Title
Functional and Mechanistic Characterization of Bacterial H-NOX/Nitric Oxide Signaling Systems

Author
Plate, Lars

Publication Date
2013

Peer reviewed|Thesis/dissertation

Functional and Mechanistic Characterization of Bacterial H-NOX/Nitric Oxide Signaling Systems

By

Lars Plate

A dissertation submitted in partial satisfaction of the

requirements for the degree of

Doctor of Philosophy

in

Molecular and Cell Biology

in the

Graduate Division

of the

University of California, Berkeley

Committee in charge:

Professor Michael A. Marletta, Chair
Professor Carolyn R. Bertozzi
Professor Michelle C. Chang
Professor Kevan M. Shokat

Spring 2013

Functional and Mechanistic Characterization of Bacterial
H-NOX/Nitric Oxide Signaling Systems

By

Lars Plate

Abstract

Functional and Mechanistic Characterization of Bacterial
H-NOX/Nitric Oxide Signaling Systems

By

Lars Plate

Doctor of Philosophy in Molecular and Cell Biology

University of California, Berkeley

Professor Michael A. Marletta, Chair

The gaseous free radical nitric oxide (NO) is firmly established as a unique signaling agent in nature. Eukaryotes employ this freely diffusible molecule in low transient concentrations as a cardiovascular signaling agent and neurotransmitter. Macrophages produce higher, cytotoxic concentrations of NO to serve as an integral piece of the host-defense against pathogens. NO signaling in vertebrates is well characterized and involves the Heme-Nitric oxide/Oxygen binding (H-NOX) domain of soluble guanylate cyclase (sGC) as a selective NO sensor. H-NOX domains are also present in many bacteria including a number of pathogens. Bacterial H-NOX proteins are often found in the same operon as signaling proteins such as histidine kinases, suggesting a role for H-NOX proteins as sensors in prokaryotic NO signaling pathways.

H-NOX-dependent control of histidine kinase autophosphorylation has been demonstrated, but little was known about the biological role or output of H-NOX two-component signaling pathways in bacteria. Here, molecular details of a bacterial H-NOX signaling network in *Shewanella oneidensis* are presented. NO regulates biofilm formation by controlling the levels of the bacterial secondary messenger cyclic diguanosine monophosphate (cyclic-di-GMP) through an unusually complex multi-component signaling network. Homologous pathways exist in the pathogen *Vibrio cholerae* and in additional gammaproteobacteria. This work and other recent studies highlight a more general role for NO in restructuring bacterial communal behavior, influencing motility and biofilm formation, host-symbiont interactions, and quorum sensing.

The connectivity of the signaling network in *S. oneidensis* was mapped by phosphotransfer profiling, which demonstrated signal integration from two histidine kinases and branching to three response regulators: HnoB, HnoC, and HnoD. Phosphodiesterase assays showed that a feed-forward loop between HnoB and HnoD response regulators with phosphodiesterase domains and phosphorylation-mediated activation intricately regulated c-di-GMP levels. *In vivo* phenotypic characterization established a direct link between NO signaling

and increased biofilm formation. Cellular adhesion in biofilms may provide a general protection mechanism for bacteria against high concentrations of reactive and damaging NO. HnoC functions as transcription factor controlling expression of the signaling components in the network. Mechanistic studies of HnoC revealed an unprecedented regulation mechanism, involving phosphorylation-induced dissociation of the response regulator tetramer. The transcriptional feedback loop created by HnoC further regulates the dynamics of the H-NOX signaling network in response to NO stimuli.

One of the phosphotransfer targets of the H-NOX-associated histidine kinase in the signaling network in *S. oneidensis* and *V. cholerae* contains a HD-GYP domain: a predicted but poorly characterized phosphodiesterase domain for cyclic-di-GMP hydrolysis. The HnoD HD-GYP domains contain degenerate residues that cause them to be catalytically inactive. To understand the functional consequence of the degeneracy and to gain general insights on the catalytic mechanism of HD-GYP domains, two catalytically active HD-GYP enzymes were characterized. The enzymes contained a binuclear iron center, and reconstitution experiments demonstrated that a heterovalent Fe(III)-Fe(II) cluster is likely required for catalysis. The absence of the metal-coordination site in HnoD eliminates any phosphodiesterase activity.

The prevalence of orphan H-NOX/histidine kinase pairs highlights the necessity for improved methods to map connectivities in two-component signaling. The identity of cognate response regulator(s) is needed to define the biological function of the signaling system. Analogous to approaches in eukaryotic kinases, protein engineering was applied to histidine kinases to permit the use of unnatural ATP analogs as substrates, which are unreactive with other enzymes. Analog-sensitive alleles of two model histidine kinases were developed, and the phosphotransfer transfer reactions to their respective response regulators were optimized. Additionally, a panel of kinase inhibitors was screened for specificity against the analog-sensitive alleles. The analog-sensitive histidine kinases could become useful for *in situ* identification of phosphotransfer partners of orphan histidine kinases.

TABLE OF CONTENT

LIST OF ABBREVIATIONS

as	analog-sensitive
ATP	adenosine-5'-triphosphate
ATPγS	adenosine-5'-O-(3-thiotriphosphate)
$BeCl_2$	beryllium chloride
BeF_x	beryllium fluoride
CA	histidine kinase catalytic and ATP-binding domain
$CaCl_2$	calcium chloride
cDNA	complementary DNA
CO	carbon monoxide
cRNA	complementary RNA
cXMP	xanthosine-3',5'-cyclic monophosphate
cyclic-di-GMP	3',5'-cyclic diguanosine monophosphate
DEA	diethanolamine
DETA NONOate	(Z)-1-[N-(2-aminoethyl)-N-(2-ammonioethyl)amino]diazen-1-ium-1,2-diolate
DGC	diguanylate cyclase
DMSO	dimethyl sulfoxide
DNA	2'-deoxyribonucleic acid
DTT	dithiothreitol
EAL	cyclic-di-GMP phosphodiesterase domain, containing an EAL motif
EDTA	ethylenediaminetetraacedic acid
FIST	F-box and intracellular signal transduction proteins
GFP	green fluorescent protein
GGDEF	cyclic-di-GMP diguanylate cyclase domain, containing a GGDEF motif
GHKL	gyrase, Hsp90, histidine kinase, MutL
GMP	guanosine-5'-monophosphate
GpG	guanylyl-(3'-5')-guanosine
GTP	guanosine-5'-triphosphate
H-NOX	Heme-Nitric Oxide/Oxygen binding domain
HD-GYP	cyclic-di-GMP phosphodiesterase domain, containing an HD-GYP motif
HEPES	4-(2-hydroxyethyl)piperazine-1-ethanesulfonic acid
His_6	hexa-histidine
HK	histidine kinase
hno	H-NOX/NO-dependent
HPLC	high performance liquid chromatography
HPR	horseradish peroxidase
Hpt	histidine-containing phosphotransfer domain
HTH	helix-turn-helix
ICP-AES	inductively coupled plasma atomic emission spectroscopy
IPTG	isopropyl *β*-D-1-thiogalactopyranoside
KOH	potassium hydroxide
LB	Luria-Bertani medium
LC-MS	liquid chromatography mass spectrometry
MBP	maltose binding protein

MCP	methyl-accepting chemotaxis protein
$MgCl_2$	magnesium chloride
mRNA	messenger RNA
NaCl	sodium chloride
NaF	sodium fluoride
NaOH	sodium hydroxide
NMR	nuclear magnetic resonance
NO	nitric oxide
NOS	nitric oxide synthase
NTA	nitrolotriacetic acid
O_2	oxygen
OD	optical density
PAP	purple acid phosphatase
PAS	Per/ARNT/SIM domain
PBS	phosphate buffered saline
PBST	phosphate buffered saline, 0.1% Tween
PCR	polymerase chain reaction
PDB	Protein Data Bank
PDE	phosphodiesterase
pGpG	5'-phosphoguanylyl-(3'-5')-guanosine
PNBM	*p*-nitrobenzyl mesylate
REC	response regulator receiver domain
RNA	ribonucleic acid
RNAP	RNA polymerase
RNS	reactive nitrogen species
ROS	reactive oxygen species
RR	response regulator
SDS-PAGE	sodium dodecyl sulfate polyacrylamide gel electrophoresis
SEC	size-exclusion chromatography
sGC	soluble guanylate cyclase
So	*Shewanella oneidensis*
TBE	Tris/borate/EDTA
TCEP	tris(2-carboxyethyl)phosphine
TCS	two-component signaling system
TEV	Tabacco Etch Virus
Tris	tris(hydroxymethyl)aminomethane
Tt	*Thermoanaerobacter tengcongensis*
Vc	*Vibrio cholerae*
WT	wild-type

LIST OF FIGURES

LIST OF TABLES

ACKNOWLEDGEMENTS

The work presented here and my personal growth as a scientist throughout my time in graduate school would not have been possible without great mentorship and teaching, countless advice and insights, and important moral backing from a large number of people. I am greatly indebted to all of them for their help and guidance.

Above all, I would like to thank my advisor and scientific mentor Michael Marletta for his limitless support. His research group was one of the primary reasons I originally applied to Berkeley for graduate studies, and my communication with him during the visit and his later endorsement over the phone were the main reasons I joined. I never regretted that decision. I was fortunate enough to be welcomed to Michael's lab during my first rotation. Since then, he has been an inspiring mentor and his supervision has been critical for my success in graduate school. I appreciate the freedom and encouragement he provides to his students to develop new research ideas and projects, even if they deviate from the main interest and expertise of the group. Michael has been instrumental in fostering a collaborative work environment and in initiating exciting joint projects that have pushed me into new research areas. The move to Scripps certainly came as a surprise, but I am grateful for how delicately Michael handled the transition, always keeping the well-being of his lab members in mind, and still encouraging us to maintain strong ties to Berkeley while in San Diego. I am excited to have moved with everyone and been given the opportunity to help build the lab, experience the stimulating, fresh work environment, and engage in new collaborations. Lastly, I truly admire Michael's leadership skills in tackling the "larger issues" of the scientific community that go beyond the day-to-day research activities. I hope that the few lessons learned will one day become helpful when I continue on my own career path.

I would also like to express my gratitude to the many other professors who have supported me throughout the years. In particular, I would like to thank the members on my thesis committee: Michelle Chang, Carolyn Bertozzi, and Kevan Shokat. Each of them has provided invaluable insights and advice for the success of my research projects and educational advancement. I am especially grateful to Kevan Shokat for always making himself available, and being extremely enthusiastic and supportive about a collaborative project with his lab. I also thank the members of the Shokat lab who have helped with advice and reagents. I am grateful to my undergraduate advisor JoAnne Stubbe at MIT for sparking my interest in biochemistry, training me in her lab, and supporting the transition to graduate school.

Much about the graduate school experience is determined by the work environment. For this reason, I consider myself extremely lucky to have worked among such friendly, collaborative, and stimulating colleagues, who have also become my good friends over the years. I am thankful to Emily Weinert and Charlie Olea, who were fantastic rotation mentors. I appreciate their initial training, their project advice and ideas, and their insights on graduate school life. It has also been a pleasure to work with Mark Herzik, collaborate on X-ray crystallography, and discuss H-NOX proteins and bacterial signal transduction with him. I am thankful that I had continued assistance from Julie Lanselle, and that I had the chance to mentor such a talented undergraduate student. I am proud of her achievements and wish her success in

graduate school. Together with Mark, it was also a great experience to mentor Charles Hespen during his rotation. I am glad that Charles decided to join the lab and that he continues working on bacterial H-NOX signaling. Eric Underbakke has been an invaluable help when it came to effective communication, teaching me better writing through his rigorous edits and sharing his Illustrator skills. I thank Hans Carlson for his help and recommendations on microbiology, especially in the early stages of the project, and for his encouragement to use genetic techniques that looked all too foreign to a biochemist. Lily Chao was instrumental in the success of this work by providing advice on *Shewanella* and by serving as the liaison to the Spormann lab at Stanford. I am grateful to Alfred Spormann and the members of his lab for helpful suggestions and material. I thank all other Marletta lab members, present and past – Basak Surmeli, Minxi Rao, Brian Smith, Sarah Wynia-Smith, Alexander Nierth, Van Vu, Christine Phillips-Piro, Sarah Bissonnette, Loes Bevers, Katy Barglow, Kaya Erbil, Josh Woodward, Michael Winter, Shirley Huang, Emily Derbyshire, Rosalie Tran, Theo Agapie, Jungjoo Yoon, Steve Reece – for their guidance and support, and for the many pleasant moments shared at lunch, over a pint of beer, or during infamously themed potlucks.

Lastly, I am infinitely grateful to my friends and housemates, and most importantly to my family, for their continuing support, encouragement, and love.

CHAPTER 1:

INTRODUCTION

Nitric Oxide Sensing by Bacteria

As a gaseous free radical, nitric oxide (NO) has long been recognized as a unique signaling agent in nature. Eukaryotes employ this freely diffusible molecule in low transient concentrations as a cardiovascular signaling agent and neurotransmitter (1). NO is also produced by macrophages at much higher, cytotoxic concentrations, where it serves as a host-defense against pathogens (2). Bacteria are exposed to a NO from endogenous and environmental sources and the exposure concentrations vary widely from cytotoxic, micromolar levels, as produced by macrophages, to sub-nanomolar levels. In bacteria, NO is formed as an intermediate in nitrogen assimilation, where nitrite is converted to NO by nitrite reductases, or as an intermediate in the dissimilatory reduction of nitrite to ammonia (3). A growing number of bacterial species with sequenced genomes have also been found to contain nitric oxide synthases, which generate NO through oxidation of L-arginine (4).

Since high NO concentrations are cytotoxic, pathogens encountering NO produced by the innate immune response have evolved mechanisms for sensing and detoxification (5-7). High levels of NO induce rapid expression of detoxifying enzymes, such as flavohemoglobin (HmpA), flavorubredoxin nitric oxide reductase (NorVW), respiratory nitric oxide reductase (NorB), and cytochrome c nitrite reductases (NrfA) (7-11). These enzymes convert NO to less toxic molecules, i.e. nitrate, nitrous oxide (N_2O), and ammonia. The expression of detoxification genes is controlled by a variety of transcription factors that are either dedicated NO sensors or secondary sensors that can react with NO but primarily respond to other signals. Examples of dedicated NO sensors are NorR, NnrR, and NsrR, which control expression of NorVW, HmpA, and other genes involved in a response to nitrosative stress (5, 12, 13). In agreement with their function in NO clearance, these transcriptional regulators have high-nanomolar to low-micromolar affinity, sufficient to sense toxic levels of NO (14, 15).

Recent studies have demonstrated that non-lethal, sub-micromolar concentrations of NO have diverse signaling roles and control bacterial communal behavior - for instance, biofilm formation and dispersal, motility, symbiosis, and quorum sensing (16-20). The archetypal NO sensors for these processes are *H*eme-*N*itric Oxide/*Ox*ygen binding (H-NOX) proteins, a newly characterized receptor family that shares high sequence homology with the heme-binding domain of the principal mammalian NO receptor, soluble guanylate cyclase (sGC). H-NOX proteins are present in more than 250 bacterial species, including several pathogens. Rather than exerting direct transcriptional control, these proteins serve as high-affinity NO sensors in more complicated downstream signaling processes. This chapter will address the structure, function, and activation mechanism of H-NOX proteins, and the recent discoveries regarding the physiological role and biochemical mechanisms of the diverse downstream signaling pathways.

Heme-Nitric Oxide/Oxygen Binding Proteins

H-NOX proteins were originally identified in a bioinformatics search for sequence homologs of the heme-binding domain of the mammalian NO receptor sGC (21). NO binding to the ferrous heme cofactor of sGC activates the cyclase domain, converting GTP to cyclic GMP, the secondary messenger for downstream signaling events (1). The N-terminal 194 residues of the sGC beta subunit were identified to be sufficient for heme binding (22). This sequence was found to contain a conserved His residue required for coordination to the central iron atom in the porphyrin (23, 24). Sequence homologs with 15-40% identity to the N-terminal heme-binding domain were subsequently identified in bacteria across many phyla, including *Proteobacteria*, *Firmicutes*, *Bacteroidetes*, *Cyanobacteria*, and *Thermotogae* (21, 25). As more genome sequences become available, there are now over 250 known bacterial species containing H-NOX proteins.

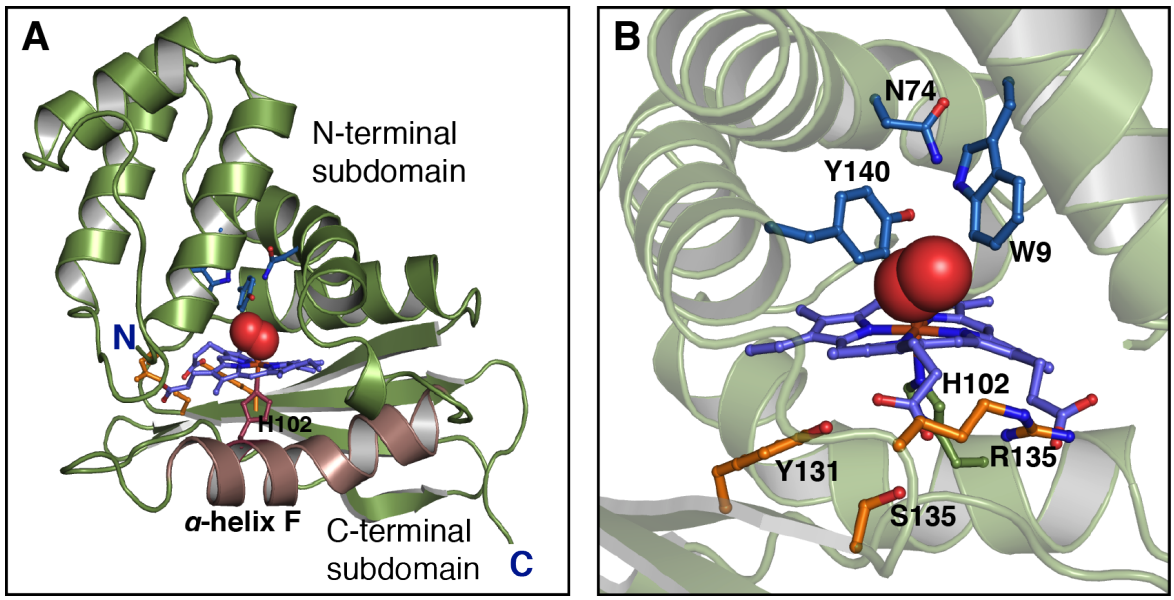

Fig. 1.1. X-ray crystal of *Thermoanaerobacter tengcongensis* (*Tt*) H-NOX
A. Structure of the H-NOX domain showing the N-terminal subdomain on top and C-terminal subdomain on the bottom with the heme cofactor buried in a pocket. The heme-coordinating H102 residue and α-helix F are at the bottom (light red).
B. Close-up of the heme-binding pocket. The H-bonding network is shown in blue, the YxSxR residues in orange.

The heme prosthetic group in the Fe(II) state is capable of coordinating several diatomic gas ligands. Consequently, a variety of heme-based gas-binding proteins exist for O_2, NO and CO (26, 27), but most of them, such as the globin family or FixL, cannot discriminate between O_2, NO and CO (27, 28). In contrast, sGC has exquisite ligand selectivity for NO and shows no measurable affinity for O_2 (1). This stringent discrimination against O_2 is a requirement for selective NO receptors, because the proteins must be capable of efficiently coordinating low nanomolar NO in the presence of greater than 1000-fold excess O_2 in aerobic environments. Characterization of several bacterial H-NOX proteins from facultative anaerobes revealed sGC-like ligand selectivity for NO (25, 29). However, a second subfamily of H-NOX proteins from

obligate anaerobes is capable of binding both O_2 and NO with high affinity (25, 30). This divergent ligand-binding behavior led to the designation of the protein family as *H*eme-*N*itric Oxide/*Ox*ygen binding (H-NOX) domains.

The first crystal structure of an H-NOX family member was from *Thermoanaerobacter tengcongensis* (*Tt* H-NOX) and it showed a novel heme-protein fold that was distinct from other heme-based gas sensors (30, 31). H-NOX domains consist of an N-terminal, helical subdomain and a C-terminal subdomain consisting of α-helix F and G, and an anti-parallel β-sheet (Fig. 1.1). The heme cofactor is deeply buried between the two subdomains and the central iron is coordinated axially to a conserved His residue on α-helix F (30, 31). Furthermore, the propionate groups of the heme form salt-bridges to an absolutely conserved YxSxR motif, which is also required for stable heme binding to the protein and activation in sGC (32) (Fig. 1.1).

Downstream effectors of H-NOX proteins

Bacterial H-NOX domains are either encoded as freestanding proteins (76% of known H-NOX sequences) or as domains of membrane-bound methyl-accepting chemotaxis proteins (MCP) (24%). H-NOX-MCP fusions are present in *Thermotogae*, *Firmicutes*, and the *Desulfovibrio* genus. Intriguingly, all of the H-NOX-MCP fusions are found in obligate anaerobes or microaerotolerant species, and their H-NOX domain contains a tyrosine in the distal heme pocket, which is a major determinant for O_2-binding (33) (Fig. 1.2.A, yellow shade). MCPs are receptors for chemical attractants or repellents, which stimulate a chemotaxic response to approach or avoid the particular stimulus (34). Therefore, based on the high affinity for O_2, the MCP-H-NOX fusions have been proposed to serve as O_2 sensors that can direct obligate anaerobes away from toxic O_2 sources (35). Alternatively, MCP-H-NOX fusions could function as NO sensors in low O_2 environments where selective pressure to exclude O_2 binding was absent during evolution of these proteins.

To obtain insight into the function of freestanding, NO-selective H-NOX proteins, the operons containing the H-NOX genes were examined for functionally-related and co-transcribed genes (Fig. 1.2.A, see Fig. A.1.A for the full list organisms and H-NOX operons). The NO-selective H-NOX genes are found in operons with other bacterial signaling genes. The majority of the operons contain histidine kinase (HK) genes directly adjacent to the H-NOX gene (112 of 209 species) (Fig. 1.2.B). HKs function in bacterial two-component signaling systems and are often membrane-incorporated proteins with periplasmic or extra-cellular sensor domains, which trigger a change in HK autophosphorylation activity in response to a chemical stimulus (36). Interestingly, no HKs adjacent to H-NOX genes are predicted to be membrane-incorporated, nor do they contain sensor domains, suggesting that the H-NOX protein can serve as sensor. Interaction between H-NOX protein and HK, as well as NO-dependent control of autophosphorylation, has indeed been observed and will be addressed later (18, 37, 38).

In two-component signaling, HKs transfer a phosphoryl group to a response regulator (RR). RRs typically contain an effector domain, and a change in phosphorylation state alters the function of the effector domain, controlling the overall output of the signaling system (36, 39). About one third of H-NOX operons with HKs also contain RR genes (Fig. 1.2.B), which likely form cognate interaction(s) with the HK (40). One such interaction can be observed in

Bacteroidetes where many operons contain RRs with LytTR DNA-binding effector domains (Fig. A.1.C). The clustering could point to a conserved function for two-component signaling systems controlling gene expression in response to NO. The RRs in H-NOX operons also contain other effector domains, including HD-GYP phosphohydrolases of cyclic-di-GMP, DNA-binding domains from the NtrC family, or they contain RRs from the CheY family which lack an effector domain altogether (39) (Fig. A.1.C). The variety of effector domains in other organisms suggests diverse roles for the H-NOX signaling pathways. Furthermore, the majority of H-NOX associated HKs are orphans, lacking a RR gene in the same operon (Fig. 1.2.B). To obtain information on the physiological role of these orphan H-NOX/HK pairs, other methods must be employed to identify the cognate RRs (16).

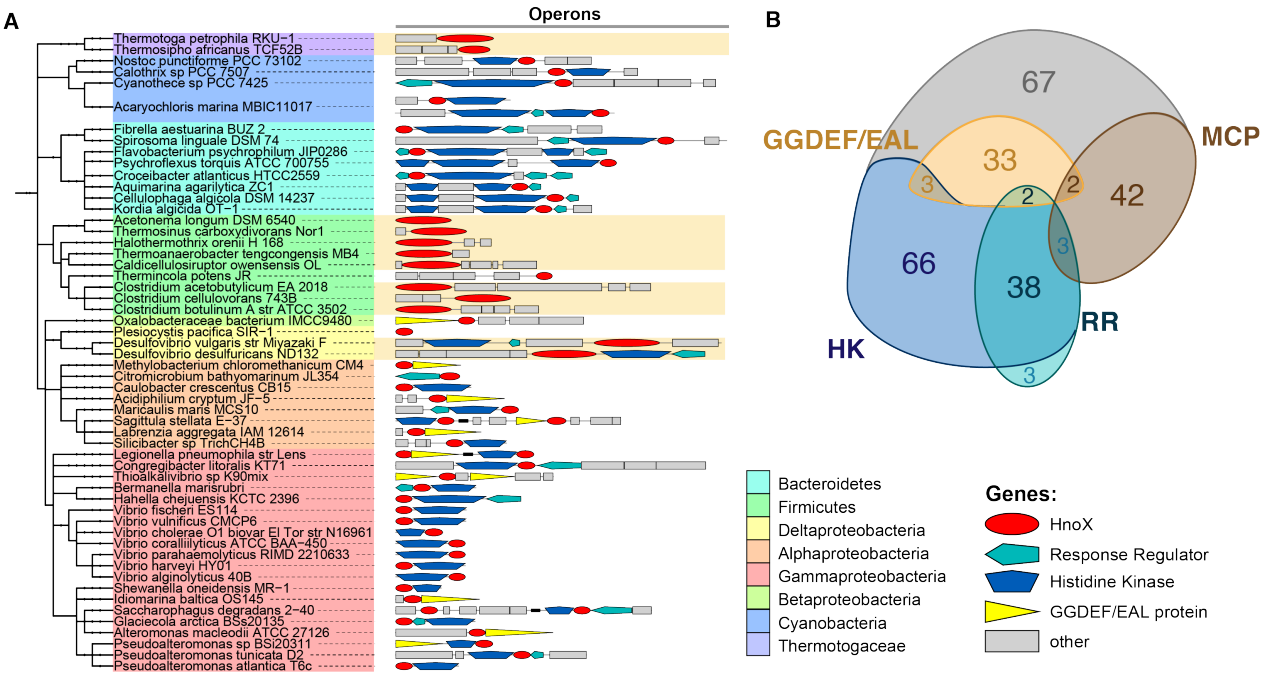

Fig. 1.2. Distribution of selected bacterial H-NOX proteins and operon organization
A. Phylogenetic tree of select bacterial species containing H-NOX genes. To the right, the gene organization of the H-NOX containing operons is displayed. Operons shaded in yellow contain predicted O_2-binding H-NOX proteins based on the presence of Tyr residue in the distal pocket. The figure was generating using the Interactive Tree of Life (41). A complete list of organisms and H-NOX operons can be found in Fig. A.1.A in Appendix A. Fig. A.1.B-D show domain organizations of the HKs, RRs and DGC/PDE proteins.
B. Euler diagram displaying the number of H-NOX containing species that have each of the listed downstream effector genes in the H-NOX operon.

A third family of frequently occurring signaling genes in the H-NOX operons are GGDEF diguanylate cyclases and EAL phosphodiesterases (Fig. 1.2.A). These proteins regulate the synthesis and/or degradation of the bacterial secondary messenger cyclic diguanosine monophosphate (cyclic-di-GMP), which controls motility behavior of bacteria through a switch from a motile to a sedentary 'lifestyle' in biofilms (42). As with HKs, interaction between an H-

NOX protein and a GGDEF-EAL protein and NO-dependent control of activity have been demonstrated and will be discussed in more detail below (17, 19).

Interestingly, certain bacteria contain two H-NOX genes in separate operons, for example *Legionella pneumophila* or *Sagitulla stellate* (Fig. 1.2.A). In these organisms, one of the duplicated genes is often associated with a HK, while the other is adjacent to a diguanylate cyclase gene. This is suggestive that both signaling modes are essential for some species.

Ligand selectivity for NO

A combination of structural studies and site-specific mutants have elucidated the mechanism for ligand discrimination in the H-NOX family. The crystal structure of *Tt* H-NOX, an O_2-binding H-NOX from an obligate anaerobe, shows a hydrogen-bonding network in the distal pocket of the heme, consisting of Y140, W9, and N74. The tyrosine residue forms a direct H-bond with the heme-bound O_2 (30) (Fig. 1.3.A). The H-bonding network is absent in the distal heme pocket of the NO-selective H-NOX protein from *Nostoc sp.* and is instead replaced by hydrophobic residues (43) (Fig. 1.3B). Multiple-sequence alignment shows that the tyrosine residue and parts of the H-bonding network are conserved in the O_2-binding H-NOX subfamily, while hydrophobic residues occupy the same position in the NO-selective H-NOX proteins, including sGC. Mutation of the Tyr to Phe in *Tt* H-NOX weakened the O_2-binding affinity, which could be rescued by introducing a compensatory Tyr (33). Introduction of a Tyr into the distal heme pocket of the NO-selective H-NOX of *Legionella pneumophila* and an sGC truncation (β1-385) allowed the formation of a weak O_2 complex, confirming that the Tyr residue is a key determinant for O_2 binding (33). Nonetheless, introduction of a Tyr into full-length sGC did not confer the ability to bind O_2 (44), suggesting that the Tyr residue is not the sole factor governing ligand selectivity.

Extensive mutagenesis studies of H-NOX proteins have revealed additional elements that influence ligand affinity, including heme distortion, conformational changes in the heme pocket, changes to protein dynamics, and a tunnel network for ligand entry and exit (45-48) (Fig. 1.3.C). In several H-NOX proteins that have been structurally characterized, the heme cofactor is severely distorted from planarity due in part to a conserved proline residue (P115 in *Tt* H-NOX) pushing up against one of the heme pyrrole rings (30, 45, 49). Relaxation of the heme distortion through a proline-to-alanine substitution leads to tighter O_2 binding (45), demonstrating that the heme geometry can influence ligand affinity. The importance of protein conformation and correct positioning of the H-bonding network for efficient O_2-binding has been demonstrated through introduction of phenylalanine residues into the heme pocket (46, 47). Added bulk in the distal pocket causes a ~1 Å upward shift of the H-bonding network and the Tyr residue away from the heme, which weakens the O_2 binding affinity more than 100-fold (46). Opening of the heme pocket and increasing flexibility of the residues covering the heme also contribute to weaker O_2 affinities (47). Furthermore, in NO-selective H-NOX proteins, a tunnel network extending from the protein surface to the heme pocket has been identified to be responsible for increased ligand flux near the heme (48). This higher ligand flow in the NO-selective H-NOX proteins could facilitate preferential binding of NO in the presence of high concentrations of O_2 because of intrinsically tighter affinities of His-ligated heme proteins for NO compared to O_2 (48, 50).

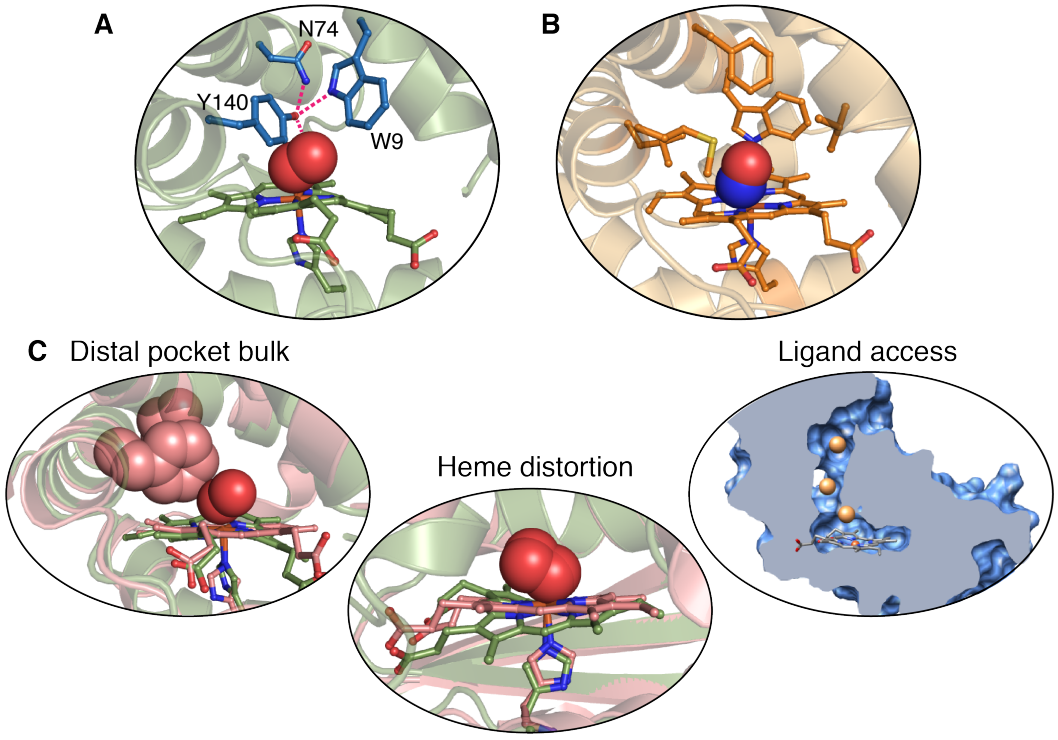

Fig. 1.3. Determinants of ligand selectivity for H-NOX proteins
A. Close-up view of the heme pocket of the O_2-binding H-NOX protein from *T. tengcongensis* (PDB: 1U55) containing the H-bonding network consisting of Y140, W9, N74.
B. Close-up view of the hydrophobic heme-pocket of the NO-selective H-NOX protein from *Nostoc sp.* (PDB: 2O09).
C. Additional factors involved in tuning the ligand binding affinity of H-NOX proteins include heme distortion, distal pocket bulk and protein flexibility, as well as ligand access through tunnels into the heme pocket.

An important distinction between O_2 and NO binding to H-NOX proteins is the coordination state of the heme. O_2 binds axially to the open coordination site on the Fe(II) forming a 6-coordinate complex, while in most H-NOX proteins, NO forms a 5-coordinate heme complex due to dissociation of the axial His residue (18, 19, 25, 29, 30, 37, 51). The transition to a 5-coordinate NO species has been described as a mechanism to increase the NO affinity because NO dissociation from the 5-coordinate heme is significantly slower (50, 52). The His-dissociation also has important consequences for the activation mechanism of H-NOX proteins and signaling to downstream effectors.

Activation mechanism

To serve as effective gas sensors in signaling pathways, H-NOX domains must be able to communicate a change in ligation state to their interacting downstream effector proteins. Structural characterization of several bacterial H-NOX proteins in different ligation states has

provided important insights into the conformational changes that are triggered by gas binding or dissociation.

A striking observation in the crystal structure of *Tt* H-NOX is the heme distortion from planarity (30). Similar heme distortion is observed in the NMR structure of *Shewanella oneidensis* (*So*) H-NOX and, to a lesser extent, in the H-NOX protein from *Nostoc* sp. (*Ns*) (43, 49). Several residues in close van-der-Waals contact with the heme pyrrole surfaces influence the heme geometry. A conserved proline residue (P115 in *Tt* H-NOX) presses against one of the pyrroles from the proximal heme pocket while a conserved hydrophobic residue (I5 in *Tt* H-NOX) on the N-terminal α-helix A is in contact with the neighboring pyrrole surface from the distal side, causing a distinct kink in the heme (Fig. 1.4.A). Intriguingly, the amount of heme distortion correlates with the movement of the N-terminal helical subdomain, which can be displaced with respect to the C-terminal domain by 3–5 Å (30, 43) (Fig. 1.4.A). This movement is the result of a 4–11º rotation around an axis along α-helix D (Fig. 1.4.A) (45, 49, 51, 53). Direct evidence for a connection between heme planarity and N-terminal rotation has been established through mutagenesis of the conserved Pro (P115) to Ala, which is sufficient to relax the heme and cause a large N-terminal shift (45). A ligand-induced change to the geometry of the heme can therefore be amplified to a larger conformational change between the N and C-terminal subdomains of the H-NOX protein.

NO binding occurs at the open-coordination site of the 5-coordinate Fe(II), forming a transient 6-coordinate complex (Fig. 1.4.B). In most H-NOX proteins, as in sGC, NO association severely weakens the bond between the Fe(II) and the distal His residue, leading to dissociation of the His and formation of a 5-coordinate Fe(II)-NO complex (Fig. 1.4.B) (25, 54). Unfortunately, structure determination of an unliganded H-NOX and a 5-coordinate NO-bound H-NOX has proved to be difficult. Instead, structural mimics of the 5-coordinate Fe(II)-NO have helped to elucidate the conformational changes resulting from NO binding and His dissociation. In both *So* and *Tt* H-NOX, the bonding connection between α-helix F and the heme has been broken by mutation of the coordinating His residue to Gly (49, 51). Heme binding to the protein was rescued through addition of imidazole as an axial ligand. Comparison of the NMR structures of WT and H103G *So* H-NOX (both CO bound) showed a similar rotational displacement of the N-terminal subdomain with respect to the C-terminal subdomain, in particular relative to the signaling α-helix F containing the heme-coordinating His residue. Accordingly, the heme in the WT structure was distorted, while rupturing the α-helix F-heme connection in the H103G mutant caused the heme to flatten (49). Activity assays of the H-NOX-associated HK confirmed that the WT CO-bound H-NOX mimicked the unliganded state, whereas the CO-bound H103G mutant resembled the activated, 5-coordinate NO-bound H-NOX state (49). Flattening of the heme and the associated N-terminal rotation with respect to α-helix F was also observed in the H102G *Tt* H-NOX structure (51). These observations lead to a heme strain model for H-NOX activation (1.4.B) (49). In the inactive, unliganded state, the heme is held in a distorted "spring-loaded" conformation through coordination of the iron to the His on α-helix F (51). NO binding to the iron and subsequent dissociation of the His release the heme, allowing it to adopt a more planar geometry. Tight van-der-Waals contacts with residues of the N-terminal subdomain, in particular I5, are responsible for translating the heme relaxation to an upward shift and rotational displacement of the entire N-terminal subdomain with respective to α-helix F. Functional validation of the heme strain model has been attained by testing the influence of H-NOX heme

conformation on the enzyme activity of an effector protein. In *Shewanella woodyi*, the H-NOX protein controls the activity of an associated DGC/PDE protein. The P117A mutation, which leads to a planar heme, is sufficient to mimic the NO-activated H-NOX state (55).

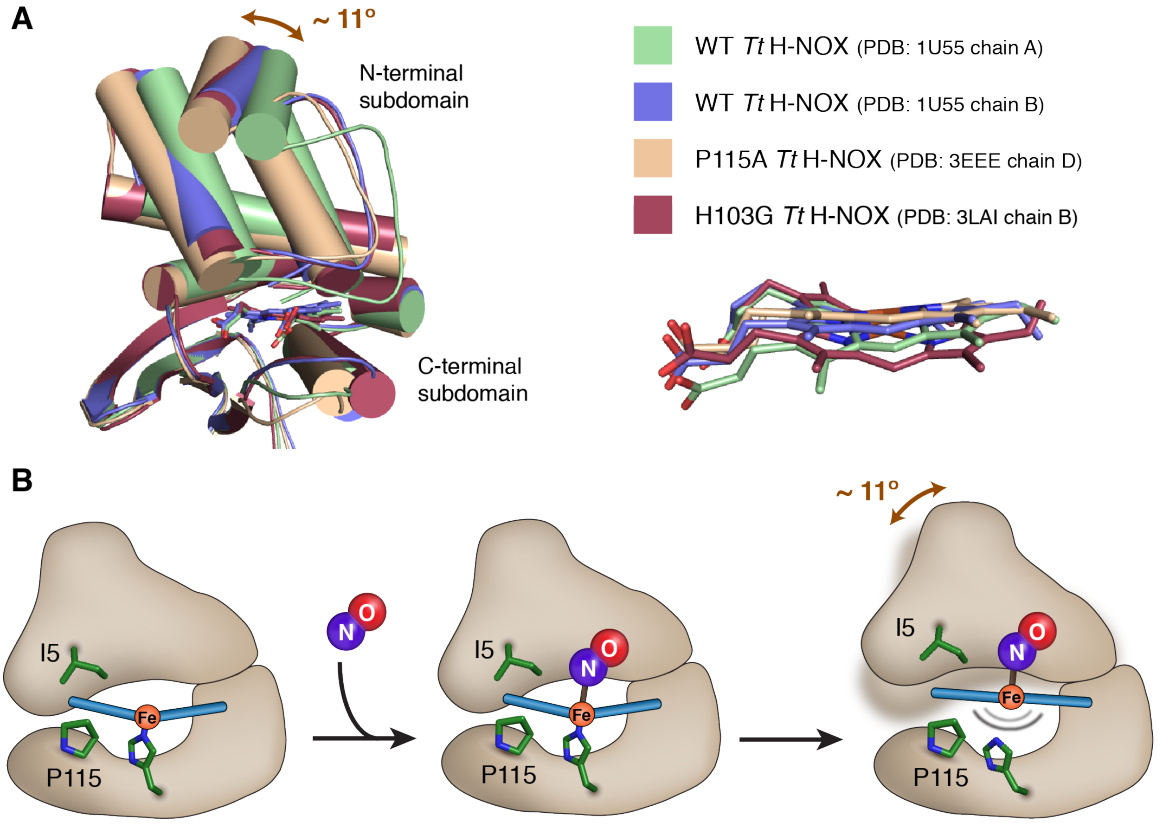

Fig. 1.4. Ligand-induced activation mechanism
A. Structural alignment of selected *Tt* H-NOX crystal structures (left) displaying the rotational displacement of the N-terminal subdomain with respect to the C-terminal subdomain. Alignment of the heme cofactors on the right displays the varying degree of heme distortion associated with each protein conformation.
B. Heme-strain model for H-NOX activation. In the unliganded H-NOX state, the heme is highly distorted due to van-der-Waals interaction between P115 and I5 (*Tt* H-NOX numbering) with two of the heme pyrroles. Initial formation of a six-coordinate Fe(II)-NO complex weakens the iron-His bond leading to His dissociation. Formation of the 5-coordinate Fe(II)-NO complex allows relaxation of the heme into a more planar geometry. Contacts between the N-terminal helix and the heme, in particular through I5, trigger an upward rotational displacement of the N-terminal subdomain (top) relative to the C-terminal subdomain (bottom).

The rotational displacement of the N-terminal subdomain relative to α-helix F (Fig. 1.4.A.) is a probable mechanism for communicating the ligation state of the H-NOX domain to associated effector. The effector domains conceivably share interaction surfaces with the H-NOX, which include α-helix F and part of the N-terminal subdomain. Recently, an involvement of these H-NOX surfaces in inter-domain contacts in sGC has been shown (56). How the H-

NOX movement is sensed and transduced into a conformational change of the effector domains is currently under investigation.

Nitric Oxide controls diverse communal behaviors

Control of motility through regulation of cyclic-di-GMP levels

Based on the operon organization of H-NOX genes adjacent to DGC and PDE genes, it was proposed that NO and the H-NOX proteins could be involved in regulation of cyclic-di-GMP metabolism (17, 21). Cyclic-di-GMP has emerged as a crucial bacterial secondary messenger controlling diverse functions, such as virulence, cell cycle progression, and motility and biofilm formation (42). Cyclic-di-GMP is produced from two equivalents of GTP by DGC domains, which contain a GGDEF motif. In turn, cyclic-di-GMP can be hydrolyzed to 5'-phosphoguanylyl-(3'-5')-guanosine (pGpG) by two different families of PDE domains: EAL or HD-GYP domains, named after conserved sequence motifs (42, 57). Organisms with DGC/PDE proteins in the H-NOX operon include mostly gammaproteobacteria (Fig. 1.2.A), including the opportunistic pathogen *Legionella pneumophila*, a parasite of amoebae that is capable of infecting human macrophages, causing Legionnaire's disease (58). Mixed-species biofilm communities in anthropogenic water supplies play an important role in the *Legionella* growth cycle and serve as nutrient and storage ground (59). A direct role for H-NOX/NO signaling in controlling biofilm formation in *L. pneumophila* has been demonstrated through genetic and biochemical experiments. Deletion of the *hnoX*1 gene produced elevated biofilm levels, consistent with a role for the signaling pathway in biofilm repression (17). Furthermore, mild overexpression of the H-NOX-associated DGC protein caused elevated biofilm formation proving an involvement of cyclic-di-GMP (17). Lastly, *in vitro* characterization of the DGC showed that the NO-bound H-NOX state activated cyclic-di-GMP synthesis, although the overall activity of the protein was relatively weak (17).

The H-NOX-dependent kinetic control of a DGC/PDE enzyme was characterized in more detail in *Shewanella woodyi*, a metabolically versatile marine organism originally isolated from squid ink (60). The H-NOX-associated DGC/PDE from *S. woodyi* (*Sw*DGC) contains active GGDEF and EAL domains, capable of both the synthesis and degradation of cyclic-di-GMP (61). This is in contrast to the homologous protein from *L. pneumophila*, which contains a degenerate EAL domain and only possesses DGC activity (17, 62). Analysis of steady-state kinetic parameters indicated that *Sw*DGC had 10-fold higher DGC activity when the H-NOX was present in the unliganded state compared to the NO-bound state. Alongside, PDE activity increased greater than 10-fold in the presence of the NO-bound state compared to the unliganded state (19). One caveat is that the overall k_{cat}/K_M for PDE activity is significantly higher than for DGC activity, even in the presence of unliganded H-NOX, suggesting that the enzyme mostly functions as a PDE and regulation of this activity is more crucial. Consistent with the NO-induced DGC-to-PDE-switch model generated from the kinetic data, lower cyclic-di-GMP concentrations and lower levels of biofilms were measured in *S. woodyi* in response to NO. Furthermore, deletion of the *hnoX* gene alleviated the decrease in biofilm formation (19).

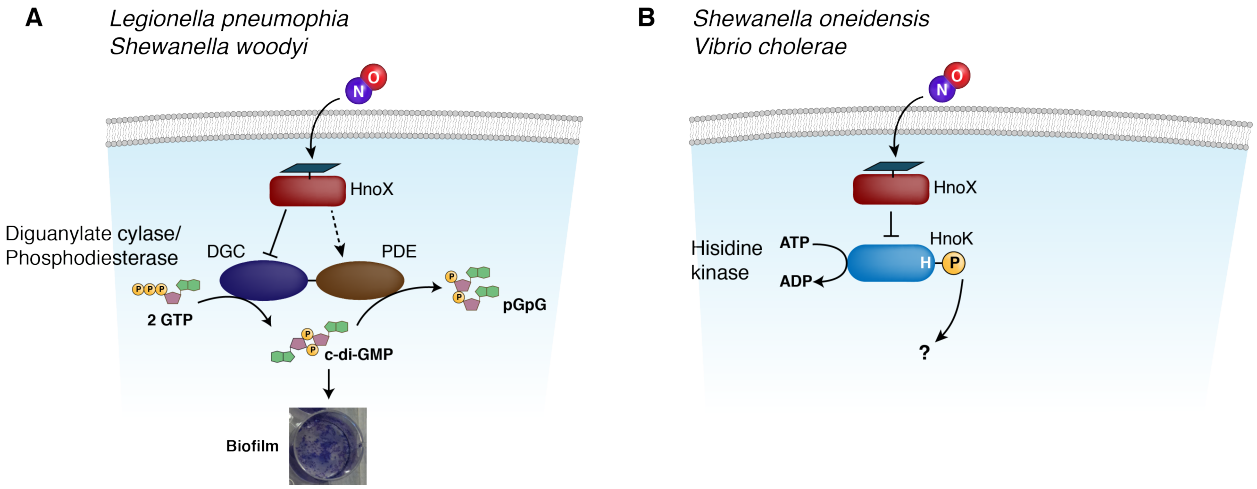

Fig. 1.5. H-NOX-dependent control of biofilm formation through regulation of cyclic-di-GMP levels
A. Model of H-NOX signaling in *L. pneumophila* and *S. woodyi*. The H-NOX protein HnoX interacts with a diguanylate cyclase/phosphodiesterase (DGC/PDE). The NO-bound H-NOX state inhibits DGC activity, and in the case of *S. woodyi*, also activates PDE activity, leading to increased c-di-GMP hydrolysis and lower biofilm formation in reponse to NO.
B. Model for the H-NOX signaling network in *S. oneidensis* and *V. cholerae* prior to the work in this thesis. The NO-bound H-NOX state inhibits autophosphorylation of the associated histidine kinase HnoK. The phosphotransfer targets of HnoK and the physiological function of the signal pathway were unknown.

Overall, the studies in *L. pneumophila* and *S. woodyi* lead to a model for H-NOX/NO-dependent biofilm dispersal described in Fig. 1.5.A. The H-NOX protein forms a regulatory complex with a co-cistronically expressed DGC/PDE protein. NO-binding to the H-NOX inhibits cyclic-di-GMP production and/or increases PDE activity, lowering cyclic-di-GMP concentrations, which causes biofilm dispersal.

Effect on host-colonization by Vibrio fischeri

Evidence that the H-NOX/NO signaling system can influence infection of a host organism has been established in a different *Vibrio* species: *V. fischeri.* This bioluminescent marine organism is engaged in a symbiosis with the Hawaiian bobtail squid *Euprymna scolopes*. *V. fischeri* colonizes the light organ of the squid. The *V. fischeri* derived bioluminescence protects the squid from predators by providing counter-illumination at night to avoid casting shadows in moon light (63, 64). A particular challenge in the initiation of symbiosis for a newly hatched *E. scolopes* is the specific acquisition of *V. fischeri* from the environment and exclusion of all other bacterial species, which are much more abundant (65). NO production by the epithelial cells lining the light organ has been shown to be an important beneficial process for symbiont colonization and partially serves as a specificity determinant for *V. fischeri* (66, 67). Consequently, the *V. fischeri* H-NOX signaling pathway was predicted to play a direct role in controlling the host-colonization.

Gene-expression profiling demonstrated that many genes in *V. fischeri* involved in iron uptake and utilization were repressed in an H-NOX and NO dependent manner (20). The

promoters for these genes contain a binding motif for the ferric-uptake regulator (Fur), and regulation of gene expression by Fur has been confirmed (68). Many of the genes are involved specifically in hemin uptake as a source of iron. This links H-NOX/NO signaling to repression of hemin acquisition and utilization (Fig. 1.6.A). The *Vf* H-NOX gene is part of an operon containing a HK gene (HnoK), and the NO-bound H-NOX inhibits the HK autophosphorylation (unpublished results) (Fig. 1.6.A). However, how HnoK is linked to regulation of Fur and the iron utilization genes remains to be determined. Unlike in *S. oneidensis* and *V. cholerae*, *V. fischeri* HnoK is a hybrid HK and contains an extra C-terminal receiver domain, which serves as an intramolecular acceptor of a phosphoryl group. This necessitates an intermediary histidine-containing phosphotransfer protein (Hpt) to shuttle the phosphoryl group from HnoK to a cognate RR (36). The partner Hpt and RR of HnoX and HnoK in this so-called phosphorelay system have yet to be identified (Fig. 1.6.A).

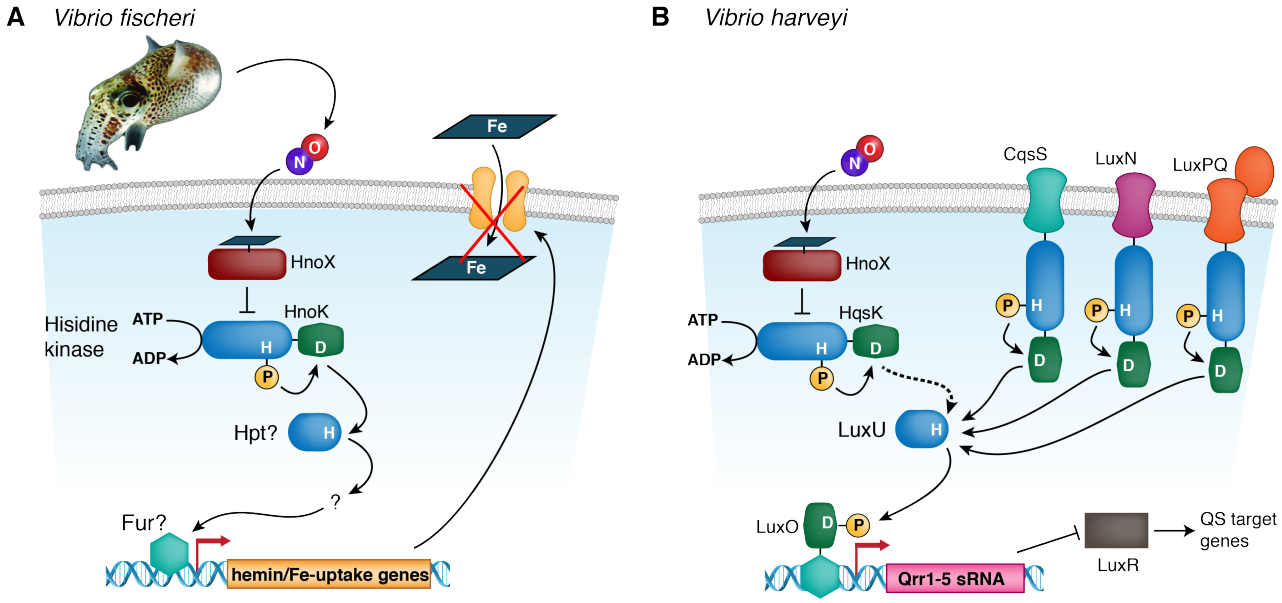

Fig. 1.6. H-NOX-dependent control of host colonization in *V. fischeri* and cross-talk with quorum sensing in *V. harveyi*

A. Model for H-NOX signaling in *V. fischeri* in the symbiosis with the Hawaiian bobtail squid *E. scolopes*. Bacteria experience NO during colonization of the squid light organ. The NO-bound state of the H-NOX inhibits autophosphorylation of the associated HK. Through an uncharacterized phosphorelay system, the NO-bound HnoX downregulates the expression of a gene set containing a Fur-binding motif in the promoter region. A subset of genes repress hemin-specific iron-uptake and utilization genes. Downregulation of intracellular iron levels in response to NO primes *V. fischeri* for exposure to ROS during the course of colonization.

B. Model for the interaction of the H-NOX signaling pathway in *V. harveyi* with the quorum sensing pathway. Quorum sensing autoinducers control the activity of three sensor HKs (CqsS, LuxN and LuxPQ). Phosphotransfer from all three HKs to a single Hpt protein, LuxU, and a RR, LuxO, integrates the quorum sensing signal. LuxO controls the expression of small regulatory RNAs Qrr1-5, which in turn repress LuxR expression. LuxU is the final transcriptional activator of the quorum sensing genes, regulating for example bioluminescence. NO-bound HnoK inhibits the activity of the associated HqsK histine kinase. HqsK is capable of also phosphorylating LuxU, linking NO sensing to expression of quorum sensing genes.

Surprisingly, deletion of the *hnoX* gene led to more efficient colonization of the squid host by *V. fischeri*, which paradoxically implicated H-NOX signaling as a deterrent in the colonization process (20). Further experiments showed that the colonization advantage of the *hnoX* deletion strain stemmed from more efficient iron utilization through hemin uptake in the low-iron environment of the light organ ducts. NO exposure in the presence of hemin as the sole iron source causes a significant slowing of growth in the wild-type strain due to downregulation of hemin uptake (20). In addition to NO, hydrogen peroxide and ROS are produced in the ducts and antechamber of the light organ (69, 70). The species generated are reminiscent of the toxicants produced by macrophages during killing. Limitation of iron uptake by *V. fischeri* during the course of colonization has been hypothesized to serve as an important strategy to avoid damage from hydroxyl radicals generated through Fenton chemistry from Fe(II) and hydrogen peroxide (20). NO exposure, which occurs even before bacteria enter the light organ ducts, is suggested to prime *V. fischeri* for ROS exposure by lowering intracellular iron levels and slowing of growth (20, 66). Consequently, H-NOX signaling is at least partially responsible for the competitive advantage of *V. fischeri* colonization compared to other bacteria present in the seawater.

V. fischeri aggregation onto mucus secreted by the light organ and subsequent transient biofilm formation are other important aspects for successful colonization of *E. scolopes* (71). Large aggregates cannot efficiently colonize the light organ crypts, but NO limits the aggregate size (67). Given the precedence for H-NOX/NO regulation of motility and biofilm levels in other organisms, an involvement in controlling *V. fischeri* aggregation is also conceivable. Regardless, a link between the H-NOX signaling pathway and biofilm formation in this organism remains to be investigated.

Cross-talk with quorum sensing

In addition to the control of motility, biofilm formation, and host-colonization, recent work suggests that H-NOX/NO signaling can influence quorum sensing, an important group behavior in which bacteria can sense their cell population density (72). Many bacteria secrete low molecular weight chemicals, called autoinducers, whose accumulated concentration can serve as readout for cell density. Autoinducer concentrations are detected by specific sensors, which trigger population-synchronized downstream signaling events in response to a rise in autoinducer concentration above a certain threshold (72). Processes regulated by quorum sensing include gene expression, motility, biofilm formation, virulence, and bioluminescence. Quorum sensing in *Vibrio harveyi*, an opportunistic pathogen of marine organisms, involves three separate autoinducers and three corresponding membrane-bound sensor HKs: CqsS, LuxN, and LuxPQ (Fig. 1.6.B). Phosphotransfer from all three HKs to a single Hpt protein, LuxU integrates the quorum sensing signal. Further downstream signaling events regulate expression of quorum sensing genes, which for example control bioluminescence (Fig. 1.6.B). High autoinducer concentrations above the threshold level switch the HK activity from autophosphorylation to phosphatase, promoting dephosphorylation of LuxU and LuxO and causing induction of gene expression by LuxR (72).

V. harveyi cultures exhibited increased bioluminescence at low culture density in the presence of low-nanomolar concentrations of NO, suggesting that NO could function as a newly

discovered autoinducer (18). NO-induced quorum sensing was dependent on the presence of the *hnoX* gene, implicating the H-NOX protein as the relevant NO sensor. As in other H-NOX/HK systems, the NO-bound H-NOX inhibited the autophosphorylation activity of the associated hybrid HK, termed HqsK (18). The link between H-NOX/NO dependent HqsK phosphorylation and the quorum sensing phosphorelay pathway was established when it was discovered that HqsK can phosphorylate LuxU (18). The H-NOX/NO sensing pathway therefore interacts directly with the quorum sensing signaling network (Fig. 1.6.B).

Nonetheless, the phosphotransfer kinetics from HqsK to LuxU were slow compared to other signaling partners, for example LuxN to LuxU (73). This raises the question whether the HsqK/LuxU interaction is cognate or the result of cross-talk between a separate H-NOX phosphorelay system and the quorum sensing network (40, 74). Further experiments are necessary to determine whether HqsK can interact with another Hpt protein, linking it to additional RR targets. Likewise, this research opens up the possibility of NO influencing quorum sensing in other organisms.

Thesis

The majority of bacterial H-NOX genes are found adjacent to HK genes, indicating that H-NOX proteins function as NO sensors in two-component signaling systems (Fig. 1.2.B). H-NOX-dependent control of HK activity was first demonstrated in *S. oneidensis* (37) and has since been studied in *Vibrio harveyi* and *Pseudoaltermonas atlantica* (18, 38). In all cases, the NO-bound state of the H-NOX inhibits HK autophosphorylation while the unliganded state either has no measurable effect on HK activity (18, 37) or increases HK autophosphorylation (38). Thus, the NO bound state of the H-NOX is inhibitory towards HKs, as it is towards DGCs (Fig. 1.5.B)

As discussed earlier, 65% of bacterial species containing a co-cistronic H-NOX/HK pair lack a cognate RR gene in the same operon, including *S. oneidensis*, and *V. cholerae* (Fig. 1.2). The work in this thesis was directed at identifying the cognate RR of these orphan H-NOX-associated HK, characterizing the H-NOX signaling system, and determining the physiological function of the NO sensing pathway in the organisms.

In **Chapter 2**, the H-NOX signaling network in *S. oneidensis* in *V. cholerae* is studied. The cognate RRs of the H-NOX associated HK, termed HnoK, were identified by phosphotransfer profiling, a kinetic profiling of all possible orphan RR candidates (16, 40). Three RR targets became phosphorylated by HnoK: HnoB, HnoC, HnoD. Subsequent biochemical characterization of the RR components demonstrated that the network was involved in adjusting cyclic-di-GMP concentrations and controlling biofilm formation. HnoB contained a phosphorylation-activated PDE effector domain. HnoD contained a degenerate HD-GYP domain, which was catalytically inactive but functioned as an allosteric inhibitor of HnoB to fine-tune PDE activity. The increased surface adhesion and biofilm formation in response to NO was proposed as a protection mechanism against this cytotoxic molecule. The presence of orthologs of the pathway components suggests a conservation of the pathway in other gammaproteobacteria.

Chapter 3 is focused on the function of HnoC, the third RR target of HnoK in the *S. oneidensis* H-NOX signaling network. HnoC serves as a transcriptional regulator and gene expression profiling identified its gene targets. It was demonstrated that HnoC controlled the expression of all the signaling components in the network, thus mediating transcriptional feedback control and regulating the dynamics of the NO response. Furthermore, the DNA-binding mechanism of HnoC and its regulation by HnoK phosphorylation were investigated.

Among the response regulators occurring in H-NOX/NO signaling pathway, HD-GYP phosphodiesterases for cyclic-di-GMP represent the least studied family. The degenerate HD-GYP response regulator HnoD from *S. oneidensis* was studied in **Chapter 2**. However, little information is known on the function and mechanism of other HD-GYP family members that are catalytically active. Therefore, **Chapter 4** is directed at the biochemical characterization of two HD-GYP phosphohydrolase enzymes. The proteins were shown to contain a binuclear iron center and the requirements for metal binding and the oxidation state of the metal site were examined.

The identification of RRs and characterization of H-NOX signaling networks in Chapters 2 and 3 revealed that current methods for mapping bacterial two-component signaling are laborious and time-consuming. **Chapter 5** is aimed at developing new tools for studying bacterial signal transduction pathways. For this purpose, analog-sensitive histidine kinases were engineered, which can accept unnatural ATP analogs as substrate that are unreactive with other enzymes. The bio-orthogonal approach could become useful for probing phosphotransfer *in situ* to identify new response regulator targets of orphan kinases. In addition, inhibitors can be developed to specifically target the analog-sensitive kinases, permitting the chemical inactivation of distinct two-component signaling pathways to probe their function.

References

1. Derbyshire, E. R., and Marletta, M. A. (2009) in *cGMP: Generators, Effectors and Therapeutic Implications* (Schmidt, H., ed.) pp. 17–31, Handbook of experimental pharmacology, Berlin Heidelberg
2. MacMicking, J., Xie, Q. W., and Nathan, C. (1997) Nitric oxide and macrophage function. *Annu. Rev. Immunol.* **15**, 323–350
3. Rodionov, D. A., Dubchak, I. L., Arkin, A. P., Alm, E. J., and Gelfand, M. S. (2005) Dissimilatory metabolism of nitrogen oxides in bacteria: comparative reconstruction of transcriptional networks. *PLoS Comput. Biol.* **1**, e55
4. Sudhamsu, J., and Crane, B. R. (2009) Bacterial nitric oxide synthases: what are they good for? *Trends Microbiol.* **17**, 212–218
5. Spiro, S. (2007) Regulators of bacterial responses to nitric oxide. *FEMS Microbiol. Rev.* **31**, 193–211
6. Fang, F. C. (2004) Antimicrobial reactive oxygen and nitrogen species: concepts and controversies. *Nat. Rev. Microbiol.* **2**, 820–832
7. Stevanin, T. M., Poole, R. K., Demoncheaux, E. A. G., and Read, R. C. (2002) Flavohemoglobin Hmp protects *Salmonella enterica* serovar typhimurium from nitric oxide-related killing by human macrophages. *Infect. Immun.* **70**, 4399–4405

8. Poole, R., and Hughes, M. (2000) New functions for the ancient globin family: bacterial responses to nitric oxide and nitrosative stress. *Mol. Microbiol.* **36**, 775–783
9. Gardner, A. M., Helmick, R. A., and Gardner, P. R. (2002) Flavorubredoxin, an inducible catalyst for nitric oxide reduction and detoxification in *Escherichia coli*. *J. Biol. Chem.* **277**, 8172–8177
10. Mills, P. C., Rowley, G., Spiro, S., Hinton, J. C. D., and Richardson, D. J. (2008) A combination of cytochrome c nitrite reductase (NrfA) and flavorubredoxin (NorV) protects *Salmonella enterica* serovar Typhimurium against killing by NO in anoxic environments. *Microbiology (Reading, Engl.)* **154**, 1218–1228
11. Stevanin, T. M., Moir, J. W. B., and Read, R. C. (2005) Nitric oxide detoxification systems enhance survival of *Neisseria meningitidis* in human macrophages and in nasopharyngeal mucosa. *Infect. Immun.* **73**, 3322–3329
12. Bush, M., Ghosh, T., Tucker, N., Zhang, X., and Dixon, R. (2011) Transcriptional regulation by the dedicated nitric oxide sensor, NorR: a route towards NO detoxification. *Biochem Soc T* **39**, 289–293
13. Tucker, N. P., Le Brun, N. E., Dixon, R., and Hutchings, M. I. (2010) There's NO stopping NsrR, a global regulator of the bacterial NO stress response. *Trends Microbiol.* **18**, 149–156
14. D'Autréaux, B., Tucker, N., Spiro, S., and Dixon, R. (2008) Characterization of the nitric oxide-reactive transcriptional activator NorR. *Meth. Enzymol.* **437**, 235–251
15. Heurlier, K., Thomson, M. J., Aziz, N., and Moir, J. W. B. (2008) The nitric oxide (NO)-sensing repressor NsrR of *Neisseria meningitidis* has a compact regulon of genes involved in NO synthesis and detoxification. *J. Bacteriol.* **190**, 2488–2495
16. Plate, L., and Marletta, M. A. (2012) Nitric oxide modulates bacterial biofilm formation through a multicomponent cyclic-di-GMP signaling network. *Mol Cell* **46**, 449–460
17. Carlson, H. K., Vance, R. E., and Marletta, M. A. (2010) H-NOX regulation of c-di-GMP metabolism and biofilm formation in *Legionella pneumophila*. *Mol. Microbiol.* **77**, 930–942
18. Henares, B. M., Higgins, K. E., and Boon, E. M. (2012) Discovery of a nitric oxide responsive quorum sensing circuit in *Vibrio harveyi*. *ACS Chem Biol* **7**, 1331–1336
19. Liu, N., Xu, Y., Hossain, S., Huang, N., Coursolle, D., Gralnick, J. A., and Boon, E. M. (2012) Nitric oxide regulation of cyclic di-GMP synthesis and hydrolysis in *Shewanella woodyi*. *Biochemistry* **51**, 2087–2099
20. Wang, Y., Dufour, Y. S., Carlson, H. K., Donohue, T. J., Marletta, M. A., and Ruby, E. G. (2010) H-NOX-mediated nitric oxide sensing modulates symbiotic colonization by *Vibrio fischeri*. *Proc. Natl. Acad. Sci. USA* **107**, 8375–8380
21. Iyer, L. M., Anantharaman, V., and Aravind, L. (2003) Ancient conserved domains shared by animal soluble guanylyl cyclases and bacterial signaling proteins. *BMC Genomics* **4**, 5–12
22. Karow, D. S., Pan, D., Davis, J. H., Behrends, S., Mathies, R. A., and Marletta, M. A. (2005) Characterization of functional heme domains from soluble guanylate cyclase. *Biochemistry* **44**, 16266–16274
23. Zhao, Y., Schelvis, J. P., Babcock, G. T., and Marletta, M. A. (1998) Identification of histidine 105 in the beta1 subunit of soluble guanylate cyclase as the heme proximal ligand. *Biochemistry* **37**, 4502–4509
24. Foerster, J., Harteneck, C., Malkewitz, J., Schultz, G., and Koesling, D. (1996) A

functional heme-binding site of soluble guanylyl cyclase requires intact N-termini of alpha 1 and beta 1 subunits. *Eur. J. Biochem.* **240**, 380–386
25. Karow, D. S., Pan, D., Tran, R., Pellicena, P., Presley, A., Mathies, R. A., and Marletta, M. A. (2004) Spectroscopic characterization of the soluble guanylate cyclase-like heme domains from *Vibrio cholerae* and *Thermoanaerobacter tengcongensis*. *Biochem.* **43**, 10203–10211
26. Farhana, A., Saini, V., Kumar, A., Lancaster, J. R., and Steyn, A. J. C. (2012) Environmental heme-based sensor proteins: implications for understanding bacterial pathogenesis. *Antioxid Redox Signal* **17**, 1232–1245
27. Gilles-Gonzalez, M.-A., and Gonzalez, G. (2005) Heme-based sensors: defining characteristics, recent developments, and regulatory hypotheses. *Journal of Inorganic Biochemistry* **99**, 1–22
28. Gilles-Gonzalez, M. A., Gonzalez, G., Perutz, M. F., Kiger, L., Marden, M. C., and Poyart, C. (1994) Heme-based sensors, exemplified by the kinase FixL, are a new class of heme protein with distinctive ligand binding and autoxidation. *Biochemistry* **33**, 8067–8073
29. Boon, E. M., Davis, J. H., Tran, R., Karow, D. S., Huang, S. H., Pan, D., Miazgowicz, M. M., Mathies, R. A., and Marletta, M. A. (2006) Nitric oxide binding to prokaryotic homologs of the soluble guanylate cyclase beta1 H-NOX domain. *J. Biol. Chem.* **281**, 21892–21902
30. Pellicena, P., Karow, D. S., Boon, E. M., Marletta, M. A., and Kuriyan, J. (2004) Crystal structure of an oxygen-binding heme domain related to soluble guanylate cyclases. *Proc. Natl. Acad. Sci. USA* **101**, 12854–12859
31. Nioche, P., Berka, V., Vipond, J., Minton, N., Tsai, A.-L., and Raman, C. S. (2004) Femtomolar sensitivity of a NO sensor from *Clostridium botulinum*. *Science* **306**, 1550–1553
32. Schmidt, P. M., Schramm, M., Schröder, H., Wunder, F., and Stasch, J.-P. (2004) Identification of residues crucially involved in the binding of the heme moiety of soluble guanylate cyclase. *J. Biol. Chem.* **279**, 3025–3032
33. Boon, E. M., Huang, S. H., and Marletta, M. A. (2005) A molecular basis for NO selectivity in soluble guanylate cyclase. *Nat. Chem. Biol.* **1**, 53–59
34. Hazelbauer, G. L., Falke, J. J., and Parkinson, J. S. (2008) Bacterial chemoreceptors: high-performance signaling in networked arrays. *Trends in Biochemical Sciences* **33**, 9–19
35. Boon, E. M., and Marletta, M. A. (2005) Ligand specificity of H-NOX domains: from sGC to bacterial NO sensors. *Journal of Inorganic Biochemistry* **99**, 892–902
36. Stock, A. M., Robinson, V. L., and Goudreau, P. N. (2000) Two-component signal transduction. *Annu. Rev. Biochem.* **69**, 183–215
37. Price, M. S., Chao, L. Y., and Marletta, M. A. (2007) *Shewanella oneidensis* MR-1 H-NOX regulation of a histidine kinase by nitric oxide. *Biochem.* **46**, 13677–13683
38. Arora, D. P., and Boon, E. M. (2012) Nitric oxide regulated two-component signaling in *Pseudoalteromonas atlantica*. *Biochem Biophys Res Commun* **421**, 521–526
39. Galperin, M. Y. (2010) Diversity of structure and function of response regulator output domains. *Curr. Opin. Microbiol.* **13**, 150–159
40. Laub, M. T., Biondi, E. G., and Skerker, J. M. (2007) Phosphotransfer profiling: systematic mapping of two-component signal transduction pathways and phosphorelays. *Meth. Enzymol.* **423**, 531–548
41. Letunic, I., and Bork, P. (2011) Interactive Tree Of Life v2: online annotation and display

of phylogenetic trees made easy. *Nucleic Acids Res* **39**, W475–8
42. Hengge, R. (2009) Principles of c-di-GMP signalling in bacteria. *Nat. Rev. Microbiol.* **7**, 263–273
43. Ma, X., Sayed, N., Beuve, A., and van den Akker, F. (2007) NO and CO differentially activate soluble guanylyl cyclase via a heme pivot-bend mechanism. *EMBO J* **26**, 578–588
44. Martin, E., Berka, V., Bogatenkova, E., Murad, F., and Tsai, A.-L. (2006) Ligand selectivity of soluble guanylyl cyclase: effect of the hydrogen-bonding tyrosine in the distal heme pocket on binding of oxygen, nitric oxide, and carbon monoxide. *J. Biol. Chem.* **281**, 27836–27845
45. Olea, C., Boon, E. M., Pellicena, P., Kuriyan, J., and Marletta, M. A. (2008) Probing the function of heme distortion in the H-NOX family. *ACS Chem Biol* **3**, 703–710
46. Weinert, E. E., Plate, L., Whited, C. A., Olea, C., and Marletta, M. A. (2010) Determinants of ligand affinity and heme reactivity in H-NOX domains. *Angew Chem Int Ed Engl* **49**, 720–723
47. Weinert, E. E., Phillips-Piro, C. M., Tran, R., Mathies, R. A., and Marletta, M. A. (2011) Controlling conformational flexibility of an O(2)-binding H-NOX domain. *Biochemistry* **50**, 6832–6840
48. Winter, M. B., Herzik, M. A., Kuriyan, J., and Marletta, M. A. (2011) Tunnels modulate ligand flux in a heme nitric oxide/oxygen binding (H-NOX) domain. *Proc. Natl. Acad. Sci. USA* **108**, E881–9
49. Erbil, W. K., Price, M. S., Wemmer, D. E., and Marletta, M. A. (2009) A structural basis for H-NOX signaling in *Shewanella oneidensis* by trapping a histidine kinase inhibitory conformation. *Proc. Natl. Acad. Sci. USA* **106**, 19753–19760
50. Tsai, A.-L., Berka, V., Martin, E., and Olson, J. S. (2012) A "sliding scale rule" for selectivity among NO, CO, and O2 by heme protein sensors. *Biochemistry* **51**, 172–186
51. Olea, C., Jr., Herzik, M. A., Jr., Kuriyan, J., and Marletta, M. A. (2010) Structural insights into the molecular mechanism of H-NOX activation. *Protein Science* **19**, 881–887
52. Yoo, B.-K., Lamarre, I., Martin, J.-L., Andrew, C. R., and Negrerie, M. (2013) Picosecond binding of the His ligand to four-coordinate heme in cytochrome c': a one-way gate for releasing proximal NO. *J Am Chem Soc* **135**, 3248–3254
53. Olea, C., Jr., Kuriyan, J., and Marletta, M. A. (2010) Modulating Heme Redox Potential through Protein-Induced Porphyrin Distortion. *J Am Chem Soc* **132**, 12794–12795
54. Stone, J. R., and Marletta, M. A. (1996) Spectral and kinetic studies on the activation of soluble guanylate cyclase by nitric oxide. *Biochemistry* **35**, 1093–1099
55. Muralidharan, S., and Boon, E. M. (2012) Heme flattening is sufficient for signal transduction in the H-NOX family. *J Am Chem Soc* **134**, 2044–2046
56. Underbakke, E. S., Iavarone, A. T., and Marletta, M. A. (2013) Higher-order interactions bridge the nitric oxide receptor and catalytic domains of soluble guanylate cyclase. *Proc. Natl. Acad. Sci. USA*
57. Schirmer, T., and Jenal, U. (2009) Structural and mechanistic determinants of c-di-GMP signalling. *Nat. Rev. Microbiol.* **7**, 724–735
58. Swanson, M. S., and Hammer, B. K. (2000) *Legionella pneumophila* pathogesesis: a fateful journey from amoebae to macrophages. *Annu Rev Microbiol* **54**, 567–613
59. Declerck, P. (2010) Biofilms: the environmental playground of Legionella pneumophila. *Environ Microbiol.* **12**, 557–566

60. Makemson, J. C., Fulayfil, N. R., Landry, W., Van Ert, L. M., Wimpee, C. F., Widder, E. A., and Case, J. F. (1997) *Shewanella woodyi* sp. nov., an exclusively respiratory luminous bacterium isolated from the Alboran Sea. *Int. J. Syst. Bacteriol.* **47**, 1034–1039
61. Liu, N., Pak, T., and Boon, E. M. (2010) Characterization of a diguanylate cyclase from *Shewanella woodyi* with cyclase and phosphodiesterase activities. *Mol Biosyst* **6**, 1561–1564
62. Rao, F., Yang, Y., Qi, Y., and Liang, Z.-X. (2008) Catalytic mechanism of cyclic di-GMP-specific phosphodiesterase: a study of the EAL domain-containing RocR from *Pseudomonas aeruginosa*. *J. Bacteriol.* **190**, 3622–3631
63. Jones, B. W., and Nishiguchi, M. K. (2004) Counterillumination in the Hawaiian bobtail squid, *Euprymna scolopes* Berry (Mollusca: Cephalopoda). *Marine Biology* **144**, 1151–1155
64. Visick, K. L., and Ruby, E. G. (2006) *Vibrio fischeri* and its host: it takes two to tango. *Curr. Opin. Microbiol.* **9**, 632–638
65. Nyholm, S. V., and McFall-Ngai, M. J. (2004) The winnowing: establishing the squid-*vibrio* symbiosis. *Nat. Rev. Microbiol.* **2**, 632–642
66. Wang, Y., and Ruby, E. G. (2011) The roles of NO in microbial symbioses. *Cell Microbiol* **13**, 518–526
67. Davidson, S. K., Koropatnick, T. A., Kossmehl, R., Sycuro, L., and McFall-Ngai, M. J. (2004) NO means "yes" in the squid-*vibrio* symbiosis: nitric oxide (NO) during the initial stages of a beneficial association. *Cell Microbiol* **6**, 1139–1151
68. Septer, A. N., Wang, Y., Ruby, E. G., Stabb, E. V., and Dunn, A. K. (2011) The haem-uptake gene cluster in *Vibrio fischeri* is regulated by Fur and contributes to symbiotic colonization. *Environ Microbiol.* **13**, 2855–2864
69. Small, A. L., and McFall-Ngai, M. J. (1999) Halide peroxidase in tissues that interact with bacteria in the host squid *Euprymna scolopes*. *J. Cell. Biochem.* **72**, 445–457
70. Visick, K. L., and Ruby, E. G. (1998) The periplasmic, group III catalase of *Vibrio fischeri* is required for normal symbiotic competence and is induced both by oxidative stress and by approach to stationary phase. *J. Bacteriol.* **180**, 2087–2092
71. Morris, A. R., and Visick, K. L. (2010) Control of biofilm formation and colonization in *Vibrio fischeri*: a role for partner switching? *Environ Microbiol.* **12**, 2051–2059
72. Ng, W.-L., and Bassler, B. L. (2009) Bacterial quorum-sensing network architectures. *Annu. Rev. Genet.* **43**, 197–222
73. Timmen, M. (2006) AI-1 Influences the Kinase Activity but Not the Phosphatase Activity of LuxN of *Vibrio harveyi*. *Journal of Biological Chemistry* **281**, 24398–24404
74. Laub, M. T., and Goulian, M. (2007) Specificity in two-component signal transduction pathways. *Annu. Rev. Genet.* **41**, 121–145

CHAPTER 2:

NITRIC OXIDE MODULATES BACTERIAL BIOFILM FORMATION THROUGH A MULTICOMPONENT CYCLIC-DI-GMP SIGNALING NETWORK[1]

Summary

This chapter describes the molecular pathway for H-NOX signaling in *Shewanella oneidensis*. NO stimulates biofilm formation by controlling the levels of the bacterial secondary messenger cyclic diguanosine monophosphate (cyclic-di-GMP). Phosphotransfer profiling was used to map the connectivity of a multicomponent signaling network that involves integration from two histidine kinases and branching to three response regulators. A feed-forward loop between response regulators with phosphodiesterase domains and phosphorylation-mediated activation intricately regulated cyclic-di-GMP levels. Phenotypic characterization established a link between NO signaling and biofilm formation. Cellular adhesion may provide a protection mechanism for bacteria against reactive and damaging NO. These results are broadly applicable to H-NOX- mediated NO signaling in bacteria.

Introduction

Nitric oxide (NO) is a ubiquitous signaling molecule in nature despite its inherent toxicity and reactivity. NO signaling in vertebrates is a well-understood process in which NO activates soluble guanylate cyclase (sGC), leading to the formation of cyclic GMP, which controls diverse downstream processes such as vasodilation and neurotransmission (1). sGC contains a unique heme domain, which selectively binds NO and has no measurable affinity for O_2. This domain is a member of a larger family of hemoprotein sensors for diatomic gases termed *H*eme-*N*itric oxide/*OX*ygen binding (H-NOX) proteins (2-4). H-NOX domains are also present in many bacteria including a number of pathogens. Bacteria encounter NO as an intermediate of denitrification or as a product of bacterial or host nitric oxide synthases. NO plays a particularly important role in host-pathogen interactions and macrophages produce NO as an antimicrobial agent (5). A variety of bacterial iron and heme-containing NO sensors confer protection by regulating expression of enzymes that convert NO to less toxic species (6, 7). The majority of these NO sensors are direct transcriptional regulators. In contrast, bacterial NO-selective H-NOX proteins are often found in the same operon as signaling proteins such as histidine kinases or diguanylate cyclases, suggesting a role as sensors in prokaryotic NO signaling pathways.

The biological function of H-NOX proteins has been studied in few organisms. In *Legionella pneumophila* and *Shewanella woodyi*, the H-NOX protein was shown to be involved

[1] This chapter was previously published as: Plate L., Marletta MA (2012) Nitric Oxide Modulates Bacterial Biofilm Formation through a Multicomponent Cyclic-di-GMP Signaling Network, *Molecular Cell* 46: 449-460

in biofilm repression by directly influencing the activity of a diguanylate cyclase/phosphodiesterase protein, which controls the level of the bacterial secondary messenger cyclic diguanosine monophosphate (cyclic-di-GMP) (8, 9). In *Vibrio fischeri*, the H-NOX protein plays a role in symbiosis with the squid *Euprymna scolopes* by regulating the expression of iron uptake genes during NO exposure in the course of colonization (10). In the majority of bacteria with H-NOX proteins, including *V. fischeri*, the *hnoX* gene is located adjacent to that of a histidine kinase (HK). Direct interaction between the H-NOX protein and the HK has been demonstrated in *Shewanella oneidensis MR-1,* a metabolically versatile bacterium with applications in bioremediation. HK autophosphorylation is controlled by the ligation state of the H-NOX protein and NO binding suppresses HK activity (11). The present study addresses signal transduction from the HK to the physiological output of the signaling pathway.

HKs are part of two-component signal transduction systems, the predominant means by which bacteria sense and adapt to diverse stimuli (12). In the simplest form, two-component signaling involves a sensor histidine kinase (HK) and a cognate response regulator (RR). Stimulus recognition by the HK sensory domain controls autophosphorylation of a conserved His residue. The H-NOX-associated HKs are unusual in that the H-NOX sensory protein is separately expressed and not fused to the HK. The second step in two-component signaling involves phosphoryl transfer from the His residue on the HK to a conserved Asp residue on the RR receiver domain. Receiver domain phosphorylation controls the activity of an attached effector domain, which governs the output of the signaling pathway (13). The effector domains are often DNA binding domains controlling a transcriptional response but can also be enzymes (e.g. diguanylate cyclases or cyclic-di-GMP phosphodiesterases). Specificity in the pathway is achieved by tuning the interactions between HK and RR (14). Mapping the connectivity between particular HKs and RRs is challenging due to the large number of two-component signaling systems in most bacterial genomes and the presence of orphan HK and RRs (i.e. HK or RR encoded without a nearby partner gene) (15). The majority of H-NOX-associated HKs, including the one in *S. oneidensis*, are orphans. Thus, the cognate RR(s) have to be identified to determine the output and the biological role of the H-NOX signaling pathway.

In this chapter, a complex signaling network was mapped in *Shewanella oneidensis*, which involves integrated and branched phosphotransfer from the H-NOX-associated HK, as well as an additional HK to three common RR targets. Phosphodiesterase assays demonstrated how two RR jointly regulated the intracellular cyclic-di-GMP pool. Biofilm assays in *S. oneidensis* provided a direct link between NO sensing and the control of cellular attachment. Conservation of the pathway in other gammaproteobacteria, such as *Vibrio cholerae*, suggests a broad role for bacterial H-NOX proteins in controlling cyclic-di-GMP levels and biofilm formation as a behavioral response to NO.

Experimental Procedures

Protein expression and purification

All proteins, except HnoX and HnoK, were cloned, expressed, and purified as follows: Genes were PCR amplified from *S. oneidensis* MR-1 or *Vibrio cholerae* genomic DNA and cloned into pENTR/TEV/D-TOPO using TOPO cloning (Invitrogen). Gateway cloning

(Invitrogen) was used for transfer of genes into the expression plasmid pHMGWA (16) appending a *N*-terminal His_6-MBP. Proteins were expressed in *E. coli* BL21(DE3)pLysS at 20ºC, induced with 1 mM IPTG and grown at 20ºC for 20 hrs. Cells were resuspended in lysis buffer (50mM sodium phosphate pH 8.0, 300mM NaCl, 10% glycerol, 1 mM pefabloc, 1 mM benzamidine, 2 mM 2-mercaptoethanol) and lysed by passage through a high-pressure homogenizer (Avestin). The lysate was centrifuged at 200,000 g for 45 min in an Optima XL-100K ultracentrifuge with a Ti-45 rotor (Beckman). The supernatant was loaded onto amylose resin (NEB), which was washed with lysis buffer. The columns were washed with 20 column volumes of lysis buffer and protein was eluted with 50 mM maltose in lysis buffer. The proteins were further purified on nickel-nitrolotriacetic acid (Ni-NTA) agarose resin (Qiagen). The resin was washed with 10 column volumes of lysis buffer supplemented with 20 mM imidazole and protein was eluted with 250 mM imidazole in lysis buffer. For HnoD used in inhibition assays, the MBP-tag was removed by overnight incubation with TEV protease (1:20 TEV:HnoD ratio) and simultaneous dialysis into TEV cleavage buffer (50 mM Tris pH 8.0, 50 mM NaCl, 1 mM dithiothreitol (DTT), 5% glycerol). Protein was passed over Ni-NTA resin and the flow-through was collected. Protein was further purified on a Superdex 200 column (GE Healthcare). HnoX (SO2144) and HnoK (SO2145) were purified as described previously (11). All proteins were exchanged into storage buffer (50 mM diethanolamine pH 8.0, 150 mM NaCl, 1 mM DTT, 5% glycerol) and flash frozen in liquid nitrogen.

Phosphotransfer profiling and phosphotransfer kinetics

S. oneidensis RRs were identified from a BLAST search and the number of RR candidates was narrowed to 20 by excluding genes adjacent to HKs as well as RR genes with known functions. Notably, we included proteins from a genome region that was particularly rich in two-component signaling proteins (SO2538-SO2547, Figure 2.1A). Phosphotransfer profiling was performed as described (17) with the following modifications: Purified HK (5 μM) in phosphorylation buffer (50 mM DEA pH 8.0, 150 mM NaCl, 5% glycerol) was pre-incubated with 1 mM ATP, 10 μCi [γ-^{32}P]-ATP (6000 Ci/mmol, Perkin-Elmer) and 5 mM $MgCl_2$ for 60 min prior to addition of the respective purified RR (5 μM). Reactions were quenched after 10 sec or 60 min by addition of 6x SDS loading dye and products were separated on 10-20% Tris-glycine SDS-PAGE gels. The gels were dried and exposed on phosphoimager plates (Molecular Dynamics) and analyzed on a Typhoon Trio (GE Healthcare). Phosphotransfer kinetics were measured in the same way and the phosphorylation signal was quantified using ImageQuant. Two or three independent experiments were averaged.

Phosphodiesterase assays

Cyclic-di-GMP was synthesized enzymatically (18). A pGpG standard was purchased from Biolog. Purified EAL protein (or HD-GYP protein) was incubated in phosphorylation buffer with 10 mM $MgCl_2$ and the reactions were initiated by addition of 0.5 mM cyclic-di-GMP. If necessary, tryptophan (1 mM) or cXMP (0.25 mM) internal standards were included. Aliquots (10 μL) were quenched at different time points by addition of 25 μL trifluoroacetic acid (2%) and 10 μL $CaCl_2$ (1 M). Volumes were adjusted to 100 μL, the samples were filtered and analyzed by HPLC on a Nova-Pak C18 4 μm (3.9 x 150 mm) column at a flow rate of 1 mL/min

using the following gradient: 0 – 6 min: 20 mM ammonium acetate – 5% acetonitrile; 7.5 min: 15 % acetonitrile; 8.4 - 9 min: 100% acetontrile; 9.1 – 13.5 min: 20 mM ammonium acetate. pGpG formation was calculated from peak integration and a standard curve of pGpG. HK (40 μM) was pre-phosphorylated with 0.5 mM ATP for 30 min prior to addition of HnoB and incubated for 15 min before initiating reactions with cyclic-di-GMP. Beryllium fluoride was prepared freshly by mixing 10 μL $BeCl_2$ (1 M) and 90 μL NaF (1 M) and 1 mM was added to the assay 15 min prior to initiation. HnoD (50 μM, unless otherwise noted) was also added 15 min before initiation. All experiments were conducted in duplicates or triplicates.

Pull-down assays between H-NOX protein and HKs

MBP-tagged HnoK, HnoS, SO2145 (100 μg) or buffer (control) was equilibrated with amylose resin (60 μL, NEB) in storage buffer for 1 hour. H-NOX protein (NO-bound, 60 μM) was added for 1 hour and washed two times with storage buffer (200 μL). Proteins were eluted with 50 mM maltose in storage buffer and separated by SDS-PAGE.

S. oneidensis strain construction

In-frame deletion strains were generated from WT *Shewanella oneidensis* MR-1 as described (19). Briefly, 750 bp upstream and downstream regions, which only contained the first and last 20 bp of each gene, were PCR amplified, fused by PCR and ligated into pDS3.0 suicide plasmid. Plamids were transformed into S17-λpir donor strain, introduced into WT *S. oneidensis* by mating, and first crossover mutants were selected on gentamicin. Gen^R colonies were grown in LB medium without NaCl and antibiotics and plated on 10% sucrose to select for second crossover mutants. Gen-sensitive colonies were screened for correct deletions by verifying the size of PCR amplifications using primers that flanked the deleted locus. For complementation, *hnoB* was PCR amplified using a 5' primer containing a ribosomal binding site and was cloned into pBAD202/D-TOPO (Invitrogen). The plasmid was transformed into the respective *S. oneidensis* strain by electroporation and selected on kanamycin. A detailed description of strains and plasmids used in this study can be found in Appendix Table B.1.

Static biofilm assays

Biofilm assays were performed in an anaerobic glovebag (Coy Laboratory Products) in 12-well or 96-well polystyrene microtiter plates. *S. oneidensis* was grown aerobically in LB medium at 30ºC overnight. Anaerobic MM mineral medium (20) supplemented with 50 mM lactate, 50 mM fumarate and 0.1% casamino acids was inoculated with 100-fold diluted overnight cultures. DETA NONOate (Cayman Chemical), prepared freshly in 10 mM NaOH, was added to 200 μM if necessary. Cells were grown statically at 29ºC and a 3 mL reference culture was grown for OD measurements and normalization. Addition of NO to *S. oneidensis* caused an 18-hour lag in growth but cultures reached the same optical density after 25 hrs (Figure B.5.B). Therefore, biofilm formation was quantified after 20 hours during log phase (Figure 2.5.A) and at 44 hours during stationary phase (Figure 2.5.B,D) and normalized to growth. Crystal violet staining after 20 hrs or 44 hrs was performed as described (21). Measurements from individual wells were combined and normalized to growth ($OD600_{nm}$) and twelve (96-well) or three (12-well) experiments from separate days were averaged.

Determination of NO concentrations in S. oneidensis growth medium

Anaerobic MM mineral medium (3 mL, see Experimental Procedures) was added to 12-well microtiter plates and individual wells were inoculated with WT *Shewanella oneidensis* (30 µL) grown aerobically in LB medium. A DETA NONOate stock was prepared freshly in 10 mM NaOH and 200 µM were added to individual wells. The plates were incubated at 27-29ºC inside an anaerobic glovebag (Coy Laboratory Products). Samples (200 µL) were removed in sealed Reacti-vials with minimal headspace and 50-100 µL samples were injected into the reaction chamber of an NO analyzer (Sievers) in liquid setup with 1 M NaOH as carrier solution. A standard curve of NO was prepared by serial dilution of a saturated solution of NO (1.98 mM) (22).

Growth curves of Shewanella oneidensis

Assays were performed in 96-well microtiter plates inside an anaerobic glovebag (Coy Laboratory Products). Overnight cultures of WT *Shewanella oneidensis* and the respective knockout strains were grown aerobically in LB. Eight wells of anaerobic MM mineral medium (200 µL) were inoculated with 100-fold diluted overnight cultures from each strain and grown at 29 ºC in a microplate reader (Molecular Device). NO was introduced to the media by addition of DETA NONOate (200 µM) from a freshly prepared stock. The plates were stirred and the OD at 600 nm was recorded every 10 min. Measurements from individual wells were combined and growth curves from three independent experiments were averaged.

Reverse transcription PCR

WT *Shewanella oneidensis* was grown anaerobically in 12-well microtiter plates in the presence and absence of DETA NONOate as above. Once cultures reached an OD_{600nm} of 0.5, they were stabilized with RNAprotect Bateria Reagent (Qiagen) and total RNA was extracted using the RNeasy Mini kit (Qiagen). Samples were treated twice with RNAse-free DNAse (Qiagen) and subsequently cleaned up using the RNeasy Mini kit until DNA was no longer detectable. cDNA was generated using SuperScript III Reverse Transcriptase (Invitrogen). Primers for short qPCR probes were designed using the RealTime PCR tool (Integrated DNA Technologies). The H-NOX signaling genes were PCR amplified with Taq DNA Polymerase (Qiagen). The constitutively expressed DNA gyrase subunit *gyrB* served as a positive control. All primer sequences from this study are available upon request.

Biofilm viability

Anaerobic *S. oneidensis* biofilms were grown in 12-well microtiter plates as described in the experimental procedures. Liquid medium and planktonic cell were removed and wells were washed once with wash buffer (10 mM HEPES pH 7.4, 150 mM NaCl). Biofilms were resuspended in the same buffer by vigorous pipetting and diluted to an $OD600_{nm}$ ~ 0.1. Cells were stained using the Live/Dead BacLight Bacterial Viability kit (Invitrogen) according to the manual. Standard mixtures of viable and dead cells were prepared by mixing live and isopropanol-treated, dead cells. Fluorescence emission spectra between 490 – 700 nm were

recorded on a Fluoromax-4C Fluorometer (Horiba Scientific) using an excitation wavelength of 470 nm. A standard curve was prepared by plotting the ratios of fluorescence intensity at 530 nm and 630 nm against the percentage of live cells in the mixture.

Results

Identification of three cognate response regulators to the H-NOX-associated histidine kinase

To map the two-component signaling pathway and identify the cognate RR(s) to the H-NOX-associated HK in *Shewanella oneidensis*, we used phosphotransfer profiling. This method probes the *in vitro* phosphotransfer between a purified HK and a panel of RR candidates and relies on the observation that *in vivo* cognate interactions display fast phosphotransfer kinetics *in vitro* (15, 23). The H-NOX-associated HK (SO2145, HnoK) was phosphorylated with [γ-^{32}P]-ATP prior to RR addition. Rapid loss of phosphorylation from the HK was observed within the first 10 sec for three RRs: SO2539, SO2540 and SO2541 (Fig. 2.1.B). This loss of signal occurred within a kinetic timeframe typical for cognate interactions and is indicative of specific phosphotransfer. Formation of phosphoaspartate esters on SO2539 and SO2541 was not observed, due to either instability of the esters or dephosphorylation by HnoK. In contrast, phosphorylated SO2540 was observed as an intense, unresolved signal after 60 min, possibly due to protein aggregation. Because of involvement in H-NOX signaling, the H-NOX-associated HK gene was named **H**-NOX/**NO**-regulated histidine **k**inase (*hnoK*) and the genes in the RR operons (Fig. 2.1.A) were named *hnoA-E*.

The vast majority of characterized two-component signaling systems display specific one-to-one connectivity between a HK and a single cognate RR. Phosphotransfer to multiple RRs *in vitro* has often been attributed to non-specific crosstalk (15). To distinguish between a branched pathway and crosstalk, the phosphotransfer kinetics between HnoK and the three RRs (HnoB, HnoC and HnoD) were examined in detail (Fig. 2.1.D). Transfer to all three RRs occurred with similar rates and was essentially complete after 10 seconds, suggesting that all three represent biologically relevant cognate interactions. Consistent with the results of the phosphotransfer profiling, only HnoC phosphorylation was detected (Figure B.1.C).

The three RRs genes are located in a region that is particularly enriched in two-component signaling genes in three adjacent operons (Fig. 2.1.A). In addition to the RRs, three HK genes (*hnoT*, *hnoS* and SO2545) are present. HnoS and SO2545 are more similar to the H-NOX-associated HK than any other HKs in the genome. The co-localization and similarity prompted us to investigate whether these HKs could be involved in the signaling pathway. To identify the cognate RRs for each HK, phosphotransfer profiling was repeated with the panel of orphan RRs. HnoS exhibited transfer to the same three RRs as HnoK (HnoB-D) (Fig. 2.1.C). In contrast, HnoT and SO2545 led to the phosphorylation of a CheY (SO2547) (Figure B.1.A and B.1.B). HnoS demonstrated a slightly faster transfer to HnoB and HnoC over HnoD (Fig. 2.1.E). Again, HnoC was the only RR with phosphoaspartate modification that was detected (Figure B.1.D).

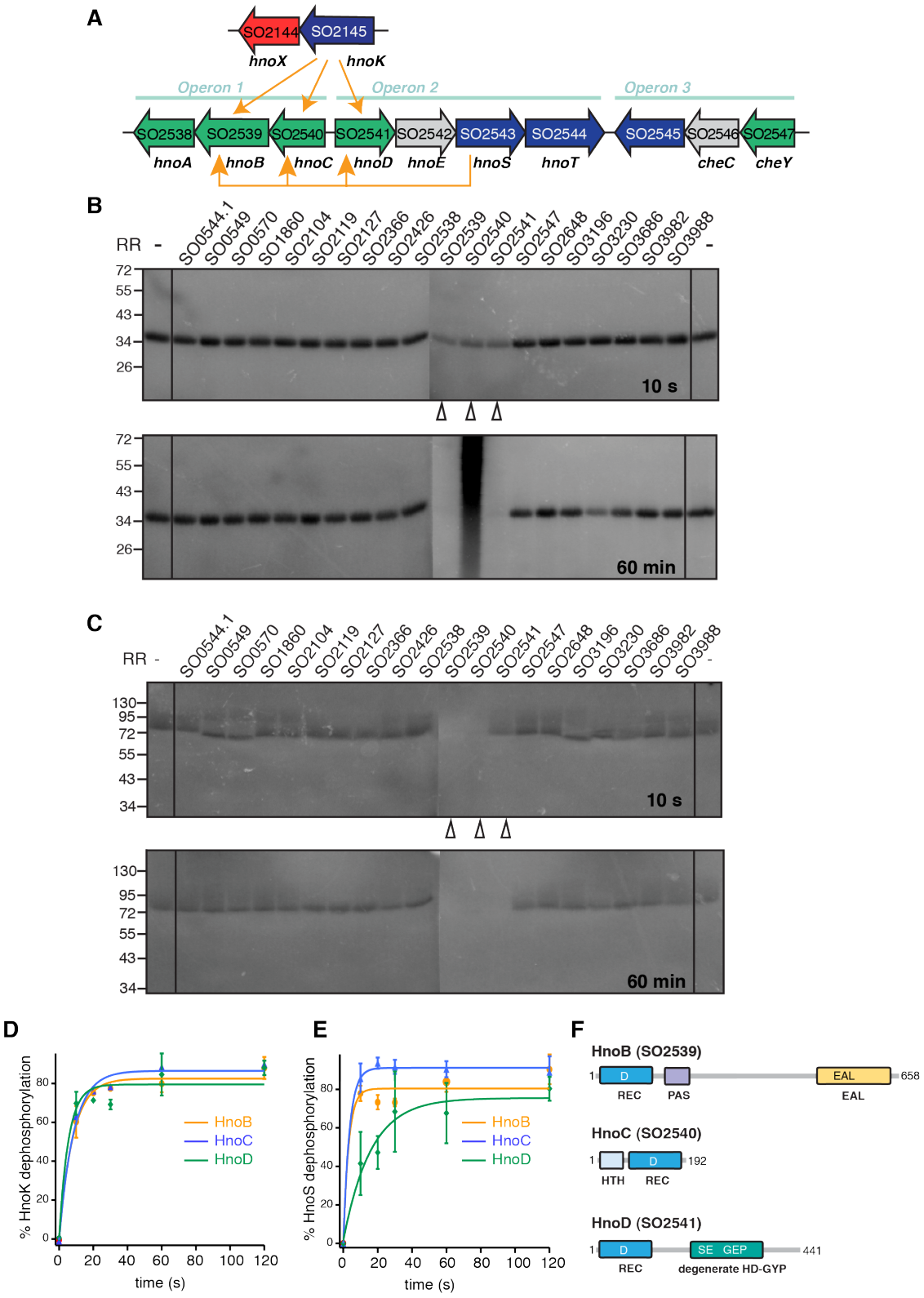
A
SO2144
SO2145
hnoX
hnoK
Operon 1
Operon 2
Operon 3
SO2538
SO2539
SO2540
SO2541
SO2542
SO2543
SO2544
SO2545
SO2546
SO2547
hnoA
hnoB
hnoC
hnoD
hnoE
hnoS
hnoT
cheC
cheY
B
RR -
SO0544.1
SO0549
SO0570
SO1860
SO2104
SO2119
SO2127
SO2366
SO2426
SO2538
SO2539
SO2540
SO2541
SO2547
SO2648
SO3196
SO3230
SO3686
SO3982
SO3988
-
72
55
43
34
26
10 s
60 min
C
RR -
130
95
72
55
43
34
10 s
60 min
D
% HnoK dephosphorylation
time (s)
HnoB
HnoC
HnoD
E
% HnoS dephosphorylation
time (s)
HnoB
HnoC
HnoD
F
HnoB (SO2539)
D
REC
PAS
EAL
EAL
658
HnoC (SO2540)
HTH
REC
192
HnoD (SO2541)
REC
SE GEP
degenerate HD-GYP
441

Fig. 2.1. Identification of cognate response regulators to the H-NOX-associated histidine kinase in *Shewanella oneidensis*

A. The H-NOX gene (*hnoX*, SO2144, red) and the H-NOX-associated HK gene (*hnoK*, SO2145, purple) form an isolated operon in *Shewanella oneidensis*. The three cognate RR genes of the H-NOX-associated HK *hnoB* (SO2539), *hnoC* (SO2540) and *hnoD* (SO2541) (green) are located in three operons that are rich in two-component signaling proteins. The adjacent HK *hnoS* (SO2543, purple) had the same three response regulators targets (yellow arrows).

B. Phosphotransfer profiling of the H-NOX-associated HK (HnoK, SO2145) to 20 orphan RRs identified three cognate phosphorylation targets (SO2539, SO2540, SO2541). The HK was pre-phosphorylated with [γ-^{32}P]-ATP and subsequently incubated with an equimolar amount of the respective RR for either 10 s or 60 min. Phosphorylation was detected by visualizing ^{32}P radioactivity after SDS-PAGE

C. HnoS (SO2543) displayed the same phosphotransfer specificity for SO2539, SO2540, SO2541.

D-E. Comparison of phophotransfer kinetics of the two HKs. All values represent the mean (n = 2 or 3) +/- SEM

F. Domain architecture of cognate response regulators, displaying the receiver domain with the conserved aspartic acid (REC, dark blue) and the varying effector domains. HnoB contains a PAS domain and an EAL PDE domain (yellow). HnoC exhibits a helix-turn-helix (HTH) DNA binding domain (light blue) and HnoD contains a degenerate HD-GYP domain (green). See also Figure B.1.

HnoT contains predicted transmembrane regions and a sensor domain, while cytoplasmic HnoS and SO2545, along with HnoK, lack these regions. To investigate whether the H-NOX protein also serves as a sensor domain for either HnoS or SO2545, like it does for HnoK (11), pull-down assays were carried out between the H-NOX protein and MBP-tagged HKs (Figure B.1.E). Consistent with previous reports, the H-NOX protein interacts with HnoK. In contrast, HnoS and SO2545 did not pull down H-NOX above background, suggesting that distinct sensor domains control activity of these HKs or that the H-NOX interaction is weak. One candidate sensor domain is the adjacent HnoE. This protein shares similarity with FIST proteins, which are predicted to bind and sense small molecules such as amino acids (24) but have not been characterized.

RR signaling output is governed by effector domains within the RRs (13). HnoB contains a PAS domain and an EAL domain, predicted to hydrolyze the bacterial secondary messenger cyclic-di-GMP (Fig. 2.1.F). HnoC contains a MerR superfamily helix-turn-helix DNA binding domain at the *N*-terminus. HnoD includes an HD-GYP domain, which is also a predicted phosphodiesterase (PDE) for cyclic-di-GMP, but the HD-GYP consensus residues crucial for activity are altered to SE-GEP in HnoD.

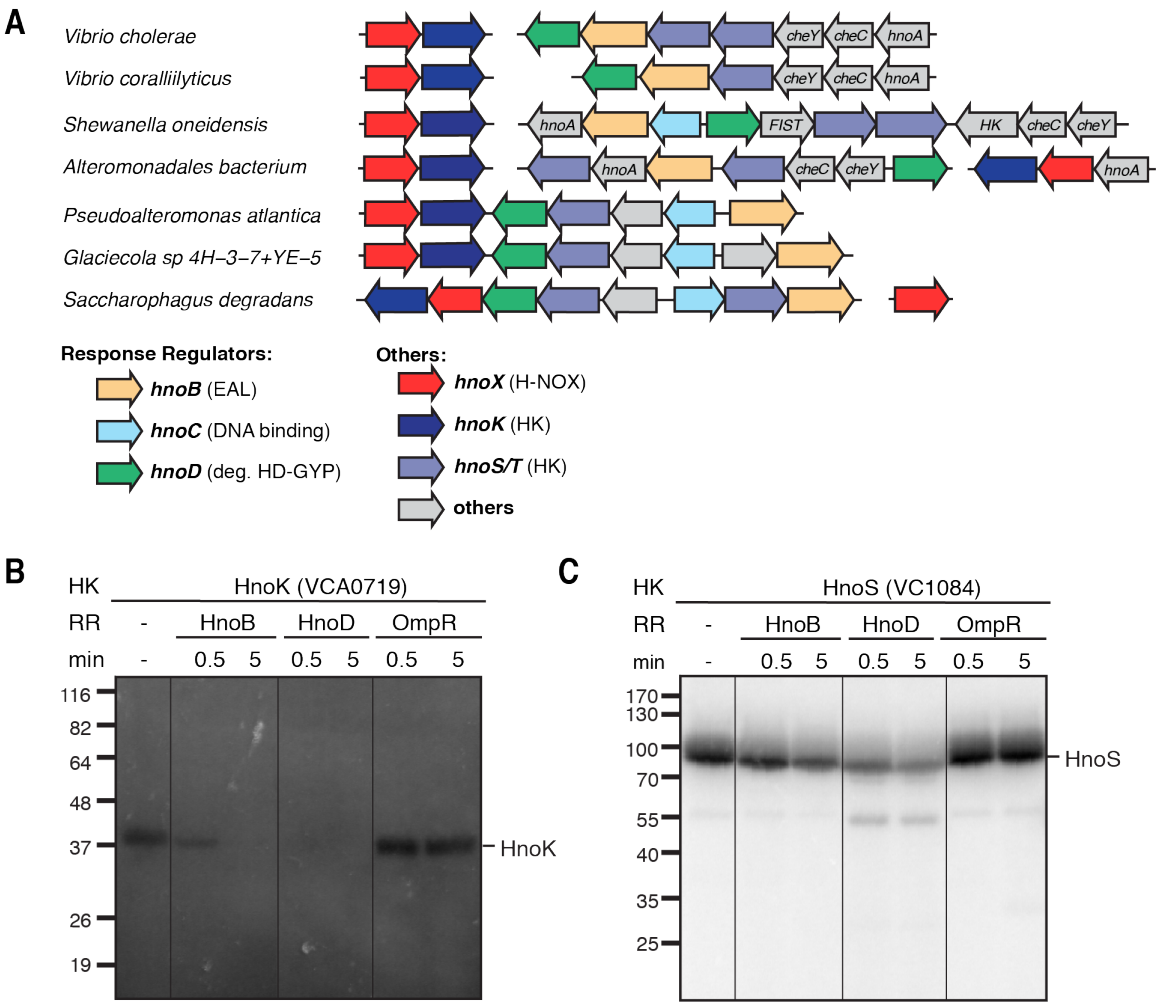

Fig. 2.2. Phosphotransfer to HnoB and HnoD orthologs
A. Organization of the *hnoX* genes (red) and associated *hnoK* HK genes (purple) as well as operons containing orthologs of the *hnoB* (yellow), *hnoC* (light blue) and *hnoD* (green) in select gammaproteobacteria. For a complete list of organisms see supplemental Figure B.2.B.
B. Phosphotransfer assay of HnoK from *Vibrio cholerae* (VCA0719) to HnoB (VC1086) and HnoD (VC1087). Assays were carried out as in Figure 2.1.
C. Phosphotransfer assay of *Vibrio cholerae* HnoS (VC1084) to HnoB and HnoD.

Phosphotransfer to response regulator orthologs in other gammaproteobacteria

The lack of RR genes in the majority of operons with *hnoXK* pairs prompted the question if other bacteria contained orthologs of the three *S. oneidensis* cognate RRs. Discerning the ortholog of a particular RR is challenging because a single organism often contains many RRs with identical architecture and effector domains (13). In particular, DNA binding domains, GGDEF diguanylate cyclase (DGC) domains, as well as EAL and HD-GYP PDE domains are very prevalent. To circumvent this multiplicity problem, we narrowed our search by taking advantage of unique sequence features in HnoD. Proteins with high sequence similarity to HnoD

were discovered in 16 other gammaproteobacteria (Figure B.2.A). Surprisingly, genes with high similarity to *hnoB* and *hnoC* were often co-localized in operons near *hnoD* (Fig. 2.2.A, and Figure B.2.B). Indeed, four species (*Saccharophagus degradans*, *Pseudoalteromonas atlantica*, *Glaciecola sp.,* and *Neptuniibacter caesariensis*) exhibited operons with the RR genes directly adjacent to the *hnoXK* operon. This organization and co-localization with the *hnoXK* genes supports a conserved functional relationship between the H-NOX and signaling proteins in other gammaproteobacteria.

To determine whether the RRs are specific cognates of HnoK in other organisms, we investigated the phosphotransfer in *Vibrio cholerae*. This pathogen would need to avoid NO produced by the host in response to infection (5, 25). *V. cholerae* harbors the *hnoXK* genes (VCA0720/VCA0719) in an isolated operon with *hnoB* (VC1086) and *hnoD* (VC1087) grouped into a separate operon containing two additional HKs. *V. cholerae* does not contain an *hnoC* ortholog. Indeed, HnoK rapidly transferred its phosphoryl group to HnoB and HnoD (Fig. 2.2.B) consistent with a cognate interaction. HnoS, one of the adjacent HKs, also displayed rapid phosphotransfer to the two RRs (Fig. 2.2.C). This suggests that signaling integration at the level of the RRs from two sensory inputs is a conserved feature between organisms.

The effect of phosphorylation on the cyclic-di-GMP phosphodiesterase activity of HnoB

HnoB contains a *C*-terminal EAL domain (Fig. 2.1.F), which is predicted to hydrolyze cyclic-di-GMP to 5'-phosphoguanylyl-(3'→5')-guanosine (pGpG) (26, 27). Sequence alignments confirmed that the conserved residues essential for PDE activity were present in HnoB (28). When HnoB was incubated with cyclic-di-GMP, formation of pGpG was observed within the first 5 min and complete turnover occurred after one hour (Fig. 2.3.A), confirming that HnoB was a functional PDE for cyclic-di-GMP.

Next, we investigated whether RR phosphorylation regulates PDE activity. To date, regulation of EAL domain activity by the phosphosphorylation state of the receiver domain has yet to be observed. To assess the effect of HnoB phosphorylation on PDE activity, assays were carried out in the absence or presence of the H-NOX-associated HK (HnoK) and ATP. HK and ATP caused a 50-fold stimulation of HnoB PDE activity (Fig. 2.3.B). In the phosphoreceiver D53A mutant, addition of HK and ATP had no effect on activity, confirming that the stimulation was specific to phosphorylation.

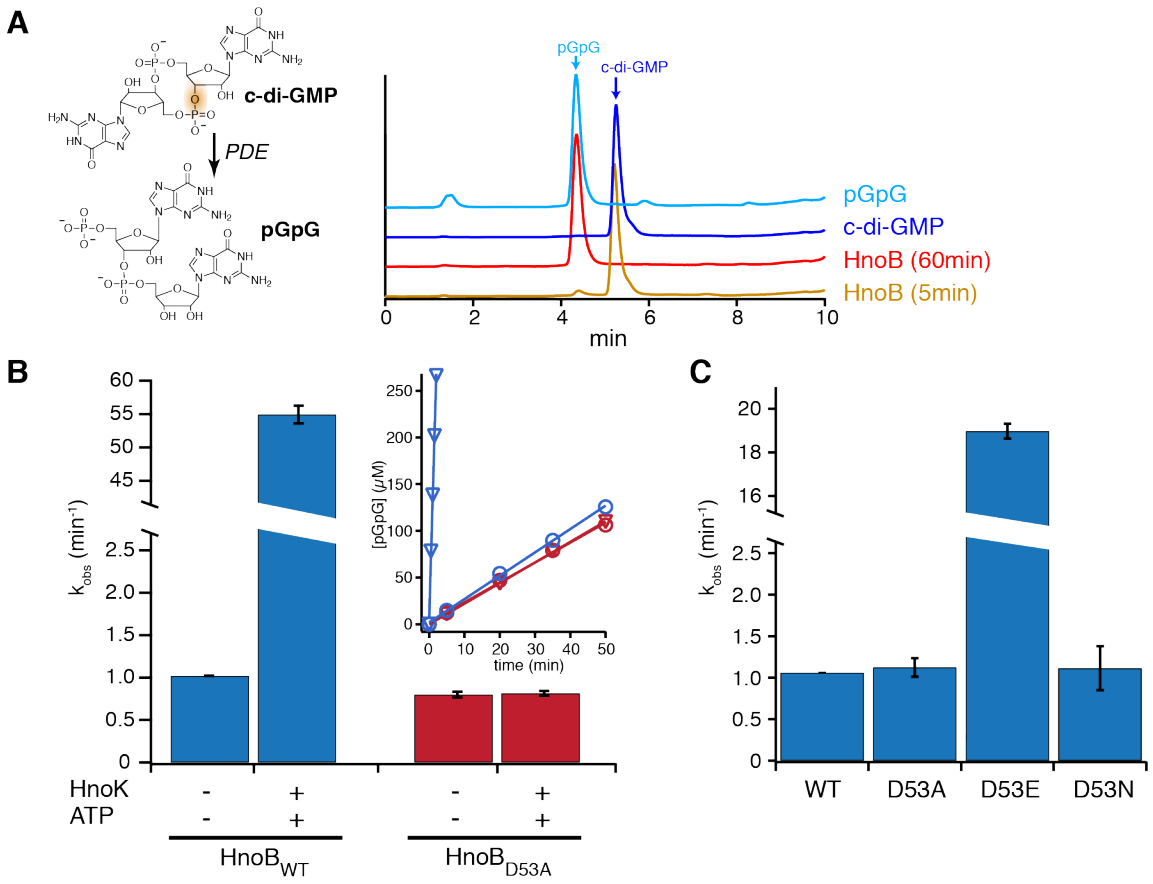

Fig. 2.3. Cyclic-di-GMP phosphodiesterase activity of HnoB
A. The structure of cyclic-di-GMP and the hydrolysis product pGpG are shown and the bond that is broken is highlighted. HPLC chromatograms (λ = 253 nm) of a cyclic-di-GMP standard (dark blue) and pGpG (light blue) are shown. Incubation of purified HnoB with cyclic-di-GMP in the presence of Mg^{2+} led to partial hydrolysis to pGpG after 5 min (yellow) and complete hydrolysis after 60 min (red).
B. PDE activity of HnoB in the presence or absence of HK (HnoK) and ATP. Purified HnoB (2.5 μM) was incubated with 20x excess HnoK, 0.5 mM ATP and 10 mM $MgCl_2$. Reactions were initiated with 0.5 mM cyclic-di-GMP, time points were drawn, acid-quenched and then analyzed by HPLC. The insert shows the kinetics of the PDE assay monitored by following pGpG formation. Phosphorylation of WT HnoB by HnoK led to 50-fold enzyme activation (blue, triangles in the insert correspond to HnoK/ATP conditions). Addition of the HK to the phosphorylation-deficient D53A HnoB mutant had no effect on activity (red). C. The phosphorylation mimic D53E mutant showed 19-fold activation of PDE activity while the phosphorylation-deficient D53A and D53N mutants displayed no change in activity compared to WT HnoB. All values represent the mean (n = 2) +/- SEM. See also Figure B.3.

To further verify stimulation of PDE activity, two different receiver domain phosphorylation mimics were tested. Mutation of the phosphoreceiver aspartate to glutamate has been shown, in certain cases, to structurally and functionally mimic the phosphorylated RR state (29, 30). The HnoB D53E mutation resulted in a 19-fold increase in the rate of pGpG formation while the rates of the D53A and D53N mutants remained unchanged compared to WT (Fig. 2.3.C). PDE activity was also measured in the presence of the RR phosphorylation mimic beryllium fluoride (BeF_x), which can serve as a structural analog for a phosphoryl group (31, 32).

Titration of increasing BeF_x concentrations resulted in a 7-fold stimulation of HnoB PDE activity (Figure B.3). Taken together, the activity of the phosphorylation mimics confirmed that the HnoB EAL domain is activated through phosphorylation of the HnoB receiver domain. Thus, HnoK and HnoS decrease cyclic-di-GMP levels by phosphotransfer-mediated activation of the HnoB EAL domain.

The degenerate HD-GYP domain of HnoD lacks phosphodiesterase activity

The second cognate RR (HnoD) of the H-NOX-associated HK contains a HD-GYP domain, which represents another family of cyclic-di-GMP PDEs (33). However, sequence alignment to other HD-GYP domains showed that the consensus residues vital for PDE activity were not conserved in HnoD (Fig. 2.4.A, Figure B.2.A). Therefore, we first tested if the degenerate HD-GYP domain of HnoD could hydrolyze cyclic-di-GMP. As a positive control, TM0186, a HD-GYP RR from *Thermotoga maritima* containing the consensus HD-GYP motifs (Fig. 2.4.A) was expressed and purified. TM0186 completely hydrolyzed cyclic-di-GMP, whereas HnoD displayed no detectable pGpG formation, even after 48 hours (Fig. 2.4.B).

HD-GYP domains belong to a larger superfamily of HD metal-dependent phosphohydrolases (33). The HD motif forms part of the metal coordination site, along with a number of conserved histidines and acidic residues (blue triangles in Fig. 2.4.A) (34). Purified TM0186 contained iron, but no metals were detected bound to HnoD by by inductively coupled plasma atomic emission spectroscopy (Fig. B.4.D) or UV/vis spectroscopy (Fig. B.4.E). Attempts to reconstitute metal binding were unsuccessful (data not shown). The inability to coordinate metal is likely one reason for the lack of HnoD PDE activity.

Degenerate EAL or GGDEF domains often retain the ability to bind nucleotides, and thereby serve a regulatory role as a receptor for cyclic-di-GMP or GTP (26, 35). No binding of either molecule was observed by equilibrium dialysis or isothermal titration calorimetry (data not shown), suggesting that the degenerate HD-GYP domain of HnoD does not act as a nucleotide receptor.

The effect of HnoD on HnoB EAL phosphodiesterase activity

Degenerate GGDEF and EAL domains can carry out alternate regulatory roles through macromolecular interactions, especially in cases when degeneracy eliminates ligand binding (36). Because of the co-localization of the *hnoD* and the EAL domain-containing *hnoB* genes in a number of species (Fig. 2.2.A, Fig. B.2.B), we speculated that a functional relationship between these two proteins could exist. Therefore, PDE assays of HnoB were carried out in the presence of excess HnoD. Addition of HnoD decreased the rate of HnoB catalyzed cyclic-di-GMP hydrolysis by 40% (Fig. 2.4.C). In contrast, addition of a control RR (*E. coli* OmpR) had no effect on HnoB activity. HnoD demonstrated detectable inhibition of HnoB activity at 10 μM HnoD (4-fold excess), and HnoB activity was further inhibited as HnoD concentration was increased (Fig. B.4.A). Pull-down assays between MBP-tagged HnoB and HnoD suggested that the interaction between the two RRs was relatively weak (Fig. B.4.B).

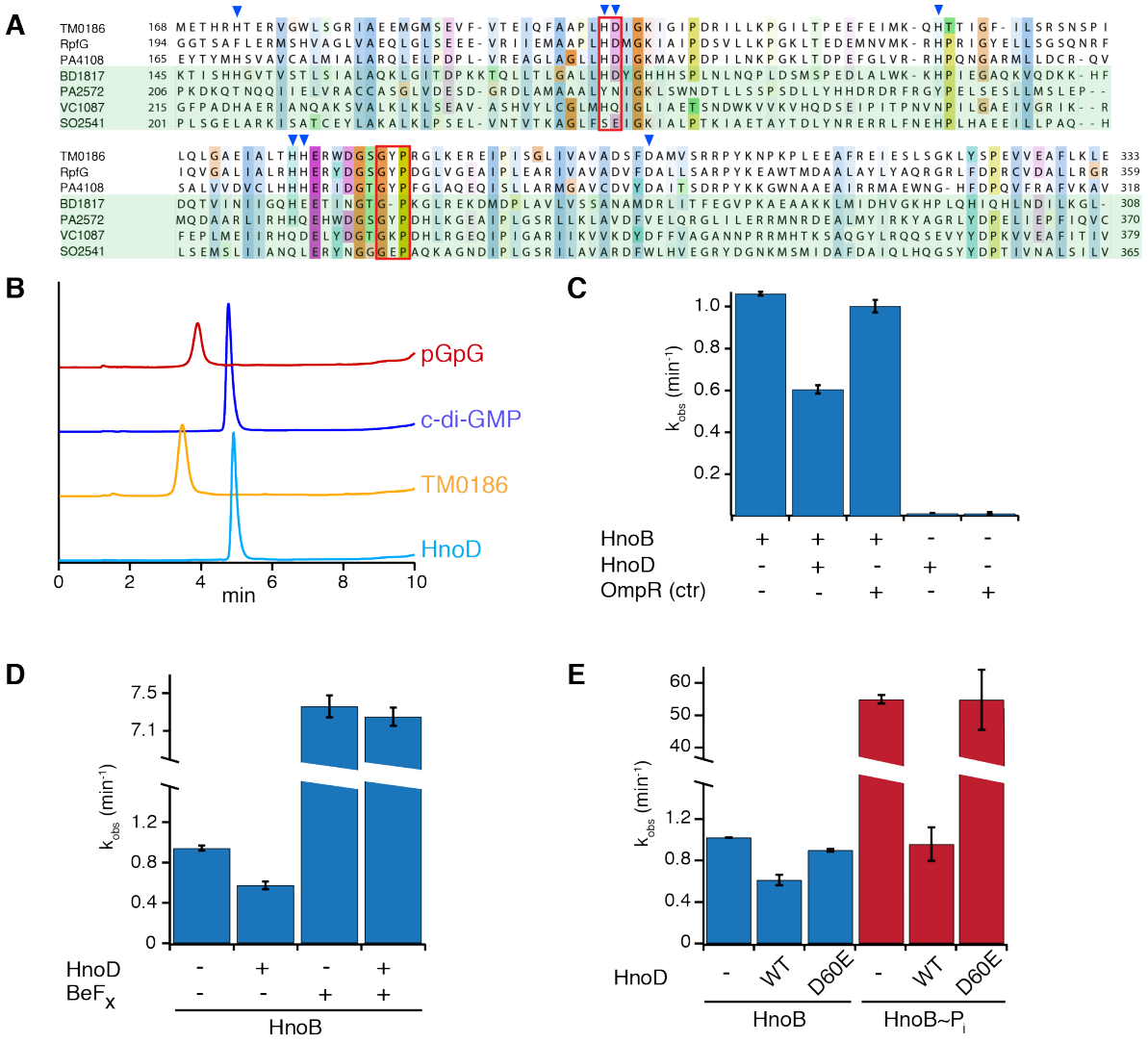

Fig. 2.4. Fine-tuning of HnoB cyclic-di-GMP hydrolysis by the degenerate HD-GYP domain of HnoD

A. Sequence alignment of HD-GYP domains from three RRs that contain the conserved sequence motif (*T. maritima* TM0186, *X. campestris* RpfG, *P. aeruginosa* PA4108) and four RR that contain some degeneracy of the conserved sequence (*Bdellovibrio* BD1817, *P. aeruginosa* PA2572, *V. cholerae* HnoD (VC1087), *S. oneidensis* HnoD (SO2541)). The HD and GYP motifs are boxed in red and residues that are ligands for binuclear iron are indicated by blue triangles.

B. HPLC chromatograms of a PDE assay with a "true" HD-GYP RR (TM0186, yellow) and the degenerate HD-GYP RR (HnoD, light blue) showed that only TM0186 hydrolyzed cyclic-di-GMP to pGpG. Standards of pGpG (red) and cyclicyclic-di-GMP (blue) are shown at the top.

C. HnoD inhibited the PDE activity of the HnoB. Purified HnoB (2.5µM) was pre-incubated with 20x excess HnoD prior to addition of cyclic-di-GMP (0.5mM).

D-E. Phosphorylation of HnoD abolished the inhibition of HnoB PDE activity. (D) Loss of inhibition in the presence of the phosphorylation mimic beryllium fluoride (BeF_x). HnoD and HnoB were preincubated with BeF_x before the reactions were initiated with cyclic-di-GMP. (E) Inhibition of HnoB by HnoD phosphoacceptor mutants. HnoB was either unphosphorylated (blue) or was pre-phosphorylated with HK (HnoK) and ATP (red). WT HnoD or the phosphorylation mimic D60E mutant was then added prior to initiation of the PDE reaction. All values represent the mean (n = 2) +/- SEM. See also Figure B.4.

The results above demonstrated that phosphorylation of HnoB by HnoK stimulated HnoB PDE activity while the non-phosphorylated HnoD inhibited HnoB. HnoD is also a phosphotransfer target of the two HKs, creating a possibility for a feed-forward loop to control PDE activity. Therefore, we examined the effect of HnoD phosphorylation on the inhibition of HnoB activity. BeF_x was employed to allow independent, simultaneous mimicking of the phosphophorylated state for both response regulators (Fig. 2.4.D). BeF_x caused an activation of HnoB PDE activity as seen before, but in the presence of HnoD and BeF_x, the reaction was no longer inhibited. This suggested that when phosphophorylated, HnoD was no longer inhibitory. To further validate this mechanism, conditions were devised under which HnoB and HnoD could be placed in the phosphorylated or phoshophorylation-mimicked state independently (Fig. 2.4.E). Phosphorylation of HnoB was controlled by addition of HnoK and ATP whereas phosphorylation of HnoD was mimicked by a D60E mutation in the phosphoreceiver domain. In the absence of HnoB phosphorylation (blue bars), the phosphorylation-mimic HnoD variant (D60E) was no longer inhibitory. When HnoB was phosphorylated by HnoK and ATP and the PDE was stimulated as expected (red bars), the D60E mutant had no inhibitory effect on this activated form of HnoB. PDE activity of HnoB was decreased in the presence of WT HnoD and HnoK/ATP because the large excess of HnoD out-competed HnoB as a substrate of the HK, leaving HnoB non-phosphorylated and unactivated. Overall, these results indicate that only the unphosphorylated state of HnoD is the inhibitory, suggesting that the inhibition is abolished by a conformational change upon phosphorylation. This was further confirmed by analyzing the inhibition of HnoD truncations (Fig. B.4.C). Inhibition of HnoB activity only occurred in the presence of the HnoD receiver domain while removal of the receiver domain relieved inhibition.

Nitric oxide induces biofilm formation

Cyclic-di-GMP controls the motility behavior of bacteria and increased levels of cyclic-di-GMP signal a transition from planktonic growth to a sessile state with biofilm formation (36, 37). We therefore hypothesized that NO may serve as a signal for biofilm formation, as the NO-bound H-NOX inhibits autophosphorylation of HnoK, leading to inactivation of HnoB and an increase in cyclic-di-GMP levels (Fig. 2.5.E). Therefore, the effect of NO on *Shewanella oneidensis* biofilm formation under static anaerobic growth was investigated. NO was introduced to the medium by adding DETA NONOate. This slow-release NO donor ($t_{1/2}$ of 56 hours at 25 ºC) led to a relatively steady NO concentration ranging between 0.4 and 2.7 μM (Fig. B.5.A). Fluorescent staining of the biofilms confirmed that these were comprised of viable cells under all conditions tested (Fig. B.5.E). In the WT strain, NO caused a significant increase in the amount of biofilm (p = 0.020 in 96-well plates in Figure 2.5.A at and p = 0.039 in 12-well plates in Figure 2.5.B) consistent with the signaling hypothesis outlined above.

Next, we assessed the contributions of the individual two-component signaling proteins to biofilm formation. Reverse transcription PCR confirmed that the *hnoX*, *hnoK* and *hnoB-D* genes were transcribed in the presence and absence of NO (Fig. B.5.C). In-frame deletion strains of *hnoX*, *hnoK*, *hnoB, hnoC,* and *hnoD* were constructed and assayed for static biofilm formation. Deletion of *hnoX* and *hnoK* resulted in biofilm formation that was comparable to WT levels in the absence of NO and had a significantly decreased response to NO (Fig. 2.5.A, Fig. B.5.D for images). This confirmed that the H-NOX had a central role in the signaling pathway as

an activator cellular attachment in response to NO (Fig. 2.5.E). HnoK also appears to stimulate NO-induced biofilm formation, based on the loss-of-function phenotype. The observed activator function of HnoK can be rationalized by invoking a dual kinase and phosphatase activity towards HnoB and HnoD (Fig. 2.5.E). Thus far, only inhibition of HnoK autophosphorylation by NO-bound H-NOX has been observed (11), but HnoK, in the presence of NO-bound H-NOX, was indeed capable of dephosphorylating its RR targets (unpublished data). This NO-induced shift of HnoK kinase towards phosphatase activity and dephosphorylation of HnoB and HnoD would lead to a decrease in HnoB PDE activity.

Deletion of the DNA-binding RR (*ΔhnoC*) resulted in a very moderate increase in biofilm amounts both in the absence and presence of NO (Fig. 2.5.B), suggesting HnoC may control some gene targets involved in biofilm formation but likely has other cellular roles. The knockout of *hnoD* displayed stimulation of biofilm formation in response to NO (Fig. 2.5.A, $p = 0.027$), which is consistent with a more subtle role in fine-tuning cyclic-di-GMP levels. In contrast, deletion of the PDE gene *hnoB* led to hyperproduction of biofilm (Fig. 2.5.B-D). Compared to WT, biofilm formation was slightly increased in the absence of NO and was significantly elevated when grown under NO ($p = 0.0001$ compared to WT+ NONOate). This increase in cellular attachment validates HnoB as a major contributor to NO-induced biofilm formation. At the same time, an additional regulator must suppress the overproduction of biofilms in the absence of NO. For instance, HnoD could control other DGC or PDE proteins besides HnoB in the organism. The *hnoB* deletion also conferred a growth advantage in the presence of NO, and the lag phase was reduced from 18 to 12 hours. (Fig. B.5.B). To further confirm that the hyperbiofilm phenotype of the *DhnoB* strain was due to loss of EAL activity, we complemented the knockout with WT *hnoB* from an arabinose inducible plasmid (pBAD202). Biofilm formation was only reset to WT levels upon expression of HnoB.

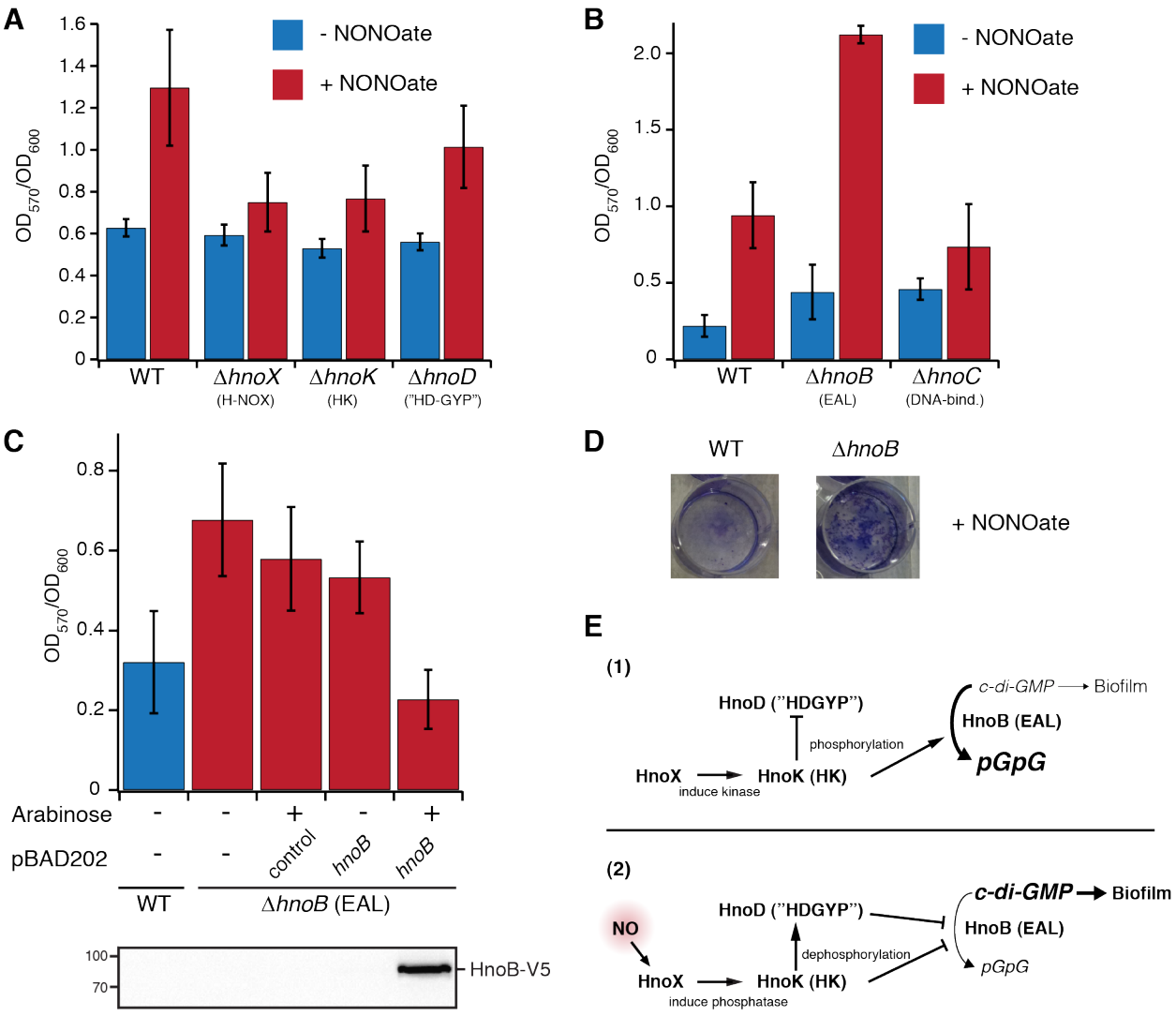

Fig. 2.5. Phenotypic analysis of two-component signaling knockouts affecting NO induced biofilm formation

A-C. Static biofilm measurements of *Shewanella oneidensis* under anaerobic growth. NO stimulated the formation of biofilms, while cell attachment in *hnoX* and *hnoK* knockouts was insensitive to NO. Knockout of the EAL RR (*hnoB*) led to a hyperbiofilm phenotype. WT *S. oneidensis* or the respective knockouts were grown anaerobically in MM medium in 96-well plates (A) or 12-well plates (B) with fumarate as electron acceptor. DETA NONOate (200 µM), a slow release NO donor, was added for NO production. Biofilm levels were quantified by measuring the absorbance at 570 nm (OD_{570nm}) after staining with crystal violet and normalized to cell growth (OD_{600nm}). (C) Complementation of the hyperbiofilm phenotype of the *hnoB* knockout. WT *S. oneidensis* and the *hnoB* knockout were transformed with pBAD202 containing the *hnoB* gene or empty vector as a control. The strains were grown as described above and expression of HnoB was induced with 0.02% arabinose. Western-blot analysis (below) confirmed expression of HnoB. All values represent the mean from independent experiments (n = 12 (A), n = 3 (B-C)) +/- SEM.

D. Images of crystal violet stained biofilms display the enhanced cell attachment of the *hnoB* knockouts compared to WT *S. oneidensis*.

E. Model for signaling interactions between components of the network in the absence (1) or presence (2) of NO. See also Figure B.5.

Discussion

H-NOX signaling proceeds through a conserved multi-component signaling system

The results from phosphotransfer profiling showed the connectivity between proteins of the bacterial H-NOX signaling pathway and unexpectedly identified three RR targets of the H-NOX-associated HK HnoK (Fig. 2.6.A): HnoB containing an EAL effector domain, HnoC, containing a DNA-binding domain, and HnoD, containing a degenerate HD-GYP domain. The RRs targets of the HnoK clustered in a genome region enriched in two-component signaling proteins, containing three additional HKs, two other RRs, a CheC phosphatase and a putative FIST sensor protein. Operons containing similar proteins have been identified in a number of H-NOX-containing gammaproteobacteria, and this conserved gene organization suggests that the proteins are functionally related members of the same signaling network (38). Based on phosphotransfer to three common RRs, HnoS and HnoK are clearly part of the same signaling network and the RRs act as a signal integration point in the network (Fig. 2.6.A). The independently expressed H-NOX protein serves as the sensor for HnoK, whereas the lack of interaction between H-NOX protein and HnoS implies that this HK must respond to an alternate stimulus.

Evidence for conservation of the integrated H-NOX signaling network involving two HKs and three RRs was obtained by confirming phosphotransfer in *Vibrio cholerae*. *V.c.* HnoK and HnoS phosphorylated both *V.c.* HnoB and HnoD. Mutation of *V.c.* HnoB (VC1086) has been shown to result in an increase in biofilm formation (39). This mirrors the phenotype of the HnoB knockout in *S. oneidensis* and provides further evidence towards functionally conserved pathways. Interestingly, no homologs to HnoC could be identified in *V. cholerae* and in several of the organisms containing HnoB and HnoD (Fig. B.2.B), suggesting that some bacteria do not depend on the HnoC-mediated transcriptional output.

A regulatory role for degenerate HD-GYP proteins in controlling EAL activity

The primary signaling response mediated by the H-NOX signaling network is to control cyclic-di-GMP levels. The effectors of this response are the PDE RRs HnoB and HnoD, containing EAL and HD-GYP domains, respectively. Regulation of PDE activity has only been demonstrated for EAL domains that are directly fused or interact with sensor domains (9, 26, 40). Phosphorylation is a hallmark of RR control (41), and here we demonstrated that the PDE activity of the HnoB EAL RR was stimulated by phosphorylation.

HnoD, the second cognate RR linked to cyclic-di-GMP metabolism, is identified as a HD-GYP domain, but active site residues responsible for coordination of crucial catalytic metals are missing in HnoD (34) rendering the protein inactive for cyclic-di-GMP hydrolysis. Compared to EAL domains, HD-GYP domains remain poorly characterized with only few reports of direct PDE activity (42, 43). Interestingly, despite the lack of PDE activity, an HnoD ortholog from *P. aeruginosa* is known to modulate swarming motility, a function typically controlled by cyclic-di-GMP levels (44). This prompted us to investigate whether HnoD regulates cyclic-di-GMP levels indirectly by controlling HnoB activity. HnoD significantly

inhibited the PDE activity of HnoB and this inhibition was dependent on the phosphorylation state of HnoD. Phosphorylated HnoD was no longer inhibitory, and this loss of inhibition was independent of HnoB phosphorylation. HnoD and HnoB thus form a coherent feed-forward loop to control cyclic-di-GMP levels (45). Unphosphorylated HnoB exhibited low activity that was further suppressed by HnoD. Phosphotransfer from HnoK or HnoS activated the PDE activity of HnoB while simultaneously preventing the inhibition by HnoD. This example of cross-regulation between two RRs to form a feed-forward loop in the same signaling network is in contrast to typical cross-regulation, which connects distinct signaling pathways, often by use of separate connector proteins (46).

This feed-forward loop in the H-NOX signaling network may allow for an extra level of tunability over the intracellular pool of cyclic-di-GMP. Precise control is required because the affinities of cyclic-di-GMP receptors span several orders of magnitude (36), thus the cellular processes controlled by cyclic-di-GMP are likely sensitive to a wide concentration range. The dual control provides the opportunity for fine-tuning the signal integration from HnoK and HnoS. The *in vivo* phosphorylation levels of the two RRs will be influenced by the dueling kinase and phosphatase activities from each HK. Gradual attenuation of PDE activity of HnoB could be achieved by biasing phosphotransfer activity from the kinases slightly towards either RR. Lastly, HnoD may regulate the activity of additional unknown downstream signaling effectors, and indeed serve as a global regulator for other EAL domain proteins, and possibly, GGDEF diguanylate cyclases. It has been shown that the functional HD-GYP RR RpfG from *X. campestris* interacts physically and functionally with multiple GGDEF proteins (47). Cyclic-di-GMP modulators are particularly enriched in the genomes of gammaproteobacteria and *S. oneidensis* contains 51 proteins with GGDEF domains, 27 with EAL domains and 20 GGDEF-EAL hybrids (20). Thus to effectively modulate the intracellular cyclic-di-GMP concentration, it may be necessary to exert a global effect on the activities of multiple EAL and GGDEF proteins.

Biofilm formation as a defense mechanism against NO

A variety of cellular processes are mediated by receptor proteins and riboswitches specific to cyclic-di-GMP (28). Cyclic-di-GMP controls flagellar motor speed (48), and in *Vibrio cholerae* and *Shewanella oneidensis,* it has been shown to upregulate gene clusters for biosynthesis of extracellular polysaccharides, which facilitate the adhesion between cells (20, 49-51). We focused the phenotypic characterization on biofilm formation in *S. oneidensis* because biofilms represent an important aspect of the life cycle for *S. oneidensis,* allowing the colonization of metal surfaces for dissimilatory metal reduction. Biofilms are equally important in the life cycle of pathogens, enhancing survival and protection from predators and antimicrobial agents (52). Static biofilm assays demonstrated a clear increase in cellular adhesion with NO treatment, which is consistent with the biochemical interactions in the signaling network (Fig. 2.6.A). H-NOX protein and the associated HK, HnoK, were positive regulators of biofilm formation because deletions of the genes rendered these cells insensitive to NO. In contrast, HnoB was a negative regulator of biofilm formation and the *hnoB* knockout resulted in elevated biofilm formation. Interestingly, in the absence of NO, the large biofilm increase of the *ΔhnoB* strain was attenuated, suggesting that other regulators were able to suppress biofilm formation. HnoD could act as suppressor and control the activity of additional cyclic-di-GMP modulators, supporting a function for HnoD as a global regulator.

To date, the only links between NO/H-NOX signaling and cyclic-di-GMP dependent changes in biofilm formation have been established in *Legionella pneumophila* and in *Shewanella woodyi.* However, in both organisms, the H-NOX controlled the activity of an adjacent diguanylate cyclase/phosphodiesterase protein directly and repressed biofilm formation (8, 9). Despite a paucity of studies addressing the biological function of bacterial NO-specific H-NOX proteins, a common role for controlling motility via cyclic-di-GMP levels is emerging. Genes encoding GGDEF and EAL proteins are occasionally found adjacent to H-NOX genes and their direct regulation by the H-NOX protein represents a simplified one-component signaling mode with a role in biofilm dispersal in response to NO. Alternatively, other gammaproteobacteria appear to have evolved a more complex signaling network, homologous to the system characterized here. This network structure can meet additional demands for fine-tuned regulation and integration from multiple signal inputs, and it has the opposite role of signaling increased biofilm formation in response to NO.

Encapsulation of bacteria into a biofilm provides a significant protective mechanism against environmental toxins and antimicrobial agents (52). At high concentration, the free radical NO and related reactive nitrogen species (RNS), such as peroxynitrite, are active antimicrobials and are detrimental to cellular growth. Thick biofilm layers and extracellular matrix encapsulation provide a protective diffusional barrier, buffering nitrosative stress at the top layers and protecting the underlying cells (Fig. 2.6.B). This mechanical protection could be especially important for *S. oneidensis* as the organism lacks any genes encoding flavohemoglobins or nitric oxide reductases, which usually remove NO enzymatically. Indeed, the Δ*hnoB* strain, which produced the highest biofilm levels, displayed a significant growth advantages in the presence of NO. Although exact NO concentrations in the natural soil or water environment of *S. oneidensis* are not known, the organism is certainly exposed to NO. *S. oneidensis* itself generates low micromolar NO as a byproduct of denitrification (11). The organism is also well known for its capacity to utilize a diverse range of metals as electron acceptors. For instance, it can grow on Fe(III) mineral surfaces releasing Fe(II) into solution (53). When concomitant with denitrification, reaction of nitrite with Fe(II) will lead to production of NO (54). Signaling for increased biofilm formation may serve as protection against the NO byproduct. Alternatively, it could serve as a signaling cue to increase surface adhesion onto the metal mineral for increased respiration efficiency.

H-NOX proteins are also present in pathogens, and an orthologous H-NOX/NO signaling network was discovered in *Vibrio cholerae*. Pathogens are exposed to high NO concentrations and nitrosative stress during the host innate immune response (5). *V. cholerae* colonizes the small intestine causing the severe diarrhea associated with cholera disease. *V. cholerae* encounters NO formed by acidified nitrite while passing through the stomach and NO generated by macrophages in the intestine (25, 55). It was recently demonstrated that *V. cholerae* strains defective in RNS defense exhibited a colonization defect in mouse intestines (25). Furthermore, biofilm formation plays an important role during *V. cholerae* infection and colonization (56). For instance, biofilm-like multicellular clumps are more infectious than planktonic cells (57). NO sensing by the H-NOX protein and the subsequent control over biofilm formation may therefore play a virulence role in *V. cholerae*.

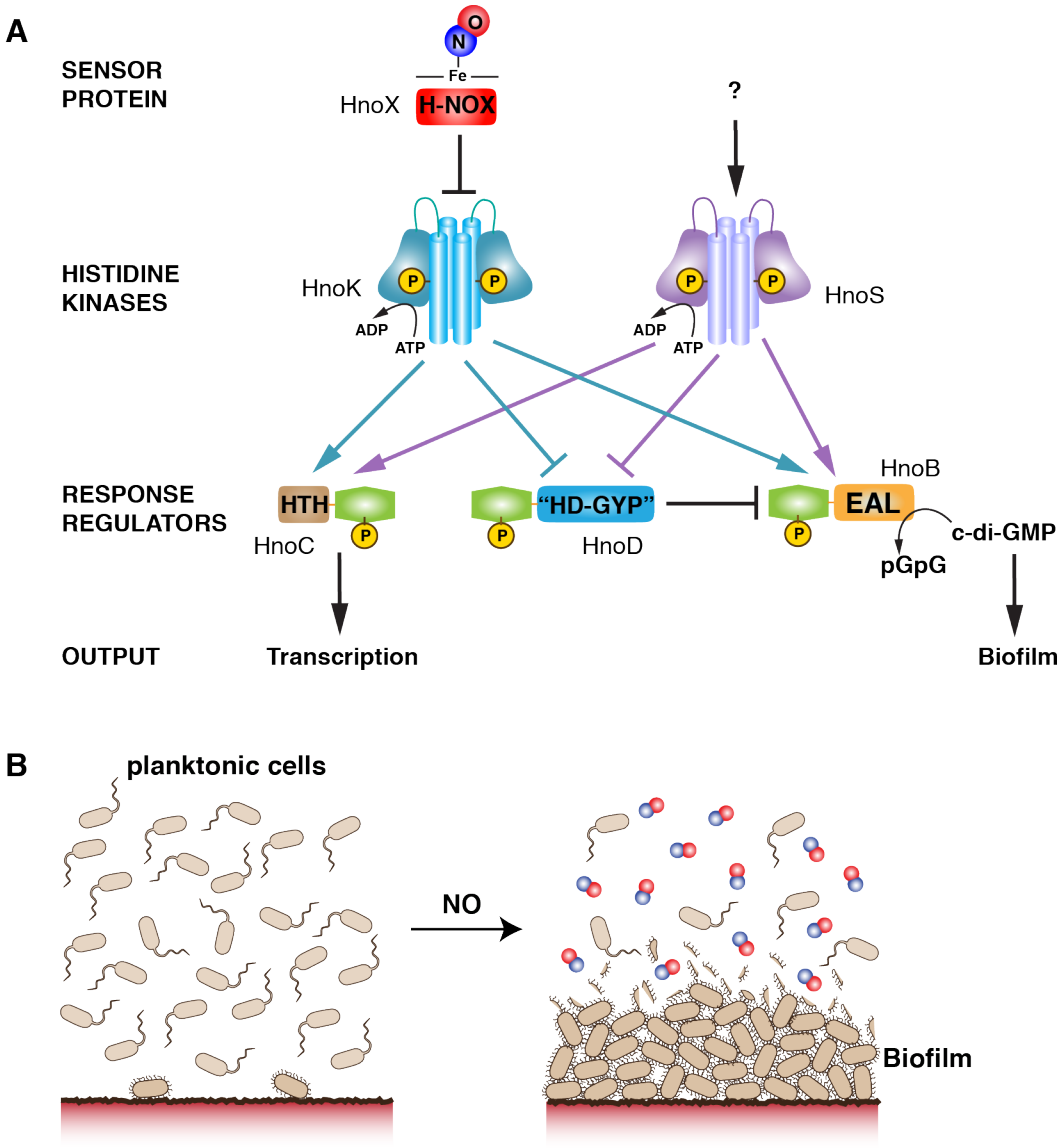

Fig. 2.6. Model of multi-component signaling network for NO-induced biofilm formation as a protection mechanism against NO

A. The complex multi-component signaling pathway is initiated by NO binding to the sensory H-NOX protein (HnoX), which then inhibits HnoK autophosphorylation. Phosphotransfer establishes a branching of the network to three response regulators. HnoB and HnoD form a feed-forward loop. Phosphorylation controls PDE activity of HnoB, which can be fine-tuned by allosteric control from HnoD. NO-controlled repression of the PDE activity leads to an increase in cyclic-di-GMP levels, which serves as a signaling cue for cellular attachment into biofilms.

B. The NO signal switches the bacterial motility pattern from planktonic growth to increased attachment onto surfaces. The thick layers of cells provide a protective barrier against diffusion of reactive and damaging NO and may protect cells in the lower layers.

Emergence of complex bacterial signal transduction networks

The complex architecture of the H-NOX signaling network characterized in this study is highly unusual and stands in contrast with the mostly linear two-component signaling pathways. Branched and integrated networks still represent a minority of the characterized pathways. However, there are emerging examples of more complex signaling structures, such as chemotaxis, differentiation in *Caulobacter crescentus* (23, 58), quorum sensing in *Vibrio harveyi* (59) , and fimbriae production in *Pseudomonas aeruginosa* (60, 61). The results reported here describe a further example of a highly complex bacterial signaling network with an intricate relationship between two HKs and three RRs. It involves signal integration, branching of outputs, and an unprecedented allosteric feed-forward loop between RR components, hallmarks of signaling cascades in higher organisms. The complexity exhibited by the NO-sensing pathway reported here suggests that sophisticated prokaryotic signaling mechanisms may be more prevalent than previously imagined.

References

1. Derbyshire, E. R., and Marletta, M. A. (2009) in *cGMP: Generators, Effectors and Therapeutic Implications* (Schmidt, H., ed.) pp. 17–31, Handbook of experimental pharmacology, Berlin Heidelberg
2. Boon, E. M., Davis, J. H., Tran, R., Karow, D. S., Huang, S. H., Pan, D., Miazgowicz, M. M., Mathies, R. A., and Marletta, M. A. (2006) Nitric oxide binding to prokaryotic homologs of the soluble guanylate cyclase beta1 H-NOX domain. *J. Biol. Chem.* **281**, 21892–21902
3. Iyer, L. M., Anantharaman, V., and Aravind, L. (2003) Ancient conserved domains shared by animal soluble guanylyl cyclases and bacterial signaling proteins. *BMC Genomics* **4**, 5–12
4. Karow, D. S., Pan, D., Tran, R., Pellicena, P., Presley, A., Mathies, R. A., and Marletta, M. A. (2004) Spectroscopic characterization of the soluble guanylate cyclase-like heme domains from *Vibrio cholerae* and *Thermoanaerobacter tengcongensis*. *Biochem.* **43**, 10203–10211
5. MacMicking, J., Xie, Q. W., and Nathan, C. (1997) Nitric oxide and macrophage function. *Annu. Rev. Immunol.* **15**, 323–350
6. Poole, R. K. (2005) Nitric oxide and nitrosative stress tolerance in bacteria. *Biochem Soc T* **33**, 176–180
7. Spiro, S. (2007) Regulators of bacterial responses to nitric oxide. *FEMS Microbiol. Rev.* **31**, 193–211
8. Carlson, H. K., Vance, R. E., and Marletta, M. A. (2010) H-NOX regulation of c-di-GMP metabolism and biofilm formation in Legionella pneumophila. *Mol. Microbiol.* **77**, 930–942
9. Liu, N., Xu, Y., Hossain, S., Huang, N., Coursolle, D., Gralnick, J. A., and Boon, E. M. (2012) Nitric oxide regulation of cyclic di-GMP synthesis and hydrolysis in *Shewanella woodyi*. *Biochemistry* **51**, 2087–2099
10. Wang, Y., Dufour, Y. S., Carlson, H. K., Donohue, T. J., Marletta, M. A., and Ruby, E. G. (2010) H-NOX-mediated nitric oxide sensing modulates symbiotic colonization by *Vibrio*

fischeri. *Proc. Natl. Acad. Sci. USA* **107**, 8375–8380
11. Price, M. S., Chao, L. Y., and Marletta, M. A. (2007) *Shewanella oneidensis* MR-1 H-NOX regulation of a histidine kinase by nitric oxide. *Biochem.* **46**, 13677–13683
12. Stock, A. M., Robinson, V. L., and Goudreau, P. N. (2000) Two-component signal transduction. *Annu. Rev. Biochem.* **69**, 183–215
13. Galperin, M. Y. (2010) Diversity of structure and function of response regulator output domains. *Curr. Opin. Microbiol.* **13**, 150–159
14. Skerker, J. M., Perchuk, B. S., Siryaporn, A., Lubin, E. A., Ashenberg, O., Goulian, M., and Laub, M. T. (2008) Rewiring the Specificity of Two-Component Signal Transduction Systems. *Cell* **133**, 1043–1054
15. Laub, M. T., and Goulian, M. (2007) Specificity in two-component signal transduction pathways. *Annu. Rev. Genet.* **41**, 121–145
16. Busso, D., Delagoutte-Busso, B., and Moras, D. (2005) Construction of a set Gateway-based destination vectors for high-throughput cloning and expression screening in *Escherichia coli*. *Anal. Biochem.* **343**, 313–321
17. Laub, M. T., Biondi, E. G., and Skerker, J. M. (2007) Phosphotransfer profiling: systematic mapping of two-component signal transduction pathways and phosphorelays. *Meth. Enzymol.* **423**, 531–548
18. Rao, F., Pasunooti, S., Ng, Y., Zhuo, W., Lim, L., Liu, A. W., and Liang, Z.-X. (2009) Enzymatic synthesis of c-di-GMP using a thermophilic diguanylate cyclase. *Anal. Biochem.* **389**, 138–142
19. Thormann, K. M., Saville, R. M., Shukla, S., and Spormann, A. M. (2005) Induction of rapid detachment in *Shewanella oneidensis* MR-1 biofilms. *J. Bacteriol.* **187**, 1014–1021
20. Thormann, K. M., Duttler, S., Saville, R. M., Hyodo, M., Shukla, S., Hayakawa, Y., and Spormann, A. M. (2006) Control of formation and cellular detachment from *Shewanella oneidensis* MR-1 biofilms by cyclic di-GMP. *J. Bacteriol.* **188**, 2681–2691
21. Lassak, J., Henche, A.-L., Binnenkade, L., and Thormann, K. M. (2010) ArcS, the cognate sensor kinase in an atypical Arc system of *Shewanella oneidensis* MR-1. *Appl. Environ. Microbiol.* **76**, 3263–3274
22. Lide, D. D. (2008) CRC Handbook of Chemistry and Physics, 89th Edition. 1–523
23. Skerker, J. M., Prasol, M. S., Perchuk, B. S., Biondi, E. G., and Laub, M. T. (2005) Two-component signal transduction pathways regulating growth and cell cycle progression in a bacterium: a system-level analysis. *PLoS Biol.* **3**, e334
24. Borziak, K., and Zhulin, I. B. (2007) FIST: a sensory domain for diverse signal transduction pathways in prokaryotes and ubiquitin signaling in eukaryotes. *Bioinformatics* **23**, 2518–2521
25. Davies, B. W., Bogard, R. W., Dupes, N. M., Gerstenfeld, T. A. I., Simmons, L. A., and Mekalanos, J. J. (2011) DNA damage and reactive nitrogen species are barriers to *Vibrio cholerae* colonization of the infant mouse intestine. *PLoS Pathog.* **7**, e1001295
26. Christen, M., Christen, B., Folcher, M., Schauerte, A., and Jenal, U. (2005) Identification and characterization of a cyclic di-GMP-specific phosphodiesterase and its allosteric control by GTP. *J. Biol. Chem.* **280**, 30829–30837
27. Tamayo, R., Tischler, A. D., and Camilli, A. (2005) The EAL domain protein VieA is a cyclic diguanylate phosphodiesterase. *J. Biol. Chem.* **280**, 33324–33330
28. Schirmer, T., and Jenal, U. (2009) Structural and mechanistic determinants of c-di-GMP signalling. *Nat. Rev. Microbiol.* **7**, 724–735

29. Lauriano, C. M., Ghosh, C., Correa, N. E., and Klose, K. E. (2004) The sodium-driven flagellar motor controls exopolysaccharide expression in *Vibrio cholerae*. *J. Bacteriol.* **186**, 4864–4874
30. Davies, K. M., Lowe, E. D., Vénien-Bryan, C., and Johnson, L. N. (2009) The HupR receiver domain crystal structure in its nonphospho and inhibitory phospho states. *J. Mol. Biol.* **385**, 51–64
31. Lee, S. Y., Cho, H. S., Pelton, J. G., Yan, D., Henderson, R. K., King, D. S., Huang, L., Kustu, S., Berry, E. A., and Wemmer, D. E. (2001) Crystal structure of an activated response regulator bound to its target. *Nat. Struct. Biol.* **8**, 52–56
32. Yan, D., Cho, H. S., Hastings, C. A., Igo, M. M., Lee, S. Y., Pelton, J. G., Stewart, V., Wemmer, D. E., and Kustu, S. (1999) Beryllofluoride mimics phosphorylation of NtrC and other bacterial response regulators. *Proc. Natl. Acad. Sci. USA* **96**, 14789–14794
33. Galperin, M. Y., Natale, D. A., Aravind, L., and Koonin, E. V. (1999) A specialized version of the HD hydrolase domain implicated in signal transduction. *J. Mol. Microbiol. Biotechnol.* **1**, 303–305
34. Lovering, A. L., Capeness, M. J., Lambert, C., Hobley, L., and Sockett, R. E. (2011) The Structure of an Unconventional HD-GYP Protein from *Bdellovibrio* Reveals the Roles of Conserved Residues in this Class of Cyclic-di-GMP Phosphodiesterases. *MBio* **2**
35. Navarro, M. V. A. S., De, N., Bae, N., Wang, Q., and Sondermann, H. (2009) Structural Analysis of the GGDEF-EAL Domain-Containing c-di-GMP Receptor FimX. *Structure* **17**, 1104–1116
36. Hengge, R. (2009) Principles of c-di-GMP signalling in bacteria. *Nat. Rev. Microbiol.* **7**, 263–273
37. Jenal, U., and Malone, J. (2006) Mechanisms of cyclic-di-GMP signaling in bacteria. *Annu. Rev. Genet.* **40**, 385–407
38. Wolf, Y. I., Rogozin, I. B., Kondrashov, A. S., and Koonin, E. V. (2001) Genome alignment, evolution of prokaryotic genome organization, and prediction of gene function using genomic context. *Genome Res.* **11**, 356–372
39. Waters, C. M., Lu, W., Rabinowitz, J. D., and Bassler, B. L. (2008) Quorum sensing controls biofilm formation in *Vibrio cholerae* through modulation of cyclic di-GMP levels and repression of vpsT. *J. Bacteriol.* **190**, 2527–2536
40. Barends, T. R. M., Hartmann, E., Griese, J. J., Beitlich, T., Kirienko, N. V., Ryjenkov, D. A., Reinstein, J., Shoeman, R. L., Gomelsky, M., and Schlichting, I. (2009) Structure and mechanism of a bacterial light-regulated cyclic nucleotide phosphodiesterase. *Nature* **459**, 1015–1018
41. Gao, R., and Stock, A. M. (2010) Molecular strategies for phosphorylation-mediated regulation of response regulator activity. *Curr. Opin. Microbiol.* **13**, 160–167
42. Hammer, B. K., and Bassler, B. L. (2009) Distinct sensory pathways in *Vibrio cholerae* El Tor and classical biotypes modulate cyclic dimeric GMP levels to control biofilm formation. *J. Bacteriol.* **191**, 169–177
43. Ryan, R. P. (2006) Cell-cell signaling in *Xanthomonas campestris* involves an HD-GYP domain protein that functions in cyclic di-GMP turnover. *Proc. Natl. Acad. Sci. USA* **103**, 6712–6717
44. Ryan, R. P., Lucey, J., O'Donovan, K., McCarthy, Y., Yang, L., Tolker-Nielsen, T., and Dow, J. M. (2009) HD-GYP domain proteins regulate biofilm formation and virulence in *Pseudomonas aeruginosa*. *Environ Microbiol.* **11**, 1126–1136

45. Mangan, S., and Alon, U. (2003) Structure and function of the feed-forward loop network motif. *Proc. Natl. Acad. Sci. USA* **100**, 11980–11985
46. Mitrophanov, A. Y., and Groisman, E. A. (2008) Signal integration in bacterial two-component regulatory systems. *Genes Dev.* **22**, 2601–2611
47. Ryan, R. P., McCarthy, Y., Andrade, M., Farah, C. S., Armitage, J. P., and Dow, J. M. (2010) Cell-cell signal-dependent dynamic interactions between HD-GYP and GGDEF domain proteins mediate virulence in *Xanthomonas campestris*. *Proc. Natl. Acad. Sci. USA*
48. Boehm, A., Kaiser, M., Li, H., Spangler, C., Kasper, C. A., Ackermann, M., Kaever, V., Sourjik, V., Roth, V., and Jenal, U. (2010) Second messenger-mediated adjustment of bacterial swimming velocity. *Cell* **141**, 107–116
49. Beyhan, S., Tischler, A. D., Camilli, A., and Yildiz, F. H. (2006) Transcriptome and phenotypic responses of *Vibrio cholerae* to increased cyclic di-GMP level. *J. Bacteriol.* **188**, 3600–3613
50. Krasteva, P. V., Fong, J. C. N., Shikuma, N. J., Beyhan, S., Navarro, M. V. A. S., Yildiz, F. H., and Sondermann, H. (2010) *Vibrio cholerae* VpsT regulates matrix production and motility by directly sensing cyclic di-GMP. *Science* **327**, 866–868
51. Thormann, K. M., Saville, R. M., Shukla, S., Pelletier, D. A., and Spormann, A. M. (2004) Initial Phases of biofilm formation in *Shewanella oneidensis* MR-1. *J. Bacteriol.* **186**, 8096–8104
52. Donlan, R. M., and Costerton, J. W. (2002) Biofilms: survival mechanisms of clinically relevant microorganisms. *Clin. Microbiol. Rev.* **15**, 167–193
53. Myers, C. R., and Nealson, K. H. (1988) Bacterial manganese reduction and growth with manganese oxide as the sole electron acceptor. *Science* **240**, 1319–1321
54. Brons, H. J., Hagen, W. R., and Zehnder, A. J. (1991) Ferrous iron dependent nitric oxide production in nitrate reducing cultures of Escherichia coli. *Arch. Microbiol.* **155**, 341–347
55. Duncan, C., Dougall, H., Johnston, P., Green, S., Brogan, R., Leifert, C., Smith, L., Golden, M., and Benjamin, N. (1995) Chemical generation of nitric oxide in the mouth from the enterosalivary circulation of dietary nitrate. *Nat. Med.* **1**, 546–551
56. Zhu, J., and Mekalanos, J. J. (2003) Quorum sensing-dependent biofilms enhance colonization in *Vibrio cholerae*. *Dev. Cell* **5**, 647–656
57. Faruque, S. M., Biswas, K., Udden, S. M. N., Ahmad, Q. S., Sack, D. A., Nair, G. B., and Mekalanos, J. J. (2006) Transmissibility of cholera: in vivo-formed biofilms and their relationship to infectivity and persistence in the environment. *Proc. Natl. Acad. Sci. USA* **103**, 6350–6355
58. Paul, R., Jaeger, T., Abel, S., Wiederkehr, I., Folcher, M., Biondi, E. G., Laub, M. T., and Jenal, U. (2008) Allosteric regulation of histidine kinases by their cognate response regulator determines cell fate. *Cell* **133**, 452–461
59. Ng, W.-L., and Bassler, B. L. (2009) Bacterial quorum-sensing network architectures. *Annu. Rev. Genet.* **43**, 197–222
60. Mikkelsen, H., Sivaneson, M., and Filloux, A. (2011) Key two-component regulatory systems that control biofilm formation in *Pseudomonas aeruginosa*. *Environ Microbiol.* **13**, 1666–1681
61. Sivaneson, M., Mikkelsen, H., Ventre, I., Bordi, C., and Filloux, A. (2011) Two-component regulatory systems in *Pseudomonas aeruginosa*: an intricate network mediating fimbrial and efflux pump gene expression. *Mol. Microbiol.* **79**, 1353–1366

CHAPTER 3:

FEEDBACK CONTROL IN THE *SHEWANELLA ONEIDENSIS* H-NOX/NITRIC OXIDE SIGNALING NETWORK THROUGH THE TRANSCRIPTIONAL REGULATOR HNOC

Summary

In this chapter, the role of HnoC - the third response regulator in the H-NOX/NO signaling network in *Shewanella oneidensis* - is characterized. A role for HnoC as a transcriptional repressor for the signaling genes in the network is described. The genes controlled by HnoC were identified by microarray analysis. Furthermore, binding of HnoC to its promoter targets was characterized in vitro and in vivo, revealing an unprecedented regulation mechanism, involving phosphorylation-induced dissociation of the response regulator tetramer. A function for HnoC in fine-tuning the dynamics of the signaling response to NO is proposed. The regulation of *hno* component expression levels allows further refinement of changes in cyclic-di-GMP concentration and biofilm formation.

Introduction

Many microbes switch from a motile to a sessile lifestyle. In that process, large numbers of cells form surface-adhered clusters known as biofilms. Microbes in biofilms are protected from hostile environmental factors (e.g. antibiotic treatment) due to encapsulation in an extracellular polysaccharide matrix and prevalent metabolic dormancy (1). As such, biofilms are associated with chronic infections of pathogens (2) and many therapeutic strategies for fighting infectious diseases are now focused on treating the bacterial biofilm state (3).

The switch from a motile lifestyle to surface attachment and biofilm formation can be influenced by many factors, including nutrient availability, quorum sensing, or specific signaling molecules (4). Signaling cues often affect the concentration of the bacterial secondary messenger cyclic-di-GMP, which stimulates biofilm formation. One molecule that has been implicated in controlling biofilm formation is nitric oxide (NO). In very low concentrations, this reactive gas molecule is an important signaling agent in both prokaryotes and eukaryotes. In contrast, high concentrations of NO are cytotoxic, a property exploited by macrophages in response to microbial infections (5). Therefore, NO forms a link between the innate immune response and biofilms as a possible microbial defense mechanism (6).

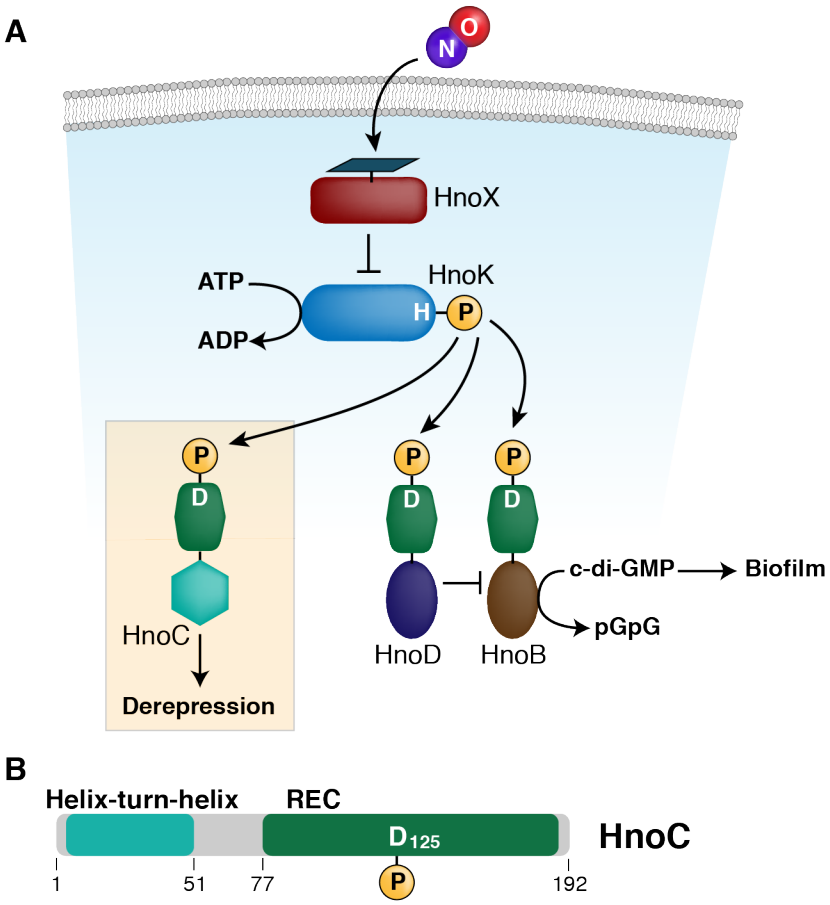

Fig. 3.1. The role of HnoC as a transcriptional regulator in the H-NOX/NO signaling network
A. Summary of the H-NOX/NO signaling network controlling biofilm formation. The histidine kinase HnoK phosphorylates three response regulators: HnoB, HnoC and HnoD. Phosphorylation activates the phosphodiesterase activity of HnoB and circumvents the inhibition of HnoB by HnoD. The stimulated HnoB activity leads to increased hydrolysis of cyclic-di-GMP and low biofilm levels. NO binding to HnoX inhibits the autophosphorylation of HnoK, lowers the phosphodiesterase activity of HnoB, and increases biofilm formation. HnoC constitutes a separate arm in the signaling network, controlling a transcriptional response.
B. The domain organization of HnoC (SO_2540). In addition to the C-terminal phosphoreceiver domain (REC) containing the site of phosphorylation (D125), HnoC contains an N-terminal helix-turn-helix DNA binding domain.

NO has been shown to both promote and inhibit biofilm formation. In *Pseudomonas aeruginosa*, NO has been associated with biofilm dispersal by decreasing cyclic-di-GMP levels, although the nature of the NO sensor and the signaling mechanism are unknown (7). In *Legionella pneumophila* and *Shewanella woodyi*, *H*eme-*N*itric oxide/*OX*ygen binding (H-NOX) proteins have been identified as selective NO sensors. The H-NOX protein controls the activity of a diguanylate cyclase and phosphodiesterase, thus influencing cyclic-di-GMP levels and biofilm dispersal (8, 9). In contrast, NO stimulates biofilm formation in *Shewanella oneidensis* and *Vibrio cholerae* (6) (and unpublished results). Here, H-NOX proteins act as sensors in a more sophisticated multi-component signaling system that elevates cyclic-di-GMP levels in response to NO. The mechanistic details of the H-NOX/NO (*hno*) signaling system have been recently

characterized (6) (Fig. 3.1.A). The NO-bound H-NOX protein (HnoX) inhibits the activity of the histidine kinase HnoK (10). Subsequently, HnoK transfers its phosphoryl group to three response regulator targets, HnoB, HnoC, and HnoD.

Response regulators mediate the functional output of the bacterial signaling system through effector domains (11, 12), which often harbor enzymatic activity, as is the case for HnoB. Phosphorylation of HnoB activates a phosphodiesterase domain, leading to increased cyclic-di-GMP hydrolysis. The second response regulator in the *hno* network, HnoD, functions as phosphorylation-dependent allosteric effector of HnoB to fine-tune cyclic-di-GMP hydrolysis. NO stimulus decreases HnoK kinase activity, lowering the phosphorylation levels of HnoB and HnoD. The diminished activity of HnoB and HnoD causes a rise in cyclic-di-GMP levels, ultimately leading to cellular attachment in biofilms (6) (Fig. 3.1.A).

In a number of gammaproteobacteria, such as *S. oneidensis*, a third response regulator, HnoC (SO_2540), adds further complexity to the *hno* signaling network. HnoC contains a DNA-binding effector domain that serve as transcriptional regulators (13). DNA-binding response regulators can be further classified into subfamilies based on structural classifications of their DNA-binding domains. The most prevalent families contain variations of helix-turn-helix (HTH) motives, such as winged-HTH in the OmpR/PhoB family, simple HTH in the NarL/FixJ family, and the two domain AAA-FIS effector in the NtrC family (13). HnoC belongs to a relatively small subfamily of DNA-binding response regulators possessing a HTH domain from the MerR family (Pfam: HTH_17) (13, 14). Currently, there are 70 members of this family listed in the Pfam database.

HnoC is predicted to function as a transcriptional regulator in the *hno* signaling network. However, the gene regulation targets of HnoC, as well as its functional role on NO-induced biofilm formation are unknown. This study establishes the transcriptional targets of HnoC and demonstrates that HnoC regulates expression of all components of the *hno* network, thus forming a transcriptional feedback loop. We propose that this loop fine-tunes the temporal dynamics of the network and motility response. Furthermore, the molecular mechanism for HnoC transcriptional repression was investigated, revealing several unprecedented regulation features in this previously uncharacterized MerR subfamily of response regulators.

Experimental Procedures

Media and growth conditions

For the microarray analysis, *S. oneidensis* MR-1 strains were grown anaerobically at 29 ºC in MM mineral medium (15), supplemented with 0.1% casamino acids, 50 mM D/L-lactate and 50 mM sodium fumarate. For the reporter assays, *S. oneidensis* strains were cultured in Luria-Bertani (LB) medium at 30ºC and supplemented with the appropriate antibiotics. Strains were grown aerobically to allow maturation of the GFP fluorophore. Previous transcript analysis showed that the *hno* genes are expressed under aerobic and anaerobic conditions (6). In all cases, cultures were inoculated at a 100-fold dilution from an aerobically grown overnight culture in LB medium. For protein expression, *E. coli* BL21 Star (DE3) was grown in expression media (45 g L^{-1} yeast extract, 11.9 mM monobasic potassium phosphate, 50.4 mM dibasic potassium

phosphate, supplemented with 100 μg mL^{-1} ampicillin). Cultures were grown under vigorous shaking (225 rpm) at 37ºC until an OD_{600} of 0.7. Subsequently, the temperature was lowered to 20ºC, the cultures were induced with 50 μM IPTG, and grown for 20 hours.

Strains

The bacterial strains used in this study are listed in Table C.2 in the Appendix. In-frame deletions of *hnoC* (SO_2540), *hnoX* (SO_2144) and *hnoK* were generated from WT *S. oneidensis* MR-1 as described (6, 16). *S. oneidensis* strains were transformed with the GFP-reporter plasmids by electroporation.

Plasmid construction

The plasmids pHMGWA-*So*HnoC and pHMGWA-*So*HnoK for HnoC and HnoK expression were generated as described previously (6). GFP-reporter plasmids to monitor transcription from the *hno* promoters were based on pPROBE-NT (17). The *hnoX*, *hnoC* and *hnoD* promoter regions stretching from the -250 to the -1 bp position, or a 250 bp HnoD intragenic control sequence, were PCR-amplified from *S. oneidensis* genomic DNA using the respective F-*Hind*III and R-*Xba*I primers. A list of all primers used in this study can be found in Table C.3 in the Appendix. The PCR products and pPROBE-NT were digested with *Hind*III and *Xba*I and ligated together to form the respective pProbe-NT::*_p-gfp* plasmids. The reporter plasmids expressing the unstable GFP variant GFP(AAV) were based on pPROBE-gfp[AAV] (17). As before, the PCR fragment of *hnoCp* was cloned into the plasmid using *Hind*III and *Xba*I restriction sites.

Microarray analysis

Four biological replicates of WT *S. oneidensis MR*-1 and Δ*hnoC* were grown in 12-well microtiter plates inside an anaerobic glovebag (Coy Laboratory Products). After 15 hrs, 2.5 mL of the culture were treated with RNAprotect (Qiagen) and total RNA was extracted from the samples using the RNeasy mini kit (Qiagen). The quality of the RNA was assessed on a Bioanalyzer. Cy5-labeled cRNA was generated using the Low Input Quick Amp WT Labeling Kit (Agilent) with 100 ng of input RNA. A custom whole-genome microarray for *S. oneidensis* MR-1, containing a minimum of 3 probes for each gene, was designed on eArray (Agilent). The samples were hybridized onto individual arrays using standard protocols provided by Agilent. The microarray data were analyzed using the *limma* package in the *R* computing environment (18-20). Data were background corrected using the normexp method with an offset of 1, and quantile normalized between arrays. Replicate probes were averaged, the data was fit to a linear model, and differentially expressed genes between strains were filtered using a *p*-value smaller than 0.05 and a fold-change between samples of at least 2. The microarray data has been deposited in NCBI's GEO database (21) and can be accessed under reference number GSE44689.

GFP-Reporter assays

S. oneidensis strains, transformed with the appropriate reporter, plasmids were grown aerobically in LB until mid-log phase (OD_{600} ~ 0.5). 15 – 20 μL of each culture were diluted into 2 mL of

pre-chilled 1.5× PBS solution. Samples were analyzed on a BD LSR II flow cytometer using a forward-scatter and side-scatter threshold of 300V. The laser settings were as follows: FSC: 580 V, SSC: 328 V, FITC: 610 V. Each dataset, consisting of 30,000 observations, was gated manually by FSC-A and SSC-A, and subsequently by SSC-A and SSC-W to exclude doublets. GFP expression was calculated as the median FITC intensity. The fluorescence intensities from three biological replicates, grown on separate days, were normalized to the intensity of *S. oneidensis* Tn7::*gfp*, a strain expressing GFP constitutively from a transposon insertion.

HnoC and HnoK expression and purification

To ensure solubility, HnoC and HnoK were expressed and purified as a C-terminal fusion to maltose binding protein (MBP). The expression and purification was performed as described (6). Briefly, the fusion protein was expressed in *E. coli* BL21 Star (DE3), induced with 50 μM IPTG. Cells were lysed by passage through a high-pressure homogenizer (Avestin) and the lysate was cleared by centrifugation. The protein was purified by affinity chromatography using amylose resin (NEB) followed by Ni-NTA resin (Qiagen). For HnoK, the MBP-tag was cleaved by treatment with TEV protease and the protein was further purified on a Superdex S200 16/60 column. Both proteins were buffer-exchange into storage buffer (50 mM diethanolamine pH 8.0, 150 mM NaCl, 5% glycerol, 1 mM dithiothreitol) and aliquots were flash-frozen in liquid nitrogen.

DNA-gel-shift assays and size-exclusion chromatography

DNA probes (250-300 bp) of the *hnoX*, *hnoC/D* and *ompR* promoter control regions were generated by PCR amplication from *S. oneidensis* genomic DNA using the respective hno_-F and hno_-R primers. The forward primer contained a 5'-6-carboxyfluorescein modification to incorporate a fluorescence label into each probe. Identical unmodified forward primers were used to create unlabeled DNA probes for the competition assay. Gel-shift assays were performed as described (22) with the following modifications: Each binding reaction (20 μL) contained 5 nM DNA probe, 1 – 500 nM HnoC, 300 μg mL^{-1} BSA, 50 μg mL^{-1} Poly(dI-dC) • Poly(dI-dC), 50 mM Tris pH 8.0, 50 mM NaCl, 5 mM $MgCl_2$, 2 mM dithiothreitol, 10 % glycerol. If needed, a 25-fold excess unlabeled competitor probe (125 nM) was added. To examine the effect of phosphorylating HnoC on DNA-binding, 5 μM HnoK and 1 mM ATP were added to the respective binding reactions. Each reaction was incubated for 30 min at room temperature and loaded with loading dye onto precast 6% DNA Retardation Gels (Life Technologies). The samples were separated by gel electrophoresis in 0.5× TBE running buffer (44.5 mM Tris, 44.5 mM boric acid, 1 mM EDTA) at 100 V for 1.5 hrs. The gels were imaged on a Pharos FX System (Biorad) using a laser excitation at 488 nm and a BP 530 nm filter. Band intensities were quantified using Image Lab software (Biorad). Size-exclusion chromatography was performed on a Bio SEC-3, 300Å, 4.6 x 300 mm column (Agilent) in 50 mM sodium phosphate pH 8.0, 150 mM NaCl at 10 ºC at a flow rate of 0.4 mL min^{-1}. Samples of HnoC (10 μM), or HnoC phosphorylated with 5-fold excess HnoK and ATP as before, were filtered and 10 μL portions injected.

DNase I footprinting

The same DNA probe from the gel-shift assay, containing a 5'-6-carboxyfluorescein modification, was used for the *hnoXp* control region. For the *hnoCD* control region, a shorter 137 bp fragment was PCR amplified, also using one primer containing a 5'-6-carboxyfluorescein modification. The footprinting protocol was modified from the literature (23). The binding reactions (100 µL) consisted of 40 nM DNA probe, 0 – 300 nM HnoC, 300 µg mL^{-1} BSA, 5 µg mL^{-1} Poly(dI-dC) • Poly(dI-dC), 50 mM Tris pH 8.0, 50 mM NaCl, 5 mM $MgCl_2$, 2 mM dithiothreitol, 10 % glycerol. After incubation at 25ºC for 30 min, 60 ng DNAse I was added. After 1 min, the reactions were quenched by addition of 100 µL 192 mM sodium acetate, 32 mM EDTA, 0.14% sodium dodecyl sulfate, and 64 µg/mL yeast RNA. The samples were phenol/chloroform extracted and the DNA was precipitated in ethanol. DNA fragments were resuspended in 10 µL TE buffer and 10 µL 95% formamide, 25 mM EDTA, boiled for 5 min, and separated on a 6% polyacrylamide, 7.5 M urea sequencing gel. The gels were imaged on a Pharos FX System (Biorad) using a laser excitation at 488 nm and a BP 530 nm filter. A Sanger sequencing ladder was generated using the Thermo Sequencing Dye Primer Manual Cycle Sequencing Kit (Affymetrix) and the same fluorescently labeled primer for generating the DNA probes.

Results

Identification of transcriptional targets of HnoC

The HnoC response regulator consists of a C-terminal phosphoreceiver (REC) domain and an N-terminal helix-turn-helix domain (Pfam HTH_17) from the MerR superfamily (Fig. 3.1.B) (13, 14). The presence of this DNA-binding effector domain in the response regulator strongly indicates that HnoC acts as a transcriptional regulator. To identify the target genes controlled by HnoC, mRNA transcript levels in *S. oneidensis* were measured using whole genome microarray analysis. Gene expression levels of a wild-type strain were compared to an *hnoC* deletion strain. Both strains were grown anaerobically to exponential phase, and total RNA was stabilized and harvested. RNA probes were generated and hybridized to a custom microarray covering the complete *S. oneidensis* genome. Four biological replicates from each strain were compared and differentially expressed transcripts were identified using a false-discovery rate of 0.05 (Fig. 3.2.A, Appendix Table C.1). Deletion of *hnoC* led to upregulation of only seven genes, indicating that HnoC functions as a highly specific transcriptional regulator for a small set of genes. Intriguingly, six of the seven upregulated features in the *hnoC* knockout strain are contained within the three *hno* operons (Fig. 3.2.B). Moreover, four of the protein products have confirmed roles in the H-NOX/NO (*hno*) signaling network, namely the NO-sensor HnoX, the kinase HnoS, and the response regulators HnoB and HnoD (6). The upregulation of genes in the *hno* operons implies that HnoC acts as a transcriptional repressor for all genes in the H-NOX/NO signaling network. Since *hnoC* is itself co-transcribed from the *hno* operons, HnoC thus creates an autoregulatory transcriptional feedback loop.

HnoC acts as transcriptional repressor in vivo

The *hno* genes of the signaling network are organized in three operons that lie in two separate loci on the *S. oneidensis* chromosome (Fig. 3.2.B). The NO sensor HnoX and the kinase HnoK are co-transcribed from an isolated operon under control of the *hnoX* promoter, henceforth termed *hnoXp*. In contrast, the response regulator genes *hnoA*, *hnoB*, *hnoC*, *hnoD*, the kinase genes *hnoS* and *hnoT*, and the uncharacterized *hnoE* gene are clustered in two adjacent operons that are transcribed in opposite directions. The two operons share a bidirectional promoter region containing the *hnoC* and *hnoD* promoters (*hnoCp* and *hnoDp*).

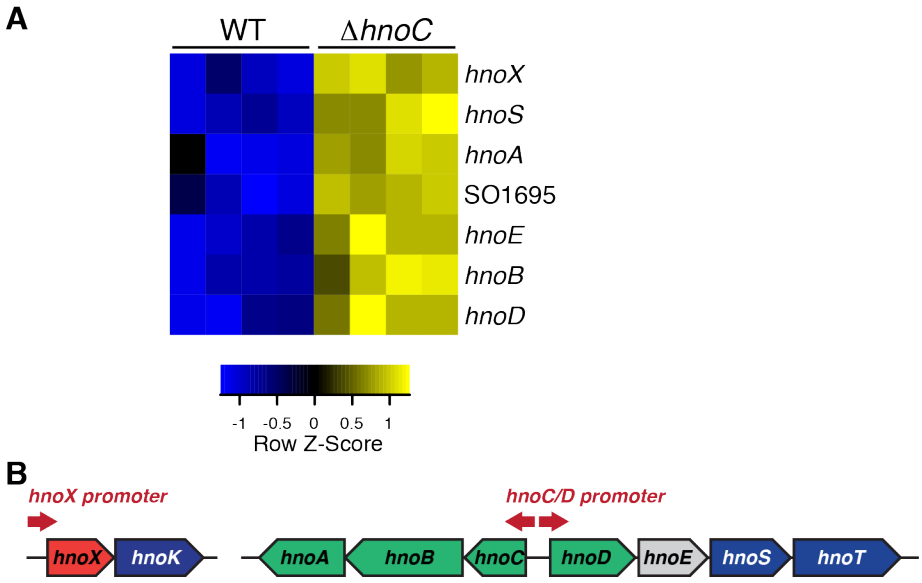

Fig. 3.2. Gene expression profiling results of hnoC *S. oneidensis* knockout
A. Heat-map summarizing the genes that show differential expression between a WT *S. oneidensis* strain and an *hnoC* knockout strain (Δ*hnoC*). Total RNA was isolated from the respective strains, labeled, and hybridized to a whole genome microarray of *S. oneidensis*. Differentially expressed transcripts were filtered using a fold-change > 2 and $p < 0.05$. Expression levels in each row were normalized to their Z-score (yellow = high expression, blue = low expression). Four biological replicates for each strain are grouped in the columns.
B. The *hno* genes are organized into three separate operons containing two distinct promoter regions: the isolated HnoX promoter and the bidirectional HnoC/HnoD promoters.

To test whether HnoC directly regulates each of the three *hno* promoters in *S. oneidensis*, we examined GFP expression driven by the *hno* promoters in a reporter assay. Stretches of 250 bp containing either the *hnoXp*, *hnoCp*, or *hnoDp* region were cloned separately into a plasmid to control eGFP expression (17). The reporter plasmids were transformed into WT *S. oneidensis*, as well as into *hnoX*, *hnoK*, and *hnoC* in-frame deletion strains. The reporter strains were grown aerobically until mid-log phase, and GFP expression was assessed by flow cytometry.

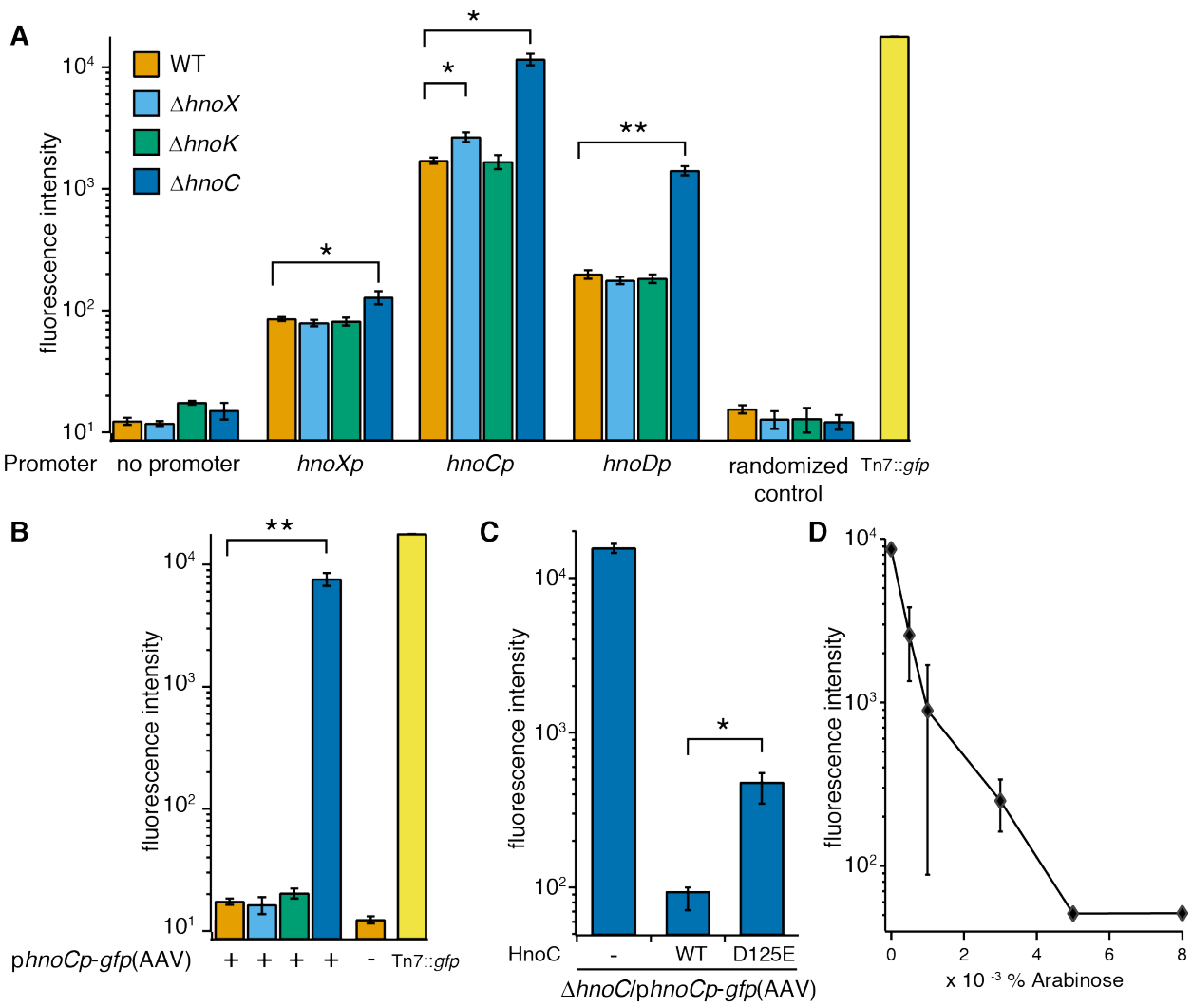

Fig. 3.3. Reporter assay measuring GFP expression from the HnoC-regulated promoters in *S. oneidensis* strains

Reporter plasmids were constructed by cloning the *hnoX*, *hnoC*, *hnoD* promoter or a negative control promoter into pProbeNT to drive eGFP expression (A) or the expression of an unstable GFP(AAV) variant (B). The plasmids were transformed into WT, Δ*hnoX*, Δ*hnoK*, or Δ*hnoC S. oneidensis* strains and GFP expression was quantified by flow cytometry. Median fluorescent intensities were normalized to a *S. oneidensis* strain, that expressed GFP constitutively (Tn7::*gfp*). Intensities from three biological replicates were averaged and the standard deviation is represented as error bars. Results from a two-tailed unpaired t-test to compare the intensities between strains are shown by asterisks (*$p < 0.05$, **$p < 0.005$).

C. Complementation of the *ΔhnoC S. oneidensis* strain with WT HnoC or the phosphorylation-mimic D125E HnoC. The pProbe-NT::*hnoCp-gfp(AAV)* construct served as reporter and HnoC expression induced from pBAD33.

D. Flow cytometry of *E. coli* DH10B co-transformed with pProbe-NT::*hnoCp-gfp(AAV)* and pBAD33-HnoC. HnoC expression was induced in individual cultures with arabinose concentrations ranging from 0.0005 % to 0.008 % (w/v).

GFP expression was undetectable in the absence of a promoter in the reporter plasmid or when a random *hnoD* intragenic sequence was inserted as a negative control (Fig. 3.3.A). In contrast, addition of *hnoXp*, *hnoCp* and *hnoDp* led to measurable GFP expression, albeit of varying intensities, suggesting that the relative strengths of the promoters differ. In the WT strain, *hnoCp* produced the highest fluorescent intensities while expression from *hnoXp* and *hnoDp* was 20-times and 9-times lower, respectively. In the *hnoC* knockout, GFP expression was significantly elevated compared to WT *S. oneidensis* in the case of all three promoters (1.5, 6.8 and 7.1-fold for *hnoXp*, *hnoCp* and *hnoDp,* respectively). The observed increase in transcription in the absence of HnoC confirms its role as a transcriptional repressor in vivo. Deletion of HnoK did not influence GFP expression even though HnoK functions as an upstream kinase of HnoC. However, a second kinase, HnoS, that can also phosphorylate HnoC is still present in this strain and might mask any effects on GFP expression (6). In contrast, a measurable increase in fluorescence was observed from the *hnoC* promoter when HnoX was deleted. This suggests a role for HnoX as an upstream supressor of HnoC. This effect is consistent with the signaling network, in which HnoX inhibits HnoK, which in turn phosphorylates HnoC. A similar increase might be concealed for the *hnoX* and *hnoD* promoter due to their lower overall induction of GFP expression.

GFP is a very stable protein with a half-life greater than 24 hours (24). Consequently, the relatively small increase in GFP expression in the HnoC knockout might be masked by high background GFP levels in the WT strain due to continual accumulation during growth. To test the true repressive power of HnoC, expression of an unstable GFP(AAV) variant that possesses a much shorter half-life (~190 min) was measured. The expression was driven by *hnoCp* (Fig. 3.3.B) (24). In this case, no measurable fluorescence could be detected in the WT, the *hnoX* deletion strain or the *hnoK* deletion strain, which confirms that much of the previously observed signal was due to slow degradation of accumulated GFP. On the other hand, the *hnoC* knockout produced very high fluorescence levels, comparable to levels of the stable GFP variant and to constitutive GFP expression from a transposon insertion. Overall, deletion of HnoC caused a 440-fold increase in GFP expression, corresponding to a high dynamic range between active transcription and full repression by HnoC. The activation of GFP expression in the *hnoC* deletion strain could be reversed by complementation with a plasmid-derived copy of the *hnoC* gene (Fig. 3.3.C). WT HnoC lowered expression to similar levels to WT *S. oneidensis*. In comparison, the aspartate to glutamate mutant of the phosphorylation site (D125E), which mimics the phosphorylated state of HnoC (6, 25, 26), only partially lowers GFP expression. This weaker repression serves as an indication that the phosphorylated state of HnoC derepresses transcription.

To test whether HnoC repression is concentration-dependent, the *hnoCp-gfp* reporter plasmid and a plasmid for arabinose-inducible expression of HnoC were co-transformed into *E. coli* DH10B. Cultures were grown to mid-log phase and HnoC was induced with varying arabinose concentrations. In the absence of arabinose and HnoC, GFP expression was high (Fig. 3.3.D). This demonstrated that *hnoCp* was also active in *E. coli*. Overexpression of HnoC led to a decrease in the fluorescence intensities and lower GFP expression. The extent of the decrease was dependent on the amount of inducer for HnoC expression. Overall, the reporter assays confirmed that HnoC functions as a strong repressor of the three *hno* promoters in vivo, and the degree of repression can be tuned by altering its concentration.

HnoC binding to hno promoter regions

The molecular mechanism by which HnoC represses transcription from the *hno* promoters was then investigated. Response regulators with DNA-binding domains typically associate directly to the promoter region or to a control region in close proximity. Activators such as members of the OmpR/PhoB or NtrC family initiate transcription by recruiting RNA polymerase (RNAP) (27, 28) or by stimulating open complex formation of a RNAP-promoter complex (29). In contrast, a repressor such as CovR prevents RNA polymerase from recognizing the promoter (30).

To test whether HnoC directly interacted with the *hno* promoter DNA, gel-shift assays were conducted between HnoC and *hno* promoter probes. Fluorescently labeled 250-300 bp probes of the control regions around each promoter were generated. The *hnoXp* probe stretches from the -200 to the +50 position of the *hnoX* gene. The *hnocC/Dp* probe contains the intergenic region between *hnoC* and *hnoD* extending from the +50 position in each gene. HnoC (50 nM) was incubated with each control region and the mixture was separated by native polyacrylamide electrophoresis (Fig. 3.4.A). HnoC produced a clear gel-shift with both the *hnoXp* and *hnoC/Dp* probe, revealing a direct interaction between the protein and DNA. For both control regions, the labeled probe binding was competed away when 25-fold excess of unlabeled probe was added. In contrast, addition of non-specific DNA had no effect on the HnoC-DNA interaction, confirming that the interaction is specific. A probe of the *ompC* promoter from *E. coli* was used as a negative control. No distinct gel shift could be observed between HnoC and this control probe, even when the HnoC concentration was raised to 500 nM (Fig. 3.4.B).

To determine the dissociation constants between HnoC and the control region probes, HnoC amounts were titrated to the *hnoXp* and *hnoC/Dp* probes in the gel-shift experiment. The fraction of bound DNA was then quantified by densitometry of the bands and binding curves between HnoC and the *hnoXp* probe (Fig. 3.4.C) and the *hnoC/Dp* probe (Fig. 3.4.D) were generated. The curves clearly show the sigmoidal shape typical for cooperative binding interactions. The data were fit to a cooperative binding model to determine dissociation constants of 2.5 and 8.8 nM and Hill coefficients of 3.2 and 2.8 for the *hnoX* and *hnoC/D* control regions, respectively. The cooperative binding behavior and magnitude of the Hill coefficient suggest that HnoC multimerizes and that at least three to four subunits participate in the association to the control region DNA. This tight binding of HnoC to the *hno* promoter region could be a mechanism to occlude RNAP from initiating transcription of the H-NOX/NO signaling genes.

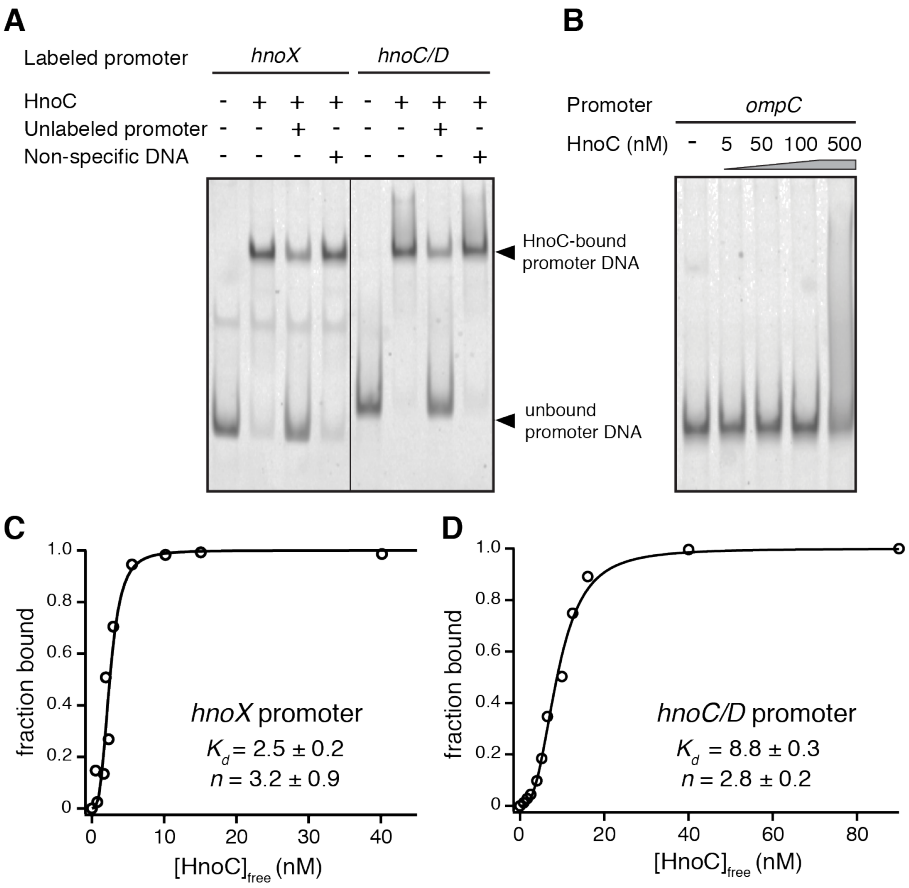

Fig. 3.4. Gel-shift binding assays between HnoC and promoter region DNA probes
Fluorescently-labeled DNA probes (5 nM) were incubated with HnoC (50 nM) and separated by native PAGE.
A. A gel-shift occurred between HnoC and the *hnoX* control region as well as the *hnoC/D* control region probe. This gel-shift was abolished with 25-fold excess unlabeled probe.
B. Gel-shift between increasing concentrations of HnoC and a control *E. coli* promoter (OmpC).
C-D. Binding curves between HnoC and the *hnoX* (C) or the *hnoC/D* control region (D). Bound and unbound DNA amounts were quantified by densitometry and fit to a cooperative binding model.

Identification of HnoC binding sites by DNA footprinting

To determine the exact binding sites of HnoC in the control region around the *hnoX* and *hnoC/D* promoters, DNA footprinting was carried out. Probes of the respective promoter control regions were digested with DNAse I in the presence of increasing amounts of HnoC to reveal which areas were protected by binding of the transcription factor. In both control regions, addition of HnoC produced a protected area corresponding to approximately 26 nucleotides (Fig. 3.5.A-B). The protected region in the *hnoX* promoter is located 5 nucleotides downstream of the -10 site and overlaps with the transcription start site. The binding location in the *hnoC/D* control region overlaps with the -10 site of the *hnoD* promoter and the -35 site of the *hnoC* promoter (Fig. 3.5.C-D). Consequently, HnoC binding can interfere with association of the RNAP holoenzyme and transcription initiation.

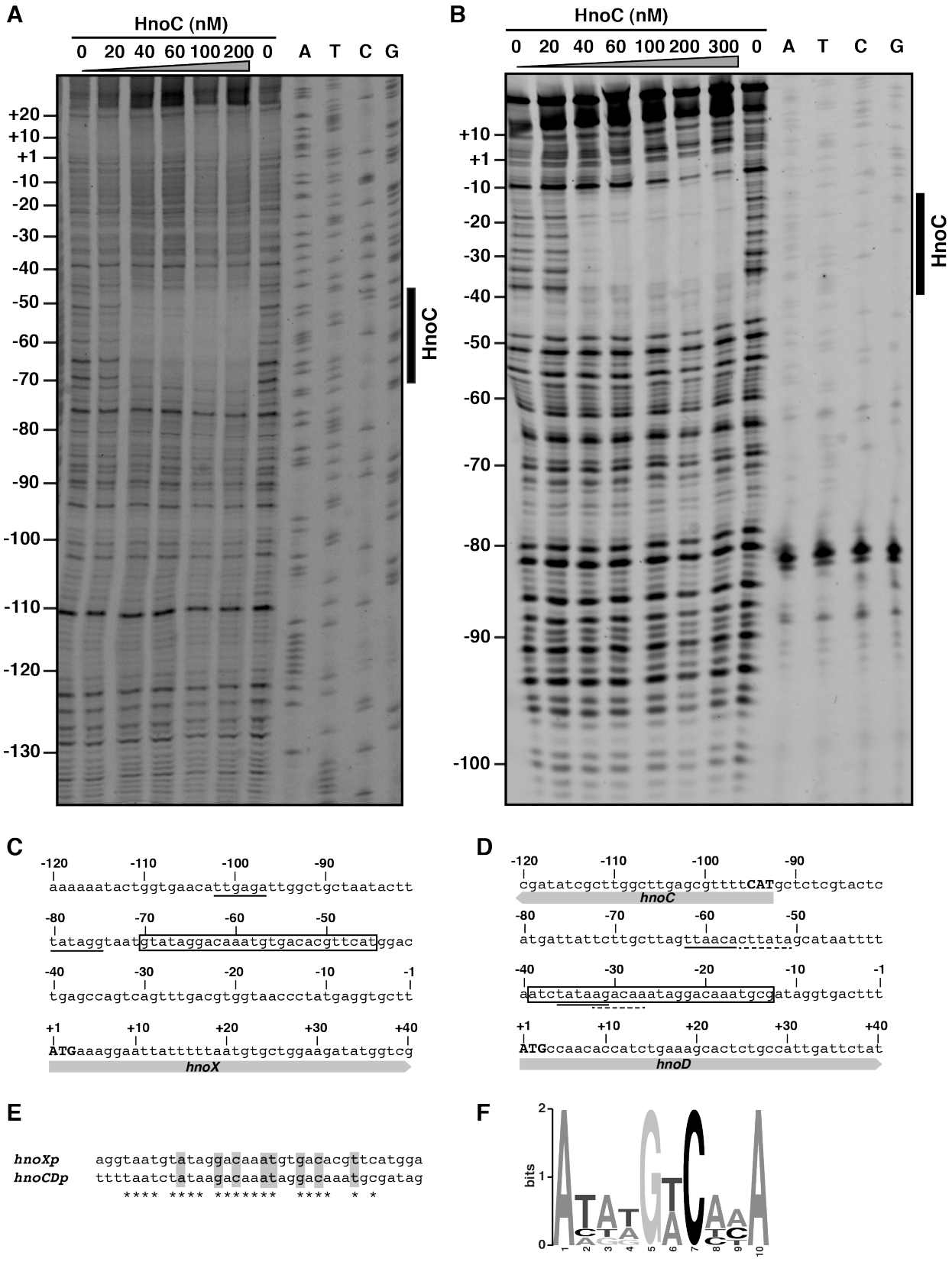
A
HnoC (nM)
0 20 40 60 100 200 0 A T C G
+20
+10
+1
-10
-20
-30
-40
-50
-60
-70
-80
-90
-100
-110
-120
-130
HnoC
B
HnoC (nM)
0 20 40 60 100 200 300 0 A T C G
+10
+1
-10
-20
-30
-40
-50
-60
-70
-80
-90
-100
HnoC
C
-120 -110 -100 -90
aaaaaatactggtgaacattgagattggctgctaatactt
-80 -70 -60 -50
tataggtaatgtataggacaaatgtgacacgttcatggac
-40 -30 -20 -10 -1
tgagccagtcagtttgacgtggtaaccctatgaggtgctt
+1 +10 +20 +30 +40
ATGaaaggaattatttttaatgtgctggaagatatggtcg
hnoX
D
-120 -110 -100 -90
cgatatcgcttggcttgagcgttttCATgctctcgtactc
hnoC
-80 -70 -60 -50
atgattattcttgcttagttaacacttatagcataatttt
-40 -30 -20 -10 -1
aatctataagacaaataggacaaatgcgataggtgacttt
+1 +10 +20 +30 +40
ATGccaacaccatctgaaagcactctgccattgattctat
hnoD
E
hnoXp aggtaatgtataggacaaatgtgacacgttcatgga
hnoCDp ttttaatctataagacaaatataggacaaatgcgatag
**** **** ******* **** * *
F
bits
2
1
0
1 2 3 4 5 6 7 8 9 10

Fig. 3.5. DNase I footprinting of *hno* promoter control regions to map the HnoC binding sites
A-B. Gel electrophoresis of DNA fragments of the *hnoX* (A) and *hnoC/D* (B) promoter control regions from the footprinting analysis. Probes were incubated with increasing amounts of HnoC and digested with DNAse I. Protected regions by HnoC are indicated by the black bar on the right. The numbering is relative to the translation start site of the *hnoX* or *hnoD* gene.
C-D. Sequence of the *hnoX* (C) and *hnoC/D* (D) promoter region. The predicted -10 and -35 promoter regions are underlined (dashed lines correspond to the *hnoC* promoter elements). The DNA regions protected by HnoC in the footprinting analysis are boxed.
E. Alignment of the DNA regions protected by HnoC. Residues forming an inverted repeat are highlighted in grey.
F. Consensus sequence for the binding half-site of an HnoC monomer. The motif was generated in MEME (31) from the known binding site in the *hnoX* and *hnoC/D* promoter, and a predicted binding site in the SO2547 promoter region.

Transcription factor dimers often bind to tandem repeat sequences. For example, OmpR/PhoB family members bind to direct repeats, where each HTH domain recognizes of 7-10 bp consensus sequence (27, 32, 33). On the other hand, MerR dimers and NarL response regulator dimers bind to inverted repeats (34, 35). Alignment of the protected DNA regions by HnoC in the *hnoX* and *hnoC/D* promoters shows several conserved stretches (Fig. 3.5.E). Intriguingly, a 20-bp area consists of two inverted repeats. This suggests that two HnoC subunit interact with the promoter DNA in a head-to-head orientation similar to other MerR family members (36).

The *S. oneidensis* genome was searched for other occurrences of this HnoC binding consensus sequence. The only other highly confident incidence of this motif was identified in the promoter region of SO_2547, an operon directly adjacent to the *hnoDEST* operon. A gel-shift assay confirmed HnoC binding to this promoter region (data not shown) suggesting that HnoC also controls expression of this operon, which encodes three chemotaxis genes. Based on the three binding sites of HnoC, each consisting of two inverted repeats, a consensus sequence for the half-site recognized by an HnoC momoner could be generated (Fig. 3.5.F). This analysis highlights that adenosine residues at position 1 and 10, as well as a G[TA]C motif in the center, are required for HnoC binding.

Effect of phosphorylation on HnoC DNA-binding

HnoC is the phosphorylation target of two histidine kinases in the *hno* signaling network, HnoK and HnoS (6). To assess the regulatory consequences of phosphorylation, the previous DNA-binding experiment was repeated with the phosphorylated form of HnoC. For this purpose, HnoC was preincubated with a large excess of HnoK and ATP prior to addition of the *hno* promoter DNA-probes. Unphosphorylated HnoC formed a homogeneous DNA-control region complex with both *hnoXp* and *hnoC/Dp*, indicated by the presence of a single band at high retention in the native gel when increasing concentrations of HnoC were added to the probe (Fig. 3.6.A and B, left panels). In contrast, when HnoK and ATP were added to phosphorylate HnoC, two additional DNA-bound species with lower retention were separated in the gel (Fig. 3.6.A and B, right panels). Addition of an inactive histidine kinase mutant (H72A HnoK) did not lead to the formation of any additional DNA-bound species, demonstrating the necessity for phosphorylation. The presence of these species can be attributed to a different HnoC:DNA binding stoichiometry or to alternate conformations of the phosphorylated HnoC-DNA complex.

Furthermore, the affinity between phosphorylated HnoC and both control regions decreased slightly compared to the unphosphorylated state. The presence of the additional DNA-bound species prevented the calculation of comparable dissociation constants for phosphorylated HnoC. Nonetheless, the intensities of the unbound DNA bands at 10 nM and 25 nM HnoC are visibly stronger for the phosphorylated state compared to the unphosphorylated, which is consistent with a weaker binding affinity of the phosphorylated HnoC.

To determine whether the mobility difference of the phosphorylated HnoC-DNA complexes could be caused by changes in multimerization, we further investigated the oligomerization state of HnoC by size-exclusion chromatography (SEC). Purified HnoC in the unphosphorylated form eluted as a single homogeneous peak with an apparent size of 175 kDa (Fig. 3.6.C, dashed line). Next, HnoK and ATP were added to generate phosphorylated HnoC. This sample eluted in two separate peaks in a 1:2 ratio, the smaller peak with an apparent size of 175 kDa and the larger peak with an apparent size of 45 kDa (dashed-dotted line). Addition of inactive H72A HnoK histidine kinase did not lead to formation of the 45 kDa peak (dotted line). The broad peak eluting between 4.3 and 5.5 min corresponds to soluble aggregate of HnoK, that forms at the concentration required for efficient HnoC phosphorylation (solid line). Given a mass of 66.3 kDa for the monomeric MBP-HnoC fusion, the smaller species with an apparent size of 45 kDa likely corresponds to an HnoC monomer, while the 175 kDa species probably constitutes a tetramer. Consequently, unphosphorylated HnoC was present uniformly as a tightly associated oligomer while phosphorylation of HnoC caused dissociation into monomers. The presence of a small 175 kDa peak in the HnoC, HnoK, and ATP sample suggests that HnoK is not capable of phosphorylating HnoC entirely under the assay conditions or that HnoC becomes partially dephosphorylated and reforms a tetramer during the chromatography run.

Overall, the SEC experiments complement the results from the gel-shift assay and demonstrate that unphosphorylated HnoC exists as an oligomer. HnoC binds to the control region DNA cooperatively and forms the tightly associated and highly retained band in the gel (Fig. 3.6.A and B, left panels). Phosphorylation by the kinase HnoK and ATP leads to dissociation of the oligomer. Due to incomplete phosphorylation, HnoC monomers are accompanied by a mixture of lower-order oligomers (trimers and dimers) and undissociated tetramers. The lower-order oligomers can still associate weakly to the control region DNA and are likely responsible for the bands at lower retention in the gel-shift assay (Fig. 3.6.A and B, right panels). In contrast to most other DNA-binding response regulators, which form tighter oligomers in the phosphorylated state (11), phosphorylation of HnoC weakens the oligomeric state and promotes subunit dissociation. Therefore, the unphosphorylated form of HnoC represents the repressive state, while phosphorylation derepresses transcription.

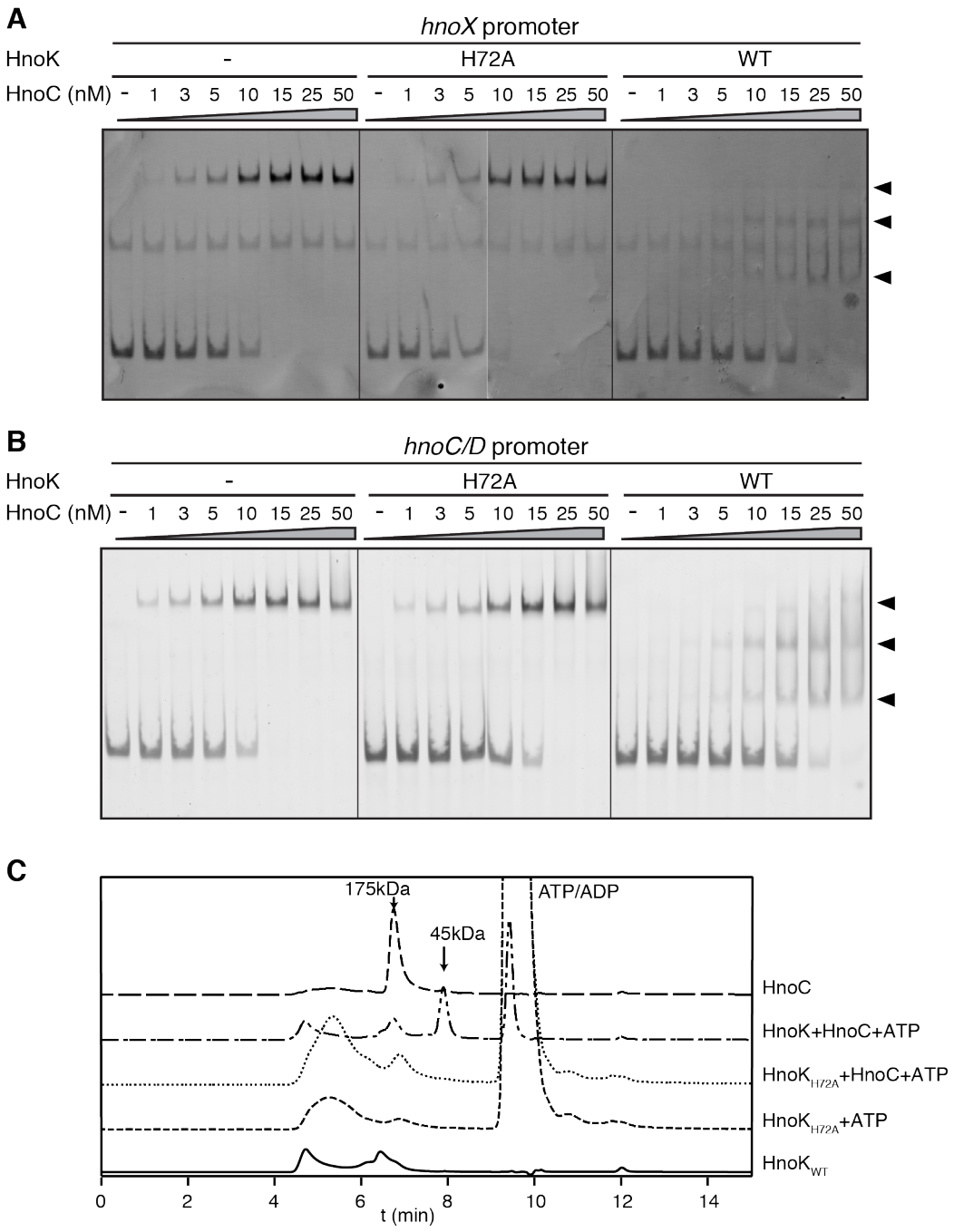

Fig. 3.6. Effect of phosphorylation on HnoC control region binding
A-B. Gel-shift binding assay between phosphorylated HnoC and DNA probes (5 nM) of the HnoX (A) or the HnoC/D promoter control region (B). HnoC was phosphorylated with excess HnoK and ATP prior to incubation with the labeled promoter probe or incubated with the inactive H72A HnoK mutant.
C. Size-exclusion chromatography of HnoK, unphosphorylated HnoC, or phosphorylated HnoC incubated with HnoK and ATP. Approximate sizes of HnoC species are indicated and were measured by comparing retention times to molecular weight standards.

Discussion

Structural and biochemical studies on a large number of DNA-binding response regulators have provided insight into the effects of receiver domain phosphorylation on transcriptional regulation by the DNA-binding domain. Despite some commonalities within subfamilies, the divergence of regulatory mechanisms even between close structural homologs is remarkable (11, 37). HnoC belongs to the relatively small MerR subfamily of DNA-binding response regulators, which thus far has been uncharacterized (13). The present study on HnoC reveals several surprising and unprecedented regulatory features that expand the repertoire of mechanistic possibilities for DNA-binding response regulators.

Size-exclusion chromatography and the observation of high cooperativity for HnoC binding to control region DNA demonstrated that unphosphorylated HnoC exists as a tetramer. Response regulator oligomerization is a common regulation method, as most DNA-binding proteins require homodimerization to bind effectively to inverted DNA repeats, which almost always constitute the target sequences. Dimerization has been observed in many response regulator subfamilies, such as for OmpR/PhoB (38-40) and NarL/FixJ members (41, 42). In contrast, it is unlikely that unphosphorylated HnoC exists as a dimer. Instead, the binding cooperativity with a Hill coefficient of approximately 3, and the apparent weight of the oligomer, which is much larger than twice the monomeric weight, points to an assembly of HnoC into tetramers (Fig. 3.6). Although the existence of a trimer cannot be fully excluded, the typical dimeric binding mode to tandem DNA sequences makes the dimer of dimer structure more probable. Nonetheless, the footprinting results only demonstrate protection of region large enough to accommodate an HnoC dimer. This suggests that two HnoC subunits in the tetramer are not in contact with DNA. A tetrameric HnoC architecture could facilitate binding to two more distantly spaced tandem recognition sequences, for example as observed for OmpR (43). If two tandem repeats are spaced apart, the large DNA-protein complex could have a role in deforming the DNA as suggested from tetrameric complexes of TorR and DosR (44-46). The HnoC tetramer could bind to two separate *hno* promoter simultaneously to bring them into close proximity.

Apart from observed NtrC hexamers, which assemble due to AAA+ ATPase domains, higher-order oligomerization states are not common. TorR has been suggested to form tetramers based on biochemical evidence (44, 45), and tetramers of the DNA-binding domain of DosR have been observed crystallographically (46), although it is not clear if these play a role in full-length DosR (47). The OmpR/PhoB-like regulator ArcA has been shown to form oligomers that are possibly larger than tetramers when phosphorylated, however, structural and functional details remain unclear (48, 49).

The HnoC tetramers form in the unphosphorylated state and bind tightly to the control region around the *hno* promoters. Based on the in vivo expression data, this state represses transcription. The footprinting data suggests a model in which the HnoC tetramer occludes RNA polymerase from initiating transcription through steric hindrance (Fig. 3.7.A). Size-exclusion chromatography demonstrated that HnoC phosphorylation weakens the multimeric interactions, causing dissociation into monomers (Fig. 3.6.C). Accordingly, the gel-shift assays indicated that multimers of intermediate size could form, which were potentially stabilized by incomplete

phosphorylation of the HnoC subunits or by DNA interactions (Fig. 3.6.A-B). These lower-order HnoC oligomers can still associate to the control region DNA, albeit with weaker affinity.

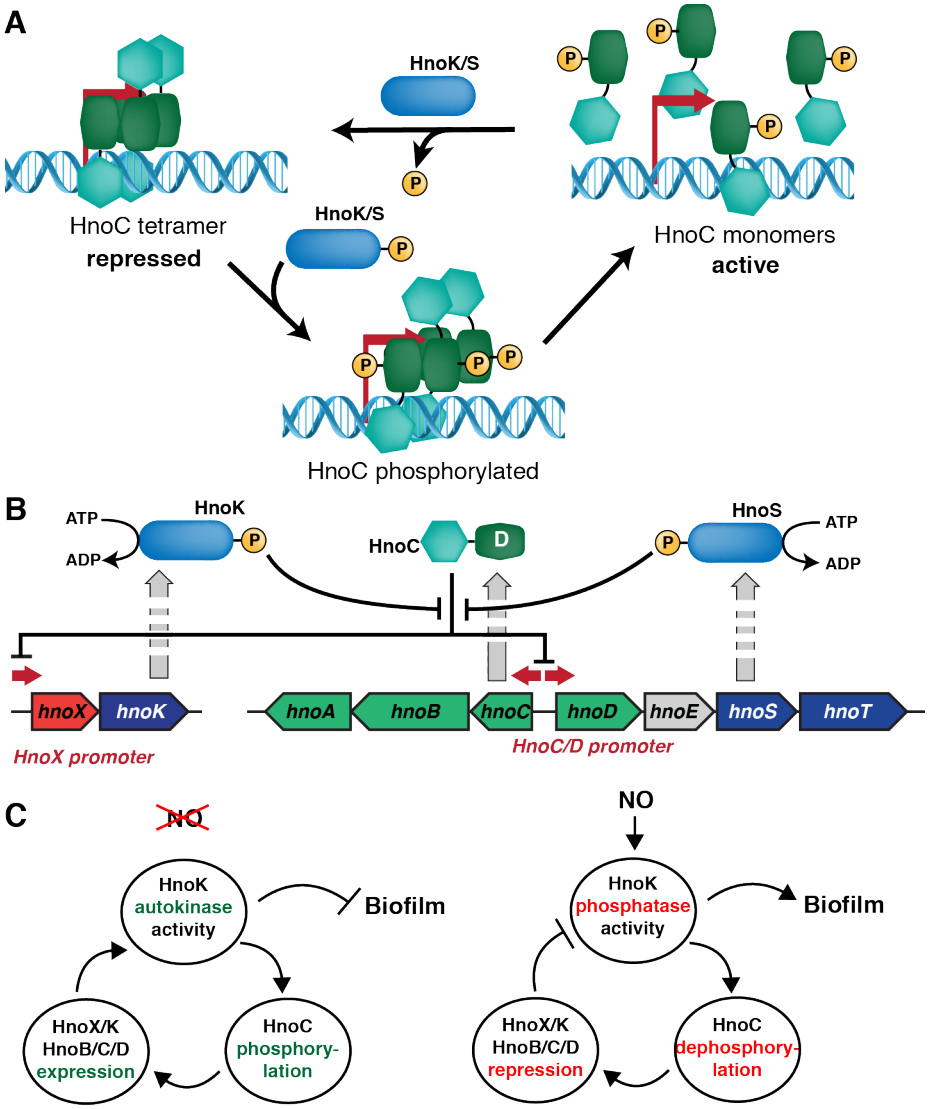

Fig. 3.7. Model for regulation of HnoC in the context of the H-NOX/NO signaling network
A. Model for regulation of HnoC by phosphorylation. Unphosphorylated HnoC forms a tetramer with tight affinity to control regions, which prevents transcription. When phosphorylated by HnoK or HnoS, HnoC tetramers become destabilized and the complex dissociates. The HnoC monomers dissociate from the control region DNA and allow transcription**.**
B. Model for the transcriptional feedback loop in the H-NOX/NO signaling network. HnoC represses transcription from the *hnoX*, *hnoC* and *hnoD* promoter, inhibiting its own expression and expression of the HnoK kinase. HnoK phosphorylates HnoC and relieves the repression.
C. Architecture of the autofeedback loops in the absence (left) and presence of NO (right). In the absence of NO, HnoK kinase activity predominates resulting in a positive feedback loop. In contrast, when NO is present, HnoK shifts towards phosphatase activity leading to a negative feedback loop.

This leads to an overall model in which phosphorylation of HnoC by a cognate kinase, HnoK or HnoS, weakens subunit interactions, initiating the dissociation of the transcription factor from the control region, and subsequently, the promoter becomes accessible for transcription (Fig. 3.7.A). This derepression mechanism through phosphorylation-induced dissociation is unprecedented. It represents a stark contrast to activation of most other response regulator transcription factors, which typically dimerize after phosphorylation and activate transcription through tighter affinity to regulatory sequences near the promoter and subsequent recruitment of RNA polymerase. For instance, members from the OmpR/PhoB family exist as monomers in the unphosphorylated state and phosphorylation induces dimerization and activation (38-40). Likewise, phosphorylation induces dimerization in NarL (41), which can both positively and negatively regulate gene expression (50). This study demonstrates that phosphorylation of the receiver domain is not limited to promoting subunit dimerization, but can also trigger dissociation of response regulator oligomers.

HnoC acts as a transcriptional regulator in the larger context of the H-NOX/NO (*hno*) signaling network, which senses NO and stimulates a change in bacterial motility by inducing surface adhesion in biofilms (6). Along with HnoB and HnoD, HnoC is one of three phosphotransfer targets of the histidine kinases HnoK and HnoS (Fig. 3.1.A) (6). This study demonstrates that HnoC is a transcriptional regulator for all of the signaling components in the pathway, repressing transcription from each of the three *hno* promoters. Since HnoC represses expression of itself and the kinases, an autoregulatory feedback loop is created (Fig. 3.7.B). The exact nature of this feedback loop, whether positive or negative, depends on the phosphorylation state of HnoC. HnoC phosphorylation is controlled by the kinase or phosphatase activities of HnoK and HnoS, which are ultimately affected by the nitric oxide signaling stimulus (Fig. 3.7.C).

Feedback control is a common feature in prokaryotic and eukaryotic signal transduction systems (51) and serves a multitude of functions (52-55). In bacteria, autoregulation of transcription factors through a negative feedback loop occurs especially frequently: for instance 40% of *E. coli* transcription factors negatively regulate their own expression (54, 56). In two-component signaling (TCS) systems, positive feedback loops are more prevalent (57). A well-characterized example is the Mg^{2+}-sensing TCS of *Salmonella enterica*. Here, the phosphorylated state of the response regulator PhoP is a positive autoregulator of PhoQ/PhoP expression and the feedback loop is required for an initial activation surge in transcription of PhoP-responsive genes, which is essential for virulence (58). Positive feedback can also slow down the response time to a stimulus, broaden the cell-to-cell variability and in extreme cases, produce bistability (52, 55). Lastly, positive feedback in TCS has been associated with a learning behavior in which increased protein levels after the first stimulus lead to a shorter activation time for the next stimulus (59).

In contrast, negative feedback speeds up the response time to a stimulus, causing a faster rise in the signaling output (54). It also produces a more uniform output level and less cell-to-cell variability (55, 60). Negative feedback can also achieve adaptation, a resetting of the signaling output after a sustained stimulus (53), and produce oscillation under certain conditions, as predicted for the CovS/CovR system (61). Overall, feedback control allows for fine-tuning of the temporal dynamics of the signaling system. Steady-state levels are not necessarily affected, as

has been demonstrated for PhoQ/PhoP, where only a high Mg^{2+} stimulus increases the steady state expression of target genes (57, 62).

Transcriptional feedback in the *hno* signaling system is complicated because the unphosphorylated and phosphorylated forms of HnoC have opposing effects on gene expression, and the level of phosphorylated HnoC is governed by the activity of two kinases, each possessing a different input signal. Furthermore, expression of HnoK and HnoS kinase is itself autoregulated through the feedback loop (Fig. 3.7.B). In the absence of NO, HnoK is active as a kinase (10), causing phosphotransfer to HnoC and consequently high expression of the *hno* signaling genes. This leads to a model in which a positive feedback loop is created when the NO concentration decreases (Fig. 3.7.C, left). When NO concentrations rise, HnoK can act predominantly as a phosphatase (6). Consequently, HnoC is dephosphorylated by HnoK, which represses expression of the *hno* signaling genes and shifts towards a negative feedback loop (Fig. Fig. 3.7.C, right). Modeling of feedback control in a similarly complex TCS has confirmed that the sign of the feedback - positive or negative - can indeed be influenced by the strength of the input signal (63). In the reporter assays in *S. oneidensis*, only a modest increase in GFP expression was observed when *hnoX* was deleted, while the *hnoK* deletion did not cause a significant change in steady-state GFP levels (Fig. 3.3.A). However, this was not surprising given the complex dynamics of the network, which integrates the kinase and phosphatase activity of HnoK and HnoS, as well as the expression levels of each protein. Nonetheless, the reporter assays clearly demonstrated that HnoC acts as a strong repressor.

Thus, it is clear that HnoC and the associated transcriptional feedback loop play an important role in fine-tuning the temporal dynamics of the *hno* signaling system and the motility response to NO. Since expression of all signaling genes in the network, including HnoB and HnoD, is influenced by the feedback loop, phosphodiesterase activity and cyclic-di-GMP levels are equally affected. For instance, shifts to high NO concentrations will not only inactivate HnoB and HnoD, but will also lower the expression levels of both proteins. This would accelerate the response time for a build up cyclic-di-GMP concentrations and biofilm formation. In contrast, a shift to lower NO levels could produce a temporary surge in HnoB expression, along with all other signaling proteins. Taking into account the increased phosphotransfer by HnoK, this would intensify the phosphodiesterase activity and accelerate the clearance of cyclic-di-GMP. This is in contrast to a steady-state response, in which the expression of the *hno* component would return to lower levels that do not completely deplete the cyclic-di-GMP pool. Consequently, the transcriptional feedback loop has an important role in regulating the NO response dynamics in the entire network.

References

1. Donlan, R. M., and Costerton, J. W. (2002) Biofilms: survival mechanisms of clinically relevant microorganisms. *Clin. Microbiol. Rev.* **15**, 167–193
2. Costerton, J. W., Stewart, P. S., and Greenberg, E. P. (1999) Bacterial biofilms: a common cause of persistent infections. *Science* **284**, 1318–1322
3. Römling, U., and Balsalobre, C. (2012) Biofilm infections, their resilience to therapy and innovative treatment strategies. *J. Intern. Med.* **272**, 541–561

4. Stanley, N. R., and Lazazzera, B. A. (2004) Environmental signals and regulatory pathways that influence biofilm formation. *Mol. Microbiol.* **52**, 917–924
5. MacMicking, J., Xie, Q. W., and Nathan, C. (1997) Nitric oxide and macrophage function. *Annu. Rev. Immunol.* **15**, 323–350
6. Plate, L., and Marletta, M. A. (2012) Nitric oxide modulates bacterial biofilm formation through a multicomponent cyclic-di-GMP signaling network. *Mol Cell* **46**, 449–460
7. Barraud, N., Schleheck, D., Klebensberger, J., Webb, J. S., Hassett, D. J., Rice, S. A., and Kjelleberg, S. (2009) Nitric oxide signaling in *Pseudomonas aeruginosa* biofilms mediates phosphodiesterase activity, decreased cyclic di-GMP levels, and enhanced dispersal. *J. Bacteriol.* **191**, 7333–7342
8. Carlson, H. K., Vance, R. E., and Marletta, M. A. (2010) H-NOX regulation of c-di-GMP metabolism and biofilm formation in *Legionella pneumophila*. *Mol. Microbiol.* **77**, 930–942
9. Liu, N., Xu, Y., Hossain, S., Huang, N., Coursolle, D., Gralnick, J. A., and Boon, E. M. (2012) Nitric oxide regulation of cyclic di-GMP synthesis and hydrolysis in S*hewanella woodyi*. *Biochemistry* **51**, 2087–2099
10. Price, M. S., Chao, L. Y., and Marletta, M. A. (2007) *Shewanella oneidensis* MR-1 H-NOX regulation of a histidine kinase by nitric oxide. *Biochem.* **46**, 13677–13683
11. Gao, R., and Stock, A. M. (2010) Molecular strategies for phosphorylation-mediated regulation of response regulator activity. *Curr. Opin. Microbiol.* **13**, 160–167
12. Stock, A. M., Robinson, V. L., and Goudreau, P. N. (2000) Two-component signal transduction. *Annu. Rev. Biochem.* **69**, 183–215
13. Galperin, M. Y. (2010) Diversity of structure and function of response regulator output domains. *Curr. Opin. Microbiol.* **13**, 150–159
14. Brown, N. L., Stoyanov, J. V., Kidd, S. P., and Hobman, J. L. (2003) The MerR family of transcriptional regulators. *FEMS Microbiology Reviews* **27**, 145–163
15. Thormann, K. M., Duttler, S., Saville, R. M., Hyodo, M., Shukla, S., Hayakawa, Y., and Spormann, A. M. (2006) Control of formation and cellular detachment from *Shewanella oneidensis* MR-1 biofilms by cyclic di-GMP. *J. Bacteriol.* **188**, 2681–2691
16. Thormann, K. M., Saville, R. M., Shukla, S., and Spormann, A. M. (2005) Induction of rapid detachment in *Shewanella oneidensis* MR-1 biofilms. *J. Bacteriol.* **187**, 1014–1021
17. Miller, W. G., Leveau, J. H., and Lindow, S. E. (2000) Improved gfp and inaZ broad-host-range promoter-probe vectors. *Mol. Plant Microbe Interact.* **13**, 1243–1250
18. Smyth, G. K. (2004) Linear models and empirical bayes methods for assessing differential expression in microarray experiments. *Stat Appl Genet Mol Biol* **3**, Article3
19. Smyth, G. K., and Speed, T. (2003) Normalization of cDNA microarray data. *Methods* **31**, 265–273
20. Ritchie, M. E., Silver, J., Oshlack, A., Holmes, M., Diyagama, D., Holloway, A., and Smyth, G. K. (2007) A comparison of background correction methods for two-colour microarrays. *Bioinformatics* **23**, 2700–2707
21. Edgar, R., Domrachev, M., and Lash, A. E. (2002) Gene Expression Omnibus: NCBI gene expression and hybridization array data repository. *Nucleic Acids Res* **30**, 207–210
22. Buratowski, S., and Chodosh, L. A. (2001) Mobility shift DNA-binding assay using gel electrophoresis. *Curr Protoc Pharmacol* **Chapter 6**, Unit6.8–Unit8
23. Bordi, C., Ansaldi, M., Gon, S., Jourlin-Castelli, C., Iobbi-Nivol, C., and Mejean, V. (2004) Genes regulated by TorR, the trimethylamine oxide response regulator of

Shewanella oneidensis. *J. Bacteriol.* **186**, 4502–4509
24. Andersen, J. B., Sternberg, C., Poulsen, L. K., Bjorn, S. P., Givskov, M., and Molin, S. (1998) New unstable variants of green fluorescent protein for studies of transient gene expression in bacteria. *Appl. Environ. Microbiol.* **64**, 2240–2246
25. Davies, K. M., Lowe, E. D., Vénien-Bryan, C., and Johnson, L. N. (2009) The HupR receiver domain crystal structure in its nonphospho and inhibitory phospho states. *J. Mol. Biol.* **385**, 51–64
26. Lauriano, C. M., Ghosh, C., Correa, N. E., and Klose, K. E. (2004) The sodium-driven flagellar motor controls exopolysaccharide expression in *Vibrio cholerae*. *J. Bacteriol.* **186**, 4864–4874
27. Kenney, L. J. (2002) Structure/function relationships in OmpR and other winged-helix transcription factors. *Curr. Opin. Microbiol.* **5**, 135–141
28. Blanco, A. G., Canals, A., Bernués, J., Sola, M., and Coll, M. (2011) The structure of a transcription activation subcomplex reveals how σ(70) is recruited to PhoB promoters. *EMBO J* **30**, 3776–3785
29. Su, W., Porter, S., Kustu, S., and Echols, H. (1990) DNA-looping and enhancer activity: association between DNA-bound NtrC activator and RNA polymerase at the bacterial glnA promoter. *Proc. Natl. Acad. Sci. USA* **87**, 5504–5508
30. Gusa, A. A., and Scott, J. R. (2005) The CovR response regulator of group A streptococcus (GAS) acts directly to repress its own promoter. *Mol. Microbiol.* **56**, 1195–1207
31. Bailey, T. L., and Elkan, C. (1994) Fitting a mixture model by expectation maximization to discover motifs in biopolymers. *Proc Int Conf Intell Syst Mol Biol* **2**, 28–36
32. Harlocker, S. L., Bergstrom, L., and Inouye, M. (1995) Tandem binding of six OmpR proteins to the ompF upstream regulatory sequence of *Escherichia coli*. *J. Biol. Chem.* **270**, 26849–26856
33. Blanco, A. G., Sola, M., Gomis-Rüth, F. X., and Coll, M. (2002) Tandem DNA recognition by PhoB, a two-component signal transduction transcriptional activator. *Structure* **10**, 701–713
34. O'Halloran, T. V., Frantz, B., Shin, M. K., Ralston, D. M., and Wright, J. G. (1989) The MerR heavy metal receptor mediates positive activation in a topologically novel transcription complex. *Cell* **56**, 119–129
35. Li, J., Kustu, S., and Stewart, V. (1994) In vitro interaction of nitrate-responsive regulatory protein NarL with DNA target sequences in the fdnG, narG, narK and frdA operon control regions of *Escherichia coli* K-12. *J. Mol. Biol.* **241**, 150–165
36. Heldwein, E. E., and Brennan, R. G. (2001) Crystal structure of the transcription activator BmrR bound to DNA and a drug. *Nature* **409**, 378–382
37. Batchelor, J. D., Doucleff, M., Lee, C.-J., Matsubara, K., De Carlo, S., Heideker, J., Lamers, M. H., Pelton, J. G., and Wemmer, D. E. (2008) Structure and regulatory mechanism of *Aquifex aeolicus* NtrC4: variability and evolution in bacterial transcriptional regulation. *J. Mol. Biol.* **384**, 1058–1075
38. Gao, R., Tao, Y., and Stock, A. M. (2008) System-level mapping of *Escherichia coli* response regulator dimerization with FRET hybrids. *Mol. Microbiol.* **69**, 1358–1372
39. Bachhawat, P., Swapna, G. V. T., Montelione, G. T., and Stock, A. M. (2005) Mechanism of activation for transcription factor PhoB suggested by different modes of dimerization in the inactive and active states. *Structure* **13**, 1353–1363

40. McCleary, W. R. (1996) The activation of PhoB by acetylphosphate. *Mol. Microbiol.* **20**, 1155–1163
41. Maris, A. E., Sawaya, M. R., Kaczor-Grzeskowiak, M., Jarvis, M. R., Bearson, S. M. D., Kopka, M. L., Schröder, I., Gunsalus, R. P., and Dickerson, R. E. (2002) Dimerization allows DNA target site recognition by the NarL response regulator. *Nat. Struct. Biol.* **9**, 771–778
42. Da Re, S., Schumacher, J., Rousseau, P., Fourment, J., Ebel, C., and Kahn, D. (1999) Phosphorylation-induced dimerization of the FixJ receiver domain. *Mol. Microbiol.* **34**, 504–511
43. Huang, K. J., Lan, C. Y., and Igo, M. M. (1997) Phosphorylation stimulates the cooperative DNA-binding properties of the transcription factor OmpR. *Proc. Natl. Acad. Sci. USA* **94**, 2828–2832
44. Simon, G., Jourlin, C., Ansaldi, M., Pascal, M. C., Chippaux, M., and Mejean, V. (1995) Binding of the TorR regulator to cis-acting direct repeats activates tor operon expression. *Mol. Microbiol.* **17**, 971–980
45. Ansaldi, M., Simon, G., Lepelletier, M., and Mejean, V. (2000) The TorR high-affinity binding site plays a key role in both torR autoregulation and torCAD operon expression in *Escherichia coli*. *J. Bacteriol.* **182**, 961–966
46. Wisedchaisri, G., Wu, M., Rice, A. E., Roberts, D. M., Sherman, D. R., and Hol, W. G. J. (2005) Structures of *Mycobacterium tuberculosis* DosR and DosR-DNA complex involved in gene activation during adaptation to hypoxic latency. *J. Mol. Biol.* **354**, 630–641
47. Wisedchaisri, G., Wu, M., Sherman, D. R., and Hol, W. G. J. (2008) Crystal structures of the response regulator DosR from *Mycobacterium tuberculosis* suggest a helix rearrangement mechanism for phosphorylation activation. *J. Mol. Biol.* **378**, 227–242
48. Toro-Roman, A., Mack, T. R., and Stock, A. M. (2005) Structural analysis and solution studies of the activated regulatory domain of the response regulator ArcA: a symmetric dimer mediated by the alpha4-beta5-alpha5 face. *J. Mol. Biol.* **349**, 11–26
49. Jeon, Y., Lee, Y. S., Han, J. S., Kim, J. B., and Hwang, D. S. (2001) Multimerization of phosphorylated and non-phosphorylated ArcA is necessary for the response regulator function of the Arc two-component signal transduction system. *J. Biol. Chem.* **276**, 40873–40879
50. Darwin, A. J., Tyson, K. L., Busby, S. J., and Stewart, V. (1997) Differential regulation by the homologous response regulators NarL and NarP of *Escherichia coli* K-12 depends on DNA binding site arrangement. *Mol. Microbiol.* **25**, 583–595
51. Brandman, O., and Meyer, T. (2008) Feedback loops shape cellular signals in space and time. *Science* **322**, 390–395
52. Mitrophanov, A. Y., and Groisman, E. A. (2008) Positive feedback in cellular control systems. *Bioessays* **30**, 542–555
53. Ma, W., Trusina, A., El-Samad, H., Lim, W. A., and Tang, C. (2009) Defining network topologies that can achieve biochemical adaptation. *Cell* **138**, 760–773
54. Rosenfeld, N., Elowitz, M. B., and Alon, U. (2002) Negative autoregulation speeds the response times of transcription networks. *J. Mol. Biol.* **323**, 785–793
55. Alon, U. (2007) Network motifs: theory and experimental approaches. *Nat Rev Genet* **8**, 450–461
56. Thieffry, D., Huerta, A. M., Pérez-Rueda, E., and Collado-Vides, J. (1998) From specific

gene regulation to genomic networks: a global analysis of transcriptional regulation in *Escherichia coli*. *Bioessays* **20**, 433–440
57. Goulian, M. (2010) Two-component signaling circuit structure and properties. *Curr. Opin. Microbiol.* **13**, 184–189
58. Shin, D., Lee, E. J., Huang, H., and Groisman, E. A. (2006) A Positive Feedback Loop Promotes Transcription Surge That Jump-Starts Salmonella Virulence Circuit. *Science* **314**, 1607–1609
59. Hoffer, S. M., Westerhoff, H. V., Hellingwerf, K. J., Postma, P. W., and Tommassen, J. (2001) Autoamplification of a two-component regulatory system results in "learning" behavior. *J. Bacteriol.* **183**, 4914–4917
60. Becskei, A., and Serrano, L. (2000) Engineering stability in gene networks by autoregulation. *Nature* **405**, 590–593
61. Mitrophanov, A. Y., Churchward, G., and Borodovsky, M. (2007) Control of *Streptococcus pyogenes* virulence: modeling of the CovR/S signal transduction system. *J. Theor. Biol.* **246**, 113–128
62. Miyashiro, T., and Goulian, M. (2008) High stimulus unmasks positive feedback in an autoregulated bacterial signaling circuit. *Proc. Natl. Acad. Sci. USA* **105**, 17457–17462
63. Ray, J. C. J., and Igoshin, O. A. (2010) Adaptable functionality of transcriptional feedback in bacterial two-component systems. *PLoS Comput. Biol.* **6**, e1000676

CHAPTER 4:

BIOCHEMICAL CHARACTERIZATION OF HD-GYP METAL-DEPENDENT PHOSPHOHYDROLASES OF CYCLIC-DI-GMP

Summary

HD-GYP domains constitute an important family of cyclic-di-GMP phosphodiesterases. Several response regulators with HD-GYP domains occur in H-NOX/NO signaling pathways, and the role of the HD-GYP protein HnoD has been studied in **Chapter 2**. HnoD is a degenerate HD-GYP domain and not catalytically active. However, very little is known about the structure and mechanism of catalytically active HD-GYP enzymes. To comprehend why HnoD is catalytically inactive, this chapter is directed at determining the sequence, structure and cofactor requirements necessary for HD-GYP activity. Two thermophilic HD-GYP proteins were isolated, the cyclic-di-GMP phosphodiesterase reaction was characterized, and the products were identified. Furthermore, the role of a binuclear metal center in enzyme catalysis was investigated.

Introduction

Cyclic diguanosine monophosphate (cyclic-di-GMP) is a widespread secondary messenger molecule that is unique to bacteria (1, 2). Although originally identified as an allosteric activator of cellulose biosynthesis in *Acetobacter xylinum* (3), it is now known as an important signaling compound controlling the motility behavior of bacteria and facilitating a change from a planktonic to a sedentary lifestyle in surface-adhered biofilms (1). In addition, cyclic-di-GMP controls a variety of other bacterial processes, including virulence and cell cycle progression (1, 4-6). Furthermore, cyclic-di-GMP can act as an immunomodulator (7) and is a target of innate immune recognition (8)

Cyclic-di-GMP is synthesized by diguanylate cyclases (DGCs), which contain GGDEF domains, named after the conserved sequence motif. In turn, phosphodiesterase (PDE) proteins hydrolyze the messenger molecule. Two separate families of PDEs, containing either an EAL or HD-GYP domain, are known (1, 9). Bacteria often contain large numbers of DGC and PDE proteins, all of which are controlled by diverse signaling pathways. The intracellular cyclic-di-GMP concentration serves as an integration point for the various signals (1). For example, **Chapter 2** discussed the NO sensing H-NOX signaling network, which controls biofilm formation through inactivation of a PDE response regulator (10). The function and regulation of GGDEF domains and the mechanism for cyclic-di-GMP synthesis are well understood from biochemical and structural studies (9, 11-13). Likewise, EAL domains have been studied extensively. Structure determination of several EAL proteins showed a TIM-barrel fold with a site for metal and cyclic-di-GMP binding at the end of the barrel (14). Catalysis is dependent on Mg(II) or Mn(II), and a two-metal-ion mechanism has been proposed in which a bridging water between the metal ions is activated for nucleophilic attack (15). However, this mechanism is

contested because some EAL structures only show one metal ion (9, 16). In contrast to GGDEF and EAL domains, the structure and function of HD-GYP PDEs is much less understood (9).

Genome analyses first identified a subfamily of HD metal-dependent phosphohydrolases. This HD-GYP subfamily, named after two conserved sequence motifs (Fig. 4.1.C), was associated with other cyclic-di-GMP signaling proteins. This suggested a function as a cyclic-di-GMP-specific PDE (17). Despite their widespread occurrence in bacterial genomes, HD-GYP PDEs have been characterized in few organisms. Several genetic studies have focused on the HD-GYP protein RpfG from the plant pathogen *Xanthomonas campestris*, which controls virulence through a cyclic-di-GMP dependent process (18-21). Decreased virulence and infection of HD-GYP deletion strains have also been observed in *Pseudomonas aeruginosa* and *Borrelia burgdorferi* (22, 23). Further, a connection between quorum sensing and HD-GYP-mediated cyclic-di-GMP signaling has been demonstrated in *Vibrio cholerae* (24).

Nonetheless, very little is known about the structure and mechanistic function of HD-GYP domains. RpfG is the only family member that has been isolated and studied *in vitro* (19). RpfG was shown to hydrolyze cyclic-di-GMP to GMP, and mutations of the histidine and aspartic acid in the HD motif eliminated enzyme activity. The importance of the aspartic acid residue for activity was confirmed in *V. cholerae* VCA0681, although the effect was measured *in vivo* and not with the isolated enzyme (25). Sultan *et al.* have recently reported measurements of cyclic-di-GMP PDE activity by the HD-GYP protein BB0374 in *Borrelia burgdorferi* cell lysates (23). However, sequence alignment with other HD-GYP domains shows that BB0374 is missing several conserved residues, including the aspartic acid of the HD motif (Fig. 4.1.C). As a result, it is unlikely that BB0374 is catalytically active, and therefore, the observed PDE activity is probably associated with a different enzyme in the *B. burgdorferi* lysate. Other HD-GYP proteins with degenerate sequence motifs (Fig. 4.1.C, shaded green) are involved in cyclic-di-GMP-controlled processes despite their lack of PDE activity (10, 22). For example as described in **Chapter 2**, the HD-GYP response regulator HnoD was shown to allosterically inhibit the PDE activity of the EAL protein HnoB (10). HnoD orthologs from several organisms (*S. oneidensis* HnoD, *V. cholerae* HnoD, *P. aeruginosa* PA2572, Fig. 4.1.C) are missing some of the conserved residues in the HD-GYP motif. But the determinants responsible for the lack of activity are not clear without first understanding the mechanistic details of active HD-GYP protein.

The recent crystal structure of a degenerate and catalytically inactive HD-GYP protein (BD1871 from *Bdellovibrio bacteriovorus*) shed some light on the function of HD-GYP proteins (Fig. 4.1.A) (26). The structure showed a binuclear metal center composed of two Fe atoms (Fig. 4.1.A), and the conserved residues involved in metal coordination were identified. (Fig. 4.1.B-C, residues marked by blue triangles in C). A bridging phosphate group and μ-hydroxyl group were observed between the two Fe ions, which are aligned in a suitable orientation for nucleophilic attack on the phosphate to initiate hydrolysis of phosphodiester bonds (Fig. 4.1.B). Unfortunately, the BD1817 HD-GYP domain is catalytically inactive and does not bind c-di-GMP, which is likely due to the missing tyrosine in the GYP motif (Fig. 4.1.C). Therefore, any other information derived from the structure on PDE enzyme function and cyclic-di-GMP binding is largely speculative.

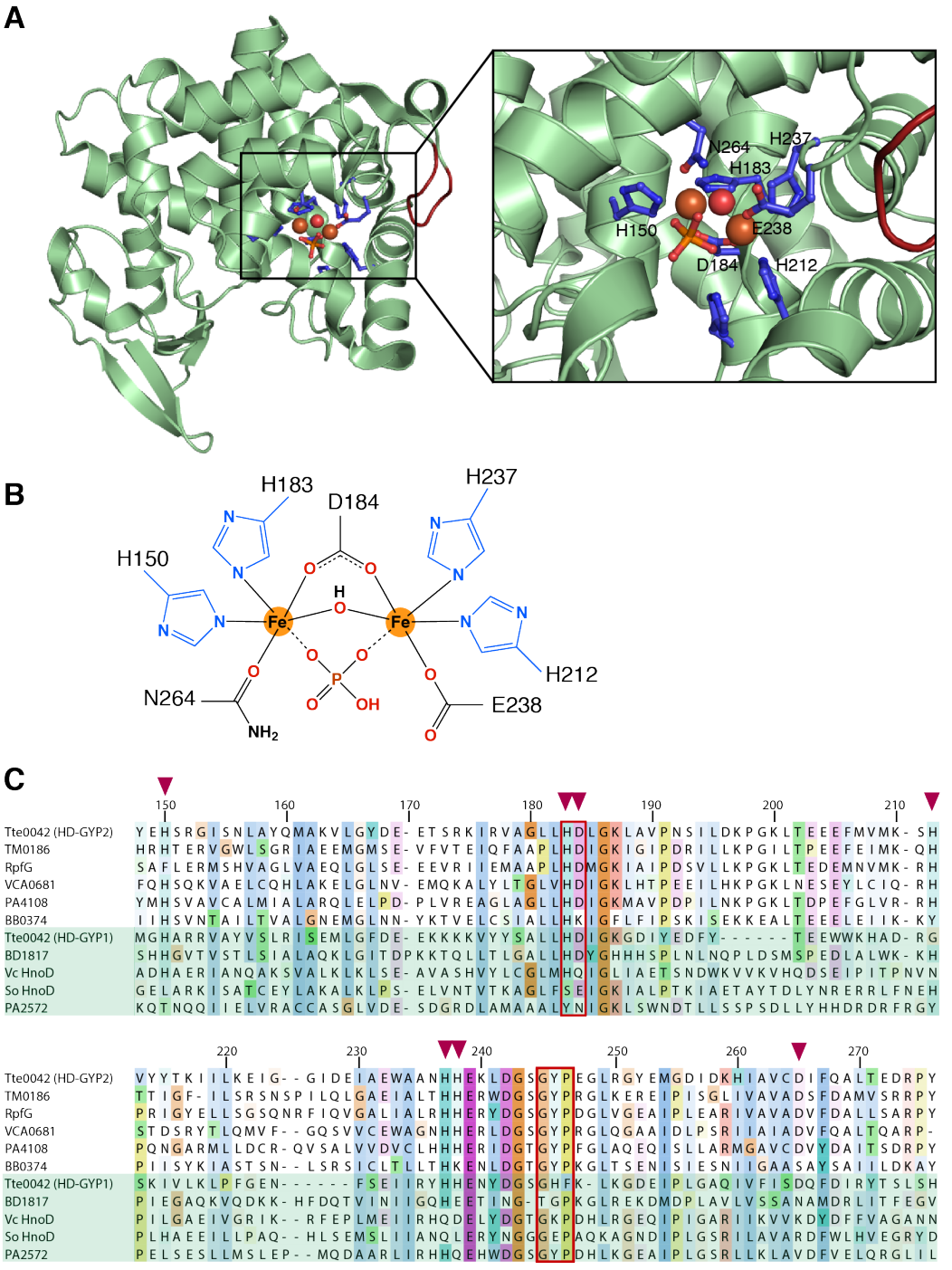

Fig. 4.1. Crystal structure and sequence alignment of HD-GYP domains

A. Crystal structure of the degenerate HD-GYP domain of BD1817 (PDB ID: 3TM8). The inlet shows the diiron center with the metal-coordinating residues highlighted.

B. Scheme of the metal-binding site of BD1817.

C. Sequence alignment of bacterial HD-GYP domains. Numbering is based on BD1817. The HD and GYP motif are boxed in red. Metal-coordinating residues are highlighted by purple triangles. The proteins shaded in green contain degenerate HD-GYP motifs.

To gain further mechanistic insight into the function of HD-GYP domains, two catalytically active family members from thermophilic organisms were isolated and biochemically characterized in the studies reported here. UV/vis spectroscopy and metal-binding analysis confirmed the presence of a binuclear iron center. Furthermore, the PDE enzyme activity of the HD-GYP proteins was determined, and the requirements for metal-coordination and the correct redox state were investigated.

Experimental Procedures

Cloning of TTE0042 and TM0186

TTE0042 and TM0186 genes were PCR-amplified from *Thermotoga maritima* genomic DNA[2]. Sequences of all primers used in this chapter can be found in Table 4.1. The PCR products and pET28b plasmid were restriction digested with NotI and NheI or NdeI and were ligated to yield His_6-TEV cleavable expression constructs for both HD-GYP proteins. To obtain expression constructs containing *N*-terminal His_6-MBP tags, the respective PCR products were cloned into pENTR/TEV/D-TOPO by TOPO cloning and subsequently transferred into pHMGWA (27). Boundaries for the $TM0186_{HD\text{-}GYP}$ construct were based on the NCBI annotation and a secondary structure prediction to place the truncation sites in predicted loops outside the HD-GYP domain. The sequences of all expression plasmids were verified.

Table 4.1. Sequence of primers used in this chapter.

Primer Name	Sequence
TM0186-NheI-f	CTAGCTAGCATGACAGTACTGATCGTGGAAG
TM0186-NotI-r	ATAGTTTAGCGGCCGCTTAACGAATACCCTCCACACC
TTE0042-NheI-f	CTAGCTAGCATGAATTTGAGTTACAATAATCTATTGTCAGC
TTE0042-NotI-r	ATAGTTTAGCGGCCGCTTAAAAAACCACTTTTTTCAAAATTTCC
TM0186pENTR-f	CACCATGACAGTACTGATCGTGGAAG
TM0186pENTR-r	TTAACGAATACCCTCCACACC
TM0186-170pENTR-f	CACCACACACAGACACACAGAGAGG
TM0186-341pENTR-r	TTACCTGTAGACATCGGTTATTTC
TTE0042pENTR-f	CACCATGAATTTGAGTTACAATAATCTATTGTCAGC
TTE0042pENTR-r	TTAAAAAACCACTTTTTTCAAAATTTCC
TM0186-170-NdeI-f	GGAATTCCATATGACACACAGACACACAGAGAGG
TM0186-341-NotI-r	ATAGTTTAGCGGCCGCTTACCTGTAGACATCGGTTATTTC

Expression and purification of HD-GYP proteins

The expression plasmids for each protein were transformed into *E. coli* Tuner (DE3) pLysS expression strain. Bacteria were grown in expression media (45 g/L yeast extract, 11.7 mM monobasic potassium phosphate, 50.3 mM dibasic potassium phosphate) containing 50 μg mL^{-1} kanamycin and 30 μg mL^{-1} chloramphenicol. Protein expression was induced at 25 ºC with 50 μM final concentration of IPTG. Cells were harvested by centrifugation after 20 hours of

[2] *T. maritima* genomic DNA was a generous gift from Dr. Rosalind Kim at LBNL.

growth. Cell pellets were resuspended in lysis buffer (50 mM DEA pH 8.0, 10% glycerol, 300 mM NaCl, 1 mM DTT supplemented with DNAseI, pefabloc, and benzamidine). For Ni-NTA purification, 20 mM imidazole was added. For TALON purifications, 5 mM imidazole was added and the NaCl concentration was raised to 500 mM. For MBP-tagged protein, the lysis buffer was 50 mM Tris pH 8.0, 10% glycerol, 150 mM NaCl, 1 mM β-mercaptoethanol, supplemented with DNAseI, pefabloc and benzamidine. Cells were lysed by passage through a high-pressure homogenizer (Avestin). The lysate was centrifuged at 200,000 g for 45 min in an Optima XL-100K ultracentrifuge with a Ti-45 rotor (Beckman). The supernatant was loaded onto a column containing either Ni-NTA agarose resin (Qiagen), TALON resin (Clontech), or amylose resin (NEB). The columns were washed with 20 column volumes of lysis buffer. Protein was eluted from the respective columns with lysis buffer, which contained either 250 mM imidazole, 50 mM imidazole, or 50 mM maltose. Approximately one third of the protein samples were concentrated and exchanged into storage buffer (50 mM Tris pH 8.0, 5% glycerol, 150 mM NaCl) by passage through a PD-10 desalting column. The other two thirds were treated with TEV protease at a 1:10 to 1:20 dilution (based on A_{280nm}) and dialyzed overnight into TEV cleavage buffer (50 mM Tris pH 8.0, 50 mM NaCl, 5% glycerol, 1 mM DTT). Ni-NTA or TALON resin was equilibrated with the lysis buffer, and the TEV-digested protein samples were passed over the columns. The columns were washed with 5 volumes of the lysis buffer. The supernatant and the wash fraction were combined and concentrated to less than 5 mL. The proteins were further purified and exchanged into storage buffer by size-exclusion chromatography on a Superdex S200 16/60 column (TTE0042, TM0186) or on a S75 16/60 column ($TM00186_{HD\text{-}GYP}$). Protein aliquots were flash-frozen in liquid nitrogen and stored at -80 ºC.

Inductively coupled plasma atomic emission spectroscopy (ICP-AES) and UV/vis spectroscopy

Protein concentrations were determined by Bradford assay. Protein samples (5 µM) were injected into an ICP-AES AAS 3100 (Perkin Elmer) at 1 mL/min and analyzed for different metals at pre-selected emission wavelengths. Standard curves for each metal were generated from dilutions of reference standard solutions (Fisher) prepared in 0.1 % nitric acid. For UV/vis spectra, protein samples were diluted into storage buffer. Spectra were recorded in 500 µL quartz cuvettes on a Cary 4E UV-visible spectrophotometer (Agilent).

Cyclic-di-GMP hydrolysis assays

Cyclic-di-GMP was synthesized enzymatically (28). A pGpG standard was purchased from Biolog. Purified HD-GYP protein (1-50 µM) was incubated in assay buffer (50 mM DEA pH 8.0, 150 mM NaCl, 5% glycerol) at 37ºC for 5 min, and the reactions were initiated by addition of 0.5 mM c-di-GMP. If necessary, tryptophan (1 mM) or cXMP (0.25 mM) internal standards were included. Initially, reactions were performed at room temperature, but the assay temperature was later raised to 37 ºC. Aliquots (10 µL) were quenched at different time points by addition of 25 µL trifluoroacetic acid (2%) and rigorous vortexing. Initially, the samples were neutralized by addition of 0.5 M KOH, though this step was later deemed unnecessary. The volumes were adjusted to 100 µL, and the samples were filtered and analyzed by HPLC on a Nova-Pak C18 4 µm (3.9 x 150 mm) column at a flow rate of 1 mL/min using the following gradient: 0-6 min: 20 mM ammonium acetate – 5% acetonitrile; 7.5 min: 15 % acetonitrile; 8.4-9

min: 100% acetontrile; 9.1-13.5 min: 20 mM ammonium acetate. pGpG formation was calculated from peak integration and a standard curve of pGpG.

Metal reduction and Ferrozine assay

HD-GYP protein (400 µL, 4 mg mL^{-1}) was degassed by at least 5 cycles of vacuum and argon flushes. Proteins samples were brought into an anaerobic glovebag and split into aliquots. Fresh reductant stock solutions (0.1 M) of TCEP, sodium ascorbate, sodium dithionite, and β-mercaptoethanol were prepared in anaerobic buffer (50 mM DEA pH 8.0, 150 mM NaCl, 5% glycerol) inside the glovebag. Reductants (5 mM final concentration) were added, and the HD-GYP samples were incubated for 24 hours at room temperature inside the glovebag. Protein samples were passed over PD-10 desalting columns to remove excess reducing agent. Protein concentrations were determined by Bradford assay.

The ferrozine assay was based on a literature protocol (29). HD-GYP protein (40 µL, approximately 2.5 – 4 mg mL^{-1}) was mixed with 80 µL 8M guanidine HCl, 50 mM Tris pH 8.0, 50 mM NaCl in a quartz microcuvette. The blank absorbance was recorded on a spectrophotometer at 562 nm. The denatured protein solution (110 µL) was mixed with 10 µL ferrozine solution (10 mM ferrozine in 100 mM ammonium acetate) and the A1 absorbance was recorded. Next, 110 µL were removed from the cuvette and mixed with 20.6 µL hydroxylamine solution (1.4 M hydroxylamine in 2 M HCl) to reduce all ferric to ferrous iron. After 10 min, 13.8 µL of 5 M ammonium acetate at pH 9.5 (adjusted with ammonium hydroxide) was added and the A2 absorbance was measured. A standard solution of 20 mM $FeCl_3$ in 10 mM HCl was prepared. This solution was further diluted to 100, 50, 20, 10, and 5 µM Fe(III) in water. These standard samples were treated as the protein samples, and the blank, A1, and A2 absorbances were measured. After subtraction of the blank, A1 and A2 absorbance were plotted against iron concentration and fitted to linear curves:

[1] $A1 = m_{A1} c_{Fe}$

[2] $A2 = m_{A2} c_{Fe}$

Solving the linear equation in (29) for $c_{Fe(II)}$ and $c_{Fe(III)}$ results in the following formulas for calculating the concentration of iron species based on the A1 and A2 absorbances and slopes of (1) and (2):

[3] $c_{Fe(II)} = \frac{A1 m_{A2} - A2 m_1}{m_{A2}(m_{A2}/\alpha - m_{A1})}$, where α is the dilution factor between A1 and A2 measurements, in this case 0.762

[4] $c_{Fe(III)} = \frac{A2 - A1\alpha}{m_{A2} - m_{A1}\alpha}$

Metal reconstitutions

HD-GYP protein samples (50 µM) were incubated with 2-fold excess (100 µM) $MnCl_2$, $FeCl_3$, $NiCl_2$, $CuCl_2$, $ZnCl_2$, $CoCl_2$ on ice for 2 hours. For reconstitution with Fe(II), the proteins were degassed as described above and brought into a glovebag. A solution of ferrous ammonium sulfate (0.1 M) was prepared in anaerobic water. The samples were treated with 2-fold excess metal and incubated inside the glove bag for 2 hours. After incubation, each enzyme sample (20 µM) was mixed with cyclic-di-GMP (1 mM). Production of pGpG was measured by HPLC as described above. For the Fe(II) reconstitution time course, a TTE0042 sample was reconstituted

in the same way, and protein aliquots (5 μM) were assayed for pGpG product at 1, 3, 5, and 21 hour time points.

Results and Discussion

Purification of HD-GYP proteins and characterization of metal binding

Two HD-GYP proteins with different domain architectures were selected for biochemical characterization: TTE0042 from *T. tengcongensis,* and TM0186 from *T. maritima*. TTE0042 consists of two HD-GYP domains, an N-terminal degenerate domain containing HD-GFH residues (Fig. 4.1.B, TTE0042(HD-GYP1)), and a C-terminal "true" HD-GYP domain (Fig. 4.1.B, TTE0042 (HD-GYP2); Fig. 4.2.A.). TM0186 is a response regulator containing a C-terminal receiver domain (REC) followed by an HD-GYP domain (Fig. 4.2.A). In addition, truncations containing only the HD-GYP domains of TTE0042 and TM0186 were constructed, consisting of residues 227-390 and 170-341, respectively. All protein constructs contained an N-terminal TEV-cleavable His_6 affinity tag. Proteins were expressed recombinantly in *E. coli* and the following three-step purification protocol was executed: Ni-NTA affinity purification, TEV cleavage of the His_6 tag followed by a subtractive Ni-NTA affinity step, and finally size-exclusion chromatography. The TTE0042 and TM0186 full-length constructs were purified to greater than 90% purity, as determined by SDS-PAGE (Fig. 4.2.B). However, of the HD-GYP domain truncations, only the TM0186 construct (hereafter called $TM0186_{HD\text{-}GYP}$) could be expressed as soluble protein and purified. The TTE0042 HD-GYP2 truncation construct was overexpressed, but formed insoluble inclusion bodies (data not shown). The poor solubility could be the result of improperly chosen truncation points, which may not fall in loop regions between protein domains. The boundaries were determined when the crystal structure of the BD1817 HD-GYP had not yet been published. Instead, the domain boundaries were based on the NCBI annotation and secondary structure prediction. If an HD-GYP2 truncation of TTE0042 is needed in the future, for example for crystallization trials, the alignment with BD1817 (Fig. 4.1.B) could help to identify better boundaries of a truncation.

HD-GYP proteins belong to the HD superfamily containing divalent cation-dependent phosphohydrolases (17, 30). Therefore, it is likely that HD-GYP proteins also coordinate cations and require metal binding for catalysis. Many metal centers in proteins display characteristic UV/vis absorption spectra. Therefore, the purified HD-GYP proteins were first characterized by UV/vis spectroscopy. In addition to the protein absorption peak at 280 nm, TTE0042 displayed two absorptions peaks at 327 nm ($\varepsilon \sim 9.8\ mM^{-1}$) and 375 nm ($\varepsilon \sim 7.8\ mM^{-1}$) and a shoulder at 495 nm ($\varepsilon \sim 1.3\ mM^{-1}$) (Fig. 4.3.A). TM0186 displayed similar absorption features in the 300 – 400 nm region. However, the peaks were not well resolved: two shoulders formed, and the extinction coefficients were approximately half of those for TTE0042 (Fig. 4.3.A). Intriguingly, the absorbance features in the 300 – 500 nm region resemble those of other characterized diiron metalloproteins. In particular, the split peaks are indicative of a diiron(III) (μ-oxo) species as, for example, in the met-form of class Ia ribonucleotide reductase or in the methydroxo state of hemerythrin (31, 32). The absorption spectra also match features observed in model (μ-oxo)(μ-carboxylato) diiron(III) complexes containing varying ligands (33). These spectrophotometric

observations serve as a first indication that the isolated HD-GYP proteins contain a diiron(III) cluster with a bridging oxide.

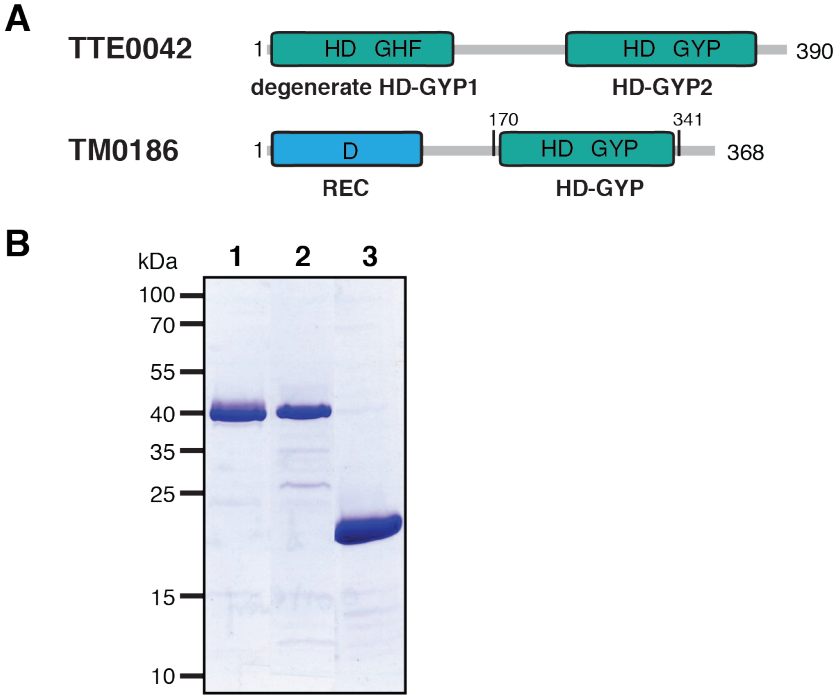

Fig. 4.2. Purification of two thermophilic HD-GYP proteins
A. Domain architecture of TTE0042 and TM0186.
B. SDS-PAGE of purified TTE042 (lane 1), TM0186 (lane 2) and $TM0186_{HD\text{-}GYP}$ (lane 3).

To confirm the identity of the bound metal and quantify the metal stoichiometry, the purified protein samples were analyzed by inductively coupled plasma atomic emission spectroscopy (ICP-AES). The binding of common divalent cations (Mg, Mn, Fe, Ni, Cu, Zn, Co) was tested. TTE0042 contained approximately 1.5 equivalents of Fe per protein after the first elution from the Ni-NTA column. The protein also contained minor amounts (0.1–0.2 equivalents) of Mn, Ni and Zn (Fig. 4.3.B, green bars). TM0186 contained smaller amounts of Fe (1.0 equivalents) than TTE0042, but also had similar trace amounts of Ni and Zn. It was then tested whether the metal ions remain bound to the protein throughout the TEV cleavage procedure and size-exclusion chromatography (SEC). The metal content was again assessed after the purification steps. Fe-content in TTE0042 increased to 2.1 equivalents, which likely arose from removal of protein impurities (Fig. 4.3.B-C, blue bars). In contrast, Fe-content in TM0186 decreased to 0.6 equivalents, indicating metal loss throughout the purification. Metal binding to $TM0186_{HD\text{-}GYP}$ was also tested. However, the sample contained even less Fe than TM0186 (0.8 equivalents after Ni-NTA column) and lost all Fe after SEC (data not shown).

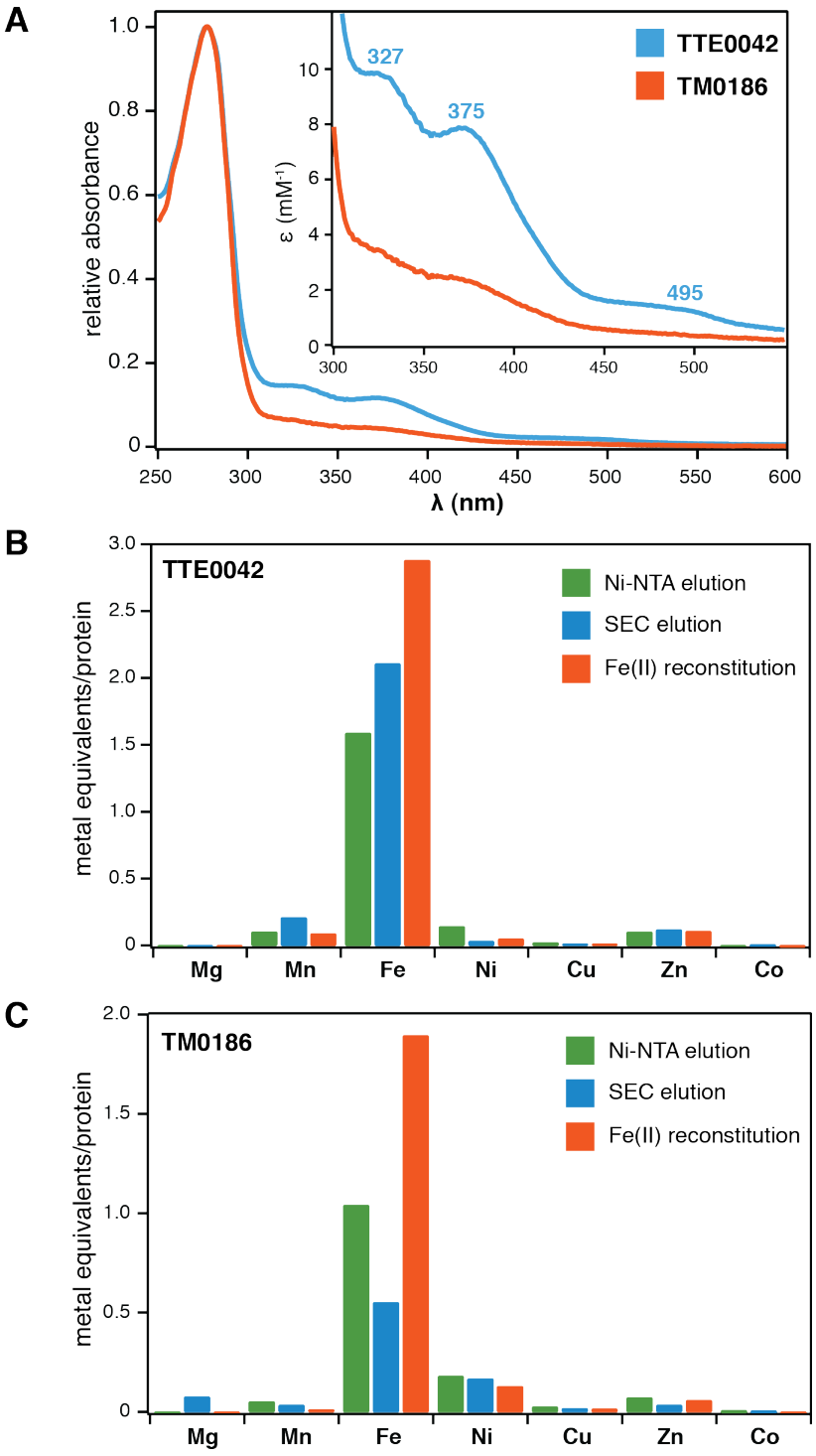

Fig. 4.3. Characterization of metal-binding by HD-GYP proteins
A. UV/vis absorption spectroscopy of TTE0042 and TM0186.
B-C. ICP-AES analysis to determine metal content of purified TTE0042 (B) and TM0183 (C).

Based on other members of the HD superfamily and the crystal structure of BD1817, a stoichiometry of 2 metals per HD-GYP domain is expected. Although TTE0042 HD-GYP1 is degenerate, the domain contains all of the predicted metal-coordination residues (Fig. 4.1.B-C). TTE0042 should therefore be capable of coordinating 4 equivalents of Fe in total: 2 equivalents per HD-GYP domain. TM0186 is predicted to bind 2 equivalents. Accordingly, the isolated HD-GYP proteins contained sub-stoichiometric amounts of metal. Metal reconstitution with Fe(II) was carried out to test whether the Fe content can be increased. Anaerobic samples were incubated with 10 equivalents of Fe(II) and subsequently, the excess iron was removed by gel filtration. ICP-AES analysis showed that the iron content of TTE0042 and TM0186 increased to 2.9 and 1.9 equivalents, respectively (Fig. 4.3.B-C, orange), indicating that iron binding can be partially restored to the predicted level.

Taken together, The ICP-AES and UV/vis characterization confirmed that the two isolated HD-GYP proteins contained a diiron center. The lower extinction coefficient in the UV/vis spectrum of TM0186 is consistent with lower iron incorporation as measured by ICP-AES. Given the loss of metal throughout the purification, the iron seemed to be more weakly associated to TM0186 than to TT0042. An involvement of imidazole in the loss of iron can be excluded because MBP-fusions of the HD-GYP proteins lost Fe to a similar degree. The fusion proteins were purified over amylose affinity resin and did not require the imidazole elution step. Nonetheless, reconstitution experiments indicated that iron binding can be restored with Fe(II). Reconstitution with Fe(III) led to much higher iron contents, indicative of non-specific metal binding to the protein, which is a known obstacle for reconstitution with Fe(III). Interestingly, small amounts of other metals were found associated to HD-GYP proteins (Fig. 4.3.B-C), in particular Mn, Ni, and Zn. TT0042 and TM0186 were also purified on TALON resin, which contains Co(II) as the immobilized affinity matrix. In this case, significant Co binding to TTE0042 and TM0186 (0.3 and 0.6 equivalents, respectively) could be observed. These observations raise the possibility that the Fe in the HD-GYP metal center can be replaced by different metal ions, most likely divalent cations, given the association of Zn(II), Ni(II), and Co(II). Substitution of similar metal ions has been observed in many other metalloenzymes and can restore enzyme activity in some cases (34-38)

The observation of a diiron center in TTE0042 and TM0186 is in agreement with the crystal structure of BD1817. RpfG from *X. campestris* is the only other HD-GYP protein that has been purified to homogeneity and shown to be enzymatically active. (19). However, UV/vis spectra and metal content were not reported. The diiron center in BD1817 was reported to contain a bridging hydroxide, consistent with the Fe-O bond-length observed (26). In contrast, the UV/vis spectrum of TTE0042 was more similar to that of μ-oxo diiron(III) cluster as found in many diiron proteins and model complexes (31-33). Another uncertainty was the oxidation state of the metal ions. Further studies with X-ray absorption, EPR and Mössbauer spectroscopy should be performed to gain more detailed insights on the coordination environment and redox state of the iron center.

Cyclic-di-GMP phosphodiesterase activity of HD-GYP proteins

Cyclic-di-GMP phosphodiesterase activity of a purified HD-GYP protein has only been demonstrated for RpfG from *X. campestris* (19). Measurements of enzyme activity for other

family members was indirect (22-24). To test the activity of the isolated TTE0042 and TM0186 and to identify the reaction products, the phosphodiesterase HPLC assay developed in chapter 2 was used. When TTE0042 and TM0186 were incubated with cyclic-di-GMP for one hour, most of the substrate was turned over, as indicated by the disappearance of the peaks corresponding to cyclic-di-GMP peaks in the HPLC traces (Fig. 4.4.A). Product peaks appeared, which eluted at a similar retention time to pGpG. Liquid chromatography-mass spectrometry (LC-MS) confirmed that the reaction product was pGpG (Fig. 4.4.C). In prior work, RpfG was shown to convert cyclic-di-GMP to GMP, thus hydrolyzing both phosphodiester bonds (19). However, no GMP formation was observed in this study. A small byproduct was observed eluting at approximately 15.5 minutes. The molecule was identified as GpG by LC-MS (Fig. 4.4.C). This suggested that TTE0042 and TM0186 could partially hydrolyze the phosphomonoester bond of the product. However, the enzymes were unable to break the second phosphodiester bond. In the future, it will be interesting to determine whether diverse HD-GYP family members truly produce different product.

Specific activities of pGpG formation for different HD-GYP samples were measured. Given the observed loss of iron, in particular for TM0186 throughout the purification procedure, the effect on enzyme activity was investigated. Directly after elution from the TALON column, TTE0042 had a specific activity of 84 (μmol pGpG) $(min)^{-1}$ (μmol of protein)$^{-1}$ and TM0186 had an equally high specific activity of 99 (μmol pGpG) $(min)^{-1}$ (μmol of protein)$^{-1}$ (Fig. 4.4.B). A subsequent gel filtration step to remove the imidazole from the buffer significantly lowered the specific activity of proteins (2.1 and 38 min^{-1}, respectively). Further purification of both proteins also lowered the activity dramatically (4.9 and 2.2 min^{-1}). In comparison, the $TM0186_{HD\text{-}GYP}$ construct was hardly active after the TALON purification step (0.9 min-1) and the activity became undetectable after further purification steps. Specific activities of different protein batches would vary noticeably. Nonetheless, the same trend - disappearance of activity throughout the purification procedure – was always observed.

Loss of activity of TM1086 can be at least partially explained by the dissociation of iron during the purification. However, the severe drop in specific activity for TTE0042 must be due to something else since the iron content remained similar throughout the purification.

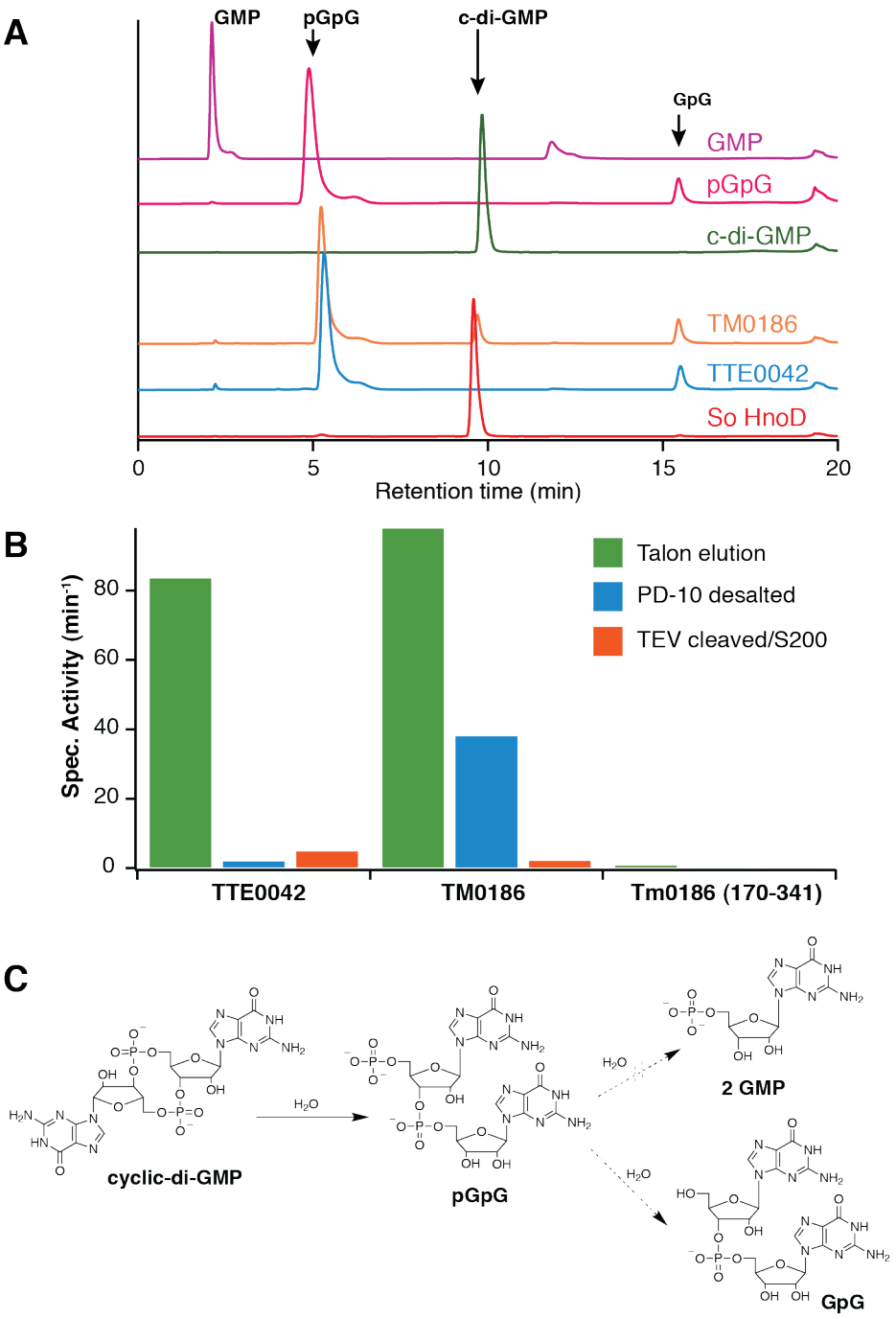

Fig. 4.4. Cyclic-di-GMP phosphodiesterase activity of HD-GYP enzymes

A. HPLC chromatogram monitoring products of HD-GYP reactions at 253 nm. Each HD-GYP (50 µM) was incubated with 1 mM cyclic-di-GMP for 1 h at room temperature. Standard compounds are shown above.

B. Measurements of specific enzyme activities throughout protein purification. Specific activity is reported as (µmol pGpG) $(min)^{-1}$ (µmol protein)$^{-1}$.

C. Chemical structures of cyclic-di-GMP substrates and pGpG and GpG products.

Reconstitution of metal center required for catalysis

While metal occupancy is clearly one requirement for catalysis, the correct oxidation state of the binuclear metal center is also important. Precedence from other binuclear metallohydrolases demonstrates that a mixed valence oxidation state is needed for catalytic activity (37). For example, purple acid phosphatases (PAPs) are well characterized phosphohydrolases with a requirement for a heterovalent Fe(III)-M(II) dimetal center where the divalent cation (M) can be either Fe, Zn, or Mn (37). Likewise, the protein phosphatase calcineurin (PP2B) contains a heterovalent Fe(III)-Zn(II) center. The Fe(III)-Fe(II) substituted enzyme is also active, while oxidation to the diferric state decreases activity (39, 40). For PAPs, it has been well documented that the oxidized diiron(III) state is catalytically inactive, but activity can be restored by incubation with Fe(II) in the presence of a reductant (β-mercaptoethanol or ascorbic acid) (35, 38, 41). Consequently, a likely explanation for the loss of HD-GYP enzymatic activity throughout the purification was oxidative inactivation of the metal-center.

Based on this hypothesis, different approaches for restoration of TTE0042 and TM0186 enzyme activity were tested. The ICP-AES measurements demonstrated that the metal coordination sites of TTE0042 and TM0186 as isolated were not fully occupied (Fig. 4.3.B-C). Therefore, divalent cations were added to examine whether the active form of the HD-GYP enzymes could be regenerated. In addition to Fe(II), a panel of other divalent cations was tested (Co, Mn, Ni, Cu, Zn). TTE0042 and TM0186 samples were incubated with 2-fold excess of each metal ion for 2 hours and cyclic-di-GMP hydrolysis was subsequently measured. The tested batch of TTE0042 and TM0186 used for the experiment was completely inactive before metal addition. For TTE0042, addition of Fe(II) significantly restored activity (Fig. 4.5.A). Several other divalent cations - Mn(II), Ni(II), Cu(II) and Zn(II) - were also able to restore activity to 40–60% of the Fe(II) activity. In contrast, Co(II) and Fe(III) were unable to stimulate cyclic-di-GMP hydrolysis. TM0186 activity could not be restored with any of the metals tested (data not shown). To obtain information on the kinetics of TTE0042 activation with Fe(II), the reconstitution was repeated, and samples were drawn at different time points to measure cyclic-di-GMP hydrolysis. The specific activity was unchanged after 1 hour but increased 4.5-fold after 3 hours (Fig. 4.5.B). Further incubation up to 21 hours did not increase the activity.

To determine the oxidation state of the protein-bound iron in TTE0042, the ferrozine method was used to discriminate between Fe(II) and Fe(III) (29). TTE0042 as isolated contained 1.8 equivalents of Fe(III) and only 0.1 equivalents of Fe(II), confirming that most of the protein-bound iron center becomes oxidized throughout the purification. After the addition of Fe(II), the enzyme contains 0.9 equivalents of Fe(II) and 2.7 equivalents of Fe(III), demonstrating incorporation of ferrous iron. The increased enzymatic activity after addition of ferrous iron is therefore likely caused by partial reconstitution of an active Fe(III)-Fe(II) center in the TT0042 active site. However, partial oxidation occurred even during this anaerobic procedure because Fe(III) content increased at the same time. A more careful procedure and higher Fe(II) incorporation could increase the activity even further.

Next, it was tested whether enzyme activity could be restored by reduction of Fe(III) in TTE0042 as isolated. A panel of different reductants was tested, and anaerobic samples of

TTE0042 were incubated with each reductant for 24 hours. Activity assays were then performed for each sample and the Fe composition was determined at the same time (Fig. 4.5.C). All of the tested compounds increased the amount of reduced Fe(II) in the protein sample to some degree: TCEP the least (0.1 equivalents), dithionite and ascorbate the most (0.6 equivalents). However, none of the molecules fully reduced the protein-bound iron. Enzyme activity correlated with the extent of reduction for TCEP and β-mercaptoethanol, where the specific activity increased from 2.9 min^{-1} to 6.4 and 9.1 min^{-1}, respectively (Fig. 4.5.C). In contrast, dithionite and ascorbate negatively affected activity even though both compounds generated the most ferrous iron. The activity decrease could be the result of iron removal from the active site by these two reductants. In fact, dithionite is used for elimination of iron from PAPs and ascorbate can coordinate Fe(II) (38). Prolonged incubation with EDTA by dialysis over 24 hours completely eliminated iron from the enzyme, which expectedly removed all detectable enzyme activity.

The attempts to restore the HD-GYP phosphohydrolase activity demonstrate that a heterovalent metal center is a likely requirement for efficient catalysis. Both addition of Fe(II) or other divalent cations, as well as reduction of Fe(III) can partially restore the enzyme activity. However, the extent of enzyme reactivation is variable from batch to batch. Further optimization is required to develop a reliable reconstitution protocol. In particular, simultaneous addition of Fe(II) and reductant should be tested, as it has been successful for reactivating PAPs (35, 38). Once a reproducible reconstitution protocol has been established, further activity assays can be performed to characterize the kinetic parameters for cyclic-di-GMP hydrolysis by HD-GYP proteins.

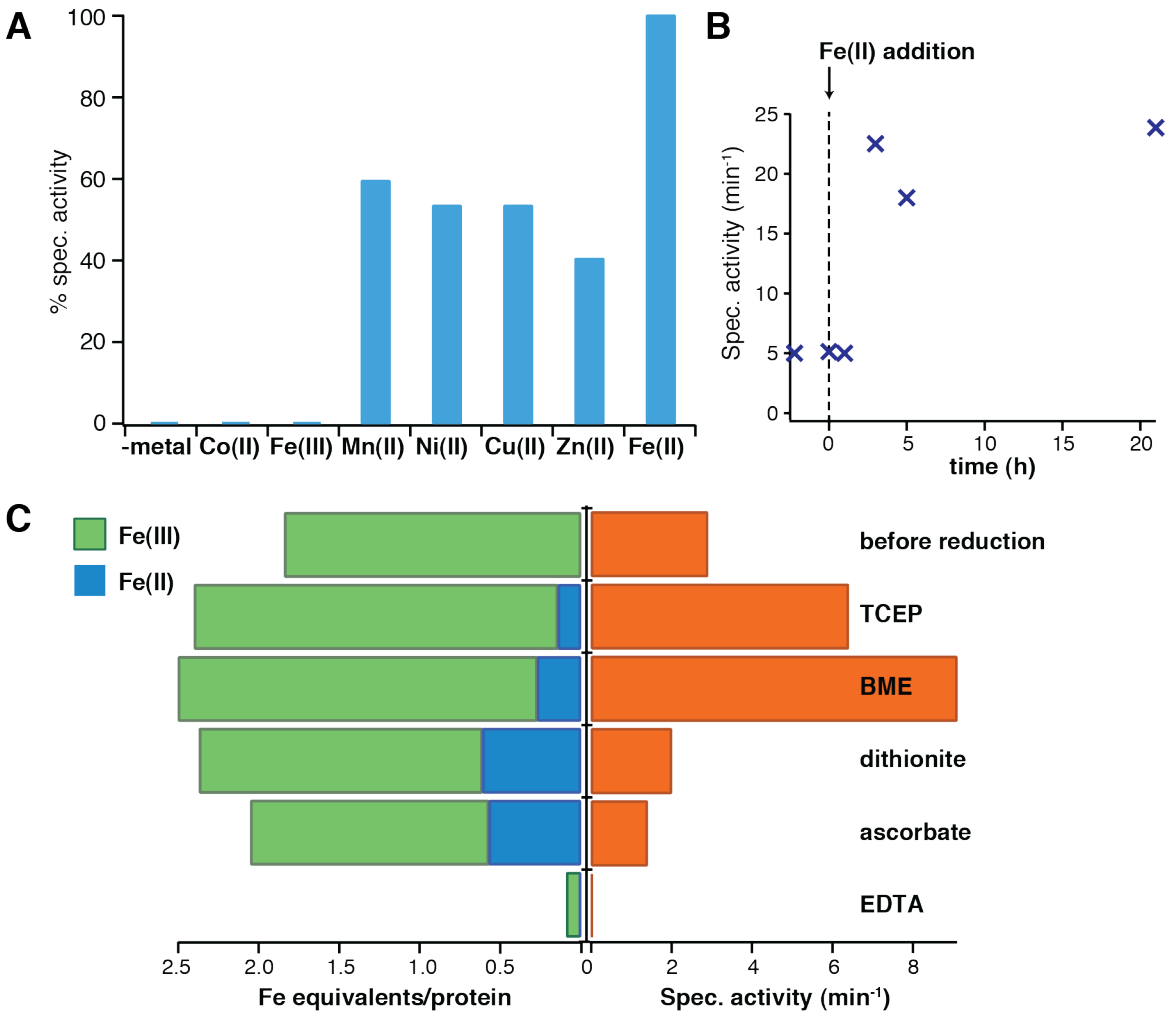

Fig. 4.5. Reconstitution of TTE0042 cyclic-di-GMP phosphodiesterase activity
A. Metal reconstitution with different divalent cations. TTE0042 was incubated with 2 equivalents of each cation for 1 h. Subsequently, pGpG production was measured at a 1 h end-point.
B. Time-course of TTE042 reconstitution with Fe(II). HD-GYP protein was incubated anaerobically with 2 equivalents of Fe(II). At the indicated time points, specific activity of pGpG production was measured.
C. Effect of iron-reduction on activity. Anaerobic TTE0042 was incubated with reductant (5 mM) or dialyzed into 50 mM EDTA for 24 h. Subsequently, iron content was determined using the ferrozine assay and specific activity of pGpG production was measured.

Conclusions

As phosphodiesterases of cyclic-di-GMP, HD-GYP proteins play an important role in mediating many cyclic-di-GMP controlled processes such as regulation of motility and virulence (18, 19, 22, 24). However, the protein family remains poorly characterized in comparison to the more thoroughly studied EAL phosphodiesterase family. The work here on TTE0042 and TM0186 establishes that pGpG is the reaction product and confirms that HD-GYP proteins contain a binuclear metal center. When expressing the proteins heterologously in *E. coli*, the metal center is mostly occupied by ferric iron, which is consistent with the metal site observed in the only crystal structure available of an HD-GYP protein (26). Reconstitution assays showed that the enzymatic activity could be partially restored through addition of Fe(II) or reduction of bound Fe(III). Therefore, HD-GYP proteins likely require a mixed valent Fe(III)-Fe(II) center for catalysis. Nonetheless, incorporation of other divalent cations in the native organisms cannot be entirely ruled out because Mn(II), Ni(II), Zn(II) and Cu(II) can partially restore activity as well. In contrast, the HnoD proteins in the H-NOX signaling network in **Chapter 2** lack any metal coordination, because most of the coordinating residues are missing. Consequently, the lack of metal coordination is a key reason for the inactivity of HnoD.

The experiments in this chapter lay the groundwork for further mechanistic studies on HD-GYP enzymes. Detailed spectroscopic experiments should address the coordination environment and redox state of the active enzyme. Moreover, site-directed mutagenesis can be employed to probe the importance of individual residues for metal-coordination, substrate binding, and catalysis. This will help elucidate the mechanism of catalysis. Finally, the thermophilic HD-GYP proteins and appropriate domain truncations should serve as excellent crystallization targets to obtain a protein structure of an active HD-GYP domain.

References

1. Hengge, R. (2009) Principles of c-di-GMP signalling in bacteria. *Nat. Rev. Microbiol.* **7**, 263–273
2. Römling, U. (2012) Cyclic di-GMP, an established secondary messenger still speeding up. *Environ Microbiol.* **14**, 1817–1829
3. Ross, P., Weinhouse, H., Aloni, Y., Michaeli, D., Weinberger-Ohana, P., Mayer, R., Braun, S., de Vroom, E., van der Marel, G. A., van Boom, J. H., and Benziman, M. (1987) Regulation of cellulose synthesis in *Acetobacter xylinum* by cyclic diguanylic acid. *Nature* **325**, 279–281
4. Tamayo, R., Pratt, J. T., and Camilli, A. (2007) Roles of cyclic diguanylate in the regulation of bacterial pathogenesis. *Annu Rev Microbiol* **61**, 131–148
5. Srivastava, D., and Waters, C. M. (2012) A tangled web: regulatory connections between quorum sensing and cyclic Di-GMP. *J. Bacteriol.* **194**, 4485–4493
6. Duerig, A., Abel, S., Folcher, M., Nicollier, M., Schwede, T., Amiot, N., Giese, B., and Jenal, U. (2009) Second messenger-mediated spatiotemporal control of protein degradation regulates bacterial cell cycle progression. *Genes Dev.* **23**, 93–104
7. Hancock, R. E. W., Nijnik, A., and Philpott, D. J. (2012) Modulating immunity as a

therapy for bacterial infections. *Nat. Rev. Microbiol.* **10**, 243–254
8. Burdette, D. L., Monroe, K. M., Sotelo-Troha, K., Iwig, J. S., Eckert, B., Hyodo, M., Hayakawa, Y., and Vance, R. E. (2011) STING is a direct innate immune sensor of cyclic di-GMP. *Nature* **478**, 515–518
9. Schirmer, T., and Jenal, U. (2009) Structural and mechanistic determinants of c-di-GMP signalling. *Nat. Rev. Microbiol.* **7**, 724–735
10. Plate, L., and Marletta, M. A. (2012) Nitric oxide modulates bacterial biofilm formation through a multicomponent cyclic-di-GMP signaling network. *Mol Cell* **46**, 449–460
11. Paul, R., Weiser, S., Amiot, N. C., Chan, C., Schirmer, T., Giese, B., and Jenal, U. (2004) Cell cycle-dependent dynamic localization of a bacterial response regulator with a novel di-guanylate cyclase output domain. *Genes Dev.* **18**, 715–727
12. Chan, C., Paul, R., Samoray, D., Amiot, N. C., Giese, B., Jenal, U., and Schirmer, T. (2004) Structural basis of activity and allosteric control of diguanylate cyclase. *Proc. Natl. Acad. Sci. USA* **101**, 17084–17089
13. Wassmann, P., Chan, C., Paul, R., Beck, A., Heerklotz, H., Jenal, U., and Schirmer, T. (2007) Structure of BeF3- -modified response regulator PleD: implications for diguanylate cyclase activation, catalysis, and feedback inhibition. *Structure* **15**, 915–927
14. Minasov, G., Padavattan, S., Shuvalova, L., Brunzelle, J. S., Miller, D. J., Baslé, A., Massa, C., Collart, F. R., Schirmer, T., and Anderson, W. F. (2009) Crystal structures of YkuI and its complex with second messenger cyclic Di-GMP suggest catalytic mechanism of phosphodiester bond cleavage by EAL domains. *J. Biol. Chem.* **284**, 13174–13184
15. Barends, T. R. M., Hartmann, E., Griese, J. J., Beitlich, T., Kirienko, N. V., Ryjenkov, D. A., Reinstein, J., Shoeman, R. L., Gomelsky, M., and Schlichting, I. (2009) Structure and mechanism of a bacterial light-regulated cyclic nucleotide phosphodiesterase. *Nature* **459**, 1015–1018
16. Rao, F., Yang, Y., Qi, Y., and Liang, Z.-X. (2008) Catalytic mechanism of cyclic di-GMP-specific phosphodiesterase: a study of the EAL domain-containing RocR from *Pseudomonas aeruginosa*. *J. Bacteriol.* **190**, 3622–3631
17. Galperin, M. Y., Natale, D. A., Aravind, L., and Koonin, E. V. (1999) A specialized version of the HD hydrolase domain implicated in signal transduction. *J. Mol. Microbiol. Biotechnol.* **1**, 303–305
18. Ryan, R. P., McCarthy, Y., Andrade, M., Farah, C. S., Armitage, J. P., and Dow, J. M. (2010) Cell-cell signal-dependent dynamic interactions between HD-GYP and GGDEF domain proteins mediate virulence in *Xanthomonas campestris*. *Proc. Natl. Acad. Sci. USA* **107**, 5989–5994
19. Ryan, R. P., Fouhy, Y., Lucey, J. F., Crossman, L. C., Spiro, S., He, Y.-W., Zhang, L.-H., Heeb, S., Cámara, M., Williams, P., and Dow, J. M. (2006) Cell-cell signaling in *Xanthomonas campestris* involves an HD-GYP domain protein that functions in cyclic di-GMP turnover. *Proc. Natl. Acad. Sci. USA* **103**, 6712–6717
20. Dow, J. M., Fouhy, Y., Lucey, J. F., and Ryan, R. P. (2006) The HD-GYP domain, cyclic di-GMP signaling, and bacterial virulence to plants. *Mol. Plant Microbe Interact.* **19**, 1378–1384
21. Slater, H., Alvarez-Morales, A., Barber, C. E., Daniels, M. J., and Dow, J. M. (2000) A two-component system involving an HD-GYP domain protein links cell-cell signalling to pathogenicity gene expression in *Xanthomonas campestris*. *Mol. Microbiol.* **38**, 986–1003
22. Ryan, R. P., Lucey, J., O'Donovan, K., McCarthy, Y., Yang, L., Tolker-Nielsen, T., and

Dow, J. M. (2009) HD-GYP domain proteins regulate biofilm formation and virulence in *Pseudomonas aeruginosa*. *Environ Microbiol.* **11**, 1126–1136
23. Sultan, S. Z., Pitzer, J. E., Boquoi, T., Hobbs, G., Miller, M. R., and Motaleb, M. A. (2011) Analysis of the HD-GYP Domain Cyclic Dimeric GMP Phosphodiesterase Reveals a Role in Motility and the Enzootic Life Cycle of *Borrelia burgdorferi*. *Infect. Immun.* **79**, 3273–3283
24. Hammer, B. K., and Bassler, B. L. (2009) Distinct sensory pathways in *Vibrio cholerae* El Tor and classical biotypes modulate cyclic dimeric GMP levels to control biofilm formation. *J. Bacteriol.* **191**, 169–177
25. Hammer, B. K., Tateda, E. S., and Swanson, M. S. (2002) A two-component regulator induces the transmission phenotype of stationary-phase *Legionella pneumophila*. *Mol. Microbiol.* **44**, 107–118
26. Lovering, A. L., Capeness, M. J., Lambert, C., Hobley, L., and Sockett, R. E. (2011) The structure of an unconventional HD-GYP protein from *Bdellovibrio* reveals the roles of conserved residues in this class of cyclic-di-GMP phosphodiesterases. *MBio* **2**
27. Busso, D., Delagoutte-Busso, B., and Moras, D. (2005) Construction of a set Gateway-based destination vectors for high-throughput cloning and expression screening in Escherichia coli. *Anal. Biochem.* **343**, 313–321
28. Rao, F., Pasunooti, S., Ng, Y., Zhuo, W., Lim, L., Liu, A. W., and Liang, Z.-X. (2009) Enzymatic synthesis of c-di-GMP using a thermophilic diguanylate cyclase. *Anal. Biochem.* **389**, 138–142
29. Viollier, E., Inglett, P., Hunter, K., Roychoudhury, A., and Van Cappellen, P. (2000) The ferrozine method revisited: Fe(II)/Fe(III) determination in natural waters. *Appl Geochem* **15**, 785–790
30. Aravind, L., and Koonin, E. V. (1998) The HD domain defines a new superfamily of metal-dependent phosphohydrolases. *Trends Biochem. Sci.* **23**, 469–472
31. Atkin, C. L., Thelander, L., Reichard, P., and Lang, G. (1973) Iron and free radical in ribonucleotide reductase. Exchange of iron and Mössbauer spectroscopy of the protein B2 subunit of the *Escherichia coli enzyme*. *J. Biol. Chem.* **248**, 7464–7472
32. Garbett, K., Darnall, D. W., Klotz, I. M., and Williams, R. J. (1969) Spectroscopy and structure of hemerythrin. *Archives of Biochemistry and Biophysics* **135**, 419–434
33. Norman, R. E., Yan, S., Que, L., Backes, G., Ling, J., Sanders-Loehr, J., Zhang, J. H., and O'Connor, C. J. (1990) (μ-Oxo)(μ-carboxylato)diiron(III) complexes with distinct iron sites. Consequences of the inequivalence and its relevance to dinuclear iron-oxo proteins. *J Am Chem Soc* **112**, 1554–1562
34. David, S. S., and Que, L., Jr. (1990) Anion binding to uteroferrin. Evidence for phosphate coordination to the iron (III) ion of the dinuclear active site and interaction with the hydroxo bridge. *J Am Chem Soc* **112**, 6455–6463
35. Twitchett, M. B., Schenk, G., Aquino, M. A. S., Yiu, D. T.-Y., Lau, T.-C., and Sykes, A. G. (2002) Reactivity of M(II) metal-substituted derivatives of pig purple acid phosphatase (uteroferrin) with phosphate. *Inorg Chem* **41**, 5787–5794
36. Merkx, M., and Averill, B. A. (1998) Ga3+ as a functional substitute for Fe3+: preparation and characterization of the Ga3+Fe2+ and Ga3+Zn2+ forms of bovine spleen purple acid phosphatase. *Biochemistry* **37**, 8490–8497
37. Mitić, N., Smith, S. J., Neves, A., Guddat, L. W., Gahan, L. R., and Schenk, G. (2006) The catalytic mechanisms of binuclear metallohydrolases. *Chem Rev* **106**, 3338–3363

38. Keough, D. T., Dionysius, D. A., de Jersey, J., and Zerner, B. (1980) Iron-containing acid phosphatases: Characterization of the metal-ion binding site of the enzyme from pig allantoic fluid. *Biochem Biophys Res Commun* **94**, 600–605
39. Yu, L., Haddy, A., and Rusnak, F. (1995) Evidence that calcineurin accommodates an active site binuclear metal center. *J Am Chem Soc* **117**, 10147–10148
40. YU, L., Golbeck, J., Yao, J., and RUSNAK, F. (1997) Spectroscopic and enzymatic characterization of the active site dinuclear metal center of calcineurin: Implications for a mechanistic role. *Biochemistry* **36**, 10727–10734
41. Pyrz, J. W., Sage, J. T., Debrunner, P. G., and Que, L. (1986) The interaction of phosphate with uteroferrin. Characterization of a reduced uteroferrin-phosphate complex. *J. Biol. Chem.* **261**, 11015–11020

CHAPTER 5:

ENGINEERING ANALOG-SENSITIVE HISTIDINE KINASES FOR POTENTIAL *IN SITU* MAPPING OF BACTERIAL PHOSPHOTRANSFER PATHWAYS[3]

Summary

In this chapter, protein engineering of histidine kinases was performed to develop new tools for studying two-component signaling systems. Analogous to prior work on eukaryotic kinases, site-specific mutations were introduced into the ATP binding site of histidine kinases permitting the use of bio-orthogonal ATP analogs as substrates. Analog-sensitive alleles of two model histidine kinases were developed and the phosphotransfer transfer reactions to their respective response regulators were optimized. Additionally, a panel of kinase inhibitors was screened for specificity against the analog-sensitive alleles. The analog-sensitive histidine kinases could be useful for identifying phosphotransfer partners of orphan histidine kinases *in situ*. This approach could serve as a replacement for the laborious *in vitro* phosphotransfer profiling employed in **Chapter 2** and it could be applied to the identification of response regulator targets of orphan H-NOX dependent histidine kinases in many organisms.

Introduction

Bacteria sense changes in the extracellular environment through two-component signaling systems (TCSs). TCSs consist of a sensor histidine kinase, which is capable of detecting a particular signal, and a response regulator, which mediates the output of the signaling cascade, often regulation of transcription or a change in secondary messenger concentration (1-3). While most TCSs consist of only one of each component, some pathways exhibit more complicated architectures involving multiple histidine kinases and response regulators (4). One complex multi-component signaling system responding to nitric oxide has been characterized in depth (**Chapters 2 and 3)** (5). TCSs regulate many essential processes of the bacterial life cycle, for example nutrient uptake, osmoregulation, chemotaxis, cell division and sporulation. In addition, TCSs play important roles in virulence and antibiotic resistance of pathogens (6-8). Since these signal transduction systems are specific to bacteria and absent in mammals, TCSs are viewed as promising targets for new antibiotics (9-11).

TCSs have been mostly studied through genetic investigations because many bacteria are genetically tractable and knockouts of TCSs genes are easily attainable. In addition, extensive biochemical studies of TCS proteins have contributed to our understanding of the autophosphorylation and phosphotransfer mechanism and regulation, as well as protein structure

[3] The work described in this chapter was performed in collaboration with Prof. Kevan Shokat from the University of California, San Francisco (UCSF). Experiments in this chapter were carried out with assistance from Julie Lanselle, an undergraduate student at UC Berkeley.

and function. However, a major challenge for studying histidine kinase and response regulator phosphorylation *in vitro* remains the instability of the phosphorylated species (12). The P – N bond of phosphohistidine has a high free energy of hydrolysis between -12 and -14 kcal mol^{-1} compared to -6.5 to -9.5 kcal mol^{-1} for the P – O bond of phosphohydroxy amino acids (13, 14). The phosphoaspartic acid on response regulators is even less stable, although it becomes stabilized by the protein scaffold (14). The kinetic stability is more variable, however phosphohistidine becomes labile at acidic pH, and phosphoaspartic acid is sensitive to both low and high pH (15). Consequently, the half-life of phosphorylated histidine kinases and response regulators in solution can be as short as several seconds, which severely hampers their characterization in TCSs. In recent years, several methods have been developed to increase the stability of the phosphorylated signaling proteins in TCSs. Some are based on the use of ATPγS as a phosphoryl donor, because the P – O bond in thiophosphorylated species is more stable (16-18). Other methods developed by Muir *et al.* focus on the incorporation of synthetic phosphohistidine analogs into the protein of interest (12).

The main challenge in assigning physiological function to a given TCS is the identification of functional connectivity between histidine kinase and response regulator genes (19). In the majority of TCSs, histidine kinase and response regulator are paired in the same operon, which infers a direct connection. However, many TCS genes are encoded as "orphans" without a partner gene nearby (20). As discussed in **Chapter 1**, most H-NOX containing TCSs fall into this category because the H-NOX/histidine kinase operons do not contain any response regulator gene. To assign a physiological function to the orphan histidine kinases, the cognate response regulators have to be identified through other means. Current methods to map TCSs include mutant screens and phenotypic characterization, bioinformatic prediction, or phosphotransfer profiling. Phenotypic analysis is limited to genetically tractable organisms and often fails to delineate more complex phosphorelay pathways or trace connectivities between components of different pathways (19). A computation approach based on co-evolution of binding interfaces between partner proteins has been successful for the correct prediction of few orphan TCS partners (21). Phosphotransfer profiling was developed as an *in vitro* kinetic profiling of a histidine kinase against a panel of purified RRs (19, 22). In **Chapter 2**, this approach was applied to the H-NOX TCS of *S. oneidensis*. Unfortunately, phosphotransfer profiling is laborious, as it requires the cloning and purification of a large number of proteins. Alternative profiling methods for faster identification of phosphotransfer targets of orphan histidine kinases are therefore desirable. Ideally, this approach would work *in situ* without the need of protein purification.

Another challenge in the study of TCSs is the lack of selective inhibitors for histidine kinases. Despite their importance as potential antibiotics, very few inhibitors of histidine kinases are available. Furthermore, for known inhibitors, the exact mechanism of action is often unknown and the compounds show poor target specificity (10, 11).

Chemical-genetics approaches applied to eukaryotic kinases were used as inspiration to develop new tools for studying histidine kinases. Eukaryotic serine/threonine and tyrosine kinases have been engineered through mutations in the ATP binding pocket to accept bio-orthogonal ATP analogs. These analogs are unreactive with other kinases permitting selective phosphorylation of the kinase of interest in a complex protein mixture (23-25). The technique

has been used to identify new phosphorylation targets of many kinases (26-30). Likewise, analog-sensitive (*as*) alleles have been successfully used to generate a number of specific inhibitors for eukaryotic kinases (31-36).

This chapter describes the engineering of histidine kinases to accept ATP analogs as substrates. Analog-sensitive alleles for two different histidine kinases were developed. Their autophosphorylation and phosphotransfer activities were characterized and optimized for complex protein mixtures. Eventually, these *as* histidine kinases and their corresponding analogs could be used to test phosphotransfer to endogenous response regulator in cell lysates or permeabilized cells. Enrichment strategies based on immunoprecipitation or chemical capture of phosphorylated proteins could be employed for identifying response regulator targets of a particular histidine kinase (29, 30, 37). Another application of *as* histidine kinases is their use as targets of inhibitors that are specific to the sensitization mutation in the ATP binding pocket. Like the ATP analogs, these inhibitors are specific to the engineered kinase variant and do not target WT kinases. Therefore, the sensitization of histidine kinases could be a promising approach as a chemical-genetics tool for targeting specific kinases of interest with an inhibitor. The method could be particularly useful for probing the function of essential histidine kinases and TCSs where deletion knockout strains are not viable.

Experimental Procedures

Selection of gate-keeper residues in histidine kinases

Positions of potential gate-keeper residues of histidine kinases were derived from the crystal structure of Tm0863 and the NMR structure of the *E. coli* EnvZ CA domain (38, 39). The histidine kinase structures and the AMP-bound crystal structure of Src (40) were aligned with Pymol using the nucleotide as reference. The alignment of the EnvZ CA domain had to be adjusted by structural homology to Tm0863 because the nucleotide was oriented in a different conformation. The T338 gate-keeper in Src was highlighted and large residues in similar positions near the N^6 amino group of adenine were identified in Tm0863 and EnvZ by visual inspection: F472 and S470 in Tm0863, and I432 and L430 in EnvZ. The F472 residue was replaced by glycine in Pymol and a benzyl group was modeled in as a N^6 substituent of adenine. No steric clashes were observed for the model structure. The sequences of selected histidine kinase CA domains were aligned with ClustalW2 and the gate-keeper positions were identified based on the residues in Tm0863 and EnvZ. An alignment of seed-sequences of the HATPase_c protein family (Pfam ID: PF02518) was obtained from the Pfam database. The alignment was trimmed around the gate-keeper residues, gaps were removed, and this shortened alignment was used to generate the sequence logo using the WebLogo interface.

Cloning of TCS genes and site-directed mutagenesis to generate gate-keeper histidine kinase mutants

The cytosolic domain of EnvZ and the phosphoreceiver domain of OmpR were PCR-amplified from *E. coli* genomic DNA (41). The cytosolic domain of *T. maritima* HpkA and DrrA

were amplified from *T. maritima* genomic DNA (42)[4]. Sequences of all primers used in this chapter can be found in Table 5.1. The EnvZ PCR product and pET20b were restriction digested with NdeI and NotI and ligated to yield pET20b-EnvZ-His_6. The $OmpR_{REC}$ PCR product was ligated into pENTR/SD/D-TOPO using TOPO cloning (Invitrogen) and subsequently transferred into pHMGWA to append an *N*-terminal His_6-MBP tag (43). The HpkA PCR product was ligated into pET28b using NdeI and NotI restriction sites to yield the His_6-TEV-HpkA expression construct. DrrA was cloned into pENTR/TEV/D-TOPO by TOPO cloning and subsequently transferred into pHMGWA. Site-directed mutagenesis was used to introduce the respective gate-keeper mutations into EnvZ and HpkA. The sequence of all expression plasmids was verified.

Table 5.1. Sequence of primers used in this chapter.

Primer Name	Sequence
EnvZ-pET20-NdeI-f	GGAATTCCATATGGCGGCTGGTGTTAAGCAAC
EnvZ-pET20-NotI-r	ATAGTTTAGCGGCCGCCCCTTCTTTTGTCGTGCCCT
OmpR-f	CACCATGCAAGAGAACTACAAGATTC
OmpR-rec-r	GCCTGGCAGTTCGTTCGCCTGAC
HpkA57-NdeI-f	GGAATTCCATATGAATCTGAAAGAAACAATTTCACG
HpKA57-NotI-r	CCTGCCGAAAAGAAGGTGAGCGGCCGCTAAACTAT
DrrA—NdeI-f	GGAATTCCATATGTACCCCCTCGGGGGATCG
DrrA-pENTR-f	CACCATGTACCCCCTCGGGGGATCG
DrrA-PENTR-r	GTCTTCCTTTCCGGGGTCTC
EnvZ-L430G-f	GCGAGCGGGGCGGGGGTTCCATTCGCGCCTGGC
EnvZ-L430G-r	GCCAGGCGCGAATGGAACCCCCGCCCCGCTCGC
EnvZ-I432G-f	GAGCGGGGCGGGCTTTCCGGTCGCGCCTGGCTGCCAGTG
EnvZ-I432G-r	CACTGGCAGCCAGGCGCGACCGGAAAGCCCGCCCCGCTC
EnvZ-L430A-f	GCGAGCGGGGCGGGGCTTCCATTCGCGCCTGGC
EnvZ-L430A-r	GCCAGGCGCGAATGGAAGCCCCGCCCCGCTCGC
EnvZ-I432A-f	GAGCGGGGCGGGCTTTCCGCGCGCGCCTGGCTGCCAGTG
EnvZ-I432A-r	CACTGGCAGCCAGGCGCGCGCGGAAAGCCCGCCCCGCTC
HpkA-T402G—f	GTGAGATCAACCAGGGAGGTCTGATGAGGGTGCTCC
HpkA-T402G—r	GGAGCACCCTCATCAGACCTCCCTGGTTGATCTCAC
HpkA-M404G-f	CAACCAGGGAACGCTGGGTAGGGTGCTCCTGCCGAAAAG
HpkA-M404G-r	CTTTTCGGCAGGAGCACCCTACCCAGCGTTCCCTGGTTG

Protein expression and purification

The expression plasmids for each protein were transformed into *E. coli* BL21(DE3) expression strain. Bacteria were grown in expression media (45 g/L yeast extract, 11.7 mM monobasic potassium phosphate, 50.3 mM dibasic potassium phosphate). Protein expression was induced at 25ºC with 50 μM to 1 mM final concentration of IPTG. Cells were harvested by centrifugation after 20 hours of growth. Cell pellets were resuspended in lysis buffer supplemented with DNAseI, pefabloc and benzamidine. The lysis buffer for EnvZ and OmpR was 50 mM DEA pH 8.0, 10% glycerol, 300 mM NaCl, 20 mM imidazole, for HpkA: 50 mM sodium phosphate pH 8.0, 10% glycerol, 300 mM NaCl, 20 mM imidazole, 2 mM 2-mercaptoethanol, and for DrrA: 50 mM sodium phosphate pH 8.0, 10% glycerol, 150 mM NaCl, 2 mM 2-mercaptoethanol. Cells were lysed by passage through a high-pressure homogenizer (Avestin). The lysate was centrifuged at 200,000 g for 45 min in an Optima XL-100K

[4] *T. maritima* genomic DNA was a generous gift from Dr. Rosalind Kim at LBNL.

ultracentrifuge with a Ti-45 rotor (Beckman). For EnvZ, OmpR and HpkA, the supernatant was loaded onto a column with Ni-NTA agarose resin (Qiagen). The columns were washed with 20 column volumes of lysis buffer and protein was eluted with 250 mM imidazole in lysis buffer. Proteins were concentrated and exchanged into storage buffer (50 mM DEA pH 8.0, 5% glycerol, 150 mM NaCl, 2 mM DTT) by passage through a PD-10 desalting column. The DrrA supernatant was loaded onto amylose resin (NEB) and washed as above. DrrA was eluted with lysis buffer containing 50 mM maltose. The protein was further purified on Ni-NTA agarose resin as above and finally exchanged into storage buffer. Protein aliquots were flash-frozen in liquid nitrogen.

Histidine kinase autophosphorylation and phosphotransfer assays using ATPγS

ATPγS was purchased from Roche and all ATPγS analogs were acquired from Axxora, the US distributor of Biolog. *p*-nitrobenzyl mesylate (PNBM) was synthesized according to literature (29). The thiophosphate ester-specific antibody was purchased from Epitomics (Cat # 2686-1). All assays were carried out in 50 mM DEA, 5% glycerol, 150 mM NaCl. $MgCl_2$ (5 mM, unless otherwise specified) was added to the buffer at the same time as ATPγS. The assay was carried out as described (16). EnvZ and OmpR were typically present at 5 μM in 20 μL reaction volumes, unless otherwise specified. Reactions were initiated by addition of 0.5 mM ATPγS or the respective analog. EnvZ reactions were incubated at room temperature, while the optimal temperature for reactions of the thermophilic HpkA was found to be 40ºC. Reactions were quenched by addition of 2.5 μL EDTA pH 8.0 (100 mM). Next, samples were treated with 1.5 μL PNBM (50 mM, dissolved in DMSO), vortexed, and incubated for 1.5 h at room temperature. SDS-loading buffer (5 μL, 6 X) was added and the samples were loaded directly onto a SDS-PAGE gel without boiling. The thiophosphorylated proteins were detected by Western blot as described (16, 37). The thiophosphate ester antibody was used as 1º antibody at a 1:5000 dilution in 3% milk in PBST (PBS, 0.1% Tween) and incubated at 4ºC overnight. Goat anti-rabbit HPR conjugate (Thermo Scientific) was used as 2º antibody at a 1:500 dilution. Bands were imaged by chemiluminescence on a Gel Doc XR imager (Biorad). Protein loading was determined by Western blot against the His_6 tag. *E. coli* lysate was generated from a 50 mL DH5α culture grown overnight in LB. Cells were harvested by centrifugation and resuspended in 1 mL assay buffer, treated with lysozyme, pefabloc and DNAseI. Cells were lysed by sonication. Cell debris was removed by centrifugation at 14,000 rpm on a tabletop centrifuge at 4ºC. The supernatant was collected and aliquots were flash frozen in liquid nitrogen.

Inhibitor screening of analog-sensitive histidine kinases

Inhibitors were provided by the Shokat group at UCSF. Each inhibitor stock was diluted to 2 mM in DMSO. Thiophosphorylation reactions were carried out with 5 μM EnvZ as above, except 1 μL inhibitor (100 μM final concentration) or DMSO were added to each tube and pre-incubated for 15 min before ATPγS addition. Reactions were quenched with EDTA after 1 min and analyzed as above. Protein amounts in each lane of the Western blot were measured by fluorescent staining using the stain-free gel system from Biorad. The thiophosphorylation signal was quantified by densitometry in Image Lab (Biorad) and adjusted to the protein amount. Each reaction was normalized to two DMSO controls. Finally, data from two to three separate experiments were averaged.

Results

Selection of gate-keeper residues

Engineering of *as* tyrosine and serine/threonine kinases to accept unnatural bio-orthogonal ATP analogs as substrates has been performed in numerous instances (23-26, 28, 30, 44). Based on co-crystal structures of different kinases with adenine nucleotides and inhibitors, a hydrophobic "gate-keeper" residue was identified near the N^6-amino group of the adenine, which was mutated to either alanine or glycine to introduce a "hole" in the ATP binding site (24, 45). For instance, T338 was selected as the gate-keeper residue in v-Src (Fig. 5.1.A) (24). The position of the gate-keeper residues is conserved among eukaryotic kinases and mutation of the homologous residue in other kinases easily generates the corresponding *as* allele (25).

Prokaryotic histidine kinases share no structural homology with eukaryotic kinases. Instead, the histidine kinase catalytic and ATP-binding (CA) domain belongs to a larger family of ATPase proteins, which also includes topoisomerase II, Hsp90, and MutL (46) Nonetheless, all histidine kinases share significant sequence homology, in particular within the CA domain as can be seen in a sequence alignment highlighting the conserved regions (Fig. 5.1.C). For this reason, the *as* method is easily transferrable to other histdine kinases once an *as* allele has been generated. The crystal structure of a *Thermotoga maritma* histidine kinase (Tm0853) as well as the NMR structure of the *E. coli* EnvZ CA domain served as a starting point for the rational design of an *as* histidine kinase (38, 39).

In the crystal structure of AMP bound v-Src, the gate-keeper residue T338 is located adjacent to the N^6-amino group slightly above the plane of the adenine (Fig. 5.1.A) (40). When visualizing the ATP-binding pocket of Tm0853 with the AMP in a similar orientation, a phenylalanine residue (T472) can be found in an analogous position near the N^6-amino group (blue). In addition, a smaller serine (S470) residue can be found protruding into the adjacent pocket, on the left side of the N^6-amino group (red). Both residues are in close enough vicinity to the ATP to function as gate-keeper residues. Next, a structural alignment of several histidine kinase CA domains was used to evaluate the conservation of these residues (Fig. 5.1.A). An ideal gate-keeper mutation should meet the following criteria (32): The residue should be large enough so that the Gly or Ala mutation extends the ATP-binding pocket far enough. To be able to generalize the change to other kinases, similar residues should occupy the position in other kinases. Furthermore, the mutation should have minimal to no effect on enzyme activity. The *as* position 1, corresponding to F472 in Tm0853, is occupied by large hydrophobic residues (F/I/V) in other histidine kinase and thus satisfies the structural requirements (Fig. 5.1.C and D). Residues at *as* position 2, corresponding to S430 in Tm0853, are less conserved and mostly occupied by smaller residues (T/S/A) (Fig. 5.1.D). Nonetheless, the *as*-2 position was also tested as a gate-keeper candidate, in particular in EnvZ, because the positions is occupied by L430. The *as*-1 position in EnvZ is filled by I432.

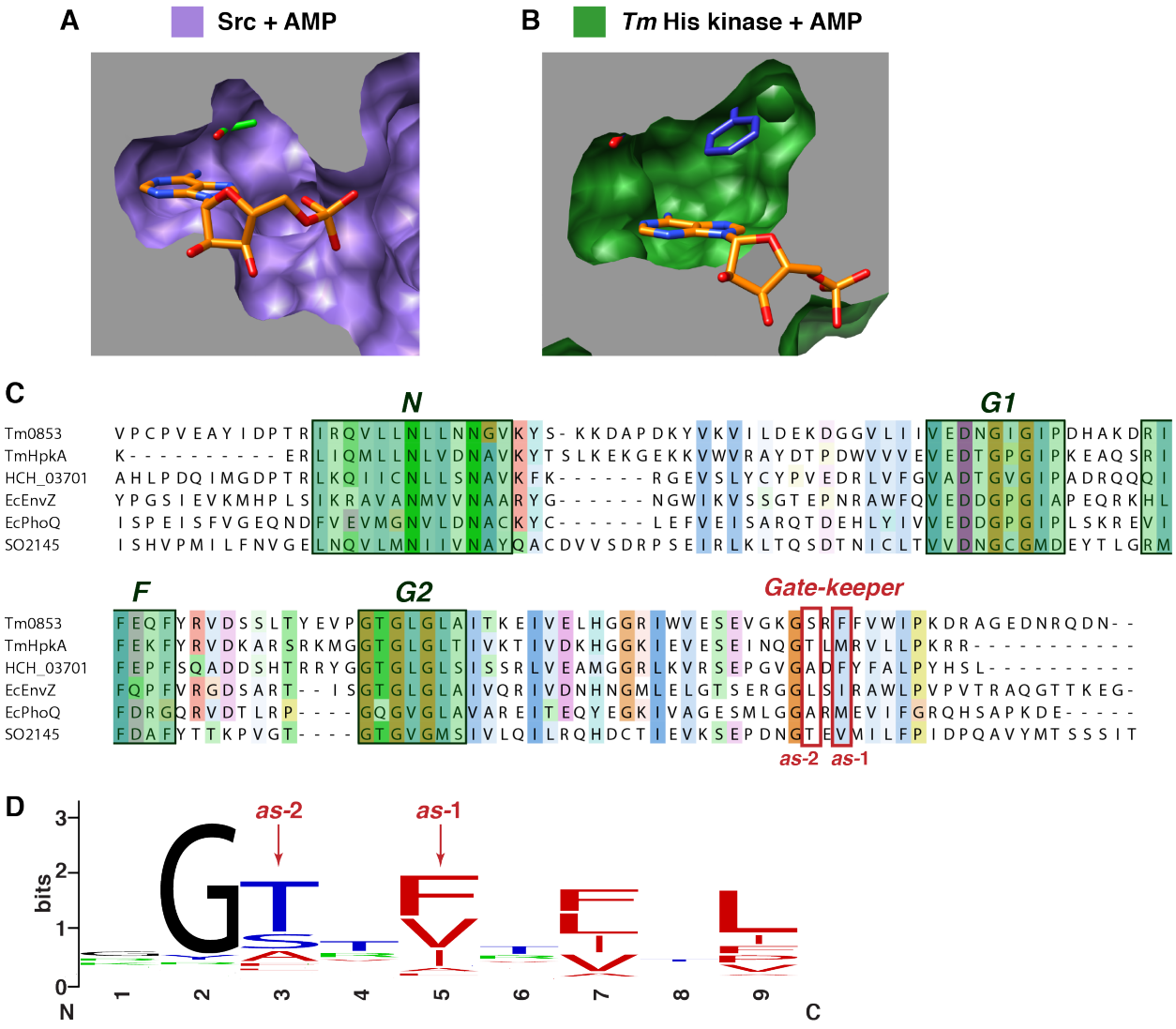

Fig. 5.1. Structural and sequence alignment of eukaryotic and histidine kinases for selection of gate-keeper residues

A. ATP-binding pocket in the crystal structure of Src kinase (PDB ID: 2SRC). Bound AMP is shown in orange and the gate-keeper T338 residue near the N^6 position of the adenine is highlighted in green.

B. ATP-binding pocket of *T. maritime* histidine kinase (Tm0853, PDB ID: 2C2A) with AMP bound. Potential gate-keeper residues are high-lighted in red (S470) and blue (F472).

C. Sequence alignment of the catalytic domain of selected histidine kinases. The conserved sequence motifs are boxed in green. Gate-keeper residues are highlighted by red boxes.

D. Conservation of gate-keeper residues in the HATPase_c protein family. The sequence logo was generated with WebLogo.

Engineering of an analog-sensitive E. coli EnvZ

After identification of potential gate-keeper residues, a suitable histidine kinase model for the protein engineering approach had to be selected. *E. coli* EnvZ is an ideal model kinase because the cytosolic C-terminal domain ($EnvZ_c$, hereinafter referred to as EnvZ) is easily

expressed and purified. The enzyme is highly active (41), and structural information on the DHp and CA are known from NMR studies (39, 47). Furthermore, OmpR, the cognate response regulator of EnvZ is known so that phosphotransfer of the *as* histidine kinase can be investigated (48).

E. coli EnvZ gate-keeper mutants were generated by site-directed mutagenesis. Each of the *as*-1 and *as*-2 positions were mutated to glycine and alanine yielding the following four EnvZ mutants: L430G, L430A, I432G, I432A. WT EnvZ and the four mutants were overexpressed in *E. coli* and purified. All mutants overexpressed and purified equally well in comparison to the WT enzyme.

Histidine kinase activity is typically measured using radioactive [γ–^{32}P]ATP, followed by gel electrophoresis and subsequent visualization of phosphorylation by imaging for ^{32}P radioactivity (41). A different method for measuring histidine kinase activity has been recently published and involves thiophosphorylation using ATPγS (16). Although autophosphorylation kinetics are slower with ATPγS, the significant advantage is that the histidine residue becomes modified to a thiophosphoramidate, which is more stable compared to the thermodynamically labile histidine phosphoramidate (49). The thiophosphorylated histidine kinase product is detected by covalent modification with the alkylating agent *p*-nitrobenzyl mesylate (PNBM), followed by Western blot detection using an antibody that has been raised against this semi-synthetic epitope (29, 37). Consequently, an additional benefit of the method is that no use of radioactive materials is required. Furthermore, a panel of ATPγS analogs, developed by Shokat *et al.* at UCSF, with modifications at the N^6 position of the adenine group, is commercially available from Biolog (29, 37). Therefore, all histidine kinase activity assays were performed with ATPγS using the semi-synthetic epitope method.

To determine the substrate specificity of WT EnvZ and the four gate-keeper mutants, a panel of ATPγS analogs was tested (Fig. 5.2.A). The substituents on the N^6 position are mostly hydrophobic but range in size. At first, an end-point thiophosphorylation assay was carried out to maximize the extent of histidine modification. WT EnvZ and each of the four mutants were incubated with the panel of ATPγS analogs for 1.5 hours and the relative extent of thiophosphorylation was detected by Western blot (Fig. 5.2.B). WT EnvZ and the four mutants reacted similarly with ATPγS, indicating that the gate-keeper mutants did not alter the enzyme activity significantly. WT EnvZ displayed very weak thiophosphorylation with three of the analogs: N^6-benzyl, N^6-isopentenyl, and N^6-furfuryl-ATPγS, and no signal with N^6-phenylethyl-ATPγS. This demonstrated that these analogs were poor substrates for the WT kinase, and thus ideal for use with the *as* versions. The L430A mutant showed phosphorylation only with ATPγS, excluding it as an *as* candidate. Likewise, I432A reacted very weakly with three of the analogs. In contrast, the two other mutants showed a strong reaction with one respective analog: L430G using N^6-furfuryl-ATPγS, and I432G using N^6-benyzl-ATPγS (indicated by red arrows in Fig. 5.2.B). These combinations were good candidates for *as* EnvZ/ATPγS analog pairs.

To further characterize the preference of the EnvZ variants for the different ATPγS substrates, a thiophosphorylation time course was measured. This should allow a rough estimation of relative substrate specificity for the different ATPγS analogs under the assay

conditions (Fig. 5.2.B). WT EnvZ reacted approximately 10 times faster with ATPγS compared to the N^6-benzyl analog and 5 times faster compared to the N^6-furfuryl analog. In contrast L430G EnvZ reacted 1.5 times faster with the N^6-furfuryl analog as compared to ATPγS. For I432G EnvZ, the thiophosphorylation is 1.5 times faster with ATPγS compared to the analog.

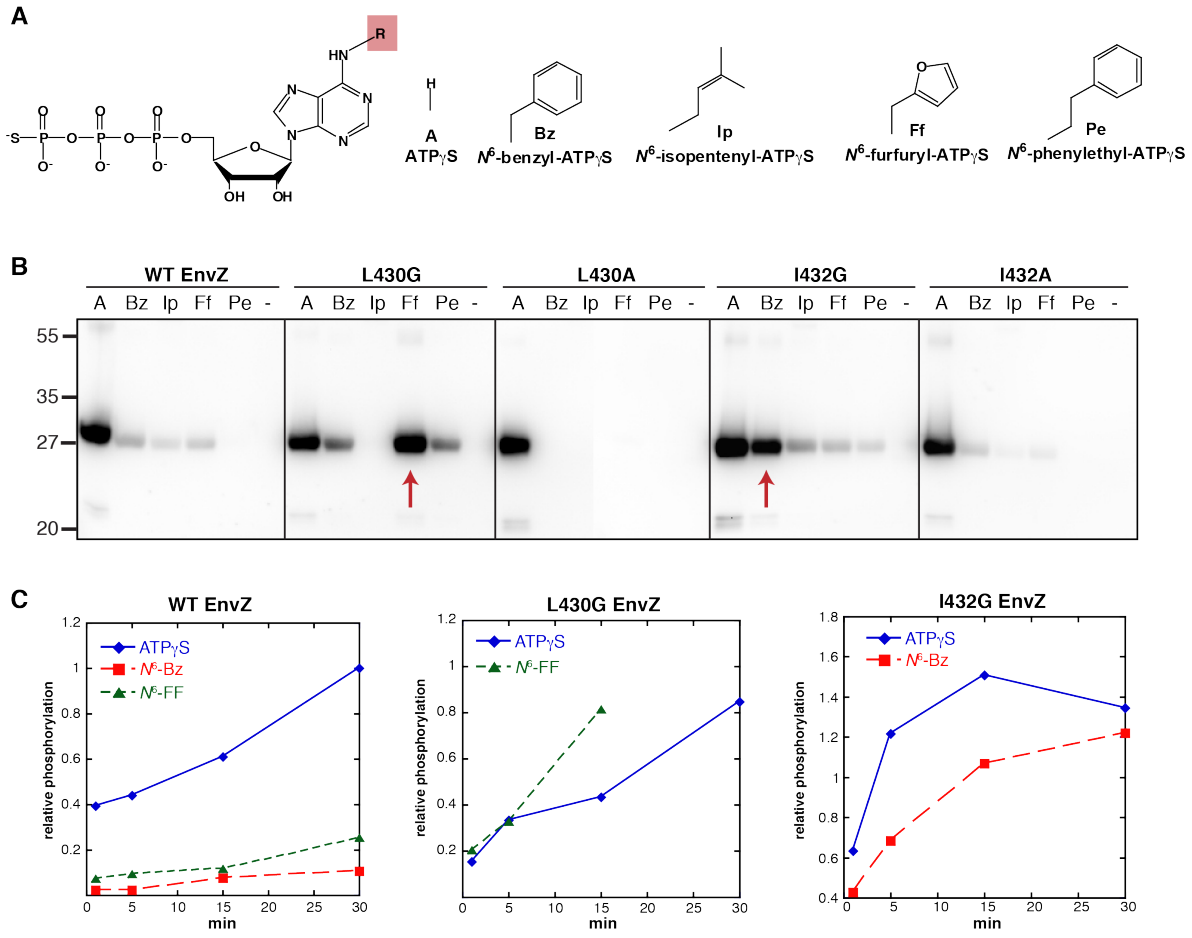

Fig. 5.2. Thiophosphorylation activity of *as* EnvZ candidates

A. Chemical structures of ATPγS analogs tested against the analog-sensitive EnvZ candidates.

B. Western-blot detection of thiophosphorylated and thioesterified EnvZ mutants testing the ATPγS analogs. EnvZ was incubated with the respective ATPγS analog for 90 min. Samples were treated with PNBM for 1.5 h and thiophosphorylation was detected by Western blot using a thiophosphate ester-specific antibody.

C. Time-course of thiophosphorylation of EnvZ mutants with different ATPγS analogs. Thiophosphorylation was detected by Western blot and quantified through densitometry of the bands.

Overall, the activity assays demonstrated that the *as* engineering approach is amenable to the EnvZ histidine kinase. Expansion of the ATP binding pocket in a similar location to the gate-keeper position in eukaryotic kinases (*as*-1 position) allowed utilization of the N^6-benzyl ATPγS substrate. Interestingly, the *as*-2 position, which is less conserved among histidine kinases but

occupied by a large hydrophobic residue in EnvZ, can also function as a gate-keeper. L430G EnvZ could be paired with the N^6-furfuryl ATPγS substrate.

Thiophosphotransfer between as EnvZ and OmpR

To use the *as* histidine kinases as tools for probing two-component signaling pathways, the engineered kinases have to retain the ability to transfer the phosphoryl group to their cognate response regulator(s). Because of higher stability of the thiophosphohistidine, transfer kinetics of the thiophosphoryl group are expected to be slower compared to phosphotransfer. To verify that the thiophosphoryl group from EnvZ could be transferred to OmpR, EnvZ was pre-treated with ATPγS for 40 minutes to maximize thiophosphorylation. Equimolar amounts of OmpR were added and aliquots of the reaction were quenched at different time points for an estimation of the transfer kinetics. Thiophosphotransfer between EnvZ and OmpR were weakly detectable after 1 minute, but became stronger and leveled out at 15 minutes (Fig. 5.3.A). As expected, the transfer was much slower than for phosphoryl groups, which is complete after 30 seconds (50). Surprisingly, the thiophosphorylation signal of EnvZ increased slightly throughout the time course, indicating that thiophosphorylation of EnvZ was faster than transfer to OmpR.

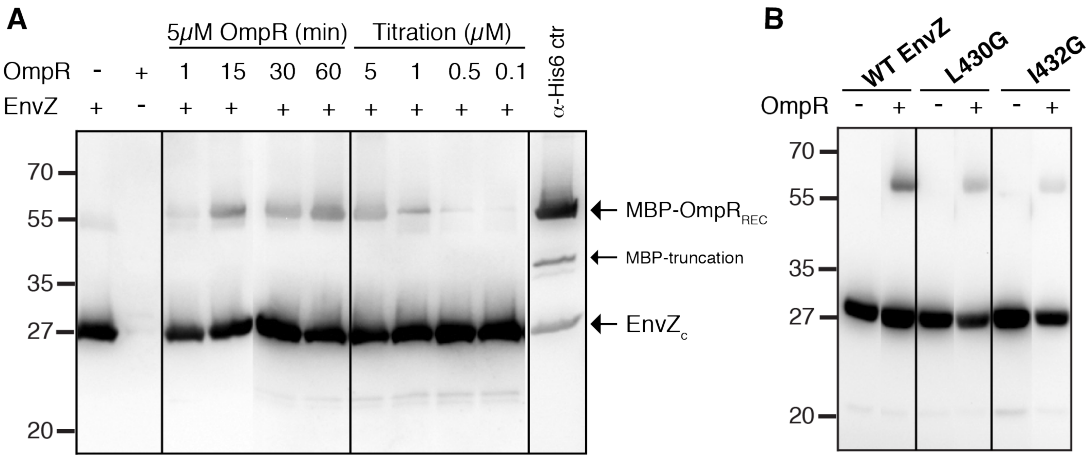

Fig. 5.3. Western-blot detection of thiophosphotransfer between EnvZ and OmpR
A. Determination of transfer kinetics and limit of detection for OmpR thiophosphorylation. EnvZ was pre-thiophosphorylated with ATPγS for 40 min prior to the addition of OmpR for indicated amounts of time or at indicated concentrations.
B. Thiophophotransfer between analog-sensitive EnvZ and OmpR using ATPγS analogs. After pre-treatment of EnvZ with the respective ATPγS analog, OmpR was added for 15 min. All samples in this figure were treated with PNBM for 1.5 h and thiophosphorylation was detected by Western blot using a thiophosphate ester-specific antibody.

For identification of unknown phosphorylation targets of orphan histidine kinases, low levels of endogenous response regulators must be detected. Fortunately, response regulators are typically expressed at much higher concentrations than the partner histidine kinases. For instance, an *E. coli* cell contains approximately 100 copies of EnvZ but 3,500 copies of OmpR

corresponding to an OmpR concentration of about 9 μM (51). In bacterial lysates, the concentration is lower. To assess the lower limit at which OmpR thiophosphorylation was still detected, a titration was performed in which the EnvZ concentration was held constant at 5 μM and the OmpR concentration was varied from 5 to 0.01 μM. OmpR thiophosphorylation was detectable as low as 0.1 μM (Fig. 5.3.A).

To verify that the gate-keeper mutations do not influence the reactions, thiophophotransfer between the EnvZ mutants and OmpR was tested. L430G and I432G EnvZ were pre-incubated with the respective ATPγS analog prior to OmpR addition (Fig. 5.3.B). For both mutants, a thiophosphorylation signaling of OmpR could be observed after 15 minutes. The signal was weaker compared to WT EnvZ suggesting slower transfer, but overall, the gate-keeper mutations showed a weak influence on the transfer reactions.

Generating analog-sensitive T. maritima HpkA mutants

Because of high sequence conservation of the histidine kinase CA domain, it should be straightforward to apply the *as* method to other histidine kinases. The approach was tested in *T. maritime* HpkA, a thermostable histidine kinase. HpkA has been studied because the phosphorylated state of its cognate response regulator DrrA has a particularly long half-life (42). Similar gate-keeper mutations to the ones used for EnvZ could were engineered into HpkA. The *as*-1 position is occupied by methionine and the *as*-2 position by threonine so site-directed mutagenesis was used to generate M404G and T402G HpkA. WT HpkA and the two mutants were expressed recombinantly in *E. coli* and purified.

To examine the substrate preference for WT HpkA and each mutant, the ATPγS analogs were tested in an end-point thiophosphorylation assay. HpkA was incubated with each ATPγS substrate for 60 min (Fig. 5.4.A). WT HpkA displayed strong thiophosphorylation with ATPγS but no detectable reactivity with any of the analogs. Likewise, T402G HpkA exclusively reacted with ATPγS, indicating that the mutant was not useful as an *as* allele of HpkA. Compared to EnvZ, where the *as*-2 position is occupied by leucine, mutation of the smaller threonine in HpkA to glycine might not increase the space in the ATP-binding pocket enough to allow the utilization of these analogs. In contrast, M404G displayed thiophosphorylation with two of the analogs: N^6-benzyl and N^6-phenylethyl-ATPγS (Fig. 5.4.A, indicated by red arrows). The weaker signal of M404G HpkA with ATPγS was the result of a lower protein loading in all M404G lanes. When normalizing to protein amounts, the reactivity with ATPγS was comparable to WT. On the other hand, the reactivity of M404G with the analogs was weaker in comparison to ATPγS. However, given that the ATPγS analogs did not show reaction with WT HpkA, the selectivity of each analog for *as* HpkA compared to WT was very high. Consequently, the M404G mutant is a suitable *as* allele of HpkA.

Next, thiophosphotransfer between HpkA and DrrA was tested. WT and M404G HpkA were pre-treated with ATPγS or the respective analogs, prior to addition of DrrA. Both WT and M404G HpkA could facilitate the phosphotransfer to DrrA using ATPγS as substrate (Fig. 5.4.B). Consistent with the results from Fig. 5.4.A, thiophosphorylation of M404G with the analogs was weaker compared to ATPγS. However, transfer of the thiophosphoryl group to DrrA

was still easily detectable. Overall, successful engineering of an *as* HpkA variant demonstrates that the approach can likely be generalized to other histidine kinases.

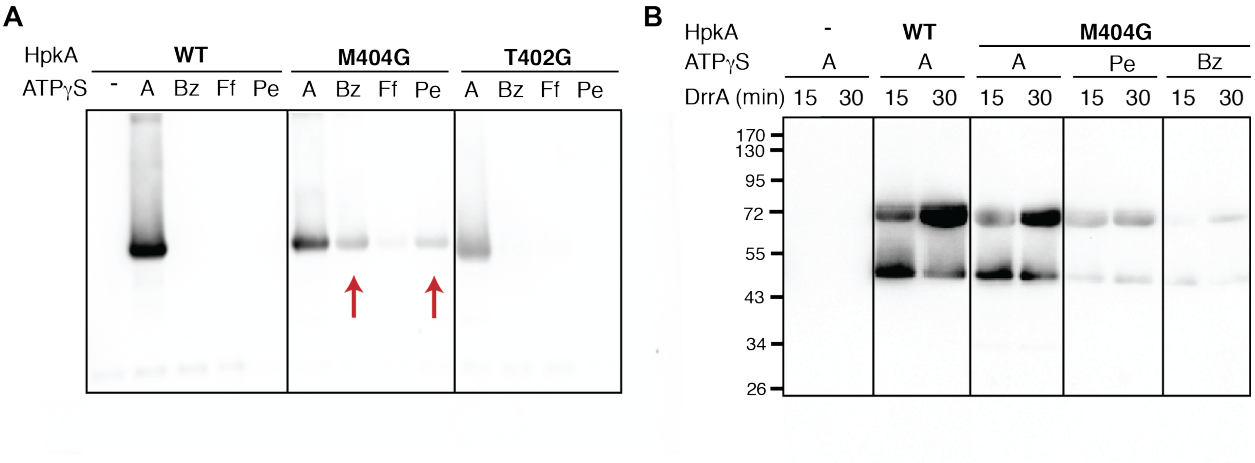

Fig. 5.4. Thiophosphorylation and phosphotransfer activity of *T. maritima* HpkA mutants with ATPγS analogs

A. Thiophosphorylation of WT, M404G and T402G HpkA with a panel of ATPγS analogs. HpkA was incubated with the respective ATPγS analog for 1 h at 40ºC.

B. Thiophosphotransfer between WT and M404G HpkA and DrrA using ATPγS and analogs. HpkA was pre-treated with ATPγS or the respective analog for 30 min at 40ºC prior to addition of DrrA for the indicated amounts of time. All samples in this figure were treated with PNBM for 1.5 h and thiophosphorylation was detected by Western blot using a thiophosphate ester-specific antibody.

Optimization of thiophosphotransfer between analog-sensitive EnvZ mutants and OmpR in complex protein mixtures

One application for *as* histidine kinases is their use in the identification of new phosphotransfer targets. For this purpose, the phosphotransfer reaction must be carried out in complex protein mixtures, for example in cellular lysates, which contain endogenous amounts of potential phosphorylation targets. Autophosphorylation of the histidine kinase must be carried out in the same mixture. Alternatively, the thiophosphorylated kinase has to be stable enough in the complex protein environment, if the phosphorylation reaction is carried out separately and then added to the mixture. For this reason, the histidine kinase thiophosphorylation and phosphotransfer conditions of EnvZ had to be optimized in the presence of cellular lysate.

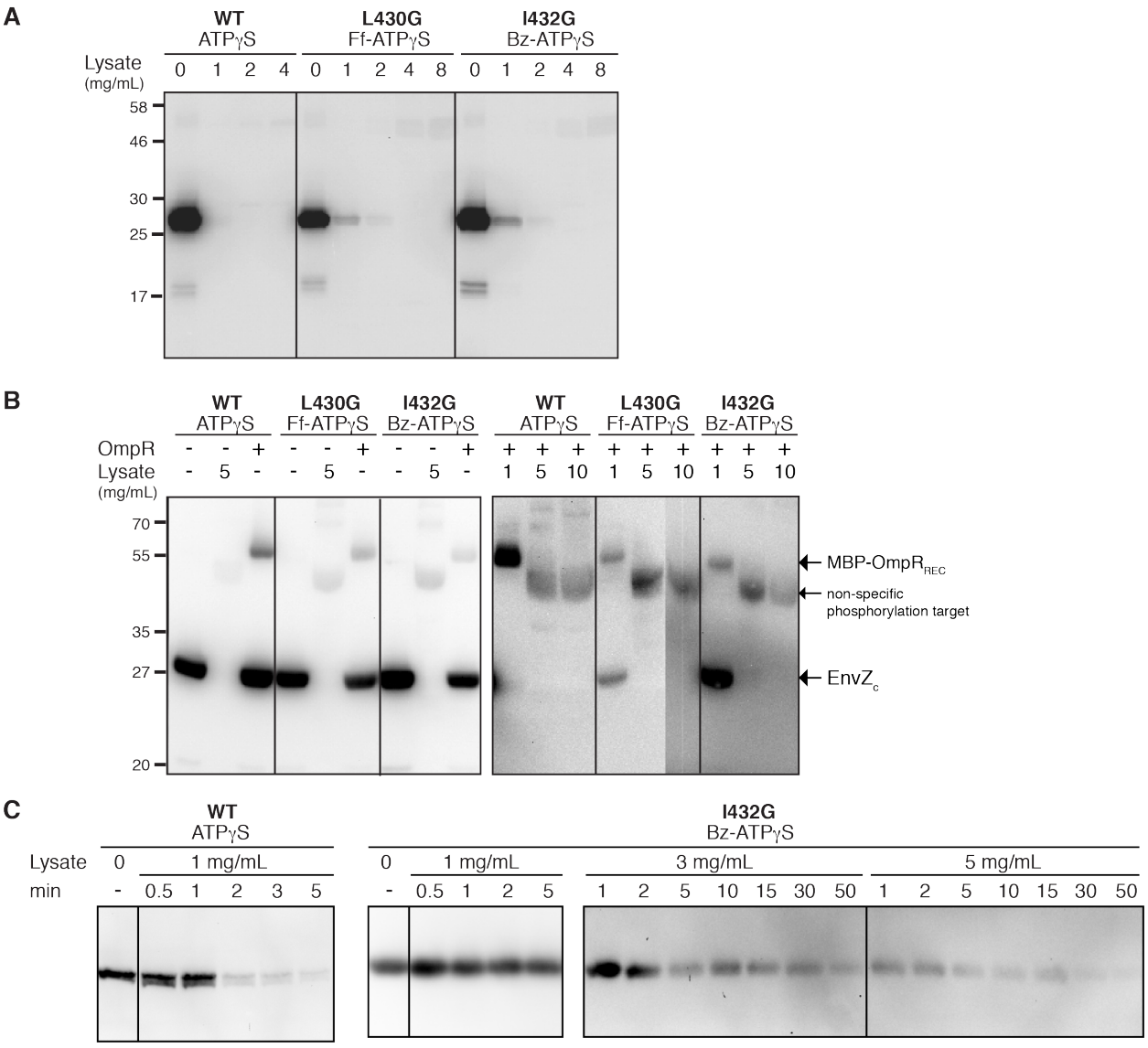

Fig. 5.5. Optimization of thiophosphotransfer conditions from EnvZ to OmpR in the presence of cellular lysate

A. End-point thiophosphorylation after 30 min of analog-sensitive EnvZ mutants and ATPγS analogs in the presence of increasing amounts of *E. coli* cleared lysate.

B. Thiophosphotransfer between EnvZ and OmpR in the presence of *E. coli* lysate. Mixtures of EnvZ, OmpR, *E. coli* cleared lysate, and ATPγS (analogs) were incubated for 30 min. The contrast in the right panel was increased 10-times compared to the left panel to visualize the thiophosphorylated proteins.

C. Dephosphorylation time-courses of WT EnvZ and mutants after addition of *E. coli* cleared lysate. EnvZ was phosphorylated with the respective ATPγS analog for 30 min prior to addition of lysate at the indicated concentrations. Reactions were quenched at the indicated time points. All samples in this figure were treated with PNBM for 1.5 h and thiophosphorylation was detected by Western blot using a thiophosphate ester-specific antibody.

To investigate the effect of an *E. coli* protein mixture on the thiophosphorylation of EnvZ, the reactions of WT EnvZ and the *as* variants were carried out in the presence of increasing amounts of *E. coli* cleared lysate (Fig. 5.5.A). The amount of lysate was quantified according to protein content as judged by the absorbance at 280 nm. Addition of lysate in concentrations of 1 mg mL^{-1} or higher completely eliminated any detectable thiophosphorylation of WT EnvZ and ATPγS. In contrast, reactions between the *as* EnvZ variants and their matching substrates were still detectable in the presence of 1 mg mL^{-1} lysate, although the extent of phosphorylation was at least 4 - 5 times lower than in the absence of cellular lysate. Higher amounts of lysates also abolished any detectable *as* EnvZ thiophosphorylation. These results demonstrated that the *as* variants and their respective ATPγS analogs were slightly better at carrying out the reactions in complex protein mixtures. This could be due to ATPγS being used up by other reactions, while the ATPγS analogs are more specific towards the *as* histidine kinase. However, increasing the concentration of ATPγS or the analogs did not raise the phosphorylation signal at 1 mg mL^{-1} lysate concentration (data not shown). This observation suggests that the low signal is predominantly the results of fast dephosphorylation.

Next, the transfer of the thiophosphoryl group between EnvZ and OmpR was examined in the presence of lysate. Mixtures of EnvZ and OmpR in equimolar concentration, as well as cleared lysate, were incubated with ATPγS or the respective analog without pre-phosphorylation (Fig. 5.5.B). Surprisingly, OmpR thiophosphorylation was detectable for WT EnvZ in the presence of 1 mg mL^{-1} lysate even though phosphorylated EnvZ was not measured (Fig. 5.5.B, right panel, left lane). Higher lysate concentrations eliminated the OmpR signal. Using the *as* EnvZ variants, thiophosphorylated OmpR was also detectable at 1 mg mL^{-1} lysate concentration. However, higher lysate amounts also eliminated any OmpR signal. Furthermore, the OmpR thiophosphorylation signals in the right panel were only visible because of an increase in contrast by 10-fold compared to the left panel of Fig. 5.5.B. Overall, the thiophosphorylation signals in the presence of lysate was much weaker compared to samples without lysate. Consequently, further optimization is needed to improve the thiophosphotransfer reactions in complex protein mixtures.

Addition of cellular lysate could promote increased phosphatase activity of the histidine kinase. Alternatively, non-specific phosphotransfer to other proteins or small-molecule phosphoacceptors and subsequent hydrolysis could be the reason for disappearance of the thiophosphorylation signal. To further investigate the cause of the weak thiophosphorylation signal of the histidine kinases in lysate, a dephosphorylation time-course was measured. EnvZ was pre-phosphorylated with ATPγS for 30 min. Subsequently, cleared lysate was added to the sample and aliquots were quenched at different time points. Addition of 1 mg mL^{-1} lysate to WT EnvZ phosphorylated with ATPγS led to rapid dephosphorylation after 2 min (Fig. 5.5.C). Thiophosphorylation of I432G EnvZ with N^6-benzyl ATPγS remained stable for 5 min after addition of 1 mg mL^{-1}, consistent with the previous results. However, higher amounts of lysate (3 and 5 mg mL^{-1}) led to increasing dephosphorylation starting after 5 min and 1-2 min, respectively. Clearly, use of the *as* variant and an ATPγS analog improved the detectability of thiophosphohistidine. However, additional enhancements are necessary to make this method amenable to the detection of phosphotransfer targets of histidine kinases.

Screening for specific kinase inhibitors of analog-sensitive EnvZ variants[5]

One benefit of histidine kinase sensitization is that the *as* variant is susceptible to specific inhibitors that cannot target the WT enzyme. This approach could facilitate the development of selective inhibitors for a histidine kinase of interest. EnvZ and HpkA *as* histidine kinases can readily accept ATP analogs with a modification at the N^6 position. Given that the same analogs are used for eukaryotic kinases, we reasoned that inhibitor scaffolds that bind competitively to the ATP binding pocket of *as* eukaryotic kinases might also be able to target the pockets of sensitized histidine kinases. A panel of 28 molecules belonging to different inhibitor classes were therefore tested. The thiophosphorylation activity of WT EnvZ, as well as L430G and I432G, with ATPγS was measured after 1 minute. Prior experiments of EnvZ thiophosphorylation demonstrated 1 min to be within the linear range of kinase activity for WT and the two *as* variants. For the initial screen, inhibitors were added to a final concentration of 100 μM.

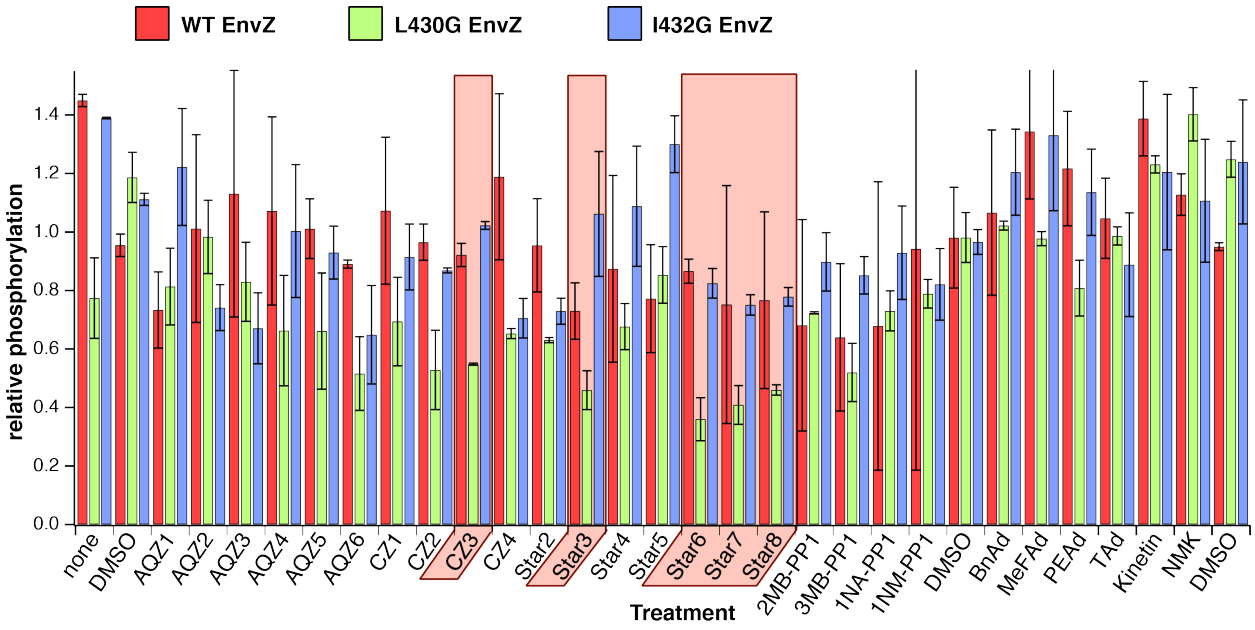

Fig. 5.6. Inhibitor screen against WT and *as* EnvZ variants
Several protein kinase inhibitors were tested for inhibition of EnvZ thiophosphorylation. WT EnvZ and *as* mutants (5μM) were pre-incubated with inhibitor (100μM). Reactions were initiated by addition of ATPγS and quenched after 1 min. Thiophosphorylation was analyzed by Western blot, quantified by densitometry and normalized to the protein load. Error bars represent standard errors from 2 (AQZ1-1NM-PP1) or 3 replicates (BnAd-NMK).

Fig. 5.6 displays the combined results from the inhibitor screen, plotting the relative phosphorylation intensity of each EnvZ variant/inhibitor combination. An exceptionally large error for some of the measured phosphorylation intensities indicated that the thiophosphorylation assay with Western blot detection is not the ideal method to screen inhibitors. It can be assumed that the large number of handling steps in the protocol is the origin of the large systematic error.

[5] Michael Lopez from the Shokat group at UCSF generously supplied the panel of inhibitors.

An enzyme coupled ATPase assay was used as an alternative activity assay with the benefit of high-throughput spectrophotometric measurements in 96-well format. However, the ATPase activity is not an ideal read-out for histidine kinase activity because ATP hydrolysis can be uncoupled from protein autophosphorylation (52).

Taken together, most compounds led to very little inhibition of EnvZ autophosphorylation activity. Even adenine analogs that were based on the ATP analogs, for example N^6-benzyl adenine (BzAd) and N^6-furfuryl adenine (kinetin), were poor inhibitors for the *as* EnvZ variants at the tested concentration. Nonetheless, a few compounds showed a promising decrease in thiophosphorylation of the *as* L430G variant while affecting WT EnvZ to a lesser extent or not at all (Fig. 5.6, compounds boxed in red). These compounds include several newly developed analogs of staurosporine from the Shokat group (Star-3, Star-6, Star-7, Star-8) (Lopez and Shokat, unpublished results). Staurosporine is one of the first known eukaryotic kinase inhibitors with high promiscuity targeting over 90 % of human kinases (39, 53, 54). To our knowledge, histidine kinase inhibition by staurosporine has never been reported. Inhibition of EnvZ autophosphorylation by these compounds is not sufficient for to make them useful tools for chemical-genetics studies of bacterial signaling systems. However, the molecules could serve as templates for designing more potent selective histidine kinase inhibitors in the future.

Discussion

The first step in designing *as* histidine kinases involved the identification of suitable residues, which can be mutated to introduce a hole in the ATP binding pocket. Despite the lack of sequence and structural similarity between eukaryotic kinases and histidine kinases, potential residues were identified near the N^6 amino group of adenine in comparable positions to the gate-keeper in eukaryotic kinases. Two positions were tested in EnvZ and HpkA histidine kinases (*as*-1 and *as*-2). Overall, the *as*-1 position is more conserved. In most cases, it is occupied by large hydrophobic residues, and it is therefore an ideal site for expanding the ATP binding pocket (Fig. 5.1.C-D). In contrast, *as*-2 often contains smaller serine, threonine, or alanine residues, a less ideal choice for introducing a hole into the ATP binding site. The difference in gate-keeper suitability is consistent with the protein engineering results of EnvZ and HpkA. In EnvZ, both positions are occupied by large hydrophobic residues, I432 and L430 respectively. As a result, both glycine mutants permit autophosphorylation by ATP analogs. In contrast, the *as*-2 position of HpkA contains a threonine residue, and the T402G mutant did not accept any ATP analogs suggesting that the binding pocket was not expanded enough. Consequently, the *as*-1 gate-keeper positions seems to be generalizable to other histidine kinases, while the *as*-2 positions needs to be evaluated on a case by case basis.

To use the *as* alleles for selective phosphorylation of a histidine kinase of interest in a background of other ATP utilizing enzymes, the ATP analogs have to be selective for the *as* enzyme. M404G HpkA/N^6-phenylethyl ATPγS form an ideal pair because the large analog is the least reactive for WT enzymes. In contrast, ATP analogs that work for *as* EnvZ variants (N^6-furfuryl and N^6-benzyl ATPγS) still demonstrated some weak reactivity with WT EnvZ (Fig. 5.2.B-C). EnvZ was engineered to accept the larger N^6-phenylethyl analog and 2nd shell mutations were introduced into the ATP binding pocket, which could lead to a further expansion

of the pocket. These were tested in combination with each primary shell gate-keeper residue. One combination, M344G/I432G, could carry out autophosphorylation with N^6-phenylethyl ATPγS (data not shown). However, the overall enzyme activity was slower compared to WT EnvZ and the I432G mutant, suggesting that the 2nd shell mutation compromised the enzyme function by destabilizing the protein. Introduction of additional mutations complicates the design of *as* histidine kinases. The method becomes less generalizable to other family members because the second mutation would have to be individually optimized.

Phosphotransfer experiments with EnvZ and HpkA and their respective response regulators demonstrated, as anticipated, that the transfer of the thiophosphoryl group is not affected by the change in the ATP binding pocket. Because of the higher stability of the P-N bond in thiophosphohistidine compared to phosphohistidine, the transfer kinetics are slower with ATPγS (Fig. 5.3.A) (16). This change in kinetics has to be considered when trying to assign physiological relevance to particular phosphotransfer events and when determining whether a histidine kinase/response regulator interaction is cognate. For example, the phosphotransfer profiling technique used in **Chapter 2** relies on comparing cognate and non-cognate phosphotransfer kinetics (19, 22), which would be altered with ATPγS.

The main challenge for using the *as* histidine kinase for identifying unknown response regulator targets remains the optimization of thiophosphorylation in complex protein mixtures. As intended, the thiophosphorylation and phosphotransfer of *as* EnvZ and their respective ATPγS analog was resistant to the presence of low amounts of bacterial cell lysate. In comparison, the reactions became undetectable for WT EnvZ and ATPγS, even in low lysate concentrations (1 mg mL^{-1}) (Fig. 5.4.A-B). Nonetheless, the same reactions were not detectable for the *as* EnvZ variants with higher concentrations of cell lysate. To be able to detect and identify endogenous levels of phosphotransfer targets of a given kinase, a balance has to be struck in finding the optimal lysate concentration. On the one hand, lysate amounts have to be sufficiently low as to not affect stability of the phosphorylated species. On the other hand they cannot be too low, or else the target proteins are too far diluted, again preventing detection. The 1 mg mL^{-1} lysate concentration at which the phosphorylation reactions can still be carried out is unfortunately too dilute. This is evident because endogenous OmpR, which is relatively abundant in *E. coli* (51, 55), does not produce a thiophosphorylation signal on any of the Western blots (Fig. 5.5). Dephosphorylation time-courses demonstrated that rapid hydrolysis was the main cause of the low thiophosphorylation signal (Fig. 5.5.C). Many factors could promote the dephosphorylation, for example stimulation of phosphatase activity of the histidine kinase or response regulator, non-specific phosphotransfer and subsequent hydrolysis, or dephosphorylation by small molecule phosphoacceptors. Clearly, additional enhancements are needed to improve the stability of the phosphorylated species in complex protein mixtures in order to use the *as* histidine kinases for detection of phosphotransfer targets.

The *as* alleles could be valuable tools for permitting precise inhibition of a particular histidine kinase by using inhibitors that are specific to the expanded ATP binding site. This could facilitate studies of many essential histidine kinases, where gene knockout strains are impossible to obtain (22). In addition, kinase inhibition could be temporally controlled, enabling detailed investigation of histidine kinase function in time-sensitive processes such as cell cycle progression and differentiation (56). The inhibitor screen of *as* EnvZ variants identified several

as specific inhibitor candidates, in particular some newly developed analogs of staurosporine. Inhibition was relatively weak (approximately 40 - 50% at 100 μM), but surprisingly comparable to other compounds identified in high-throughput screens (57). However, none of the compounds screened in this work show inhibition levels that are potent enough. Further optimization is required and the tested molecules could serve as first scaffolds.

The histidine kinase CA belongs to the larger GHKL protein family of ATPases, which includes topoisomerase II, Hsp90, and MutL (46). Because of high sequence and structure conservation within this family, the engineering approach tested here is also applicable to other family members. The gate-keeper positions of the histidine kinase CA domain are also present in other family members, allowing simple construction of the *as* alleles. This could open the door for developing new tools for targeting and manipulating members of other GHKL subfamilies.

References

1. Stock, A. M., Robinson, V. L., and Goudreau, P. N. (2000) Two-component signal transduction. *Annu. Rev. Biochem.* **69**, 183–215
2. Cheung, J., and Hendrickson, W. A. (2010) Sensor domains of two-component regulatory systems. *Curr. Opin. Microbiol.* **13**, 116–123
3. Galperin, M. Y. (2010) Diversity of structure and function of response regulator output domains. *Curr. Opin. Microbiol.* **13**, 150–159
4. Goulian, M. (2010) Two-component signaling circuit structure and properties. *Curr. Opin. Microbiol.* **13**, 184–189
5. Plate, L., and Marletta, M. A. (2012) Nitric oxide modulates bacterial biofilm formation through a multicomponent cyclic-di-GMP signaling network. *Mol Cell* **46**, 449–460
6. Raghavan, V., and Groisman, E. A. (2010) Orphan and hybrid two-component system proteins in health and disease. *Curr. Opin. Microbiol.* **13**, 226–231
7. Gooderham, W. J., and Hancock, R. E. W. (2009) Regulation of virulence and antibiotic resistance by two-component regulatory systems in Pseudomonas aeruginosa. *FEMS Microbiology Reviews* **33**, 279–294
8. Groisman, E. A. (2001) The pleiotropic two-component regulatory system PhoP-PhoQ. *J. Bacteriol.* **183**, 1835–1842
9. Gotoh, Y., Eguchi, Y., Watanabe, T., Okamoto, S., Doi, A., and Utsumi, R. (2010) Two-component signal transduction as potential drug targets in pathogenic bacteria. *Curr. Opin. Microbiol.* **13**, 232–239
10. Watanabe, T., Okada, A., Gotoh, Y., and Utsumi, R. (2008) Inhibitors targeting two-component signal transduction. *Adv. Exp. Med. Biol.* **631**, 229–236
11. Francis, S., Wilke, K. E., Brown, D. E., and Carlson, E. E. (2013) Mechanistic insight into inhibition of two-component system signaling. *Medchemcomm* **4**, 269–277
12. Kee, J.-M., and Muir, T. W. (2012) Chasing phosphohistidine, an elusive sibling in the phosphoamino acid family. *ACS Chem Biol* **7**, 44–51
13. Attwood, P. V., Piggott, M. J., Zu, X. L., and Besant, P. G. (2007) Focus on phosphohistidine. *Amino Acids* **32**, 145–156
14. Stock, J. B., Stock, A. M., and Mottonen, J. M. (1990) Signal transduction in bacteria. *Nature* **344**, 395–400
15. Stock, J. B., Surette, M., Levit, M., and Park, P. (1995) in *Two-Component Signal*

Transduction (Hoch, J. A., and Silhavy, T. J., eds.), ASM Press, Washington, DC
16. Carlson, H. K., Plate, L., Price, M. S., Allen, J. J., Shokat, K. M., and Marletta, M. A. (2010) Use of a semisynthetic epitope to probe histidine kinase activity and regulation. *Anal. Biochem.* **397**, 139–143
17. Wilke, K. E., Francis, S., and Carlson, E. E. (2012) Activity-based probe for histidine kinase signaling. *J Am Chem Soc* **134**, 9150–9153
18. Pirrung, M. C., James, K. D., and Rana, V. S. (2000) Thiophosphorylation of histidine. *J Org Chem* **65**, 8448–8453
19. Laub, M. T., Biondi, E. G., and Skerker, J. M. (2007) Phosphotransfer profiling: systematic mapping of two-component signal transduction pathways and phosphorelays. *Meth. Enzymol.* **423**, 531–548
20. Laub, M. T., and Goulian, M. (2007) Specificity in two-component signal transduction pathways. *Annu. Rev. Genet.* **41**, 121–145
21. Procaccini, A., Lunt, B., Szurmant, H., Hwa, T., and Weigt, M. (2011) Dissecting the specificity of protein-protein interaction in bacterial two-component signaling: orphans and crosstalks. *PLoS ONE* **6**, e19729
22. Skerker, J. M., Prasol, M. S., Perchuk, B. S., Biondi, E. G., and Laub, M. T. (2005) Two-component signal transduction pathways regulating growth and cell cycle progression in a bacterium: a system-level analysis. *PLoS Biol.* **3**, e334
23. Shah, K., Liu, Y., Deirmengian, C., and Shokat, K. M. (1997) Engineering unnatural nucleotide specificity for Rous sarcoma virus tyrosine kinase to uniquely label its direct substrates. *Proc. Natl. Acad. Sci. USA* **94**, 3565–3570
24. Liu, Y., Shah, K., Yang, F., Witucki, L., and Shokat, K. M. (1998) Engineering Src family protein kinases with unnatural nucleotide specificity. *Chem Biol* **5**, 91–101
25. Blethrow, J., Zhang, C., Shokat, K. M., and Weiss, E. L. (2004) Design and use of analog-sensitive protein kinases. *Curr Protoc Mol Biol* **Chapter 18**, Unit 18.11
26. Shah, K., and Shokat, K. M. (2002) A chemical genetic screen for direct v-Src substrates reveals ordered assembly of a retrograde signaling pathway. *Chem Biol* **9**, 35–47
27. Eblen, S. T., Kumar, N. V., Shah, K., Henderson, M. J., Watts, C. K. W., Shokat, K. M., and Weber, M. J. (2003) Identification of novel ERK2 substrates through use of an engineered kinase and ATP analogs. *J. Biol. Chem.* **278**, 14926–14935
28. Ubersax, J. A., Woodbury, E. L., Quang, P. N., Paraz, M., Blethrow, J. D., Shah, K., Shokat, K. M., and Morgan, D. O. (2003) Targets of the cyclin-dependent kinase Cdk1. *Nature* **425**, 859–864
29. Allen, J. J., Lazerwith, S. E., and Shokat, K. M. (2005) Bio-orthogonal affinity purification of direct kinase substrates. *J Am Chem Soc* **127**, 5288–5289
30. Blethrow, J. D., Glavy, J. S., Morgan, D. O., and Shokat, K. M. (2008) Covalent capture of kinase-specific phosphopeptides reveals Cdk1-cyclin B substrates. *Proc. Natl. Acad. Sci. USA* **105**, 1442–1447
31. Bishop, A. C., Ubersax, J. A., Petsch, D. T., Matheos, D. P., Gray, N. S., Blethrow, J., Shimizu, E., Tsien, J. Z., Schultz, P. G., Rose, M. D., Wood, J. L., Morgan, D. O., and Shokat, K. M. (2000) A chemical switch for inhibitor-sensitive alleles of any protein kinase. *Nature* **407**, 395–401
32. Bishop, A. C., Buzko, O., and Shokat, K. M. (2001) Magic bullets for protein kinases. *Trends Cell Biol.* **11**, 167–172
33. Kraybill, B. C., Elkin, L. L., Blethrow, J. D., Morgan, D. O., and Shokat, K. M. (2002)

Inhibitor scaffolds as new allele specific kinase substrates. *J Am Chem Soc* **124**, 12118–12128
34. Liu, Y., Kung, C., Fishburn, J., Ansari, A. Z., Shokat, K. M., and Hahn, S. (2004) Two cyclin-dependent kinases promote RNA polymerase II transcription and formation of the scaffold complex. *Mol Cell Biol* **24**, 1721–1735
35. Larochelle, S., Merrick, K. A., Terret, M.-E., Wohlbold, L., Barboza, N. M., Zhang, C., Shokat, K. M., Jallepalli, P. V., and Fisher, R. P. (2007) Requirements for Cdk7 in the assembly of Cdk1/cyclin B and activation of Cdk2 revealed by chemical genetics in human cells. *Mol Cell* **25**, 839–850
36. Jaeschke, A., Karasarides, M., Ventura, J.-J., Ehrhardt, A., Zhang, C., Flavell, R. A., Shokat, K. M., and Davis, R. J. (2006) JNK2 is a positive regulator of the cJun transcription factor. *Mol Cell* **23**, 899–911
37. Allen, J. J., Li, M., Brinkworth, C. S., Paulson, J. L., Wang, D., Hübner, A., Chou, W.-H., Davis, R. J., Burlingame, A. L., Messing, R. O., Katayama, C. D., Hedrick, S. M., and Shokat, K. M. (2007) A semisynthetic epitope for kinase substrates. *Nat. Methods* **4**, 511–516
38. Marina, A., Waldburger, C. D., and Hendrickson, W. A. (2005) Structure of the entire cytoplasmic portion of a sensor histidine-kinase protein. *EMBO J* **24**, 4247–4259
39. Tanaka, T., Saha, S. K., Tomomori, C., Ishima, R., Liu, D., Tong, K. I., Park, H., Dutta, R., Qin, L., Swindells, M. B., Yamazaki, T., Ono, A. M., Kainosho, M., Inouye, M., and Ikura, M. (1998) NMR structure of the histidine kinase domain of the E. coli osmosensor EnvZ. *Nature* **396**, 88–92
40. Xu, W., Doshi, A., Lei, M., Eck, M. J., and Harrison, S. C. (1999) Crystal structures of c-Src reveal features of its autoinhibitory mechanism. *Mol Cell* **3**, 629–638
41. Yoshida, T., Phadtare, S., and Inouye, M. (2007) Functional and structural characterization of EnvZ, an osmosensing histidine kinase of E. coli. *Meth. Enzymol.* **423**, 184–202
42. Goudreau, P. N., Lee, P. J., and Stock, A. M. (1998) Stabilization of the phospho-aspartyl residue in a two-component signal transduction system in Thermotoga maritima. *Biochemistry* **37**, 14575–14584
43. Busso, D., Delagoutte-Busso, B., and Moras, D. (2005) Construction of a set Gateway-based destination vectors for high-throughput cloning and expression screening in Escherichia coli. *Anal. Biochem.* **343**, 313–321
44. Larochelle, S., Batliner, J., Gamble, M. J., Barboza, N. M., Kraybill, B. C., Blethrow, J. D., Shokat, K. M., and Fisher, R. P. (2006) Dichotomous but stringent substrate selection by the dual-function Cdk7 complex revealed by chemical genetics. *Nat Struct Mol Biol* **13**, 55–62
45. Witucki, L. A., Huang, X., Shah, K., Liu, Y., Kyin, S., Eck, M. J., and Shokat, K. M. (2002) Mutant tyrosine kinases with unnatural nucleotide specificity retain the structure and phospho-acceptor specificity of the wild-type enzyme. *Chem Biol* **9**, 25–33
46. Dutta, R., and Inouye, M. (2000) GHKL, an emergent ATPase/kinase superfamily. *Trends in Biochemical Sciences* **25**, 24–28
47. Tomomori, C., Tanaka, T., Dutta, R., Park, H., Saha, S. K., Zhu, Y., Ishima, R., Liu, D., Tong, K. I., Kurokawa, H., Qian, H., Inouye, M., and Ikura, M. (1999) Solution structure of the homodimeric core domain of Escherichia coli histidine kinase EnvZ. *Nat. Struct. Biol.* **6**, 729–734

48. Aiba, H., Mizuno, T., and Mizushima, S. (1989) Transfer of phosphoryl group between two regulatory proteins involved in osmoregulatory expression of the ompF and ompC genes in Escherichia coli. *J. Biol. Chem.* **264**, 8563–8567
49. Lasker, M., Bui, C. D., Besant, P. G., Sugawara, K., Thai, P., Medzihradszky, G., and Turck, C. W. (1999) Protein histidine phosphorylation: increased stability of thiophosphohistidine. *Protein Sci* **8**, 2177–2185
50. Aiba, H., Nakasai, F., Mizushima, S., and Mizuno, T. (1989) Phosphorylation of a bacterial activator protein, OmpR, by a protein kinase, EnvZ, results in stimulation of its DNA-binding ability. *J. Biochem.* **106**, 5–7
51. Cai, S. J., and Inouye, M. (2002) EnvZ-OmpR interaction and osmoregulation in Escherichia coli. *J. Biol. Chem.* **277**, 24155–24161
52. Trajtenberg, F., Grana, M., Ruetalo, N., Botti, H., and Buschiazzo, A. (2010) Structural and Enzymatic Insights into the ATP Binding and Autophosphorylation Mechanism of a Sensor Histidine Kinase. *Journal of Biological Chemistry* **285**, 24892–24903
53. Dar, A. C., and Shokat, K. M. (2011) The Evolution of Protein Kinase Inhibitors from Antagonists to Agonists of Cellular Signaling. *Annu. Rev. Biochem.* **80**, 769–795
54. Karaman, M. W., Herrgard, S., Treiber, D. K., Gallant, P., Atteridge, C. E., Campbell, B. T., Chan, K. W., Ciceri, P., Davis, M. I., Edeen, P. T., Faraoni, R., Floyd, M., Hunt, J. P., Lockhart, D. J., Milanov, Z. V., Morrison, M. J., Pallares, G., Patel, H. K., Pritchard, S., Wodicka, L. M., and Zarrinkar, P. P. (2008) A quantitative analysis of kinase inhibitor selectivity. *Nat. Biotechnol.* **26**, 127–132
55. Wang, M., Weiss, M., Simonovic, M., Haertinger, G., Schrimpf, S. P., Hengartner, M. O., and Mering, von, C. (2012) PaxDb, a Database of Protein Abundance Averages Across All Three Domains of Life. *Mol. Cell Proteomics* **11**, 492–500
56. Kirkpatrick, C. L., and Viollier, P. H. (2012) Decoding Caulobacter development. *FEMS Microbiology Reviews* **36**, 193–205
57. Hubbard, J., Burnham, M. K. R., and Throup, J. P. (2003) in *Histidine Kinases in Signal Transduction* (Inouye, M., and Dutta, R., eds.), Academic Press, San Diego, CA

CHAPTER 6:

FUTURE DIRECTIONS

The recent discoveries in H-NOX signaling demonstrate an array of behavioral outputs influenced by NO, that range from control of motility and biofilm formation, to regulation of host-colonization, and to involvement in quorum sensing. In **Chapters 2 and 3**, the characterization of the H-NOX signaling network in *S. oneidensis* and *V. cholera* elucidated the mechanistic details of how NO triggers increased biofilm formation. Homologous systems exist in other gammaproteobacteria, but the full distribution of bacterial species with H-NOX proteins (Fig. A.1.A) displays that we currently only understand the physiological role of a small subset of H-NOX signaling pathways.

This leaves room for further exploration and functional characterization of H-NOX signaling pathways in phyla other than the gammaproteobacteria. Some organisms have obvious RRs in the H-NOX operons. In particular, *Bacteroidetes* contain CheY-like RRs or ones with LytTR DNA-binding domains. This suggests a role for H-NOX/NO signaling in chemotaxis or execution of specific transcriptional programs in response to NO. Gene expression analysis by microarray or RNAseq can identify the transcriptional targets of the LytTR RRs. The same technique can find transcriptional targets of NtrC-like RRs in several other H-NOX containing organisms. In the future, phosphotransfer profiling will remain a useful technique to identify the cognate RRs of the many other H-NOX/HK systems without easily discernable cognate RRs. Furthermore, the biological function of the H-NOX-MCP fusions in chemotaxis is unknown. Biochemical studies by other members of this research group currently investigate the influence of H-NOX ligation state on the chemotaxis autophosphorylation and phosphotransfer reactions. Genetic studies with *hnoX* deletion strains in these anaerobic species will address whether the H-NOX is required for chemotactic behavior in response to NO or O_2. As diverse H-NOX pathways from other species are characterized in the future, the repertoire of physiological functions will likely expand.

The prevalence of orphan H-NOX/HK pairs highlights the necessity for new tools to map TCSs more efficiently. Without knowledge of the cognate RRs, assignment of physiological function to the signaling system is not possible. While phosphotransfer profiling and computational prediction are often useful, they have many limitations (1, 2). For example, protein isolation becomes increasingly laborious for phosphotransfer profiling in organisms with large numbers of orphan RRs. Bioinformatic mapping algorithms perform well for predicting interactions in simple TCSs, but the method has not been adapted to multi-step phosphorelay systems, such as the majority of H-NOX TCSs. Consequently, the *in situ* mapping strategy for TCSs - based on the development of analog-sensitive histidine kinases in **Chapter 5** - could be extremely useful. Due to instability of the thiophosphohistidine and thiophosphoaspartic acid modifications in the presence of complex protein mixtures, large improvements are necessary for the enrichment and detection of phosphorylated RR targets. Instead of relying on a stable phosphoanhydride bond for affinity enrichment, a modified strategy could exploit selective

chemical reactivity of the phosphoaspartic acid species. For example, sodium borohydride has been used for reduction of phosphoaspartate to yield homoserine, which could be detected by mass spectrometry (3). Alternatively, milder reductants could be identified to yield the intermediate aspartate semialdehyde. The aldehyde group could then serve as a reactive handle for selective labeling and enrichment with alkoxyamines or hydrazides.

The H-NOX signaling network uncovered in *S. oneidensis* and *V. cholera* involves a second histidine kinase, HnoS: it can phosphorylate the same RR targets involved in cyclic-di-GMP degradation. Like HnoK, HnoS lacks any associated sensor domain. The identity of the sensor domain and the detected signal are currently unknown, but the FIST protein HnoE is a likely candidate. Bioinformatic analysis of FIST proteins suggests an involvement in signal transduction pathways and predicts small molecules such as amino acids as ligands (4). However, no FIST family members have been biochemically characterized. To define the role of HnoS in the H-NOX signaling network, HnoE should be cloned and purified, and binding to HnoS should be tested. If the FIST protein interacts with HnoS, common metabolites and small molecules should be assayed for association and control of HnoS autophosphorylation activity. To assign a physiological function to HnoS and HnoE, *S. oneidensis* deletion strains of both genes could be screened in phenotype microarrays for defects in growth or biofilm formation (5).

Given the important role for NO in the mammalian immune response, it will be exciting to uncover H-NOX-mediated countermeasures involved in bacterial pathogenesis. Since *L. pneumophila* directly infects alveolar macrophages causing gamma interferon mediated iNOS activation, the pathogens are potentially exposed to cytotoxic levels of NO during the course of infection (6, 7). However, the role of NO in clearance of *L. pneumophila* infections remains controversial (8-11). In *V. cholerae*, biofilms have been shown to enhance infectivity (12, 13), and additionally, defense against reactive nitrogen species (RNS) is important for host colonization (14, 15). Therefore, host NO-induced biofilms could play a significant role in enhancing *V. cholerae* infection. Further studies are required to elucidate the exact role of H-NOX/NO signal pathway in the infection process. Deletion strain of the *hnoX*, *hnoK*, *hnoB* and *hnoD* gene should be constructed in *V. cholerae* to assess their effect on biofilm formation. To investigate whether H-NOX signaling influences *V. cholerae* virulence, mouse colonization studies should be conducted with the *hno* deletion strains. Mice should be inoculated competitively with WT and a respective *hno* deletion strain. Subsequent recovery of the colonized species and quantification of each strain will deliver a competitive index. This value reports whether the *hno* deletion strains exhibit decreased virulence compared to WT (14). Use of an isogenic $iNOS^{-/-}$ mouse and neutralization of stomach acid to remove acidified nitrite will eliminate host-derived sources of NO (14). These controls could prove a direct involvement of NO in the virulence defect of any *hno* deletion strains.

Biofilms play an important role in persistent bacterial infections and resistance to antibiotics. Antimicrobial agents cannot diffuse into the bottom layers of the biofilms and biofilm-associated cell are often metabolically dormant (16, 17). Novel treatment strategies for bacterial infections therefore should focus on combatting biofilms in combination with antibiotic use (18). Low doses of NO have been shown to lead to biofilm dispersal in *Pseudomonas aeruginosa* and have therefore been proposed as antibiofilm agent (19-21). However, *P. aeruginosa* does not contain an H-NOX protein, and the signaling events linking NO exposure to

decreased cyclic-di-GMP levels are unknown. A similar strategy of NO-mediated biofilm dispersal could be effective in *L. pneumophila* and *S. woodyi* where NO signaling decreases cyclic-di-GMP concentrations (22, 23). However, this treatment is not generalizable because other gammaproteobacteria, such as *V. cholerae* and *S. oneidensis,* demonstrate higher biofilm formation in response to NO (24). In this case, the H-NOX/NO signaling components could be appropriate targets for developing antibiofilm agents. Since cyclic-di-GMP concentrations are a major determinant of biofilm formation and also a switch between chronic and acute infection, the cyclic-di-GMP metabolizing enzymes represent attractive therapeutical targets (18). Inhibitors of DGC should lower cyclic-di-GMP levels and prevent biofilm formation. Activators of PDEs should have a similar effect. Since the cyclic-di-GMP metabolizing enzymes are widely conserved between bacterial species, any small molecule inhibitor or activator could be broadly effective. The PDE RR HnoB was shown to have a strong influence on biofilm formation, and the protein could be isolated and was amenable to *in vitro* enzyme activity assays. Likewise, the HD-GYP enzymes in **Chapter 5** could be used as targets. A high-throughput compatible colorimetric activity assay measuring inorganic phosphate release could be designed in the future. Subsequently, this assay could be used to screen small molecule libraries to identify activators of PDE activity. If H-NOX/NO signaling is discovered to play a role in *V. cholerae* virulence, any compounds acting on the H-NOX signaling network could also directly affect the infection process.

References

1. Laub, M. T., Biondi, E. G., and Skerker, J. M. (2007) Phosphotransfer profiling: systematic mapping of two-component signal transduction pathways and phosphorelays. *Meth. Enzymol.* **423**, 531–548
2. Procaccini, A., Lunt, B., Szurmant, H., Hwa, T., and Weigt, M. (2011) Dissecting the specificity of protein-protein interaction in bacterial two-component signaling: orphans and crosstalks. *PLoS ONE* **6**, e19729
3. Purich, D. L. (2002) Use of sodium borohydride to detect acyl-phosphate linkages in enzyme reactions. *Meth. Enzymol.* **354**, 168–177
4. Borziak, K., and Zhulin, I. B. (2007) FIST: a sensory domain for diverse signal transduction pathways in prokaryotes and ubiquitin signaling in eukaryotes. *Bioinformatics* **23**, 2518–2521
5. Bochner, B. R. (2009) Global phenotypic characterization of bacteria. *FEMS Microbiology Reviews* **33**, 191–205
6. Swanson, M. S., and Hammer, B. K. (2000) Legionella pneumophila pathogesesis: a fateful journey from amoebae to macrophages. *Annu Rev Microbiol* **54**, 567–613
7. MacMicking, J., Xie, Q. W., and Nathan, C. (1997) Nitric oxide and macrophage function. *Annu. Rev. Immunol.* **15**, 323–350
8. Yamamoto, Y., Klein, T. W., and Friedman, H. (1996) Immunoregulatory role of nitric oxide in Legionella pneumophila-infected macrophages. *Cell. Immunol.* **171**, 231–239
9. Brieland, J. K., Remick, D. G., Freeman, P. T., Hurley, M. C., Fantone, J. C., and Engleberg, N. C. (1995) In vivo regulation of replicative Legionella pneumophila lung infection by endogenous tumor necrosis factor alpha and nitric oxide. *Infect. Immun.* **63**, 3253–3258

10. Heath, L., Chrisp, C., Huffnagle, G., LeGendre, M., Osawa, Y., Hurley, M., Engleberg, C., Fantone, J., and Brieland, J. (1996) Effector mechanisms responsible for gamma interferon-mediated host resistance to Legionella pneumophila lung infection: the role of endogenous nitric oxide differs in susceptible and resistant murine hosts. *Infect. Immun.* **64**, 5151–5160
11. Neumeister, B., Bach, V. R., Faigle, M., and Northoff, H. (2001) Induction of iNOS in human monocytes infected with different Legionellaspecies. *FEMS Microbiol Lett* **202**, 31–38
12. Zhu, J., and Mekalanos, J. J. (2003) Quorum sensing-dependent biofilms enhance colonization in Vibrio cholerae. *Dev. Cell* **5**, 647–656
13. Faruque, S. M., Biswas, K., Udden, S. M. N., Ahmad, Q. S., Sack, D. A., Nair, G. B., and Mekalanos, J. J. (2006) Transmissibility of cholera: in vivo-formed biofilms and their relationship to infectivity and persistence in the environment. *Proc. Natl. Acad. Sci. USA* **103**, 6350–6355
14. Davies, B. W., Bogard, R. W., Dupes, N. M., Gerstenfeld, T. A. I., Simmons, L. A., and Mekalanos, J. J. (2011) DNA damage and reactive nitrogen species are barriers to Vibrio cholerae colonization of the infant mouse intestine. *PLoS Pathog.* **7**, e1001295
15. Stern, A. M., Hay, A. J., Liu, Z., Desland, F. A., Zhang, J., Zhong, Z., and Zhu, J. (2012) The NorR regulon is critical for Vibrio cholerae resistance to nitric oxide and sustained colonization of the intestines. *MBio* **3**, e00013–12
16. Donlan, R. M., and Costerton, J. W. (2002) Biofilms: survival mechanisms of clinically relevant microorganisms. *Clin. Microbiol. Rev.* **15**, 167–193
17. Costerton, J. W., Stewart, P. S., and Greenberg, E. P. (1999) Bacterial biofilms: a common cause of persistent infections. *Science* **284**, 1318–1322
18. Römling, U., and Balsalobre, C. (2012) Biofilm infections, their resilience to therapy and innovative treatment strategies. *J. Intern. Med.* **272**, 541–561
19. Barraud, N., Schleheck, D., Klebensberger, J., Webb, J. S., Hassett, D. J., Rice, S. A., and Kjelleberg, S. (2009) Nitric oxide signaling in Pseudomonas aeruginosa biofilms mediates phosphodiesterase activity, decreased cyclic di-GMP levels, and enhanced dispersal. *J. Bacteriol.* **191**, 7333–7342
20. Barraud, N., Hassett, D. J., Hwang, S.-H., Rice, S. A., Kjelleberg, S., and Webb, J. S. (2006) Involvement of nitric oxide in biofilm dispersal of Pseudomonas aeruginosa. *J. Bacteriol.* **188**, 7344–7353
21. Barraud, N., Storey, M. V., Moore, Z. P., Webb, J. S., Rice, S. A., and Kjelleberg, S. (2009) Nitric oxide-mediated dispersal in single- and multi-species biofilms of clinically and industrially relevant microorganisms. *Microb Biotechnol* **2**, 370–378
22. Carlson, H. K., Vance, R. E., and Marletta, M. A. (2010) H-NOX regulation of c-di-GMP metabolism and biofilm formation in Legionella pneumophila. *Mol. Microbiol.* **77**, 930–942
23. Liu, N., Xu, Y., Hossain, S., Huang, N., Coursolle, D., Gralnick, J. A., and Boon, E. M. (2012) Nitric oxide regulation of cyclic di-GMP synthesis and hydrolysis in Shewanella woodyi. *Biochemistry* **51**, 2087–2099
24. Plate, L., and Marletta, M. A. (2012) Nitric oxide modulates bacterial biofilm formation through a multicomponent cyclic-di-GMP signaling network. *Mol Cell* **46**, 449–460

APPENDIX

Appendix A

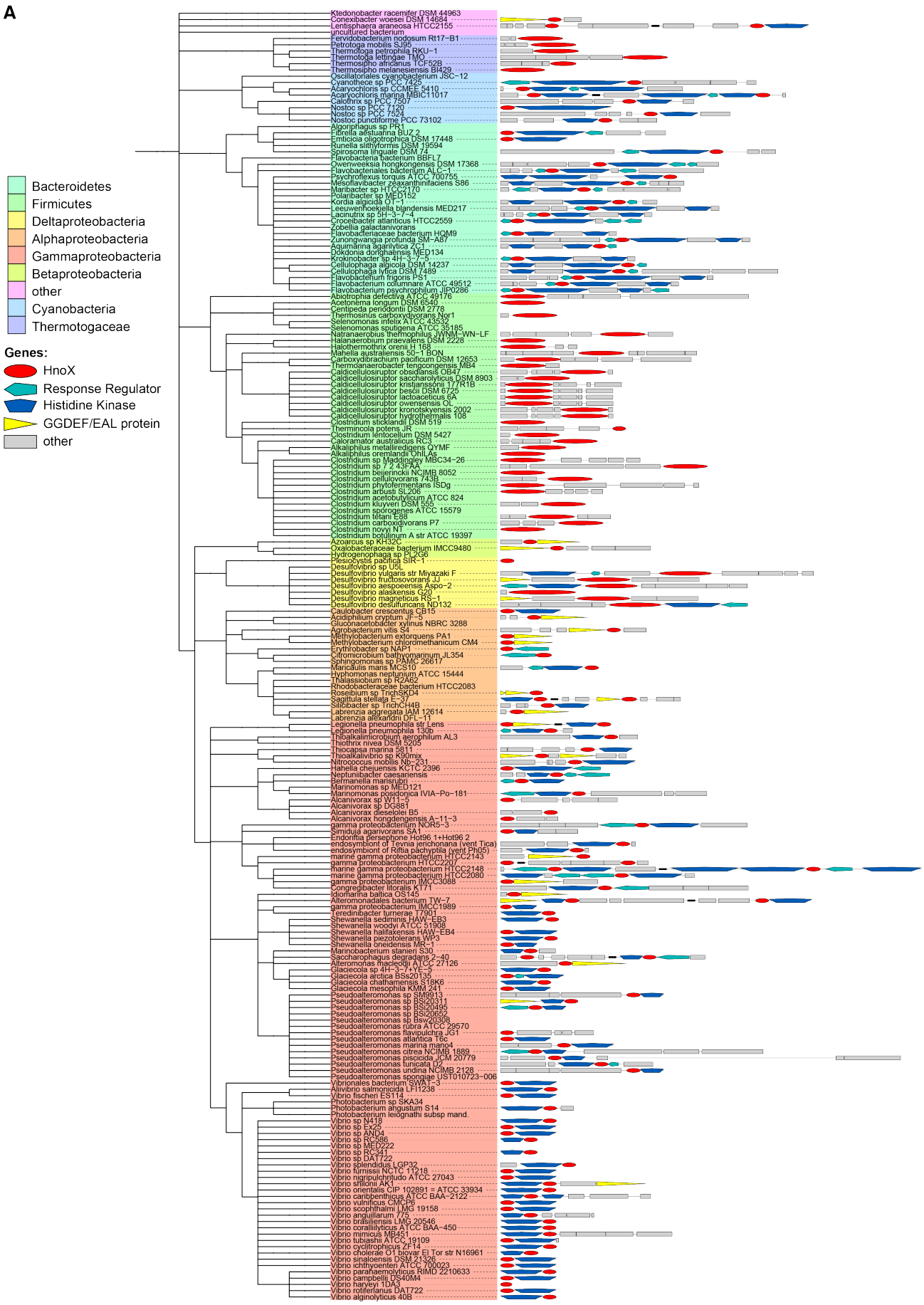
A
Bacteroidetes
Firmicutes
Deltaproteobacteria
Alphaproteobacteria
Gammaproteobacteria
Betaproteobacteria
other
Cyanobacteria
Thermotogaceae
Genes:
HnoX
Response Regulator
Histidine Kinase
GGDEF/EAL protein
other

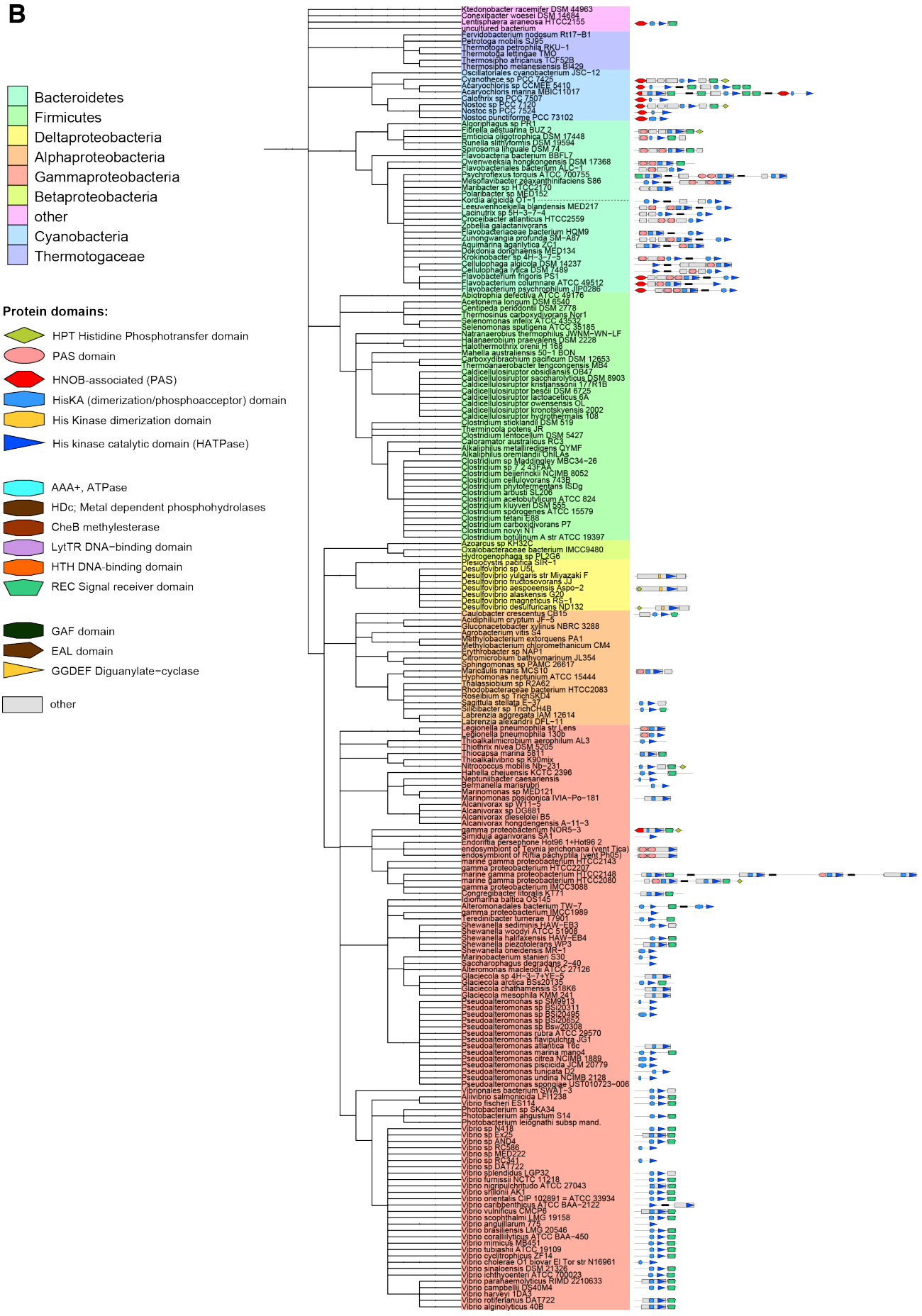
B
Bacteroidetes
Firmicutes
Deltaproteobacteria
Alphaproteobacteria
Gammaproteobacteria
Betaproteobacteria
other
Cyanobacteria
Thermotogaceae
Protein domains:
HPT Histidine Phosphotransfer domain
PAS domain
HNOB-associated (PAS)
HisKA (dimerization/phosphoacceptor) domain
His Kinase dimerization domain
His kinase catalytic domain (HATPase)
AAA+, ATPase
HDc; Metal dependent phosphohydrolases
CheB methylesterase
LytTR DNA-binding domain
HTH DNA-binding domain
REC Signal receiver domain
GAF domain
EAL domain
GGDEF Diguanylate-cyclase
other

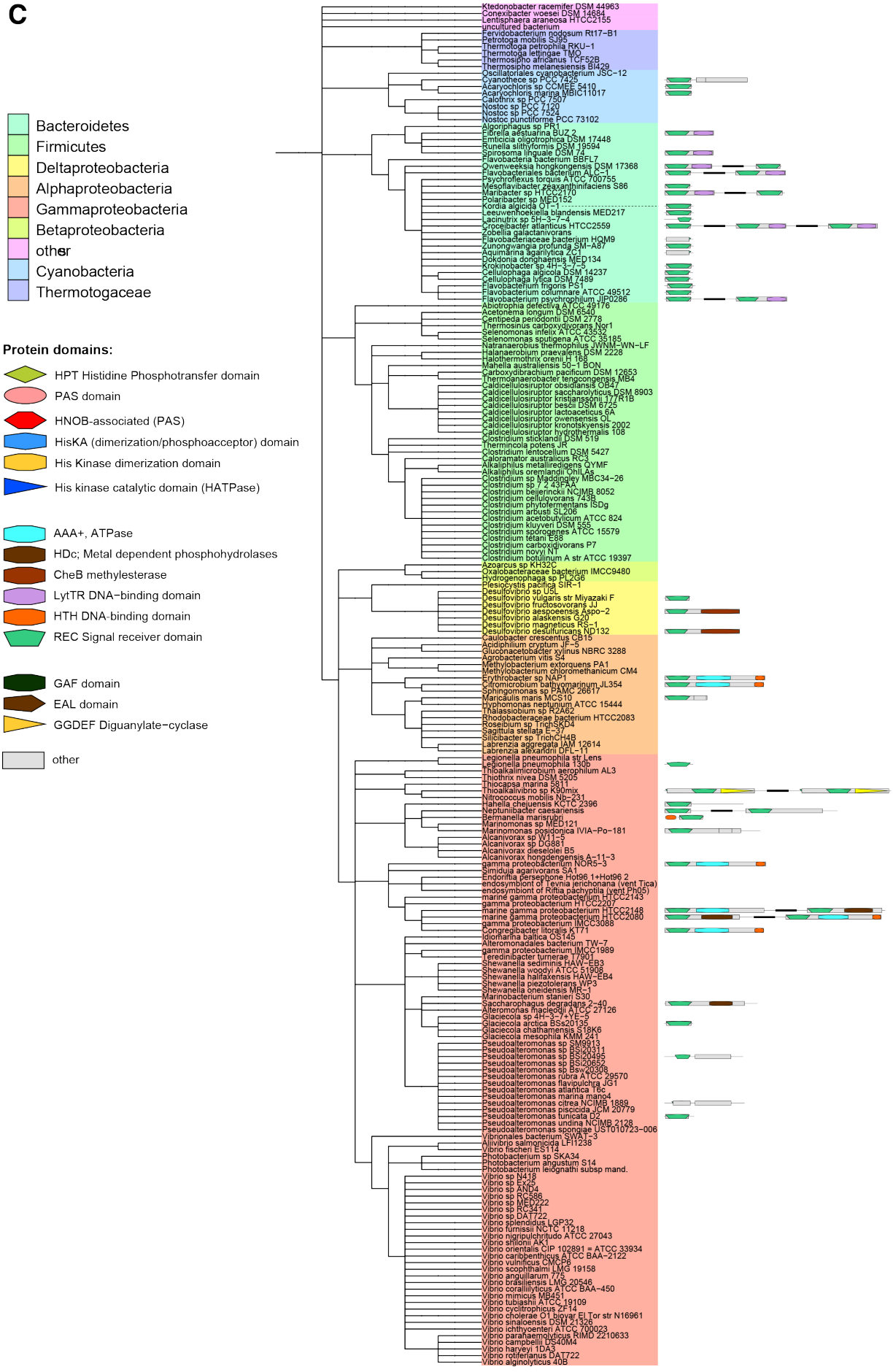
C
Bacteroidetes
Firmicutes
Deltaproteobacteria
Alphaproteobacteria
Gammaproteobacteria
Betaproteobacteria
other
Cyanobacteria
Thermotogaceae
Protein domains:
HPT Histidine Phosphotransfer domain
PAS domain
HNOB-associated (PAS)
HisKA (dimerization/phosphoacceptor) domain
His Kinase dimerization domain
His kinase catalytic domain (HATPase)
AAA+, ATPase
HDc; Metal dependent phosphohydrolases
CheB methylesterase
LytTR DNA-binding domain
HTH DNA-binding domain
REC Signal receiver domain
GAF domain
EAL domain
GGDEF Diguanylate-cyclase
other

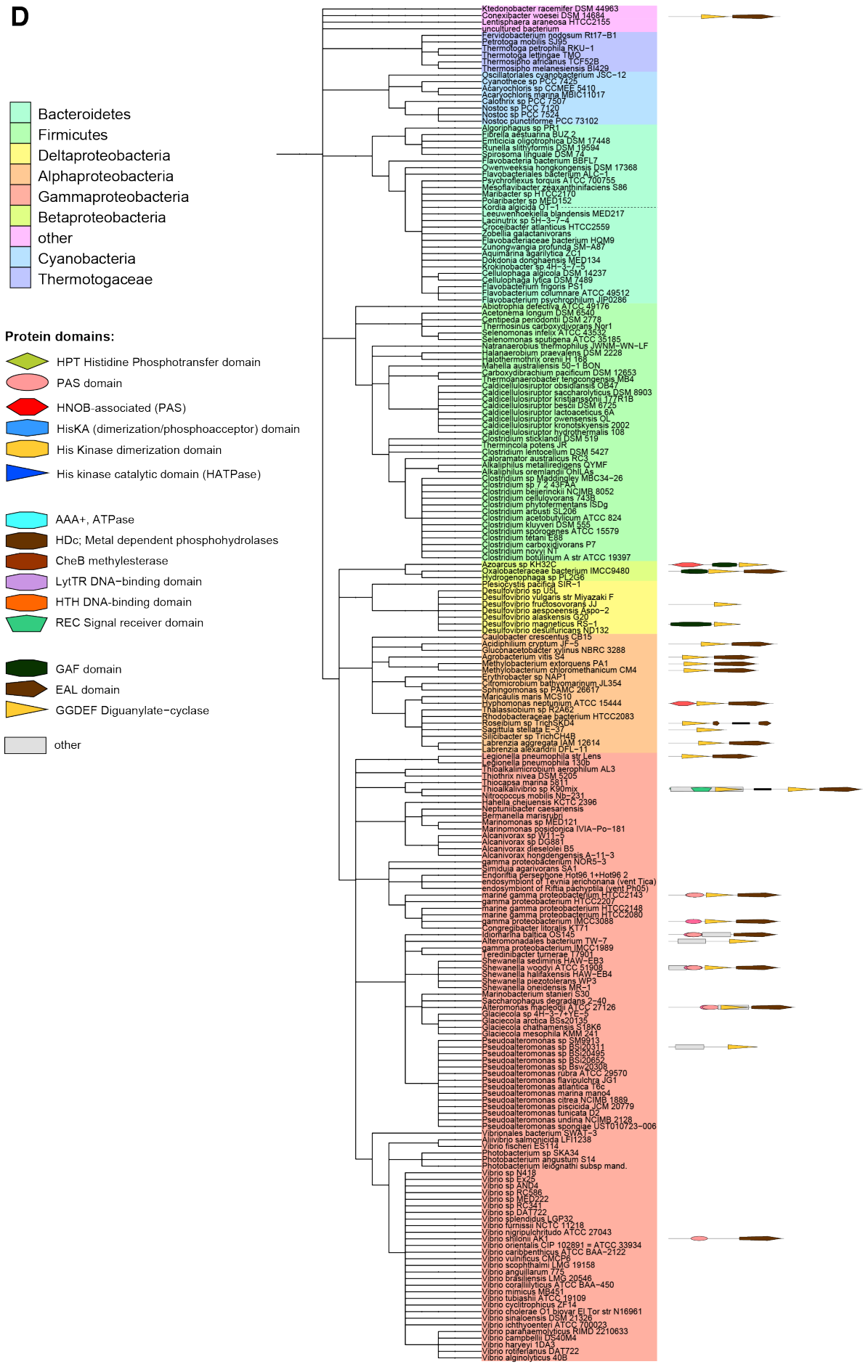
D
Bacteroidetes
Firmicutes
Deltaproteobacteria
Alphaproteobacteria
Gammaproteobacteria
Betaproteobacteria
other
Cyanobacteria
Thermotogaceae
Protein domains:
HPT Histidine Phosphotransfer domain
PAS domain
HNOB-associated (PAS)
HisKA (dimerization/phosphoacceptor) domain
His Kinase dimerization domain
His kinase catalytic domain (HATPase)
AAA+, ATPase
HDc; Metal dependent phosphohydrolases
CheB methylesterase
LytTR DNA-binding domain
HTH DNA-binding domain
REC Signal receiver domain
GAF domain
EAL domain
GGDEF Diguanylate-cyclase
other

Fig. A.1. Organization of operons containing H-NOX genes
A. Operon organization
B. Domain architectures of histidine kinases in H-NOX operons
C. Domain architectures of response regulators in H-NOX operons
D. Domain architectures of GGDEF and EAL proteins in H-NOX operons

Appendix B

Table B.1. Plasmids and bacterial strains used in Chapter 2

Strain or plasmid	Relevant genotype	Reference
Bacterial Strains		
S. oneidensis		
MR-1	*Shewanella oneidensis* MR-1 wild-type	(1)
Δ*hnoX*	MR-1 Δ*hnoX*	This work
Δ*hnoK*	MR-1 Δ*hnoK*	This work
Δ*hnoB*	MR-1 Δ*hnoB*	This work
Δ*hnoC*	MR-1 Δ*hnoC*	This work
Δ*hnoD*	MR-1 Δ*hnoD*	This work
Δ*hnoB*/pBAD202	Δ*hnoB* pBAD202 Kan^R	This work
Δ*hnoB*/p*hnoB*	Δ*hnoB* pBAD-RBS-*hnoB* Kan^R	This work
E. coli		
BL21(DE3)pLysS	*F- ompT hsdSB (r_B-m_B-) gal dcm (DE3) pLysS* Cam^R, Expression strain	Invitrogen
S17-λpir	*thi pro recA hsdR* [RP4-2Tc::Mu-Km::Tn7] λ*pir* Tp^R Sm^R	(2)
Plasmids		
pDS3.0	R6K ori, *RK2 mob, sacB,* Gen^R, suicide plasmid for in-frame deletions	Alfred Spormann, Stanford University
pDS*hnoX*	*hnoX* deletion fragment in pDS3.0	This work
pDS*hnoK*	*hnoK* deletion fragment in pDS3.0	This work
pDS*hnoB*	*hnoB* deletion fragment in pDS3.0	This work
pDS*hnoC*	*hnoC* deletion fragment in pDS3.0	This work
pDS*hnoD*	*hnoD* deletion fragment in pDS3.0	This work
pBAD202		Invitrogen
pBAD202-RBS-*hnoB*	*hnoB*-V5-His_6 in pBAD202 Kan^R	This work
pHMGWA	Expression plasmid (N-terminal His_6-MBP-tag), Amp^R	(3)

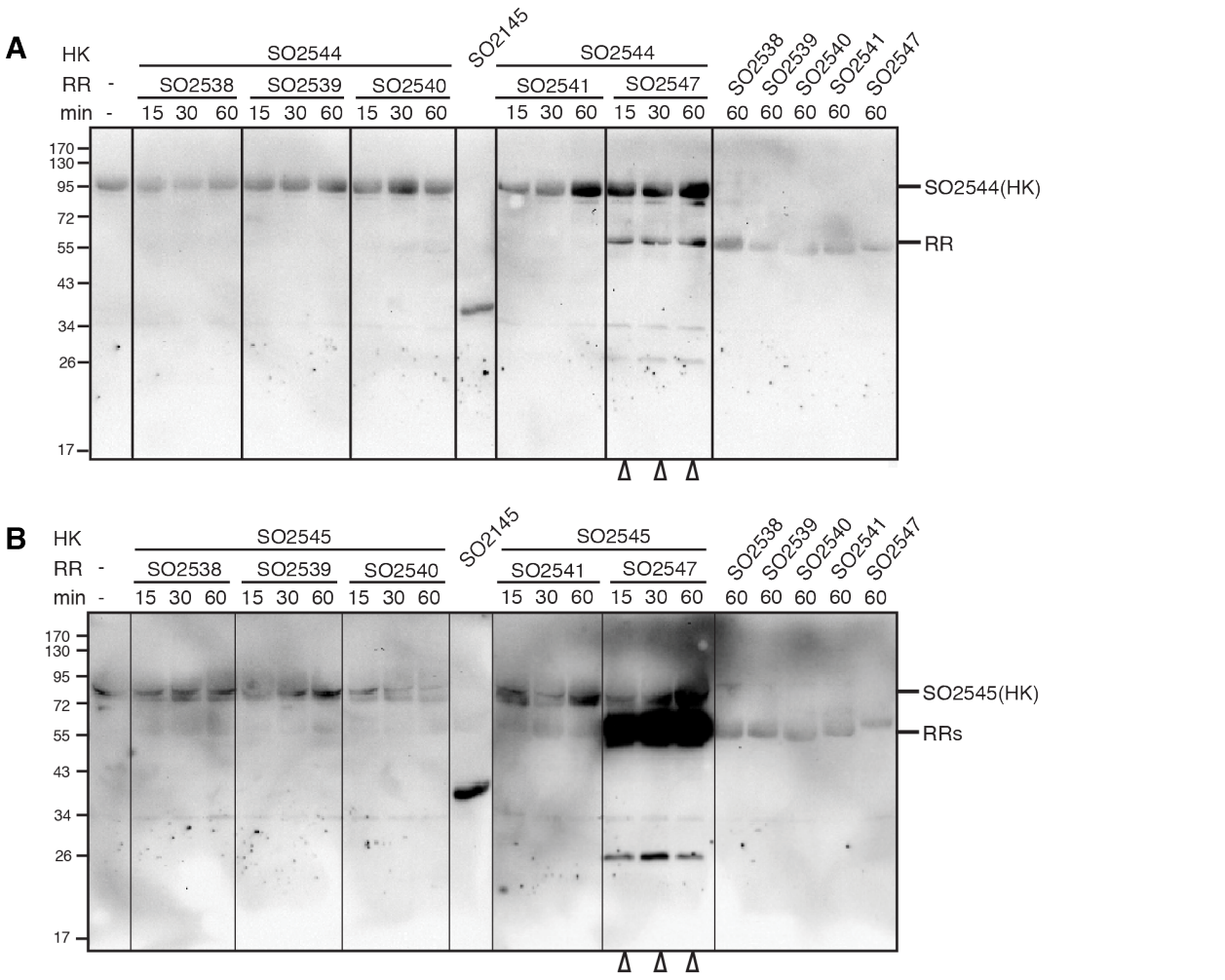
A
HK
RR
min
SO2544
SO2145
SO2544
SO2538
SO2539
SO2540
SO2541
SO2547
15 30 60
60
170
130
95
72
55
43
34
26
17
SO2544(HK)
RR
B
SO2545
SO2145
SO2545
SO2545(HK)
RRs
C
sec
10 20 30 60 120
HnoB
HnoK
HnoC
HnoD
D
HnoS
E
HK bait
HnoK
HnoS
SO2545
HKs (MBP-tagged)
H-NOX

Fig. B.1. Characterization of additional HKs in the RR operons, related to Figure 2.1

A. Phosphotransfer profiling of HnoT with the five RR in the adjacent operons (HnoA-D, SO2547). HK activity for HnoT was not observed with [γ-^{32}P]-ATP but was detected with ATPgS. The HK was pre-thiophosphorylated and then incubated with an equimolar amount of the respective RR for 15-60 min. Thiophosphorylation was detected by Western blot using a thiophosphoester specific antibody (4, 5). Thiophosphotransfer was only observed to the CheY RR (SO2547) (open triangles).

B. Phosphotransfer profiling between SO2545 and the same five RRs. The experiment was conducted as above. Thiophosphotransfer was only observed to the CheY RR (SO2547) (open triangles).

C. Comparison of phosphotransfer kinetics between HnoK and HnoB-D. The phosphorimage corresponds to representative raw data for Figure 1D. Signal of phosphorylated RR product was only observed for HnoC.

D. Comparison of phosphotransfer kinetics between HnoS and HnoB-D. The phosphorimage corresponds to representative raw data for Figure 1E.

E. Pull-down assay between the different cytosolic HKs (HnoK, HnoS, SO2545) and the H-NOX protein. MBP-tagged HK (100 μg) or buffer (control) was equilibrated with amylose resin, incubated with the NO-bound H-NOX protein (60 μM) and washed two times. Proteins were eluted with maltose and separated by SDS-PAGE. H-NOX protein was enriched when the H-NOX associated HK (HnoK) was used as bait (left lane) confirming a strong interaction. None of the other two HKs pulled down a significant amount of the H-NOX protein compared to the control.


A
PA2572
VOA_000533
VMB_24580
VC1087
VIC_001073
PTD2_05105
HCH_04027
MED92_01309
Sde_3805
amb1_19285
MADE_17750
Patl_1534
Glaag_2797
SO2541
PSM_B0118
ATW7_01230
MED92_01279
CPS_3241
RED65_02609

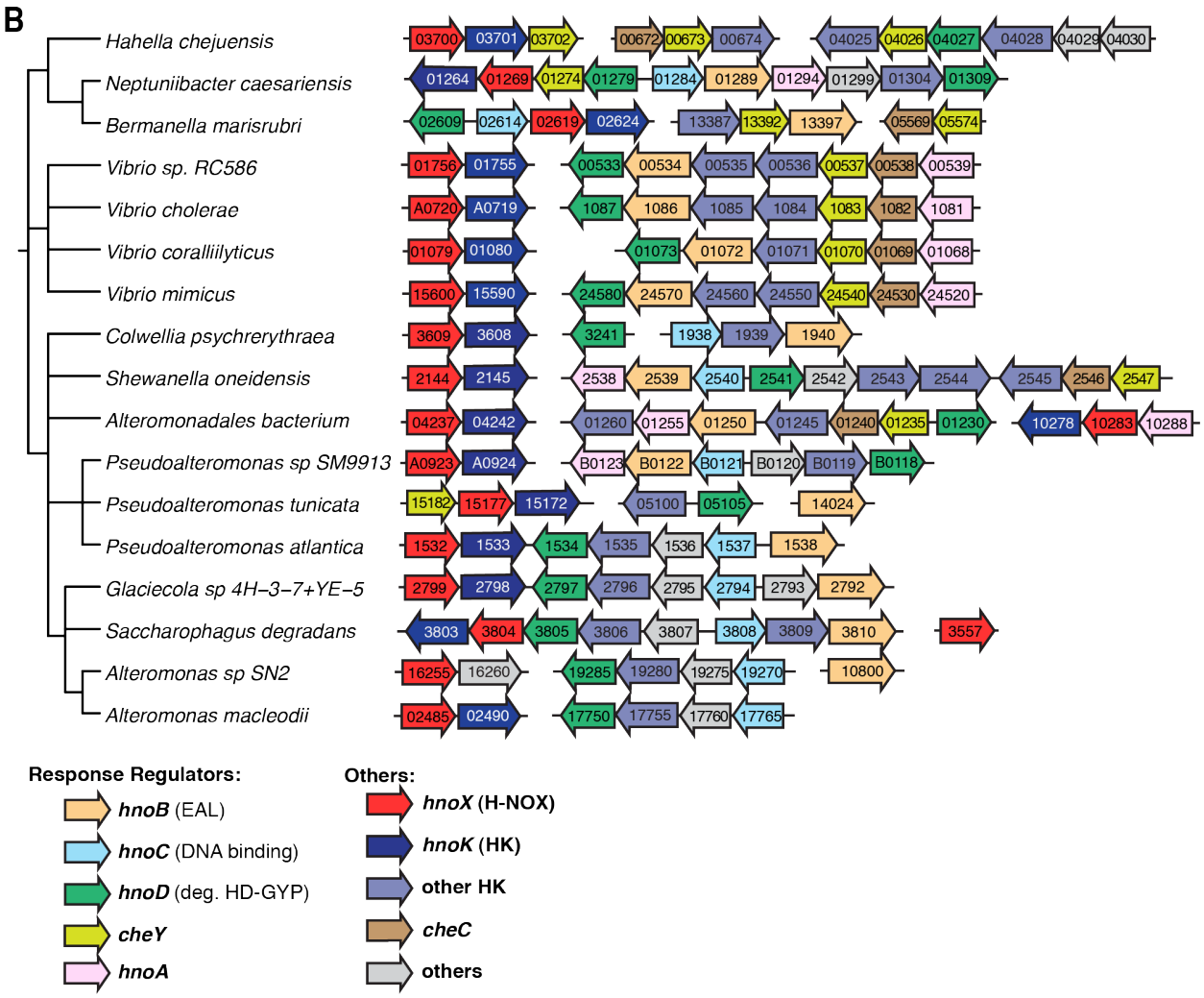

Fig. B.2. Gene organization of RR orthologs, related to Figure 2.2

A. Sequence alignment of HnoD orthologs in H-NOX containing organisms: *Vibrio sp.* VOA_000533, *Vibrio mimicus* VMB_24580, *Vibrio cholerae* VC1087, *Vibrio coralliilyticus* VIC_001073, *Pseudoalteromonas tunicata* PTD2_05105, *Hahella chejuensis* HCH_04027, *Neptuniibacter caesariensis* MED92_01309, *Saccharophagus degradans* Sde_3805, *Alteromonas sp. SN2* ambt_19285, *Alteromonas macleodii* MADE_17750, *Pseudoalteromonas atlantica* Patl_1534, *Glaciecola sp.* Glaag_2797, *Shewanella oneidensis* SO2541, *Pseudoalteromonas sp.* PSM_B0118, *Alteromonadales bacterium TW-7* ATW7_01230, *Neptuniibacter caesariensis* MED92_01279, *Colwellia psychrerythraea* CPS_3241, *Bermanella marisrubri* RED65_02609. Proteins were identified in a PSI-Blast search that looked specifically for a degenerate HD-GYP consensus motif and for the presence of a conserved C-terminal domain (shaded in yellow). The RRs align well to the *Pseudomonas aeruginosa* PA2572 (top row), which has been shown to control swarming motility and virulence (Ryan et al., 2009). The receiver domain is shaded in purple, the degenerate HD-GYP domain in green and the C-terminal domain in yellow. Red boxes highlight the position of the degenerate HD and GYP motifs and the aspartate phosphoacceptor is marked by a red triangle.

B. Organization of the *hnoX* genes (red) and associated *hnoK* HK genes (purple) as well as operons containing orthologs of the EAL RR (*hnoB*, yellow), DNA-binding RR (*hnoC*, light blue) and degenerate HD-GYP RR (*hnoD*, green) in other gammaproteobacteria. Numbers represent locus tags.

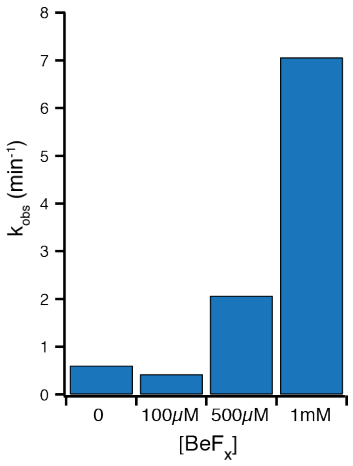

Fig. B.3. Stimulation of PDE activity of HnoB by the phosphorylation mimic beryllium fluoride, related to Figure 2.3

HnoB was incubated with the indicated concentrations of the RR phosphorylation mimic beryllium fluoride (BeF_x) prior to PDE activity assays. Increasing amounts of BeF_x caused a stimulation of activity, which was maximal at 1 mM. This was consistent with activation observed by direct phosphorylation (Figure 2.3.B) and by the D53E mutant phophosphorylation mimic (Figure 2.3.C).

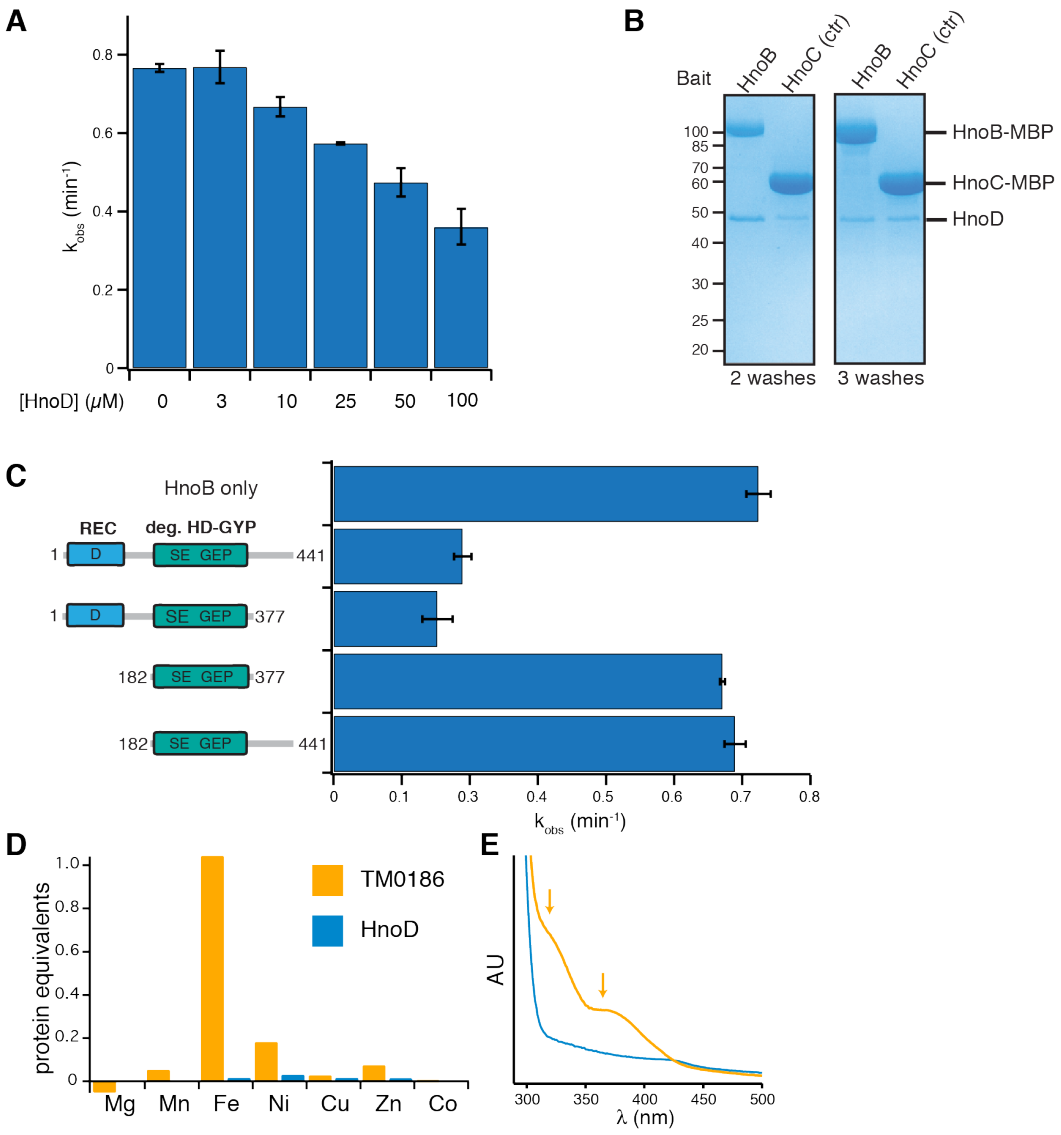

Fig. B.4. Inhibition of HnoB PDE activity by HnoD, related to Figure 2.4

A. Titration of HnoD inhibition of PDE activity. HnoB (2.5 μM) was incubated with varying amounts of HnoD (0 - 100 μM) prior to assaying HnoB PDE activity. Significant inhibition of PDE activity was first observed at 4-fold excess of HnoD (10 μM) and higher concentrations continued to decrease the activity.

B. Pull-down assay between the HnoB and HnoD to detect interactions. MBP-tagged HnoB and HnoC (control RR) were used as bait and the assay was conducted as in Fig. B.1.C. After two washes, a small difference in the amount of HnoD pulled down by HnoB compared to the control RR could be observed, but a more stringent third wash eliminated this difference.

C. Inhibition of HnoB PDE activity by HnoD truncations. HnoB was incubated with full length HnoD (residues 1-441) or three different truncations (residues 1-377, 182-377, 182-441) prior to the PDE assays. Only constructs containing the receiver domain (REC) were inhibitory (1-441, 1-377).

D. Metal content of purified HnoD and *T. maritima* TM0186 was determined by inductively coupled plasma atomic emission spectroscopy (ICP-AES). TM0186 (yellow) contained one equivalent of iron while HnoD (blue) contained no amount of metal ions above background.

E. UV/vis spectroscopy of TM0186 showed two shoulders at 320 and 370 nm that are characteristic of bound iron. These shoulders were absent in HnoD. All values represent the mean (n = 2) +/- SEM.

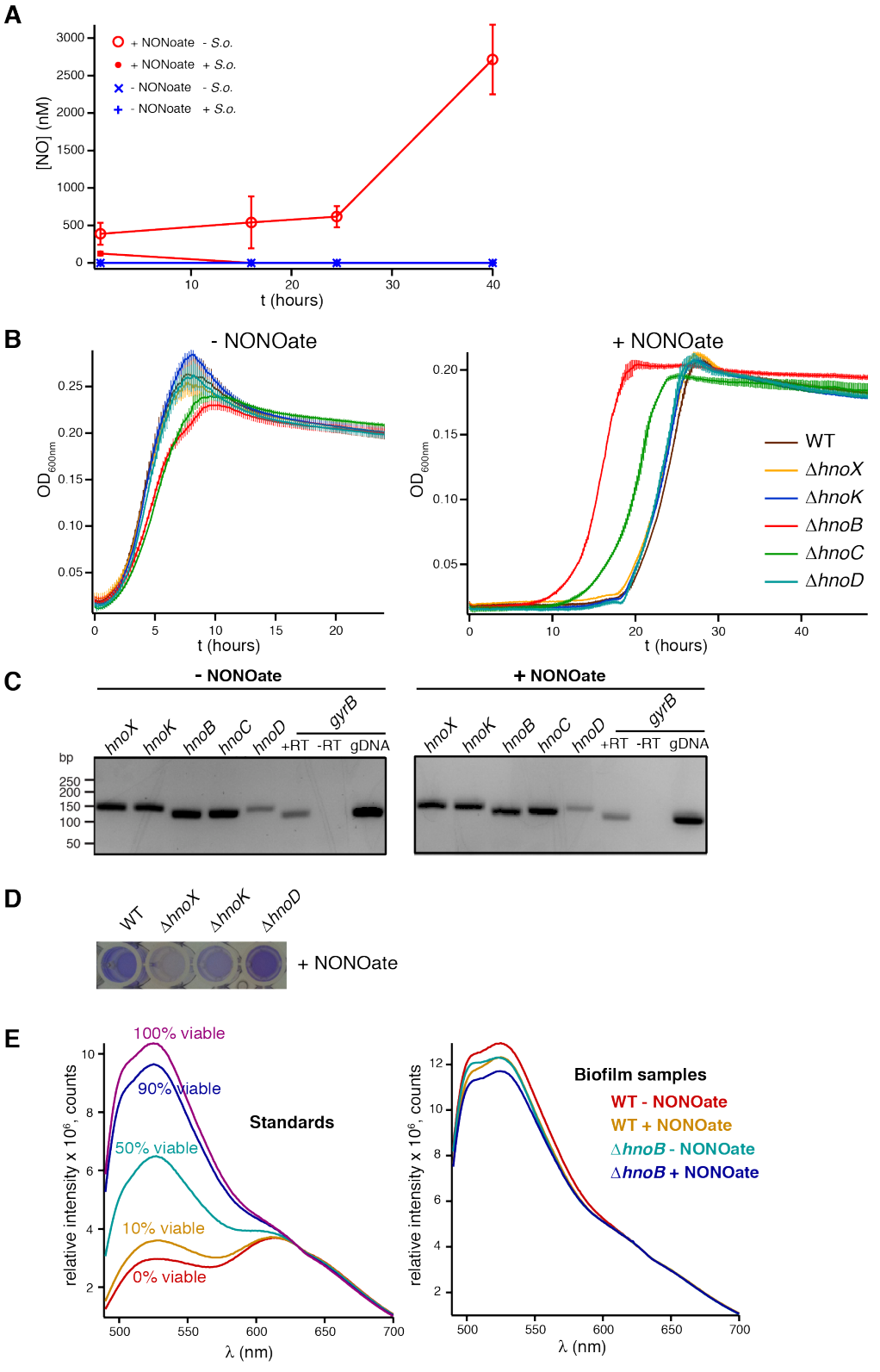
A
+ NONoate - S.o.
+ NONoate + S.o.
- NONoate - S.o.
- NONoate + S.o.
[NO] (nM)
t (hours)
B
- NONOate
+ NONOate
OD600nm
t (hours)
WT
ΔhnoX
ΔhnoK
ΔhnoB
ΔhnoC
ΔhnoD
C
- NONOate
+ NONOate
hnoX
hnoK
hnoB
hnoC
hnoD
gyrB
+RT
-RT
gDNA
bp
250
200
150
100
50
D
WT
ΔhnoX
ΔhnoK
ΔhnoD
+ NONOate
E
100% viable
90% viable
50% viable
10% viable
0% viable
Standards
relative intensity x 10^6, counts
λ (nm)
Biofilm samples
WT - NONOate
WT + NONOate
ΔhnoB - NONOate
ΔhnoB + NONOate

Fig. B.5. Characterization of two-component signaling knockouts in the presence and absence of NO, related to Figure 2.5

A. NO concentrations in anaerobic medium during growth of *Shewanella oneidensis* biofilms. WT *S. oneidensis* was grown in 12-well plates in the presence or absence of 200 μM DETA NONOate. Solution NO concentrations were measured using a NO analyzer (Sievers). In the absence of NONOate, there was no detectable NO in the cultures and control medium (blue, limit of detection ~ 50 nM). When NONOate was added, NO concentrations between 0.5 and 3 μM were measured in the control medium over 40 hours (red open circles). In the presence of *S. oneidensis*, the NO concentration was significantly lower (125 nM to non-detectable, red solid circles), implying that *S. oneidensis* consumed NO. Nonetheless, because of the high affinity of the H-NOX proteins for NO (picomolar), the H-NOX will form a complex with NO even at low nM concentrations. Values represent the mean from three independent measurements +/- SEM.

B. Anaerobic growth curves of WT *Shewanella oneidensis* and two-component signaling knockout strains. In the absence of NONOate, the strains did no exhibit any difference in growth. In the presence of NONOate, strains underwent a lag of 18 hours before growth is observed. The lag phase was shortened to 12 hours in the *ΔhnoB* strain and to 15 hours in the *ΔhnoC* strain. All strains reached the same optical density in stationary phase. Values represent the mean from three independent experiments +/- SEM.

C. Reverse transcription PCR of signaling genes during growth in the presence or absence of NO. RNA was extracted from WT *S. oneidensis* grown anaerobically with or without 200 μM DETA NONOate. cDNA was generated and transcription of *hnoX*, *hnoK*, and the three RR (*hnoB-D*) was demonstrated by PCR using primers for a 120-150 bp probe from each gene. Transcripts of all signaling proteins were present in both conditions. The DNA gyrase subunit *gyrB* was used as a positive control. A PCR product of *gyrB* was present when amplified from genomic DNA (gDNA) but was absent when no reverse transcriptase was added to the RNA extracts (-RT).

D. Images of crystal violet staining of biofilms from respective knockouts in 12-well plates.

E. Viability of *S. oneidensis* cells in biofilms. Anaerobic biofilms in 12-well plates were washed once to remove any planktonic cells and resuspended by vigorous pipetting. Cells were stained with the Live/Dead BacLight Bacterial Viability kit and the fluorescence emission spectra were measured. Standard mixtures of live and isopropanol-treated, dead *S. oneidensis* cells (left) showed that viable cells produced an increase in fluorescence at 530 nm compared to the fluorescence at 630 nm. All biofilm samples (right) displayed fluorescence emission spectra similar to viable cells. Quantification of viability demonstrated that cells in all biofilm samples were > 100% viable compared to the standards.

Appendix C

Table C.1: Microarray results comparing transcription between WT and Δ*hnoC Shewanella oneidensis*

Locus	Name	Description	log2(fold change) ΔHnoC/WT	Average Expression	Adjusted P value
SO2540	hnoC	response regulator	-3.510323528	5.906959489	0.002084669
SO2542	hnoE	signaling protein with FIST domain	2.302060492	7.706436939	0.002084669
SO2144	hnoX	NO-binding sensor protein	1.374867046	6.352462867	0.003399945
SO2541	hnoD	response regulator	2.936361615	9.883016636	0.003399945
SO2539	hnoB	cyclic diguanylate phosphodiesterase with response regulator receiver modulation and PAS sensing domain	2.714773097	7.36373823	0.003399945
SO2543	hnoS	cytoplasmic sensor histidine kinase	1.331881481	5.872132984	0.003399945
SO1695		diguanylate cyclase with PAS sensory domain	1.278079274	5.169052591	0.009059454
SO2538	hnoA	response regulator	1.948753811	6.598965031	0.046116401
SO_t009	#N/A	#N/A	0.695759767	9.098137543	0.158982273
SO_t041	#N/A	#N/A	0.751920385	9.099661249	0.208286571
SO_t033	#N/A	#N/A	0.839005965	9.137431492	0.208286571
SO2145	hnoK	histidine kinase	0.539653092	4.894146092	0.289225598
SO2544	HnoT	hybrid sensor histidine kinase	0.918997579	5.360964458	0.29442185
SO_t019	#N/A	#N/A	0.658022335	7.562045008	0.29442185
SO_t010	#N/A	#N/A	0.702254466	9.038106632	0.31587802
SO2305	lrp	leucine-responsive regulatory protein, Lrp	-0.582500287	9.25840033	0.343389121
SO2546	cheC	inhibitor of MCP methylation, CheC	1.202740596	5.588742712	0.442934982
SO2547	cheY_4	chemotaxis response regulator, CheY_4	1.710563427	7.363774849	0.47444228
SO3720	hemG_3	protoporphyrinogen oxidase, HemG_3	-0.71469302	10.60035205	0.47444228
SO2545	0	cytoplasmic sensor histidine kinase with PAS sensory domain	0.495752398	4.609812327	0.47444228
SO2623	aat	leucyl/phenylalanyl-tRNA--protein transferase, Aat	0.797140703	6.422351365	0.47444228
SO0728	0	conserved hypothetical protein	-0.447733184	7.455594449	0.47444228
SO3391	0	ATP-dependent protease, family S16 unassigned peptidases	0.679565396	5.539895944	0.47444228
SO_t015	#N/A	#N/A	0.580204805	7.429202754	0.497678493
SO4317	0	cell surface calcium-binding protein with BNR repeats	1.823379866	8.522781987	0.497678493
SO3863	modA	ABC molybdenum transporter, periplasmic ligand-binding subunit, ModA	-0.473272823	4.968685647	0.497678493

Table C.2: **Strains and plasmids used in Chapter 3**

Strain or plasmid	Relevant genotype	Reference
Bacterial Strains		
S. oneidensis		
MR-1	*Shewanella oneidensis* MR-1 wild-type	Alfred Spormann (Stanford)
Δ*hnoX*	MR-1 Δ*hnoX*	This work
Δ*hnoK*	MR-1 Δ*hnoK*	This work
Δ*hnoB*	MR-1 Δ*hnoB*	This work
Δ*hnoC*	MR-1 Δ*hnoC*	This work
Tn7::*gfp*	MR-1 Tn7::*gfp*	This work
E. coli		
BL21(DE3)pLysS	F- *ompT hsd*S_B (r_B-m_B-) *gal dcm rne131* (DE3), Expression strain	Life Technologies
Plasmids		
pHMGWA-*So*HnoC	His_6-MBP-TEV_c-HnoC, Amp^R, expression plasmid for HnoC	This work
pHMGWA-*So*HnoK	His_6-MBP-TEV_c-HnoC, Amp^R, expression plasmid for HnoK	This work
pPROBE-NT	pBBR1, *gfp*, Kan^R	(6)
pPROBE-*gfp*[AAV]	pBBR1, *gfp*(AAV), Kan^R	(6)
pProbe-NT::*hnoXp-gfp*	pBBR1, *hnoXp_gfp*, Kan^R	This work
pProbe-NT::*hnoCp-gfp*	pBBR1, *hnoCp_gfp*, Kan^R	This work
pProbe-NT::*hnoDp-gfp*	pBBR1, *hnoDp_gfp*, Kan^R	This work
pProbe-NT::*ctrp-gfp*	pBBR1, *Controlp_gfp*, Kan^R	This work
pProbe-NT::*hnoCp-gfp*[AAV]	pBBR1, *hnoCp_gfp*(AAV), Kan^R	This work

References

1. Venkateswaran, K., Moser, D. P., Dollhopf, M. E., Lies, D. P., Saffarini, D. A., MacGregor, B. J., Ringelberg, D. B., White, D. C., Nishijima, M., Sano, H., Burghardt, J., Stackebrandt, E., and Nealson, K. H. (1999) Polyphasic taxonomy of the genus Shewanella and description of Shewanella oneidensis sp. nov. *Int. J. Syst. Bacteriol.* **49 Pt 2**, 705–724
2. Simon, R., Priefer, U., and Pühler, A. (1983) A Broad Host Range Mobilization System for In Vivo Genetic Engineering: Transposon Mutagenesis in Gram Negative Bacteria. *Nat. Biotechnol.* **1**, 784–791
3. Busso, D., Delagoutte-Busso, B., and Moras, D. (2005) Construction of a set Gateway-based destination vectors for high-throughput cloning and expression screening in Escherichia coli. *Anal. Biochem.* **343**, 313–321
4. Allen, J. J., Li, M., Brinkworth, C. S., Paulson, J. L., Wang, D., Hübner, A., Chou, W.-H., Davis, R. J., Burlingame, A. L., Messing, R. O., Katayama, C. D., Hedrick, S. M., and Shokat, K. M. (2007) A semisynthetic epitope for kinase substrates. *Nat. Methods* **4**, 511–516
5. Carlson, H. K., Vance, R. E., and Marletta, M. A. (2010) H-NOX regulation of c-di-GMP metabolism and biofilm formation in Legionella pneumophila. *Mol. Microbiol.* **77**, 930–942
6. Miller, W. G., Leveau, J. H., and Lindow, S. E. (2000) Improved gfp and inaZ broad-host-range promoter-probe vectors. *Mol. Plant Microbe Interact.* **13**, 1243–1250